21808

National Library of Canada
Bibliothèque nationale du Canada

CANADIAN THESES ON MICROFICHE

THÈSES CANADIENNES SUR MICROFICHE

NAME OF AUTHOR/*NOM DE L'AUTEUR* EDWIN OKO ENGMANN.

TITLE OF THESIS/*TITRE DE LA THÈSE* TRANSVERSE MIXING CHARACTERISTICS OF OPEN AND ICE-COVERED CHANNEL FLOWS.

UNIVERSITY/*UNIVERSITÉ* ALBERTA

DEGREE FOR WHICH THESIS WAS PRESENTED/*GRADE POUR LEQUEL CETTE THÈSE FUT PRÉSENTÉE* Ph. D

YEAR THIS DEGREE CONFERRED/*ANNÉE D'OBTENTION DE CE DEGRÉ* 1974

NAME OF SUPERVISOR/*NOM DU DIRECTEUR DE THÈSE* DR. ROLF KELLERHALS

Permission is hereby granted to the NATIONAL LIBRARY OF CANADA to microfilm this thesis and to lend or sell copies of the film.

The author reserves other publication rights, and neither the thesis nor extensive extracts from it may be printed or otherwise reproduced without the author's written permission.

L'autorisation est, par la présente, accordée à la BIBLIOTHÈQUE NATIONALE DU CANADA de microfilmer cette thèse et de prêter ou de vendre des exemplaires du film.

L'auteur se réserve les autres droits de publication; ni la thèse ni de longs extraits de celle-ci ne doivent être imprimés ou autrement reproduits sans l'autorisation écrite de l'auteur.

DATED/*DATÉ* September 23rd '74 SIGNED/*SIGNÉ* Engmann

PERMANENT ADDRESS/*RÉSIDENCE FIXÉ* FACULTY OF ENGINEERING,
UNIV. OF SCIENCE & TECH.,
KUMASI, GHANA.

NL-91 (11-73)

THE UNIVERSITY OF ALBERTA

TRANSVERSE MIXING CHARACTERISTICS OF OPEN AND ICE-COVERED CHANNEL FLOWS

by

©

EDWIN OKO ENGMANN

A THESIS
SUBMITTED TO THE FACULTY OF GRADUATE STUDIES AND RESEARCH
IN PARTIAL FULFILMENT OF THE REQUIREMENTS FOR
THE DEGREE OF DOCTOR OF PHILOSOPHY

DEPARTMENT OF CIVIL ENGINEERING

EDMONTON, ALBERTA

FALL 1974

THE UNIVERSITY OF ALBERTA

FACULTY OF GRADUATE STUDIES AND RESEARCH

The undersigned certify that they have read, and recommend to the Faculty of Graduate Studies and Research, for acceptance, a thesis entitled TRANSVERSE MIXING CHARACTERISTICS OF OPEN AND ICE-COVERED CHANNEL FLOWS submitted by Edwin Oko Engmann in partial fulfilment of the requirements for the degree of Doctor of Philosophy.

Rolf Kellerhals
Supervisor

R Gerard

David J Wilson

P. H. Bouthillier

N Rajaratnam

J. Wilhe Dick
External Examiner

Date September 5th 1974

ABSTRACT

The effect of an ice-cover on transverse spreading of a tracer released at a constant and steady rate into a turbulent channel flow is investigated. Velocity and tracer concentration measurements are conducted at various sections downstream of the tracer source in both a straight and a meandering flume for open-water and ice-cover conditions.

Transverse diffusion coefficients (E_z) in the straight channel tests are computed by the method of moments and by a formula based on similarity considerations. Transverse mixing coefficients (E_{zw}) in the meandering channel tests are evaluated using the moments and integral methods based on the convective-diffusion equation expressed in a meandering coordinate system.

It is shown that the transverse diffusion coefficient for ice-cover conditions in a straight channel is approximately 50% smaller than the corresponding coefficient for open water conditions but when these coefficients are normalised with the product of shear velocity, u_* , and hydraulic radius, R , they do not differ significantly. Analysis of the available data on transverse diffusion does not indicate a clear dependence of E_z/u_*R on W/R , where W is channel width.

The magnitude of the transverse mixing coefficient in meandering channel tests and for ice-cover conditions is found to be approxi-

mately 4 times smaller than the corresponding coefficient for open-water condition. Values of E_{zw}/u_*R are higher for open-water than for ice-cover conditions for similar flow conditions. The longitudinal variation of the transverse mixing coefficient is found to be strongly related to the growth, decay and reversal of the spiral motions.

Field investigations of transverse mixing in the Lesser Slave River confirm the reduction in mixing capacity due to an ice-cover.

ACKNOWLEDGEMENTS

The author wishes to express his sincere gratitude to Dr. R. Kellerhals for his sustained advice, guidance and encouragement throughout the course of this study. The author is also indebted to Dr. Gerard who devoted much time to read the manuscript and for his useful suggestions.

Thanks are due to Dr. Rajaratnam and Dr. Beltaos for their comments and interest in this study and also to Dr. Wilson for helpful comments.

Technical assistance given by Messrs. D. McGowan, R. Gitzel and S. Lovell in constructing and maintaining the laboratory equipment are gratefully acknowledged. Mr. G. Steadman and Mr. C. Chiang assisted with some of the measurements and the author is thankful.

The present study was supported by the National Research Council of Canada. The field tests were made possible through a loan of manpower and equipment by the Highway and River Engineering Division of Alberta Research. The author was supported by an award of Scholarship offered by the Commonwealth Scholarship and Fellowship Committee, Govrnment of Canada. Study leave was granted to the author by the University of Science and Technology, Kumasi, Ghana. These are gratefully acknowledged.

Last but not least, the author is immesurably indebted to his wife, Florence, for her encouragement and sympathetic understanding throughout the years of graduate study.

TABLE OF CONTENTS

Page

Abstract

Acknowledgements

Table of Contents

List of Tables

List of Figures

List of Symbols

CHAPTER 1 - INTRODUCTION

1.1 General

1.2 Objectives

1.3 Structure of Report

CHAPTER 2 - REVIEW OF PAST STUDIES

2.1 The Convective-Diffusion Equation

2.2 Solutions of the Convective-Diffusion Equation for Transverse Diffusion in Straight Channels

2.3 Evaluation of the Transverse Diffusion Coefficient for Straight Channels

2.4 Transverse Mixing in Meandering Channels

CHAPTER 3 - ANALYTICAL INVESTIGATIONS

3.1 Similarity Analysis for Straight Channels

3.2 The 2-Dimensional Lateral Diffusion Equation

Page

3.3 Methods for Evaluating the Transverse Exchange Coefficient ....

3.3.1 Method of Moments ....

3.3.2 Integral Method ....

CHAPTER 4 - LABORATORY EQUIPMENT AND METHODS ....

4.1 Introduction and Experimental Objectives ...

4.2 Experimental Equipment ....

4.2.1 Straight Flume ....

4.2.2 Meandering Flume ....

4.2.3 Bed Roughness and Ice-Cover ....

4.2.4 Velocity Measuring System ....

4.2.4.1 Straight Flume ....

4.2.4.2 Meandering Flume ....

4.2.5 Yaw Probe ....

4.2.6 Tracer and Injection System ....

4.2.7 Concentration Measuring System ......

4.2.7.1 Straight Flume ....

4.2.7.2 Meandering Flume ....

4.2.8 Co-ordinate Positioner ....

4.2.9 Data Acquisition System for Velocity Measurements ....

4.3 Experimental Procedure ....

4.3.1 Identification Code for Flumes and Experiments ....

Page

4.3.2 Description of a Typical Experiment ..

4.3.2.1 Straight Flume ....

4.3.2.2 Meandering Flume ....

CHAPTER 5 - PRESENTATION OF VELOCITY MEASUREMENTS ....

5.1 Straight Flume ....

5.1.1 Hydraulic Data ....

5.1.2 Velocity Measurements ....

5.2 Characteristics of Flow in Meandering Channels ....

5.2.1 General ....

5.2.2 Velocity Measurements in Open Meandering Flume ....

5.2.2.1 Longitudinal Velocity Component ....

5.2.2.2 Transverse Velocity Component ....

5.2.2.3 Angle of Deviation of Velocity Vector ....

5.2.3 Velocity Measurements in Ice-Covered Meandering Channels ....

5.2.3.1 Longitudinal Velocity Component ....

5.2.3.2 Transverse Velocity Component ....

5.2.3.3 Horizontal Angle of Deviation of Velocity Vector ....

Page

CHAPTER 6 - PRESENTATION OF CONCENTRATION MEASUREMENTS AND DISCUSSION OF RESULTS ....

6.1 Straight Flume ....

6.1.1 Transverse Distribution of Tracer Concentration ....

6.1.2 Moments of the Transverse Tracer Flux Distribution ....

6.1.2.1 Calculation of Moments .....

6.1.2.2 Growth of the Second Moments with Longitudinal Distance ....

6.1.3 The Transverse Exchange Coefficient ..

6.1.3.1 Determined by the Method of Moments ....

6.1.3.2 Determined by the Similarity Analysis ....

6.1.4 Effect of a Smooth Ice-Cover on the Exchange Coefficient ....

6.1.5 Factors Affecting the Normalised Exchange Coefficient ....

6.1.6 Attenuation of Peak Concentration ...

6.2 Meandering Flume ....

6.2.1 Concentration Measurements ....

6.2.2 Evaluation of Transverse Exchange Coefficient ....

6.2.2.1 Method of Moments ....

6.2.2.2 Integral Method ....

6.2.3 The Normalised Transverse Mixing Coefficient ....

Page

6.2.4 Parameters Controlling E_{zw}/u_*R ....

CHAPTER 7 - FIELD INVESTIGATIONS ....

7.1 Description of Test Reach ....

7.2 Experimental Procedure ....

7.2.1 Velocity Measurements ....

7.2.2 Tracer Measurements ....

7.3 Experimental Results ....

7.3.1 Ice-Cover ....

7.3.2 Hydraulic Data ....

7.3.3 Tracer Distributions ....

7.4 Computation of the Transverse Mixing Coefficient, E_{zw} ....

CHAPTER 8 - SUMMARY, CONCLUSIONS AND RECOMMENDATIONS ....

8.1 Conclusions ....

8.2 Results Related to Straight Flume ....

8.3 Results Related to Meandering Flume ....

8.4 Results Related to Field Investigations .....

8.5 Recommendations ....

LIST OF REFERENCES ....

APPENDIX A - VELOCITY MEASUREMENTS ....

LIST OF TABLES

Page

CHAPTER 2

2-1 Summary of Previous Measurements of the Transverse Diffusion Coefficient in Open Channel Flows (partly adlopted from Okoye, 1970) ....

CHAPTER 4

4-1 Classification of Flume and Experiments ....

CHAPTER 5

5-1 Summary of Hydraulic Data for Straight Flume Experiments ....

5-2 Summary of Hydraulic Data for Meandering Flume Experiments ....

5-3 Comparison of Observed and Computed $\psi_{y\,o}$ Values .....

CHAPTER 6

6-1 Numerical Values of X, M_2(X) and A in Equation 6.5 ...

6-2 Comparison of E_z Values as Determined by the Method of Moments and Similarity Analysis ....

6-3 Summary of Measured Exchange Coefficients and Related Parameters ....

6-4 Summary of Decay Exponents for the Attenuation of Depth-Averaged Peak Concentration ....

6-5 Summray of Numerical Values of M_2(X), B(X) and E_{zw} ...

6-6 Summary of Results ....

6-7 Comparison of E_{zw}/u_*R for the same Reach and Source Position and Similar Flow Conditions ....

6-8 Numerical Values of Variables in Equation 6.27 ......

CHAPTER 7

7-1 Hydraulic Data for Winter Conditions ....

Page

7-2 Hydraulic Data for Open Water Conditions ....

7-3 Numerical Values of Some Variables in Equations 7.7 and 7.8 ....

7-4 Dependence of E_{zw}/u_*R on Point about which Moments of Tracer Flux are taken or Value of Cumulative Discharge about which Moments of Tracer Concentration are taken ....

7-5 Numerical Values of $M_{2q}(X)$, $B_q(X)$ and E_{zw} in Equation 7.11 ....

7-6 Some Field Measurements of the Normalised Transverse Mixing Coefficient ....

LIST OF FIGURES

Page

CHAPTER 3

3.1 Definition Sketch for Meandering Channel.....

CHAPTER 4

4.1 General View of Straight Flume, Showing Floating Ice-cover..............................
4.2a Plan View of Meandering Flume.................
4.2b Photograph of Meandering Flume................
4.3 Flume Bed Roughness, expanded sheet metal, 1/16 in. thick. ....
4.4 Partial View of Meandering Flume showing Ice-cover (1/2 in. plywood boards) in Position ....
4.5 Nose Form of Yaw Probe (not to scale) ....
4.6 Calibration Coefficient, K_4 , for Yaw Probe ..
4.7 Curve of K_5 versus ....
4.8 Sketch of Tracer Injection System ....
4.9 Calibration Curve for Rotameter ....
4.10 Sampling Rake used for Tracer Measurements ..
4.11 Data Acquisition System ....
4.12 Data Acquisition and Processing System .....
4.13 Schematic Sketch of Meandering Flume showing Sections used for Velocity and Concentration Measurements ....

CHAPTER 5

5.1 Measured Velocity Profiles, Run 106 ....

LIST OF FIGURES

CHAPTER 5 - (Cont'd) Page

5.2 Velocity Distributions in Ice-covered Channel.

5.3 Velocity Contours for Run 203, velocities on isovels in ft/sec ....

5.4 Velocity Profile near Rough Bed for Ice-cover Tests ....

5.5 Velocity Profile near Ice-cover for Ice-cover Tests ....

5.6 Vertical Distributions of Longitudinal Velocity Runs 301/2/3
a) Sections $\theta_1 = 0$ TO $\pi/2$ ....
b) Sections $\theta_1 = 2\pi/3$ TO $\theta_2 = \pi/6$ ....
c) Sections $\theta_2 = \pi/3$ TO $5\pi/6$ ....

5.7 Lateral Distributions of Depth-averaged Longitudinal Velocity
a) Runs 301/2/3 ....
b) Runs 304/5/6 ....
c) Runs 307/8 ....

5.8 Longitudinal Variation of the Dimensionless Mean Square Velocity Deviation, ...

5.9 Vertical Distributions of Transverse Velocity Runs 301/2/3
a) Sections $\theta_1 = 0$ TO $\pi/2$ ....
b) Sections $\theta_1 = 2\pi/3$ TO $\theta_2 = \pi/6$ ....
c) Sections $\theta_2 = \pi/3$ TO $5\pi/6$ ....

5.10 Longitudinal Variation of the Strength of Spiral Motion near Channel Centreline for Open Channel ....

5.11 Transverse and Longitudinal Variation of Strength of Spiral Motion, Run 407

5.12 Vertical Distributions of Horizontal Angle of Deviation of Velocity Vector, ψ, Runs 301/2/3
a) Sections $\theta_1 = 0$ TO $\pi/2$ ....
b) Sections $\theta_1 = 2\pi/3$ TO $\theta_2 = \pi/6$ ....
c) Sections $\theta_2 = \pi/3$ TO $5\pi/6$ ....

LIST OF FIGURES

CHAPTER 5 - (cont'd)

Page

5.13 Vertical Distributions of Longitudinal Velocity
- a) Sections $\theta_1 = 0$ TO $\pi/2$ ....
- b) Sections $\theta_1 = 2\pi/3$ TO $\theta_2 = \pi/6$ ....
- c) Sections $\theta_2 = \pi/3$ TO $2\pi/3$ ....

5.14 Lateral Distributions of Depth-averaged Longitudinal Velocity
- a) Runs 401/2/3 ....
- b) Runs 404/5/6 ....
- c) Runs 407/8 ....

5.15 Vertical Distributions of Trnaverse Velocity, Runs 404/5/6
- a) Sections $\theta_1 = 0$ TO $\pi/2$ ....
- b) Sections $\theta_1 = 2\pi/3$ TO $\theta_2 = \pi/6$ ....
- c) Sections $\theta_2 = \pi/3$ TO $2\pi/3$ ....

5.16 Longitudinal Variation of the Strength of Spiral Motion, S , near Channel Centerline for Ice-cover Experiments ....

5.17 Vertical Distributions of Horizontal Angle of Deviation of Velocity Vector, ψ, Runs 404/5/6.
- a) Sections $\theta_1 = 0$ TO $\pi/2$ ....
- b) Sections $\theta_1 = 2\pi/3$ TO $\theta_2 = \pi/6$ ....
- c) Sections $\theta_2 = \pi/3$ TO $2\pi/3$ ....

CHAPTER 6

6.1 Lateral Distributions of Depth-averaged Concentration at Various Distances Downstream of Source.
- a) Run 203 ....
- b) Run 101 ....
- c) Run 202 ....
- d) Run 102 ....

6.2 Graph of Normalised Concentration against Normalised Distance, Runs 106 and 206 ......

6.3 Growth of Variance of Tracer Flux with Distance Downstream of Source for Open Channel Tests .

LIST OF FIGURES

CHAPTER 6 - (cont'd) Page

6.4 Growth of Variance of Tracer Flux with Distance Downstream of Source for Ice-cover Tests. ....

6.5 Transverse Concentration Profiles at Different Levels for first Section of Tracer Measurement

6.6 Longitudinal Variation of $M_2(X)$ and A for near Side Tracer Injection ....

6.7 Longitudinal Variation of the Transverse Exchange Coefficient, E_z, for Side Injection .

6.8 Variation of the Normalised Exchange(Diffusion) Coefficient, E_z/u_*d_* with Aspect Ratio W/d_* ..

6.9 Variation of the Normalised Exchange(Diffusion) Coefficient, E_z/u_*R, with Dimensionless Width W/R ....

6.10 Variation of the Normalised Transverse Diffusion Coefficient, E_z/u_*R, with Friction Factor, f , using Miller andRichardson's(1974) Data ....

6.11 Decay of Normalised Peak Concentration, C_{1m} , with Dimensionless Distance, X_1 ....

6.12 Transverse Distributions of Depth-averaged Tracer Concentration at various Sections Downstream of Source
- a) Run 401 ....
- b) Run 403 ....
- c) Run 404 ....
- d) Run 405 ....
- e) Run 302 ....
- f) Run 304 ....

6.13 Transverse Concentration Profiles at Various Flow Levels
- a) Runs 401,403,408 and at Section $\theta_1 = 2\pi/3$. ....
- b) Runs 302,304,306 and at Section $\theta_1 = \pi/2$. ....

LIST OF FIGURES

CHAPTER 6 - (cont'd)

Page

6.14a Coefficient of Variation Curves for Ice-cover Tests ....

6.14b Coefficient of Variation Curves for Open Channel Tests ....

6.15a Longitudinal Variation of M_2 and B for various Test Runs ....

6.15b Longitudinal Variation of M_2 and B for various Test Runs ....

6.16 Longitudinal Variation of B_1, B_2, B_3 and B
- a) Runs 401/2/3 ....
- b) Runs 404/5/6 ....
- c) Runs 302/4/6 ....
- d) Runs 307/8 ....

6.17 Longitudinal and Lateral Variations of the Mixing Coefficient, E_{zw}
- a) Run 405 ....
- b) Run 403 ....
- c) Run 402 ....
- d) Run 306 ....

6.18a Longitudinal Variation of the Normalised Transverse Exchange(Mixing) Coefficient ......

6.18b Longitudinal Variation of the Normalised Transverse Exchange(Mixing) Coefficient ......

6.19 Longitudinal Variation of the Averaged Normalised Transverse Mixing Coefficient for Different Flow Conditions ....

CHAPTER 7

7.1 Plan of Study Reach ....

7.2 Relief on Ice Underside ....

7.3 Velocity Contours ....

LIST OF FIGURES

CHAPTER 7 - (cont'd)

Page

7.4 Transverse Profiles of Velocity and Depth at Sections A and C (Open-Water) ....

7.5 Tracer Distributions
  a) Winter ....
  b) Summer ....

7.6 Variations of $(M_2)c$ and B with X for Summer and Winter Tests ....

7.7 Lateral Variation of Terms in B(X) ....

7.8 Longitudinal Variation of the Normalised Transverse Mixing Coefficient, E_{zw}/u_*R .....

APPENDIX A

A.1 Vertical Distributions of Longitudinal Velocity, Runs 304/6
  a) Sections $\theta_1 = 0$ TO $\pi/2$ ....
  b) Sections $\theta_1 = 2\pi/3$ TO $\theta_2 = \pi/6$ ....
  c) Sections $\theta_2 = \pi/3$ TO $5\pi/6$ ....

A.2 Vertical Distributions of Longitudinal Velocity Runs 307/8
  a) Sections $\theta_1 = 0$ TO $\pi/2$ ....
  b) Sections $\theta_1 = 2\pi/3$ TO $\theta_2 = \pi/6$ ....
  c) Sections $\theta_2 = \pi/3$ TO $5\pi/6$ ....

A.3 Vertical Distributions of Transverse Velocity Runs 304/6
  a) Sections $\theta_1 = 0$ TO $\pi/2$ ....
  b) Sections $\theta_1 = 2\pi/3$ TO $\theta_2 = \pi/6$ ....
  c) Sections $\theta_2 = \pi/3$ TO $5\pi/6$ ....

A.4 Vertical Distributions of Transverse Velocity Runs 307/8
  a) Sections $\theta_1 = 0$ TO $\pi/2$ ....
  b) Sections $\theta_1 = 2\pi/3$ TO $\theta_2 = \pi/6$ ....
  c) Sections $\theta_2 = \pi/3$ TO $5\pi/6$ ....

LIST OF FIGURES

APPENDIX A - (cont'd)

Page

A.5 Vertical Distributions of Horizontal Angle of Deviation of Velocity Vector, Runs 304/6
  a) Sections $\theta_1 = 0$ To $\pi/2$ ....
  b) Sections $\theta_1 = 2\pi/3$ To $\theta_2 = \pi/6$ ....
  c) Sections $\theta_2 = \pi/3$ To $5\pi/6$ ....

A.6 Vertical Distributions of Horizontal Angle of Deviation of Velocity Vector, Runs 307/8
  a) Sections $\theta_1 = 0$ To $\pi/2$ ....
  b) Sections $\theta_1 = 2\pi/3$ To $\theta_2 = \pi/6$ ....
  c) Sections $\theta_2 = \pi/3$ To $5\pi/6$ ....

A.7 Vertical Distributions of Longitudinal Velocity , Runs 401/2/3
  a) Sections $\theta_1 = \pi/6$ To $2\pi/3$ ....
  b) Sections $\theta_1 = 5\pi/6$ To $\theta_2 = \pi/3$ ....
  c) Sections $\theta_2 = \pi/2$ To $5\pi/6$ ....

A.8 Vertical Distributions of Longitudinal Velocity, Runs 407/8
  a) Sections $\theta_1 = \pi/6$ To $2\pi/3$ ....
  b) Sections $\theta_1 = 5\pi/6$ To $\theta_2 = \pi/3$ ....
  c) Sections $\theta_2 = \pi/2$ To $5\pi/6$ ....

A.9 Vertical Distributions of Transverse Velocity, Runs 401/2/3
  a) Sections $\theta_1 = \pi/6$ To $2\pi/3$ ....
  b) Sections $\theta_1 = 5\pi/6$ To $\theta_2 = \pi/3$ ....
  c) Sections $\theta_2 = \pi/2$ To $5\pi/6$ ....

A.10 Vertical Distributions of Transverse Velocity, Runs 407/8
  a) Sections $\theta_1 = \pi/6$ To $2\pi/3$ ....
  b) Sections $\theta_1 = 5\pi/6$ To $\theta_2 = \pi/3$ ....
  c) Sections $\theta_2 = \pi/2$ To $5\pi/6$ ....

A.11 Vertical Distributions of Horizontal Angle of Deviation of Velocity Vector, Runs 401/2/3
  a) Sections $\theta_1 = \pi/6$ To $2\pi/3$ ....
  b) Sections $\theta_1 = 5\pi/6$ To $\theta_2 = \pi/3$ ....
  c) Sections $\theta_2 = \pi/2$ To $5\pi/6$ ....

A.12 Vertical Distributions of Horizontal Angle of Deviation of Velocity Vector, Runs 407/8
  a) Sections $\theta_1 = \pi/6$ To $2\pi/3$ ....
  b) Sections $\theta_1 = 5\pi/6$ To $\theta_2 = \pi/3$ ....
  c) Sections $\theta_2 = \pi/2$ To $5\pi/6$ ....

LIST OF SELECTED SYMBOLS

A_o	area of tracer injector
b	distance from channel axis to vertical over which $\tau = 0.5\ \tau_m$
$\tilde{c}$	instantaneous local concentration
c	local mean concentration
$\bar{c}$	depth-averaged concentration
$\bar{c}_m$	maximum depth-averaged concentration
C_1	normalized depth-averaged concentration $\bar{c}/C_o$
C_o	tracer concentration at fully mixed conditions and no tracer losses
C_s	tracer concentration at source
d_*	average flow depth
D	local depth of flow
E_z	average transverse diffusion coefficient over a channel reach
E_{zw}	average transverse mixing coefficient over a channel reach
f	Darcy-Weisbach's friction factor
g	gravitational acceleration
h_1	metric coefficient $= 1 \pm z/r_c$
H_o	static head
H_1,H_2,H_3	total heads indicated by three tubes of yaw probe
k	normalised transverse exchange (diffusion or mixing) coefficient
K_1,K_2,K_3,K_4,K_5	coefficients for yaw probe

L	length of test reach
m_p	p^{th} central moment of tracer concentration distribution p = 0, 1, 2, ...
M_p	p^{th} moment of the tracer flux about z_o p = 0, 1, 2, ...
$(M_2)a$	actual or calculated second moments of tracer flux distribution
$(M_2)c$	corrected second moments of tracer flux distribution
q	velocity vector
q_*	cumulative discharge
q_{st}	discharge through a stream tube
Q	total discharge
Q_s	volumetric discharge rate of tracer
r_c	centerline radius of curvature
R	hydraulic radius
R_N	Reynolds Number
S	strength of spiral motion
S_f	slope of energy line
S_o	flume bed slope
$\tilde{u}, \tilde{v}, \tilde{w}$	local instantaneous velocity components in the x, y and z directions, respectively
u, v, w	local mean velocities in the x, y and z directions, respectively
$\bar{u}, \bar{v}, \bar{w}$	depth-averaged components of velocity in the x, y and z directions, respectively
u',v',w'	deviations of local velocity components from the corresponding depth-averaged values
u_*	shear velocity

u_{max}	maximum longitudinal velocity
U_o	mean flow velocity
U_1	normalised average velocity U_o/u_*
W_1, W_2	transverse coordinates of channel sides
W_s	maximum width of river at water surface or ice-cover underside
W_{sm}	average maximum width of river for a reach
x	longitudinal distance parallel to channel axis
X_1	dimensionless longitudinal distance $= x/d_*$
y	vertical distance measured downwards from free water-surface or ice-cover underside
$\tilde{y}$	vertical distance measured from channel bed
z	lateral distance normal to channel axis
z_o	lateral distance from channel axis to point of tracer release
β	dimensionless transverse distance
δ	dimensionless mean square velocity deviation
ε_{ij}	diffusion tensor
$\varepsilon_x, \varepsilon_y, \varepsilon_z$	turbulent mass transfer coefficients in the x, y and z directions, respectively
ε_d	lateral dispersion coefficient
$\bar{\varepsilon}_z$	depth-averaged transverse diffusion coefficient
$\bar{\varepsilon}_{zw}$	depth-averaged transverse mixing coefficient
η	lateral distance from point of tracer release
ν	kinematic viscosity
κ	von Karman's constant
ϕ	function defining the variation of $\bar{\varepsilon}_z$

ϕ_w	function defining the variation of $\overline{\varepsilon}_{zw}$
ψ	horizontal angle of deviation of velocity vector
σ_z^2	variance of tracer concentration distribution
σ_{fz}^2	variance of the tracer flux distribution
τ_o	bed shear stress
θ_1, θ_2	radial angle from beginning of first and second bends, respectively

CHAPTER 1

INTRODUCTION

1.1 General

In recent years the ecological balance of many rivers has been seriously upset by unregulated disposal of pollutants. Because rivers perform functions that are essential to man's survival pollution control presents itself as a major technological challenge. Dilution of a pollutant by a river is rarely a satisfactory solution for a major pollution problem, yet most solutions involve dilution processes. Continued study and research on mixing of pollutants in natural rivers are, therefore, important.

Although a good amount of knowledge on mixing in open channel flows has been accumulated in the past two decades, there is still room for enlarging our understanding of the processes involved and particularly for more reliable predictions of the spreading of pollutants.

Transverse (across channel) mixing is important in rivers because it exerts a large influence on the rate of longitudinal dispersion (Fischer, 1967). Knowledge of the transverse exchange (diffusion or mixing) coefficient is also a prerequisite in estimating the crossing distance and the distance required to achieve a given degree of mixing. Considerable practical importance therefore attends the estimation of rates of transverse mixing of pollutants especially in areas where location of water intakes is crucial.

Most rivers in Canada are ice-covered for nearly 5 months of the year and pollution problems in these rivers are almost always most critical during winter due to generally low winter flows and suppression of oxygen uptake from the atmosphere. However, no laboratory or field measurements of the transverse mixing characteristics of ice-covered channels appear to have been reported so far.

1.2 Objectives

It is the principal objective of this investigation to provide information on transverse diffusion and mixing in straight and meandering ice-covered channel flows. The specific objectives are:

(i) to develop working equations for evaluating the transverse diffusion and mixing coefficients in channels of arbitrary shape,

(ii) to obtain experimental data in the laboratory and field for corresponding open and ice-covered channel flows, and

(iii) to analyse the experimental results and evaluate the effect of ice-covers on the diffusion and mixing phenomena.

Experiments were, therefore, designed to fulfil these objectives.

1.3 Structure of Report

This section deals with the form of presentation.

In Chapter 2 previous studies on transverse diffusion and mixing are reviewed and simplifications of the 3-dimensional convective diffusion equation into forms amenable to solution and the limitations of some known solutions are discussed.

Chapter 3 deals with the analytical considerations. Two methods are proposed for evaluating the transverse mixing coefficient in meandering and straight channels of arbitrary cross-section.

Chapter 4 summarises the experimental arrangement and procedures while the experimental results relating to both straight and meandering flumes are presented and discussed in Chapters 5 and 6.

Chapter 7 contains the experimental procedure, results and a discussion of these results for field tests on the Lesser Slave River (Alberta).

Overall summary and conclusions of both laboratory and field investigations form the subject of Chapter 8.

CHAPTER 2

REVIEW OF PAST STUDIES

2.1 The Convective-Diffusion Equation

The study of turbulent mixing involves the analysis of material transport by a turbulent fluid. A comprehensive approach to the problem demands both careful experimentation and considerable theoretical insight. The usual theoretical approach is by way of a mass balance or conservation equation for the quantity being transported. The principle of mass balance for some scalar quantity, c , (herein called a tracer) in an arbitrary and stationary control volume states:

Rate of mass increase within the control volume =
rate of mass inflow into the control volume +
rate of mass production with the control volume

If it is assumed that the tracer undergoes only the process of dilution and that its fluid properties are identical to those of the ambient fluid then the principle of mass balance may be stated mathematically as follows:

$$\frac{\partial}{\partial t}(\rho c) + \frac{\partial}{\partial x_i}(\rho u_i c) = \frac{\partial}{\partial x_i}\left(D_m \frac{\partial(\rho c)}{\partial x_i}\right) \qquad (2.1)$$

where x_i is the co-ordinate in the i^{th} direction; $i = 1, 2, 3$; u_i is the instantaneous fluid velocity in the x_i direction; ρ is the fluid density; D_m is the molecular diffusion coefficient; t is time; and c is the tracer concentration expressed herein as a mass ratio. Equation 2.1 describes the movement of the tracer completely. It is valid for turbulent flows and provided it can be solved would yield the instantaneous values of c.

In general, however, the fluctuations of u_i in turbulent flow are not known and in many cases knowledge of the fluctuations of c is not required. For turbulent flows, it has therefore become customary to use an equation which describes the transport of the tracer in terms of the mean (temporal) values $\tilde{u}_i$ and $\tilde{c}$. If the flow is incompressible, Equation 2.1 reduces to:

$$\frac{\partial c}{\partial t} + \frac{\partial}{\partial x_i}(u_i c) = \frac{\partial}{\partial x_i}\left(D_m \frac{\partial c}{\partial x_i}\right) \tag{2.2}$$

For turbulent flows, we can resolve instantaneous values of u_i and c into mean and fluctuating components such that:

$$\begin{aligned} u_i &= \tilde{u}_i + u_i'' \\ c &= \tilde{c} + c'' \end{aligned} \tag{2.3}$$

where $\tilde{u}_i$ and $\tilde{c}$ are the mean components; u_i'' and c'' are the fluctuating components.

Substituting Equation 2.3 into Equation 2.2, applying the Reynolds averaging procedure and using the continuity principle results in the following equation:

$$\frac{\partial \tilde{c}}{\partial t} + \frac{\partial}{\partial x_i}(\tilde{u}_i \tilde{c}) = \frac{\partial}{\partial x_i}(-\widetilde{u_i''c''}) + \frac{\partial}{\partial x_i}\left(D_m \frac{\partial \tilde{c}}{\partial x_i}\right) \qquad (2.4)$$

The magnitude of the molecular diffusion term is usually much less than the turbulent term on the RHS of Equation 2.4 and can be ignored in the present context. The velocity-concentration covariance terms $\widetilde{u_i''c''}$ represent the transport of tracer by the turbulent fluctuations. Transformation of Equation 2.4 into a form amenable to solution hinges on the interpretation of the $\widetilde{u_i''c''}$ terms.

A turbulent diffusion* coefficient, ε , is generally introduced at this point, just as Boussinesq did for the transport of momentum, such that:

$$\widetilde{u_i''c''} = \varepsilon \frac{\partial \tilde{c}}{\partial x_i} \qquad (2.5a)$$

Because $\widetilde{u_i''c''}$ and $\partial\tilde{c}/\partial x_i$ are vector quantities, the turbulent diffusion coefficient, ε , must either be a scalar or a tensor of the second order (Hinze, 1959). If ε is considered to be a scalar then Equation 2.5a applies. It may be remarked here that it is in general unlikely that the turbulent diffusion coefficient will be constant throughout the entire flow field. If ε is a second order tensor, then Equation 2.5a should read:

---

* The terms diffusion, dispersion and mixing as used in this report have the following meaning. Diffusion connotes transport that is associated primarily with the mean (temporal) product of velocity and concentration as defined in Equation 2.6. Dispersion is transport associated with the product of mean concentration and velocity differences. Mixing denotes transport caused by both diffusion and dispersion.

$$\widetilde{u_i''c''} = \varepsilon_{ij} \frac{\partial \tilde{c}}{\partial x_j} \qquad i,j = 1, 2, 3 \tag{2.5b}$$

According to Fischer (1970), whether one considers the diffusion coefficient to be a scalar or tensor is usually of little import, for neither is an exact representation of the turbulent diffusion process. In what follows, therefore, we shall refer only to the longitudinal, vertical and transverse diffusion coefficients, ε_x, ε_y and ε_z and these coefficients will be regarded as local properties of the turbulence field.

Apart from the work of McQuivey and Keefer (1972) the velocity-concentration covariance terms in Equation 2.4 have not been successcully measured. McQuivey and Keefer measured the longitudinal velocity-concentration covariance term $\widetilde{u''c''}$ in a shear flow and evaluated the longitudinal diffusion coefficient, ε_x , from the relation:

$$\varepsilon_x = - \widetilde{u''c''} \,/\, \frac{\partial \tilde{c}}{\partial x}$$

They obtained ε_x values which were within ± 20% of the corresponding surface values determined from floating particle studies. They found the Boussinesq-type turbulent exchange coefficient to be an adequate model for describing the diffusion process in the longitudinal direction.

Equation 2.4 is now expanded to conventional rectangular cartesian notation with $x_1, x_2, x_3 = x, y, z$ and $u_1, u_2, u_3 = u, v, w$; it is noted that:

$$
\begin{aligned}
-\widetilde{u''c''} &= \varepsilon_x \frac{\partial \tilde{c}}{\partial x} \\
-\widetilde{v''c''} &= \varepsilon_y \frac{\partial \tilde{c}}{\partial y} \qquad (2.6) \\
-\widetilde{w''c''} &= \varepsilon_z \frac{\partial \tilde{c}}{\partial z}
\end{aligned}
$$

Neglecting molecular diffusion and dropping the time-averaging bars we obtain the general convective-diffusion equation for a tracer in a turbulent flow:

$$
\frac{\partial c}{\partial t} + \frac{\partial (uc)}{\partial x} + \frac{\partial (vc)}{\partial y} + \frac{\partial (wc)}{\partial z} = \frac{\partial}{\partial x}\left(\varepsilon_x \frac{\partial c}{\partial x}\right) + \frac{\partial}{\partial y}\left(\varepsilon_y \frac{\partial c}{\partial y}\right) + \frac{\partial}{\partial z}\left(\varepsilon_z \frac{\partial c}{\partial z}\right) \qquad (2.7)
$$

In applications to open channel flows, x, y and z will represent distances in the longitudinal, vertical and transverse directions respectively, with u, v and w as the corresponding velocities.

Equation 2.7 is still too complex for a general solution in a realistic situation. Generally, solution of Equation 2.7 for open channel flows must account for a variety of factors such as velocity gradients in all directions, channel shape, roughness, obstructions, bends and the variation in the turbulent diffusion and mixing coefficients. No existing theory does this adequately. Most investigations have been devoted to one or more of the following:

1. Establishment of some basis for predicting the turbulent

39

mixing coefficients and the concentration distribution downstream from a tracer source,

2. Transformation of Equation 2.7 into forms more amenable to solution either by making appropriate assumptions or by spatial averaging procedures,
3. Finding approximate solutions by finite difference techniques using digital computers.

Considerable progress has been made for the simple idealized case of uniform 2-dimensional flows which are approximated in laboratory flumes. Investigations of this type of flow have been made by Glover (1964), Elder (1959), Sayre and Chang (1968), Okoye (1970).

2.2 Solutions of the Convective-Diffusion Equation for Transverse Diffusion in Straight Channels

To facilitate solution of Equation 2.7 for uniform turbulent flow in a straight and wide rectangular channel, complete analogy with molecular diffusion is assumed. The transfer coefficients ε_x, ε_y and ε_z are assumed constant and the longitudinal velocity u is replaced by U_o, the cross-sectional average velocity. It is assumed that any variations of u within the cross-section and any secondary flow effects can be absorbed into ε_x, ε_y and ε_z. With these assumptions Equation 2.7 reduces to:

$$\frac{\partial c}{\partial t} + U_o \frac{\partial c}{\partial x} = \varepsilon_x \frac{\partial^2 c}{\partial x^2} + \varepsilon_y \frac{\partial^2 c}{\partial y^2} + \varepsilon_z \frac{\partial^2 c}{\partial z^2} \qquad (2.8)$$

Solutions of Equation 2.8 for various initial and boundary conditions have been presented by Carslaw and Jaeger (1959), Glover (1964). For a continuous point source in a straight rectangular channel with a large width-depth ratio, Equation 2.8 can be reduced to 2-dimensions by integrating with respect to depth and noting that there is no tracer transport across the wetted perimeter and across the water surface. Equation 2.8 then becomes:

$$U_o \frac{\partial \bar{c}}{\partial x} = \varepsilon_x \frac{\partial^2 \bar{c}}{\partial x^2} + \varepsilon_z \frac{\partial^2 \bar{c}}{\partial z^2} \tag{2.9}$$

where $\bar{c} = \bar{c}(z,x)$ is the depth-averaged concentration. The solution is (Sayre and Chang, 1968):

$$\bar{c}(z,x) = \frac{Q_s C_s}{2\pi d_* \sqrt{\varepsilon_x \varepsilon_z}} e^{\frac{U_o x}{2\varepsilon_x}} K_o\left[\frac{U_o}{2\varepsilon_x} \sqrt{x^2 + \frac{\varepsilon_x}{\varepsilon_z} z^2}\right] \tag{2.10}$$

in which Q_s = volumetric tracer discharge

C_s = tracer concentration at source

d_* = flow depth

$K_o[\ ]$ = modified Bessel function of the second kind, of order zero

When the distance downstream from the tracer source is large enough such that:

$$\left(\frac{\varepsilon_x}{\varepsilon_z}\right)\frac{z^2}{x^2} << 1 \qquad \text{and} \qquad x >> \frac{2\varepsilon_x}{U_o}$$

Equation 2.10 converges to:

$$\overline{c}(z,x) = \frac{Q_s C_s}{U_o d_*} \frac{e^{-\frac{z^2 U_o}{4\varepsilon_z x}}}{2\sqrt{\pi\varepsilon_z x/U_o}} \qquad (2.11)$$

This represents the solution of Equation 2.9 under conditions of negligible longitudinal diffusion. Equation 2.11 can be applied to a straight channel of finite width provided the tracer is well mixed over the depth and a significant amount of tracer has not reached the side-walls.

A more general solution of Equation 2.9 applicable to channels of both infinite and finite width is given by Sayre and Chang (1968). For the general case where the tracer source is located a lateral distance from the origin (center of channel), they employed the method of superposition and treated the side-walls as reflecting barriers to obtain:

$$\overline{c}(z,x) = \overline{c}(z-\zeta,x) + \sum_{n=1}^{\infty} [\overline{c}(nW - \zeta + (-1)^n z,x) + \overline{c}(- nW - \zeta + (-1)^n z,x)] \qquad (2.12)$$

where $-W/2 \leq z \leq W/2$ and n = number of reflection cycles. The terms on the right hand side of Equation 2.12 are evaluated from Equation 2.11. Equations 2.11 and 2.12 are in fairly good agreement with experimental observations in straight rectangular channels.

Another method for solving Equation 2.7 was recently proposed by Yotsukura and Cobb (1972) for straight prismatic channels of arbitrary cross-section. They neglected longitudinal turbulent diffusion, assumed a steady state, but accounted for transverse variation in depth. They showed that the transverse diffusion equation for this situation is:

$$\bar{u} D \frac{\partial \bar{c}}{\partial x} = \frac{\partial}{\partial z} \left(\bar{\varepsilon}_z D \frac{\partial \bar{c}}{\partial z} \right) \qquad (2.13)$$

where $\bar{u}$, D, $\bar{\varepsilon}_z$ are functions of z only; $\bar{\varepsilon}_z$ and $\bar{u}$ being depth-averaged values. If the origin is located at one bank, the boundary condition at the channel edges ($z = 0, W$) is:

$$\bar{\varepsilon}_z D \frac{\partial \bar{c}}{\partial z} = 0 \qquad (2.14)$$

The conservation of tracer is expressed as:

$$J_s = \gamma \int_0^W \bar{u}\, \bar{c}\, D\, d z \qquad (2.15)$$

where γ is the specific weight of water.

Yotsukura and Cobb then defined a new independent variable q_*, the cumulative discharge, measured from one bank as:

$$q_* = \int_0^z \bar{u}\, D\, d z$$

This can be used as an alternative transverse co-ordinate. By using q_* to replace z they transformed Equations 2.13, 2.14 and 2.15 to:

$$\frac{\partial \bar{c}}{\partial x} = \frac{\partial}{\partial q_*}\left(\bar{\varepsilon}_z \bar{u}D^2 \frac{\partial \bar{c}}{\partial q_*}\right) \tag{2.16}$$

$$\bar{\varepsilon}_z \bar{u}D^2 \frac{\partial \bar{c}}{\partial q_*} = 0 \quad \text{at} \quad q_* = 0 \text{ and } Q$$

and: $$J_s = \gamma \int_0^Q \bar{c}\,dq_*$$

respectively. To obtain a solution to Equation 2.16 they assumed that it can be approximated by:

$$\frac{\partial \bar{c}}{\partial x} = \overline{\bar{\varepsilon}_z \bar{u}D^2}\, \frac{\partial^2 \bar{c}}{\partial q_*^{\,2}} \tag{2.16a}$$

where the Diffusion Factor $\overline{\bar{\varepsilon}_z \bar{u}D^2} = \frac{1}{Q}\int_0^Q \bar{\varepsilon}_z \bar{u}D^2 dq_*$.

They finally applied the method of images used by Sayre and Chang (1968) to obtain a series solution for Equation 2.16a. This theoretical model seems to agree well with field data. The approximation of the variable parameter $\bar{\varepsilon}_z \bar{u}D^2$ by its cross-sectional average $\overline{\bar{\varepsilon}_z \bar{u}D^2}$ however needs more verification.

2.3 Evaluation of the Transverse Diffusion Coefficient for Straight Channels

The turbulence which is responsible for vertical diffusion also causes diffusion across the channel. The vertical diffusion coefficient can be derived by assuming (i) equivalence between mass and momentum transfer (Reynolds analogy) and (ii) that the shear stress $\tau_{xy} = -\rho\widetilde{u''v''}$ is linearly distributed over the flow depth. The following relation is obtained:

$$\varepsilon_y = \frac{-\widetilde{u''v''}}{\frac{du}{dy}} = \frac{\frac{\tau_o}{\rho}(1 - \tilde{y}/D)}{\frac{du}{dy}} \qquad (2.17)$$

where τ_o is the bed shear stress. So far, no analytical relationship has been derived between the vertical and transverse diffusion coefficients. The transverse diffusion coefficient, ε_z , must at present be evaluated empirically from experimentally observed concentration distributions.

The local transverse diffusion coefficient, ε_z , in a two-dimensional open channel flow is known to vary over the flow depth, (Okoye 1970, Fischer 1973). It increases from zero on the channel bed to a maximum near the free water surface. In general, one is interested in the overall spreading of a contaminant in a stream and the use of an average transverse diffusion coefficient over a channel reach, E_z , simplifies the computations considerably.

Two approaches have been used in the past to obtain E_z from the convective-diffusion equation. The first approach is the Method of Moments first introduced by Aris (1956). Basically, the method involves multiplying the governing convective-diffusion equation by z^p and integrating with respect to z from $-\infty$ to ∞. The resulting equation is then expressed in terms of the moments of the experimental or theoretical $\overline{c}$ distribution which are defined as:

$$m_p(x) = \int_{-\infty}^{\infty} z^p \overline{c}(z,x)dz \quad ; \quad p = 0, 1, 2... \qquad (2.18)$$

and then solved for the various moments.

In principle, any desired degree of detail can be achieved by solving for high values of p. In practice, however, the zeroth, first, second and third moments are sufficient for calculating statistical parameters which are useful for describing some aspects of the diffusion process. The method of moments has been used extensively, for example, by Okoye (1970), Sayre and Chang (1968), Holley et al (1972).

For a continuous point source in a 2-dimensional open channel flow, it can be shown by the method of moments that:

$$E_z = \frac{U_o}{2} \frac{d\sigma_z^2}{dx} \qquad (2.19)$$

provided the tracer cloud has not encountered the channel walls and the locus of the centroid of the transverse tracer concentration distribution at various sections downstream of the source is parallel to the channel axis (z=0). In Equation 2.19, $\sigma_z^2 = m_2/m_o$ and is often called the variance of the $\overline{c}$ distribution; m_o and m_2, for this situation, are the zeroth and second central moments respectively.

Equation 2.19 can also be obtained by first finding the variances corresponding to Equation 2.10 and Equation 2.11 which are:

$$\sigma_z^2 = \frac{2E_z}{U_o}\left(x + \frac{2E_x}{U_o}\right) \tag{2.20}$$

and

$$\sigma_z^2 = \frac{2E_z x}{U_o} \tag{2.21}$$

respectively. Differentiation of Equations 2.20 and 2.21 then gives the same result as Equation 2.19. The second method used for finding E_z is designated "the simulatio[illegible]thod" (Yotsukura et al, 1970). It is a trial and error substitution of the appropriate diffusion coefficient into a numerical or analytical solution of the governing equation until the best fit between calculated and observed concentration distributions is achieved.

A summary of previous measurements of the transverse diffusion coefficient in open channel flows is given in Table 2.1. Laboratory experiments with dissolved tracers in straight flumes have yielded values of the normalized diffusion coefficient $E_z/u_* d_*$ (=k) ranging from 0.10 to 0.23, where u_* is the shear velocity, d_* is the overall average depth, and E_z is the average value of transverse diffusion coefficient over a channel reach. Okoye (1970) found the aspect ratio, defined as W/d_*, to be the most significant parameter controlling the transverse spreading of a tracer injected continuously into a straight rectangular open channel flow. The dimensionless

TABLE 2-1 SUMMARY OF PREVIOUS MEASUREMENTS OF THE TRANSVERSE DIFFUSION COEFFICIENT IN OPEN CHANNEL FLOWS

(Partly adopted from Okoye 1970)

Source	Channel Bottom Roughness	Tracer	Injection Depth y/d_*	Test Reach meters	Channel Width W m	Mean Flow Depth d_* cm	Hydraulic Radius R cm	Mean Velocity U_o cm/s	Shear Velocity u_* cm/s	Aspect Ratio W/D	$\frac{E_z}{u_* d_*}$
Elder (1959)	Smooth	Permanganate Soln.	1.0	2.2	0.36	1.2	1.125	21.6	1.59	30	0.16
Sayre and Chang (1968)	Wooden Cleats	Fluorescent Dye	0.25 0.50 0.75	35.0	2.38	14.7 24.5 37.1	13.1+ 20.3+ 28.3+	23.5 34.4 47.8	3.90 4.90 6.04	16.2 9.7 6.4	0.170 0.169 0.165
Sullivan (Okoye 1970)	Smooth	Gentian Violet Dye	over the entire depth	5.5	0.76	7.3 8.95 10.2	6.12 7.25 8.05	22.9 18.5 15.3	1.21 0.99 0.83	10.4 8.5 7.45	0.133 0.110 0.107
Kalinske and Pien (Okoye 1970)	Smooth	HCl and Alcohol Mixture	0.39	1.5	0.69	15.8	10.83	94.5	5.19	4.37	0.08
Holley and Abrahams (1973a)		Fluorescent Dye	0.50	16.5	1.23	9.7	8.4	11.7	6.21	12.7	0.16
Miller and Richardson (1974)	Wooden Blocks	Fluorescent Dye	(13 mm. above wooden blocks)	7.62	0.60	12.47-13.20	8.85-9.22	30.48-81.38	3.01-16.31	4.7	0.0975-0.177
Okoye (1970)	Smooth	Salt Soln.	0.368 0.322 0.051 0.632	7.5m	0.85	1.52-17.34	1.47 12.3	27.1-42.8	1.57-2.26	4.9-56	0.094-0.197
				17m	1.10	1.69-21.97	1.64-15.7	30.0-50.4	1.40-2.65	5-65	0.106-0.235
	Rough			17m	1.10	6.81-17.07	6.06-13.03	35.3-42.8	3.64-5.12	6.45-16.2	0.108-0.143

Note: d_* is cross-sectional average depth.

diffusion coefficient, k , increases with an increase in the aspect ratio.

2.4 Transverse Mixing in Meandering Channels

The characteristics of transverse mixing in turbulent open channel flows with curved boundaries is extremely complex. The Fickian-type Equation 2.9 which successfully predicted the spreading of tracer for straight uniform channels with a known E_z is found to give unsatisfactory results for curved channels. This is attributable to a combination of various factors such as depth, width and velocity variations, growth, decay and reversal of the secondary motion and variable turbulence structure. Recent studies by Fischer (1969), Yotsukura et al (1970) and Chang (1971) have, however, contributed immensely to our understanding of the mixing in meandering channels.

The first study of transverse mixing in bends of turbulent open channel flows was reported by Fischer (1969). He derived an expression for predicting the lateral dispersion coefficient, ε_d , based on the following assumptions: (i) lateral dispersion is analogous to longitudinal dispersion and (ii) that the transverse velocity distribution in the vertical can be described by Rozovskii's transverse velocity distribution for fully developed turbulent flow in an open channel bend. Fischer verified his analytical findings experimentally in a meandering flume having a 330° bend with a radius of curvature of 206 cm and a width of 76.3 cm. His observed values of ε_d agreed with the predicted values within a factor of 2. The large discrepancy arises because the bend was too short for the secondary flow pattern to have reached the fully developed stage. Fischer also attributes the errors to the sensitivity of the result to small changes in the input parameters, which are often not accurately known. The procedure is not a practical method for estimating the transverse dispersion coefficient in natural streams because the condition of fully developed bend flow is never obtained in natural streams. Nevertheless, Fischer demonstrated that the dominant effect of curvature is generally to increase the normalized lateral mixing coefficient compared to that usually observed in a straight channel. His normalized dispersion coefficients ranged from 0.52 to 2.4, and this is about 2 to 10 times larger than the observed values for straight laboratory channels.

A simulation procedure was used by Yotsukura, Fischer and Sayre (1970) to predict the transverse mixing coefficient in a six-mile reach of the Missouri River near Blair, Nebraska. The procedure is a numerical solution of the convective-diffusion equation. The steps involved are briefly explained. The river channel is first divided transversely into 20 stream tubes carrying constant and equal discharge. The mass transfer between stream tubes is assumed to be entirely diffusive and any effects of secondary currents are absorbed in the diffusion term. The governing equations are then expressed in finite difference form and solved by trial and error until the mixing coefficient gives a calculated concentration distribution close to the observed data. For the six-mile reach of the Missouri River near Blair, Yotsukura et al obtained an average value for E_z of 0.6 $u_* d_*$ by the simulation technique compared with 0.7 $u_* d_*$ from the Method of Moments.

Chang (1971) proposed two methods for finding the lateral mixing coefficients, namely, a simulation procedure and an integral method. His analytical derivations are based on the convective diffusion equation expressed in a meandering co-ordinate system (Sayre and Fukuoka, 1973):

$$\frac{\partial c}{\partial t} + \frac{1}{h_1}\frac{\partial (cu)}{\partial x} + \frac{\partial (cv)}{\partial y} + \frac{1}{h_1}\frac{\partial (h_1 cw)}{\partial z} = \frac{1}{h_1^{2}}\frac{\partial}{\partial x}\left(\varepsilon_x \frac{\partial c}{\partial x}\right) + \frac{\partial}{\partial y}\left(\varepsilon_y \frac{\partial c}{\partial y}\right) + \frac{1}{h_1}\frac{\partial}{\partial z}\left(h_1 \varepsilon_z \frac{\partial c}{\partial z}\right) \tag{2.23}$$

and the continuity equation:

$$\frac{\partial u}{\partial x} + h_1 \frac{\partial v}{\partial y} + \frac{\partial (h_1 w)}{\partial z} = 0 \tag{2.24}$$

where the x-axis coincides with the centerline of the channel; y is measured downward from the free water surface orthogonally to the x-axis, and z is measured laterally from the channel axis orthogonal to both x and y. Depending on whether the channel is straight or curved, the surface z = constant can be either a plane parallel to the x-axis or a cylindrical surface concentric with the x-axis. In Equations 2.23 and 2.24:

$$h_1 = 1 + \frac{z}{r_c} \quad \text{for a bend curving to the left}$$

$$h_1 = 1 \quad \text{for a straight reach} \qquad (2.25)$$

$$h_1 = 1 - \frac{z}{r_c} \quad \text{for a bend curving to the right}$$

and r_c is the radius of curvature of the channel axis.

The simulation technique employed by Chang is similar to that used by Yotsukura et al. He integrated the steady state form of Equation 2.23 and Equation 2.24 over the cross-sectional area of the j'th stream tube to obtain:

$$q_{st} \frac{\partial C_j}{\partial x} = \left[h_1 D(\bar{\varepsilon}_z + \varepsilon_d) \frac{\partial \bar{c}}{\partial z}\right]_{z_j-1}^{z_j} \qquad (2.26)$$

in which q_{st} = discharge in a stream tube, z_j denotes the boundary between the (j+1)'th and j'th stream tubes, C_j is average concentration with the j'th stream tube, ε_d is the transverse dispersion coefficient given by:

$$\overline{w'c'} = -\varepsilon_d \frac{\partial \bar{c}}{\partial z} \qquad (2.27)$$

where w' and c' are deviations from the depth-averaged values of $\bar{w}$ and $\bar{c}$.

Chang then solved Equation 2.26 numerically to find the best value of the lateral mixing coefficient, E_{zw} $(= \bar{\varepsilon}_z + \varepsilon_d)$, which gave good agreement between the calculated and observed concentration distributions. The use of Equation 2.27 is subject to debate since negative values of ε_d can be obtained. In such a case the dispersion ceases to be of the gradient type.

The Integral Method rests on the same reasoning as the previous method but provides a direct method for finding the local lateral mixing coefficient from experimental data. Chang integrated Equation 2.23 and Equation 2.24 over an area extending from the left bank to any desired stream tube boundary z_1 and arrived at the relation:

$$E_{zw} = \frac{\frac{\partial}{\partial x} \int_0^{z_1} \int_0^{D} u\, c\, dy\, dz}{h_1 D \left. \frac{\partial \bar{c}}{\partial z} \right|_{z_1}} \qquad (2.28)$$

Chang's results indicated a strong periodic variation of the lateral mixing coefficient in the longitudinal direction with the simulation and the integral methods giving similar patterns in the variation of E_{zw}. However, the integral method predicted values of E_{zw} approximately twice as large as the simulation method. It is noted that the integral method is more susceptible to errors because of the inaccuracies involved in taking derivatives of experimental data. Chang obtained normalized mixing coefficients ranging from 0.6 to 1.2 with the simulation method.

Holley, Siemons and Abrahams (1972) have put forward a method for predicting the lateral mixing coefficient, E_{zw} (the Generalized Change of Moment Method). Moments of the tracer flux ($D \bar{u} \bar{c}$) distribution are used rather than that of the concentration distribution. The method incorporates transverse variations in depth, turbulent exchange coefficients, longitudinal and transverse velocities into the depth-averaged convective diffusion equation. They tried various expressions for the variation of the exchange coefficient across the channel. These were:

$$E_{zw} = kd_*u_* = k_1 d_* U_o \tag{2.29}$$

$$\bar{\varepsilon}_{zw} = k_2 D \bar{u} \tag{2.30}$$

$$\bar{\varepsilon}_{zw} = k_3 \frac{U_o}{\sqrt{d_*}} D^{3/2} \tag{2.31}$$

where d_* is the overall average depth and k_1, k_2, k_3 are dimensionless mixing coefficients and $\bar{\varepsilon}_{zw}$ is the local depth-averaged mixing coefficient. U_o is used in Equation 2.29 simply as a matter of convenience. In Equation 2.30, $\bar{\varepsilon}_{zw}$ is assumed to vary as the product of local depth and local depth-averaged velocity while in Equation 2.31 $\bar{\varepsilon}_{zw}$ is taken to be proportional to the product of local depth and local shear velocity. Equation 2.31 is arrived at by use of Chezy's equation.

Holley et al recognized the limitations of Equations 2.29, 2.30 and 2.31. They found that the type of variation assumed for $\bar{\varepsilon}_{zw}$ can have a significant effect on the value of k_2 or k_3 determined from measured concentration distributions. Nevertheless, the use of local values of depth, velocity and shear velocity appears to be reasonable since they represent the accumulated effects of various upstream factors which also influence the local value of $\overline{\varepsilon}_{zw}$.

This chapter has presented a review of previous studies on transverse diffusion and mixing in straight and curved open channel flows. No laboratory or field measurements of the transverse diffusion or mixing characteristics in ice-covered channels appear to have been reported so far. Investigations on transverse diffusion and mixing in ice-covered channel flows are therefore urgently needed.

25

CHAPTER 3

ANALYTICAL INVESTIGATIONS

3.1 Similarity Analysis for Straight Channels

Consider the case of a continuous release of tracer at a steady rate into a steady uniform turbulent flow in a wide straight rectangular channel with no side-wall effects. If longitudinal diffusion is assumed to be negligible and ε_z constant within test reach then Equation 2.9 reduces to:

$$U_o \frac{\partial \bar{c}}{\partial x} = \varepsilon_z \frac{\partial^2 \bar{c}}{\partial z^2}$$

For practical application ε_z can be replaced by E_z, the average over a reach of length x, such that:

$$U_o \frac{\partial \bar{c}}{\partial x} = E_z \frac{\partial^2 \bar{c}}{\partial z^2} \qquad (3.1)$$

To make Equation 3.1 dimensionless, the following dimensionless variables are introduced into Equation 3.1:

$$U_1 = \frac{U_o}{u_*}\ , \quad C_1 = \frac{\bar{c}}{C_o}\ , \quad X_1 = \frac{x}{d_*}$$

$$k = \frac{E_z}{u_* d_*}\ , \quad \beta = \frac{z}{d_*} = \frac{z}{W}\frac{W}{d_*} = \frac{z}{W}\lambda$$

where λ is the aspect ratio and C_o is tracer concentration when fully diluted. The resulting equation is:

$$U_1 \frac{\partial C_1}{\partial X_1} = k \frac{\partial^2 C_1}{\partial \beta^2} \tag{3.2}$$

It is a well-known fact that as the tracer cloud spreads the depth-averaged concentration along the tracer centerline decreases. Experimental evidence (to be given in Chapter 6) indicates that the normalized concentration profiles, $C_1\ (x,\beta)$, at various sections can be made congruent by appropriate choice of scaling parameters for C_1 and β. Under such conditions the profiles are said to be "similar". The requirement for "similar" C_1 profiles may be stated as the property that any two C_1 profiles located at different X_1 differ only by a scale factor in C_1 and β. This can be stated mathematically as:

$$\frac{C_1 \left\{ (X_1)_1 \ , \ \dfrac{\beta}{g[(X_1)_1]} \right\}}{C_{1m}\ [(X_1)_1]} = \frac{C_1 \left\{ (X_1)_2 \ , \ \dfrac{\beta}{g[(X_1)_2]} \right\}}{C_{1m}\ [(X_1)_2]} \tag{3.3}$$

where $C_{1m}(X_1)$ and $g(X_1)$ are the scaling parameters for C_1 and β respectively and $C_{1m}(X_1)$ is the normalized peak concentration.

An obvious characteristic scaling parameter for the tracer cloud would be its dimensionless width at the section under consideration. However, exact demarcation of the cloud boundary would be difficult. An alternative scaling parameter is the dimensionless transverse distance between the tracer centerline and the vertical along which $C_1(X_1, \beta) = 0.5\ C_{1m}(X_1)$, denoted here by $b_1(X_1)$ $(= \frac{b}{W} \lambda)$.

27

Note that b is one-half the transverse distance between the verticals along which $\overline{C} = 0.5\ \overline{C}_m$ and $\overline{C}_m$ is depth-averaged peak concentration.

If similarity does exist, one could assume the following relation:

$$\frac{C_1}{C_{1m}} = f(\beta/b_1) = f(\alpha) \tag{3.4}$$

where $\alpha = \beta/b_1$. Substitution of Equation 3.4 into Equation 3.2 yields:

$$\frac{\partial}{\partial X_1}[C_{1m}f] = \frac{k}{U_1}\frac{\partial^2}{\partial \beta^2}[C_{1m}f]$$

$$f\,\frac{\partial C_{1m}}{\partial X_1} - C_{1m}f'\,\frac{\alpha}{b_1}\,\frac{db_1}{dX_1} = \frac{k}{U_1}\,\frac{C_{1m}}{b_1^{\,2}}\,f'' \tag{3.5}$$

where $f' = df/d\alpha$ and $f'' = d^2f/d\alpha^2$. Equation 3.5 can be rewritten as:

$$\frac{f}{f''}\left[\frac{\partial C_{1m}}{\partial X_1}\Bigg/\frac{k}{U_1}\frac{C_{1m}}{b_1^{\,2}}\right] - \frac{\alpha f'}{f''}\left[\frac{C_{1m}}{b_1}\frac{db_1}{dX_1}\Bigg/\frac{k}{U_1}\frac{C_{1m}}{b_1^{\,2}}\right] = 1 \tag{3.6}$$

The R.H.S. of Equation 3.5 is independent of X_1, therefore the L.H.S. must also be independent of X_1. This implies that:

$$\left[\frac{\partial C_{1m}}{\partial X_1}\right]\Bigg/\left[\frac{k}{U_1}\ \frac{C_{1m}}{b_1^{\,2}}\right] = \text{constant} \propto X_1^{\,o} \tag{3.7}$$

and:

$$\left[\frac{C_{1m}}{b_1}\ \frac{db_1}{dX_1}\right]\Bigg/\left[\frac{k}{U_1}\ \frac{C_{1m}}{b_1^{\,2}}\right] = \text{constant} \propto X_1^{\,o} \tag{3.8}$$

If it is assumed further that:

$$C_{1m} \propto X_1^{\,p}$$

and:

$$b_1 \propto X_1^{\,q} \qquad (3.9)$$

where p and q are as yet undetermined exponents, Equation 3.6 or Equation 3.7 yields:

$$q = \frac{1}{2} \qquad (3.10)$$

To evaluate the other exponent, p , an additional equation is required. This is obtained from the condition that there is no loss or decay of tracer, that is:

$$Q_s = d_* U_o \int \bar{c} \, d\, z \qquad (3.11)$$

where Q_s , the rate of injection of tracer into the flow, is equal to $U_o A_o C_s$. A_o is the area of the tracer injector and C_s is concentration of tracer at source.

When Equation 3.11 is simplified using the appropriate scaling parameters, the following relation is obtained:

$$b_1 C_{1m} = \frac{A_o (C_s / C_o)}{d_*^{\,2} \int f d\alpha} \qquad (3.12)$$

The R.H.S. of Equation 3.12 is again independent of X_1 , so that the L.H.S. must also be independent of X_1 for the equation to be valid at

29

any section. Introduction of Equation 3.6 into Equation 3.12 results in:

$$X_1^{q} \; X_1^{p} = \text{constant} = X_1^{o}$$

$$\therefore \quad p + q = 0 \qquad (3.13)$$

From Equation 3.9 and Equation 3.13, we obtain:

$$p = -\frac{1}{2} \qquad (3.14)$$

Therefore:

$$C_{1m} \propto X_1^{-1/2} \quad \text{or} \quad C_{1m} = \frac{A_1}{\sqrt{X_1}} \qquad (3.15)$$

$$b_1 \propto X_1^{1/2} \quad \text{or} \quad b_1 = A_2\sqrt{X_1} \qquad (3.16)$$

where A_1 and A_2 are constants for a particular flow situation. The form of the function f may be found by first substituting Equation 3.15 and Equation 3.16 into Equation 3.5. The following equation is obtained:

$$\frac{2k}{U_1 A_2^{\,2}} f'' + \alpha f' + f = 0$$

or:

$$\frac{2k}{U_1 A_2^{\,2}} f'' + \frac{d}{d\alpha}(\alpha f) = 0 \qquad (3.17)$$

Equation 3.17 can be integrated twice with respect to α , recognizing that when $\alpha = 0$, $f(o) = 1$ and $f'(o) = 0$. The solution of Equation

3.17 becomes:

$$f(\alpha) = e^{-\frac{U_1 A_2^2 \alpha^2}{4k}} = \frac{C_1}{C_{1m}} \qquad (3.18)$$

The distribution of C_1/C_{1m} is therefore Gaussian. Equation 3.18 also implies that for a given flow situation in a very wide rectangular channel, away from side-wall effects, the concentration profiles at various downstream sections is described by a single curve.

When $\alpha = 1$, $C_1 = 0.5\ C_{1m}$ and from Equation 3.18 we get:

$$k = \frac{U_1 A_2^2}{4 \ln 2} \qquad (3.19)$$

Combining Equation 3.19 with Equation 3.16 we obtain an expression for E_z:

$$E_z = \frac{b^2 U_o}{4 x \ln 2} \qquad (3.20)$$

Equation 3.19 suggests that the normalized transverse exchange or diffusion coefficient depends only on U_1 ($= U_o/u_*$) or the friction factor if A_2 is a universal constant. The effect of width was effectively removed by confining the analysis to the central portion of the flow away from the side-walls. Although most of the above results are well-known, the derivation is novel and shows that for a given flow situation in a rectangular channel the lateral concentration profiles at various sections can be represented by a single curve. Equation 3.20 also provides a quick method for evaluating the transverse exchange coefficient,

E_z , given the average velocity U_o and the lateral depth-averaged concentration profile at a downstream section.

3.2 The Two-Dimensional Lateral Diffusion Equation

The convective diffusion equation for turbulent flow in a meandering co-ordinate system may be written as:

$$\frac{\partial c}{\partial t} + \frac{1}{h_1}\frac{\partial (uc)}{\partial x} + \frac{\partial (vc)}{\partial y} + \frac{1}{h_1}\frac{\partial}{\partial z}(h_1 wc) = \frac{1}{h_1^{\,2}}\frac{\partial}{\partial x}\left(\varepsilon_x \frac{\partial c}{\partial x}\right) + \frac{\partial}{\partial y}\left(\varepsilon_y \frac{\partial c}{\partial y}\right) + \frac{1}{h_1}\frac{\partial}{\partial z}\left(h_1 \varepsilon_z \frac{\partial c}{\partial z}\right) \tag{2.23}$$

where $h_1 = 1 + z/r_c$ for a bend curving to the left

$= 1 - z/r_c$ for a bend curving to the right

$= 1$ for a straight reach

ε_x, ε_y, ε_z are the turbulent diffusion coefficients in the x (longitudinal), y (vertical) and z (lateral) directions; u, v, w are the time-averaged velocity components in the x, y and z directions respectively; and c is the local time-averaged concentration.

There is no mass transfer across the channel boundaries or the water surface by either convection or diffusion. These boundary conditions can be stated mathematically as:

$$v = 0 \; ; \; \varepsilon_y \frac{\partial c}{\partial y} = 0 \quad \text{at the water surface}$$

$$u = 0 \; ; \; v = 0 \; ; \; w = 0 \; ; \; \varepsilon_x = 0 \; ; \; \varepsilon_y = 0 \; ; \; \varepsilon_z = 0 \quad \text{at the solid boundaries} \tag{3.21}$$

Solution of Equation 2.23 requires a detailed knowledge of the distributions of local velocity and turbulent diffusion coefficients and it is also very cumbersome to work with Equation 2.23. To facilitate the analysis, the equations can be reduced to 2-dimensions by averaging over the local depth, D.

Consider non-uniform flow in a channel of arbitrary cross-section and a continuous, steady release of tracer into the channel at a fixed location. Longitudinal diffusion does not have a significant effect on the steady-state concentration distribution and can be neglected (Sayre and Chang, 1968). If the transverse diffusion coefficient, ε_z , is assumed not to vary appreciably over a considerable portion of the flow depth then the steady-state case of Equation 2.23 can be written as:

$$\frac{1}{h_1}\frac{\partial(uc)}{\partial x} \quad \frac{\partial(vc)}{\partial y} + \frac{1}{h_1}\frac{\partial}{\partial z}(h_1 wc) =$$

$$\frac{\partial}{\partial y}\left(\varepsilon_y \frac{\partial c}{\partial y}\right) + \frac{1}{h_1}\frac{\partial}{\partial z}\left(h_1 \bar{\varepsilon}_z \frac{\partial c}{\partial z}\right) \tag{3.22}$$

where $\bar{\varepsilon}_z$ is depth-averaged transverse diffusion coefficient.

Define:

$$\begin{aligned}
u(x, y, z) &= \bar{u}(x, z) + u'(x, y, z)\\
v(x, y, z) &= \bar{v}(x, z) + v'(x, y, z)\\
w(x, y, z) &= \bar{w}(x, z) + w'(x, y, z)\\
c(x, y, z) &= \bar{c}(x, z) + c'(x, y, z)
\end{aligned} \tag{3.23}$$

where the bar again denotes a depth-averaged quantity (for example, $\bar{u} = \frac{1}{D} \int_{0}^{D} u\,dy$) and the prime designates a local deviation from the depth-averaged value. Equations 3-23 are now substituted into 3.22 and the resulting equation integrated term by term with respect to y from zero to D. The order of integration and differentiation are interchanged, where necessary, using Leibnitz's Rule. The resulting equation is:

$$\frac{\partial}{\partial x}\{D(\bar{u}\,\bar{c} + \overline{u'c'})\} + \frac{\partial}{\partial z}\{Dh_1(\bar{w}\,\bar{c} + \overline{w'c'})\} = \frac{\partial}{\partial z}\{Dh_1\bar{\varepsilon}_z \frac{\partial \bar{c}}{\partial z}\} \qquad (3.24)$$

The first term in Equation 3.24 refers to the longitudinal differential convection or dispersion. Except close to the tracer source the convection dispersion term $\overline{u'c'}$ is usually much smaller than $\bar{u}\,\bar{c}$ and can often be neglected. The second term represents differential convective mass transport in the lateral direction. If $\bar{\varepsilon}_z$, $\bar{u}$, $\bar{w}$, $\overline{u'c'}$ and $\overline{w'c'}$ are known or can be predicted, Equation 3.24 can be solved for the steady-state concentration distribution at any downstream section from the tracer source.

Normally, $\bar{\varepsilon}_z$ is assumed to have a constant value within a channel reach but it seems probable that significant changes in depth or velocity within a channel reach may cause significant changes in $\bar{\varepsilon}_z$. At present there is, however, insufficient information about the turbulence responsible for diffusion to permit mathematical representation of the variation of $\overline{\varepsilon}_z$. For the time being, the variation of $\overline{\varepsilon}_z$ can be expressed as follows:

$$\overline{\varepsilon}_z = E'_z\phi(x, z) \tag{3.25}$$

where E'_z is a constant for a given flow condition and ϕ defines the variation of $\overline{\varepsilon}_z$. It is to be noted that when $\phi = 1$, $E'_z = E_z$, the average transverse diffusion coefficient over a channel reach. As mentioned previously in Section 2.4, some plausible assumptions regarding ϕ have been put forward by Holley et al (1972). However, no matter what assumption is made for ϕ , E'_z has to be evaluated experimentally. Introducing Equation 3.25 into Equation 3.24 gives the 2-dimensional lateral diffusion equation:

$$\frac{\partial}{\partial x}\{D(\overline{u}\,\overline{c} + \overline{u'c'})\} + \frac{\partial}{\partial z}\{Dh_1(\overline{w}\,\overline{c} + \overline{w'c'})\} = E'_z\frac{\partial}{\partial z}\{Dh_1\phi\frac{\partial \overline{c}}{\partial z}\} \tag{3.24a}$$

Since E'_z is the principal transverse diffusion parameter subsequent analysis and discussion of results particularly related to the straight flume experiments will concentrate on it.

3.3 Methods for Evaluating the Transverse Exchange Coefficient

Three general methods are presently used to evaluate the transverse exchange (diffusion or mixing) coefficient, E_z , in channel flows. These are (i) The Simulation Method (ii) The Method of

Moments and (iii) The Integral Method. These methods were briefly reviewed in Chapter 2. Essentially the same amount of tracer concentration and hydraulic data is required by all the three methods for evaluation of E_z, but the Integral and Moments methods have the advantage of computational simplicity. On the other hand, the procedure of simulating the mixing process is superior to the Integral and Moments techniques because it can be used to predict the tracer concentration distribution downstream of a tracer source if the transverse exchange coefficient, E_z, is known.

Two methods for evaluating E_z based on the Integral and Moments methods are proposed here. The method of moments is used in the present analysis to determine an overall transverse exchange coefficient within a channel reach. The Integral approach attempts to determine the distribution of the average transverse exchange coefficient across and along the channel.

3.3.1 Method of Moments

The method of moments was first described by Aris (1956) and has since been used widely in numerical work. It suffers from the disadvantage that no direct expression for either the $\bar{c}$ or $D \bar{u} \bar{c}$ distribution is obtainable. However, knowledge of the first few moments of the $\bar{c}$ or $D \bar{u} \bar{c}$ distribution gives a great deal of information about the distribution itself. Although in principle higher order moments of a distribution about any value can be computed, a meaning cannot necessarily be attached to the resulting values. In practice, only the first four moments are used because accuracy in estimating higher order moments from experimental data decreases rapidly as the order of the moments increases.

In applying the moments technique here, Equation 3.24a is multiplied through by η^2 and then integrated with respect to η to give:

$$\int_{W_1}^{W_2} \left[\frac{\partial}{\partial x}\{D(\bar{u}\,\bar{c} + \overline{u'c'})\}\right] \eta^2 d\eta \; +$$

$$\int_{W_1}^{W_2} \frac{\partial}{\partial \eta}\{D(1 \pm \frac{\eta + z_o}{r_c})(\bar{w}\,\bar{c} + \overline{w'c'})\} \eta^2 d\eta \; =$$

$$E_z' \int_{W_1}^{W_2} \frac{\partial}{\partial \eta}\{D(1 \pm \frac{\eta + z_o}{r_c})\, \phi\, \frac{\partial \bar{c}}{\partial \eta}\} \eta^2 d\eta \qquad (3.26)$$

in which $\eta = z - z_o$; $h_1 = 1 \pm \frac{z}{r_c} = 1 \pm \frac{\eta + z_o}{r_c}$. z_o represents the transverse distance from the channel axis to a fixed but arbitrary cylindral surface which is concentric with the channel axis. For the present analysis z_o is taken as the lateral distance from the channel axis to the cylindral surface passing through the point of tracer release and concentric with the channel axis. Note that in Equation 3.26, W_1 and W_2 represent transverse distances to the channel edges from z_o.

The second and third terms in Equation 3.26 can be integrated by parts. Some of the resulting terms go to zero because there is no transfer of mass at the flow boundaries. Again, Liebnitz's rule for interchanging the order of integration and differentiation is used. With some further rearrangement of the z-diffusion term and after dividing through by the tracer flux which is constant, we obtain:

$$\frac{d}{dx}\left[\frac{\int_{W_1}^{W_2} D(\bar{u}\,\bar{c} + \overline{u'c'})\,\eta^2 d\eta}{\int_{W_1}^{W_2} D\,\bar{u}\,\bar{c}\,d\eta}\right] - \frac{2\int_{W_1}^{W_2} D\eta\left(1 \pm \frac{\eta + z_o}{r_c}\right)(\bar{w}\,\bar{c} + \overline{w'c'})\,d\eta}{\int_{W_1}^{W_2} D\,\bar{u}\,\bar{c}\,d\eta}$$

$$= 2E'_z\left[\frac{\overbrace{\int_{W_1}^{W_2} \phi D\,\bar{c}\left(1 \pm \frac{2\eta + z_o}{r_c}\right) d\eta}^{\textcircled{A}} + \overbrace{\int_{W_1}^{W_2} \phi\bar{c}\eta\left(1 \pm \frac{\eta + z_o}{r_c}\right)\frac{\partial D}{\partial \eta}\,d\eta}^{\textcircled{B}}}{\int_{W_1}^{W_2} D\,\bar{u}\,\bar{c}\,d\eta}\right]$$

$$- 2E'_z\left[\frac{\overbrace{\int_{W_1}^{W_2} \phi\frac{\partial}{\partial \eta}\left\{D\bar{c}\eta\left(1 \pm \frac{\eta + z_o}{r_c}\right)\right\} d\eta}^{\textcircled{C}}}{\int_{W_1}^{W_2} D\,\bar{u}\,\bar{c}\,d\eta}\right] \qquad (3.27)$$

The diffusion term is found to be a combination of three terms. Term A is expected to remain reasonably constant along the channel. Term B expresses the importance of depth variations within a cross-section and goes to zero when D has a constant value across the section. Term C contributes to the diffusion term only when a significant amount of tracer reaches the side-walls. The magnitude and longitudinal variation of the different terms in Equation 3.27 will be discussed in Chapter 6.

Equation 3.27 is proposed and used in this report for evaluation of E_z' from known distributions of $\bar{w}$, $\bar{u}$, $\bar{c}$, $\overline{u'c'}$, $\overline{w'c'}$, D and ϕ. The above analysis differs from that of Holley et al (1972) only in the use of the meandering co-ordinate system but illustrates more clearly the effects of curvature and depth variations on the mixing.

One limitation in using simplified forms of Equation 3.27 is worth mentioning. In principle, the same value for E_z' will be obtained irrespective of where η is measured from provided the variations of $\bar{u}$, $\bar{w}$, $\bar{c}$, $\overline{u'c'}$, $\overline{w'c'}$, D and ϕ within the reach under consideration are correctly accounted for. If ϕ does vary within a channel reach, as is generally the case, but is assumed constant ($\phi = 1$), then Equation 3.27 will give different values of E_z' depending on where η is measured from. In such a case E_z' ($= E_z$) can be regarded only as a first estimate. Discussion of this problem is deferred until Chapter 7. Equation 3.27 can now be applied to several flow situations.

Case 1 - Meandering Channels

If the distribution of w is unknown, which is generally the case, the effects of transverse velocities on the mixing must be absorbed into a modified exchange coefficient, $\bar{\varepsilon}_{zw}$. From Equation 3.24 we have:

$$\frac{\partial}{\partial x}\{D(\bar{u}\,\bar{c} + \overline{u'c'})\} = \frac{\partial}{\partial z}\{Dh_1(\bar{\varepsilon}_z \frac{\partial \bar{c}}{\partial z} - \bar{w}\,\bar{c} - \overline{w'c'})\}$$

$\bar{\varepsilon}_{zw}$ is defined as $\bar{\varepsilon}_{zw}\frac{\partial \bar{c}}{\partial z} = \bar{\varepsilon}_z \frac{\partial \bar{c}}{\partial z} - \bar{w}\,\bar{c} - \overline{w'c'}$. In analogy with the earlier definition of E'_z , $\bar{\varepsilon}_{zw}$ can be written as:

$$\bar{\varepsilon}_{zw} = E'_{zw}\, \phi_w(x, z) \tag{3.28}$$

where E'_{zw} is constant within a channel reach for a particular flow condition and ϕ_w describes the variation of $\bar{\varepsilon}_{zw}$. Equation 3.27 can now be simplified to give:

$$\frac{d}{dx}\;\frac{\int_{W_1}^{W_2} D(\bar{u}\,\bar{c} + \overline{u'c'})\;\eta^2 d\eta}{\int_{W_1}^{W_2} D\,\bar{u}\,\bar{c}\;d} =$$

$$2E'_{zw}\left[\frac{\int_{W_1}^{W_2} \phi_w D\bar{c}(1 \pm \frac{2\eta + z_o}{r_c})d\eta + \int_{W_1}^{W_2} \phi_w \bar{c}\eta(1 \pm \frac{\eta + z_o}{r_c})\,\frac{\partial D}{\partial \eta}\,d\eta}{\int_{W_1}^{W_2} D\,\bar{u}\,\bar{c}\;d\,\eta}\right]$$

$$- 2E'_{zw} \left[\frac{\int_{W_1}^{W_2} \phi_w \frac{\partial}{\partial \eta} \{D\bar{c}\eta \; (1 \pm \frac{\eta + z_o}{r_c})\} \, d\eta}{\int_{W_1}^{W_2} D \, \bar{u} \, \bar{c} \; d \, \eta} \right] \qquad (3.29)$$

Equation 3.29 is well suited for application to both laboratory and field data. It is to be noted that since D = 0 when $\eta = W_1$ and W_2 for most rivers, the last term in the numerator of the RHS of Equation 3.29 goes to zero. Equation 3.29 then assumes the form:

$$\frac{d}{dx} \left[\frac{\int_{W_1}^{W_2} D(\bar{u} \; \bar{c} + \overline{u'c'})\eta^2 d\eta}{\int_{W_1}^{W_2} D \, \bar{u} \, \bar{c} \; d \, \eta} \right] =$$

$$2E'_{zw} \frac{\left[\int_{W_1}^{W_2} \phi_w D\bar{c}(1 \pm \frac{2\eta + z_o}{r_c}) d\eta + \int_{W_1}^{W_2} \phi_w \bar{c}\eta (1 \pm \frac{\eta + z_o}{r_c}) \frac{\partial D}{\partial \eta} \, d\eta \right]}{\int_{W_1}^{W_2} D \, \bar{u} \, \bar{c} \; d \, \eta} \qquad (3.30)$$

Equation 3.30 provides a direct means of evaluating the transverse exchange coefficient, E'_{zw} , if the lateral distributions of $\bar{u}$, $\bar{c}$, $\overline{u'c'}$

41

and D within a number of cross-sections are known and a reasonable assumption can be made for ϕ_w. Subsequent discussions of results related to the meandering flume and field investigations will concentrate on E'_{zw}.

In a practical situation, the meandering co-ordinates may be fitted to a natural river using a large scale map of the river. The thalweg is taken as the longitudinal, x , axis. If the thalweg is not accurately known, the centerline of the river at the water surface or ice-cover underside may also be taken as the longitudinal axis. The river reach of interest is divided by trial and error into sub-reaches which are either single bends that can be approximated with circular arcs or straight reaches. The centerline radius of the bends are then geometrically determined.

Transverse distances are measured normal from the x-axis in the horizontal plane. these distances are considered negative when measured towards the center of curvature and vice versa. Vertical distances are measured downwards from the free water surface or ice-cover underside (see Figure 3.1).

Case 2 - Straight Channels

For straight channels with arbitrary cross-section $r_c = \infty$ but w is not necessarily zero. Transverse velocities caused by changes in channel geometry with longitudinal distance may significantly alter the mixing. If transverse velocities can be accurately determined

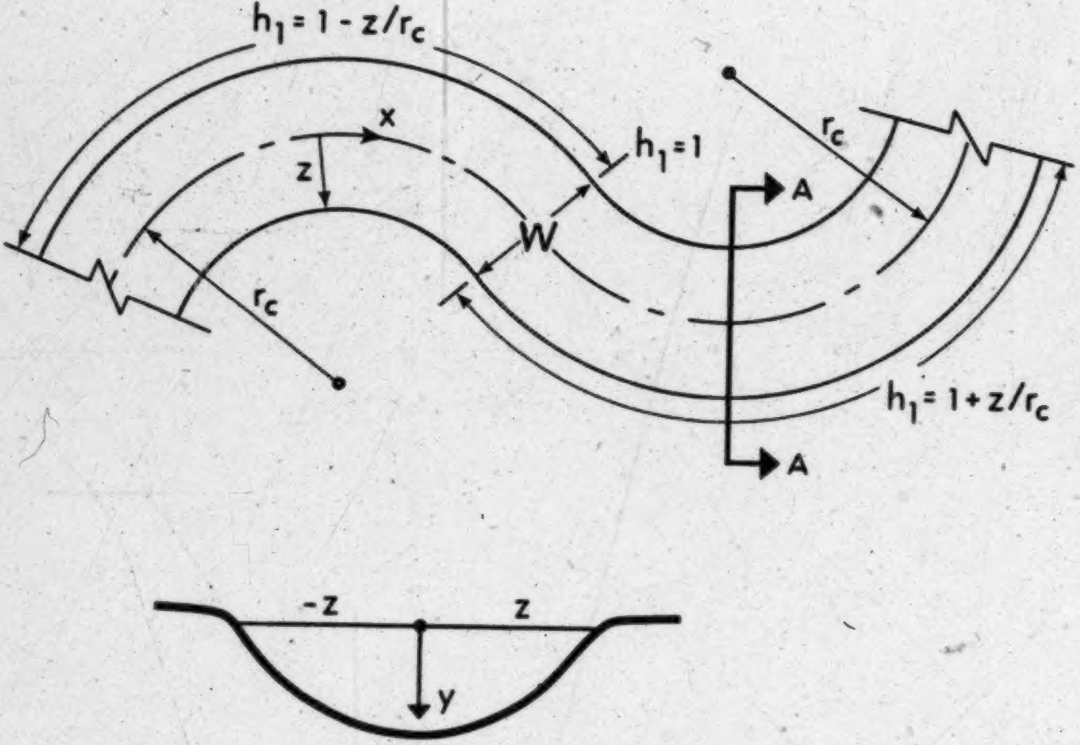
$h_1 = 1 - z/r_c$
x
z
$h_1 = 1$
W
r_c
r_c
A
A
$h_1 = 1 + z/r_c$
-z
z
y

SECTION A-A

FIGURE 3.1 DEFINITION SKETCH FOR MEANDERING CHANNEL

then the relevant equation to use is Equation 3.27 with $r_c = \infty$. Otherwise the effects of transverse velocities must again be included in the diffusion coefficient as was done in Case 1. The appropriate equation in this case is either Equation 3.29 or Equation 3.30 with $r_c = \infty$.

For the simplest case of uniform turbulent flow in a prismatic rectangular channel $\partial D/\partial\eta = 0$. If $\overline{u'c'}$ is negligible, Equation 3.27 reduces to:

$$\frac{d}{dx}\left[\frac{\int_{W_1}^{W_2} \bar{u}\,\bar{c}\,\eta^2 d\eta}{\int_{W_1}^{W_2} \bar{u}\,\bar{c}\,d\,\eta}\right] = \frac{2E'_z \int_{W_1}^{W_2} \phi[\bar{c} - \frac{\partial}{\partial\eta}(\bar{c}\eta)]d\eta}{\int_{W_1}^{W_2} \bar{u}\,\bar{c}\,d\,\eta} \qquad (3.31)$$

Away from the side-wall boundary layers $\bar{u}$ is a constant $(= U_o)$ and ϕ can be taken as equal to 1.0. If $E'_z\phi$ is replaced by E_z and provided no tracer has reached the channel walls, Equation 3.31 can be written as:

$$E_z = \frac{U_o}{2}\cdot\frac{d}{dx}\left[\int_{W_1}^{W_2} \bar{c}\eta^2 d\eta \Bigg/ \int_{W_1}^{W_2} \bar{c}d\eta\right] \qquad (3.32)$$

or: $$E_z = \frac{U_o}{2}\cdot\frac{d\sigma_z^2}{dx} \qquad (2.19)$$

Equation 3.32 is the well-known formula for finding the diffusion coefficient for uniform turbulent flow in straight rectangular channels (Sayre and Chang, 1968, Okoye, 1970). Going through the various flow situations has been instructive in demonstrating the general applicability of Equation 3.27.

3.3.2 Integral Method

Integration of Equation 3.24a with respect to z, from one bank (denoted by W_1) to an arbitrary z, gives:

$$\int_{W_1}^{z} \frac{\partial}{\partial x}\{D(\bar{u}\;\bar{c} + \overline{u'c'})\}\,dz + \int_{W_1}^{z} \frac{\partial}{\partial z}\{Dh_1(\bar{w}\;\bar{c} + \overline{w'c'})\}\,dz =$$

$$E'_z \int_{W_1}^{z} \frac{\partial}{\partial z}\{Dh_1\phi\,\frac{\partial \bar{c}}{\partial z}\}\,dz$$

which can be simplified to:

$$\frac{d}{dx}\int_{W_1}^{z} D(\bar{u}\;\bar{c} + \overline{u'c'})dz + Dh_1(\bar{w}\;\bar{c} + \overline{w'c'}) = E'_z\,Dh_1\phi\,\frac{\partial \bar{c}}{\partial z} \qquad (3.33)$$

$$= \bar{\varepsilon}_z\,Dh_1\,\frac{\partial \bar{c}}{\partial z} \qquad (3.33a)$$

Equation 3.33a can be used to determine the lateral variation of $\bar{\varepsilon}_z$ across a channel reach. Chang (1971) used a similar procedure but divided the channel into stream tubes carrying equal discharge. His

z_1-values represented the boundary between the stream tubes and he combined the dispersion term $\overline{w'c'}$ with $\bar{\varepsilon}_z\, \partial\bar{c}/\partial z$ by assuming $\overline{w'c'} = \varepsilon_d\, \partial\bar{c}/\partial z$ where ε_d is a dispersion coefficient. The only drawback in using Equation 3.33a is that it is susceptible to errors because of the inaccuracies involved in taking derivatives of experimental tracer concentration data. To circumvent this difficulty, Equation 3.33a can be integrated once more with respect to z from W_1 to z, to give:

$$\int_{W_1}^{z} \left\{\frac{d}{dx} \int_{W_1}^{z} D(\bar{u}\,\bar{c} + \overline{u'c'})dz\right\} dz + \int_{W_1}^{z} Dh_1(\bar{w}\,\bar{c} + \overline{w'c'})dz$$

$$= E'_z \int_{W_1}^{z} Dh_1\phi\, \frac{\partial\bar{c}}{\partial z}\, dz \qquad (3.34)$$

Without too much loss in detail an average ϕ can be assumed between W_1 and z such that $E_z = E'_z\phi_{avg}$ and the above equation can be written as:

$$\int_{W_1}^{z} \left\{\frac{d}{dx} \int_{W_1}^{z} D(\bar{u}\,\bar{c} + \overline{u'c'})dz\right\} dz + \int_{W_1}^{z} Dh_1(\bar{w}\,\bar{c} + \overline{w'c'})dz\ .$$

$$= E_z \left\{ \Big[Dh_1\bar{c}\Big]_{W_1}^{z} - \int_{W_1}^{z} \bar{c}\, \frac{\partial(Dh_1)}{\partial z}\, dz \right\} \qquad (3.35)$$

Equation 3.35 will give some indication of the variation of the average exchange coefficient over transverse portions of a channel reach by performing the above integrations for different z-values across the channel. If the effects of transverse velocities are not separated but are lumped with the diffusion term in the usual way, then Equation 3.35 can be modified to give:

$$\int_{W_1}^{z} \left\{ \frac{d}{dx} \int_{W_1}^{z} D(\bar{u}\,\bar{c} + \overline{u'c'})dz \right\} dz$$

$$= E_{zw} \left\{ \left[Dh_1\bar{c} \right]_{W_1}^{z} - \int_{W_1}^{z} \bar{c} \frac{\partial (Dh_1)}{\partial z} dz \right\} \qquad - (3.36)$$

Equation 3.36 is a new expression which is proposed for evaluating E_{zw} provided variations of $\bar{u}$, $\bar{c}$, $\overline{u'c'}$ and D within a channel reach are known or can be estimated.

CHAPTER 4

LABORATORY EQUIPMENT AND METHODS

4.1 Introduction and Experimental Objectives

This chapter describes the laboratory equipment and experimental procedures. The laboratory experiments were performed in both a straight and a meandering flume at the University of Alberta Civil Engineering Graduate Hydraulics Laboratory. The experiments had two primary objectives:

1. To evaluate the effect of an ice-cover on the diffusion and mixing phenomena, and
2. To provide information on the transverse diffusion and mixing characteristics in straight and meandering ice-covered channel flows.

4.2 Experimental Equipment

4.2.1 Straight Flume

A general view of the straight flume is shown in the photograph of Figure 4.1. The flume was rectangular in cross-section, approximately 60 ft. long, 4.0 ft. wide, 2.0 ft. deep and had an adjustable slope. The side walls were of plexiglass and the floor was plywood covered with a smooth layer of fiber-glass resin.

Water was pumped from a storage sump into the flume head tank through a 12 inch overhead pipe fitted with valves and a recording

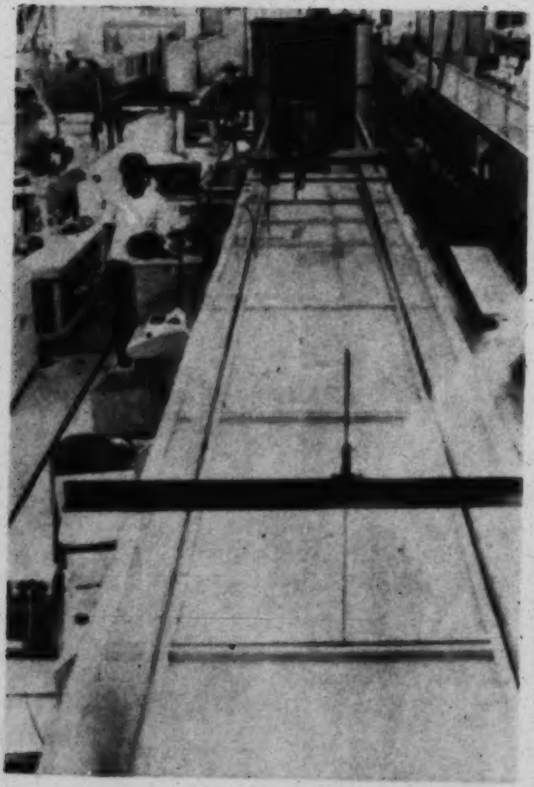

FIGURE 4.1 GENERAL VIEW OF STRAIGHT FLUME SHOWING FLOATING ICE-COVER.

8 inch Foxboro magnetic flowmeter. Downstream of the flume the water flowed into a small channel and back into the sump. A 6 ft. long floating horizontal board was installed at the upstream end of the flume to smooth the flow. Depths of flow were measured manually along the centerline of the flume with point gauges.

4.2.2 Meandering Flume

The meandering flume was 62.5 ft. long, 2.5 ft. wide and 1.0 ft. deep. Figure 4.2 is a schematic diagram of the flume. This flume had two identical but reversed 180° circular bends with a centerline radius of 9 ft. Because of insufficient laboratory space it was not possible to join the two bends with a straight section as naturally occurs in most rivers. The flume width of 2.5 ft. enabled width to depth ratios of up to 20 to be obtained. In this respect, the experiments in this flume were performed under conditions which approximated those of a natural stream.

A 5 ft. long straight reach connected the first bend to the head tank. The flume bed was made with 3/4 inch plywood and the sidewalls with 1/8 inch thick aluminium sheets. Joints were sealed with a silicon sealant and the entire flume painted.

This flume rested on ten wooden supports, each fitted with a pair of 3/4 inch bolts for slope adjustment. It shared the same pumping, flowmetering and water storage facilities with the straight flume. At the inlet, water was discharged vertically downwards into the inlet

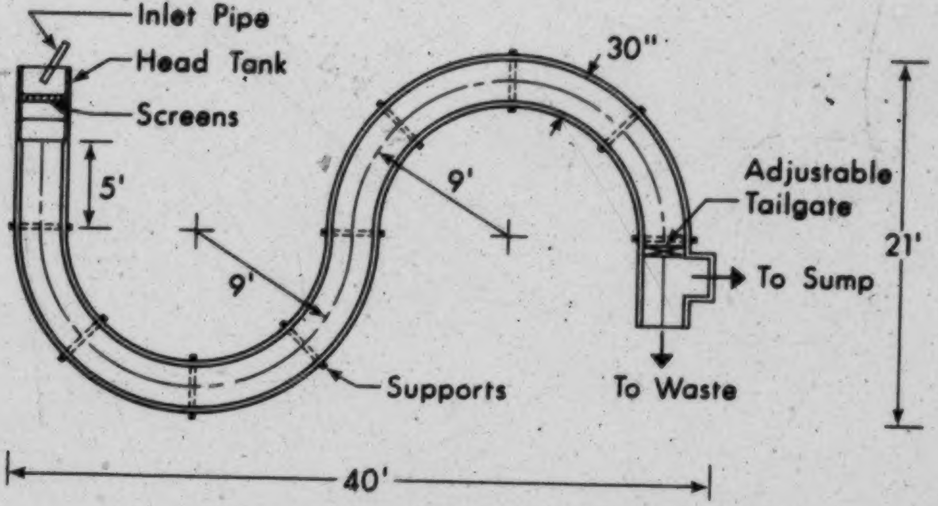
Inlet Pipe
Head Tank
Screens
5'
9'
9'
30"
Adjustable Tailgate
To Sump
21'
Supports
To Waste
40'

FIGURE 4.2a PLAN VIEW OF MEANDERING FLUME

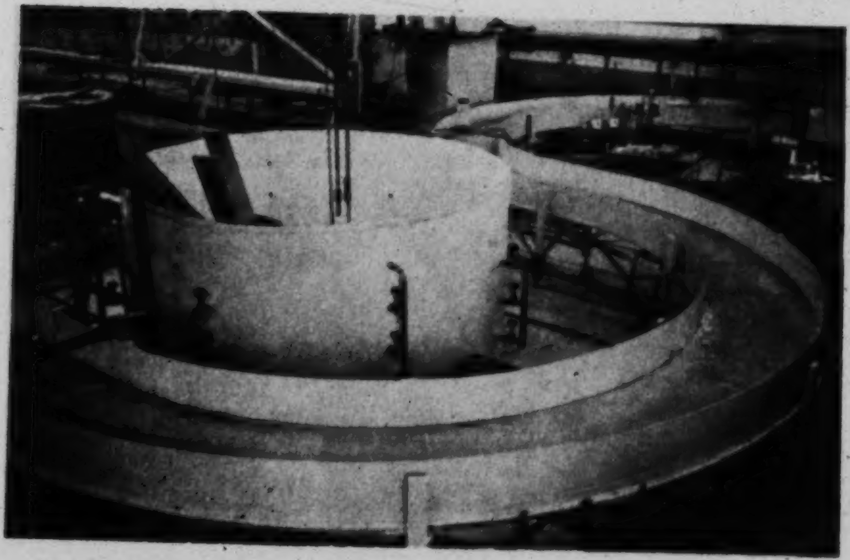

FIGURE 4.2b PHOTOGRAPH OF MEANDERING FLUME.

tank through an 8 inch pipe. A set of vertical screens was installed in the inlet tank to smooth the flow into the flume.

In all experiments, flume water was recirculated during velocity measurements but run to waste during tracer concentration measurements. The sump water was replenished continuously from the city mains during the concentration measurements. Because discharge from the city mains was limited it was not possible to perform tests with large flow depths.

4.2.3 Bed Roughness and Ice-Cover

In general, the bottom resistance to flow in an ice-covered stream is different from that of the ice-cover. To simulate this condition in the laboratory, expanded sheet metal, 1/16 inch thick was used as bottom roughness in both the straight and meandering flumes (see Figure 4.3) for some experiments. The ice cover was simulated with painted 1/2 inch plywood boards stiffened along the edges with 2" x 2" wooden strips to reduce warping (see Figures 4.1 and 4.4).

At the connection between these plywood boards a horizontal spacing of approximately 1.0 inch was left to facilitate velocity and concentration measurements. The weight of the "ice-cover" was 2.0 lbs. per ft^2. It floated free on the water in both flumes. The "ice-cover" inevitably warped in spite of the wooden strips used to stiffen it. Experiments were therefore performed with flow depths greater than 0.10 ft. to minimise the effects of the warping of the "ice-cover" on the flow.

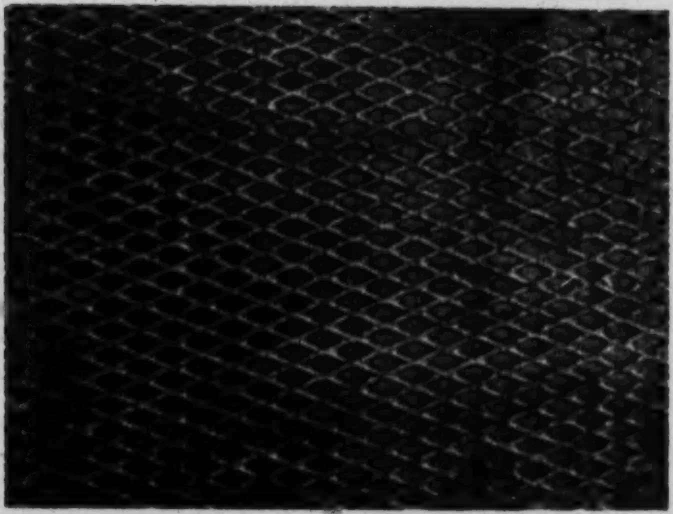

FIGURE 4.3 FLUME BED ROUGHNESS-EXPANDED SHEET METAL 1/16in. thick.

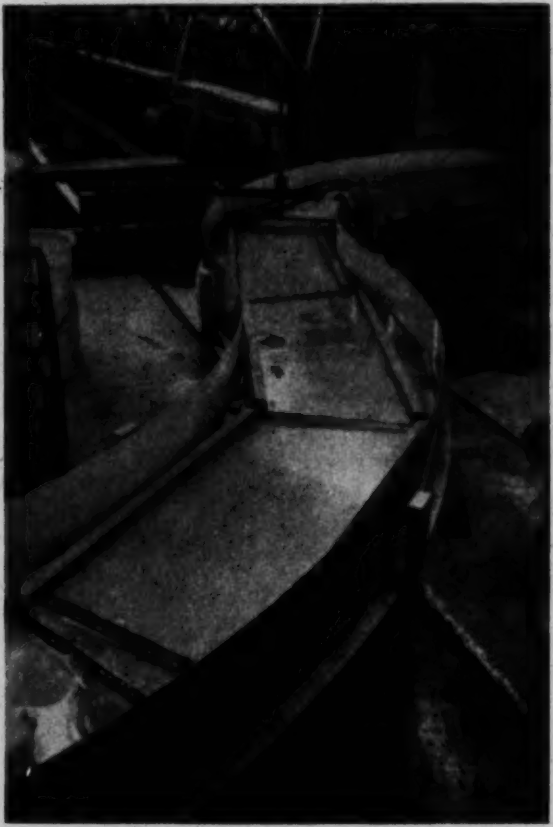

FIGURE 4.4 PARTIAL VIEW OF MEANDERING FLUME SHOWING ICE-COVER (1/2 in. plywood boards) IN POSITION.

4.2.4 Velocity Measuring System

4.2.4.1 Straight Flume: Velocities were measured with a 1/8 inch diameter pitot-static tube. The difference between dynamic and static pressures was measured with a variable reluctance differential pressure transducer with a 0.5 psid full-scale diaphragm (Pace model P1D).

This pressure transducer was connected to a multi-channel carrier demodulator so that its output could be scanned using a Data Acquisition System. The transducer was calibrated by applying static differential heads of zero to 1 inch of water to the pitot-static tube and adjusting the demodulator for a linear output of zero to 10 volts. This calibration was checked before and after each experiment. The differential pressures obtained from the transducer were converted to velocities, without a turbulence correction, and then averaged.

Because of the relatively slow sample interval of the paper punch system, each channel of the demodulator was provided with variable damping circuits to reduce the frequency response of the transducer output to a level suitable for input to the data acquisition system.

4.2.4.2 Meandering Flume: Water velocities in the meandering flume were determined by a three-tube yaw probe capable of giving the magnitude and the direction of the velocity vector component in a horizontal plane. The principle of the probe is described later. The probe was similar to that used by Rajaratnam and Muralidhar (1967). It

54

was made of 3 mm O.D./1.8 mm I.D. stainless steel tubing. At the nose of the probe the side tubes were chamfered at 45° as shown in Figure 4.5.

Differences in dynamic pressure between the two outer tubes and the central tube were measured with two (Pace model P90D) differential pressure transducers equipped with a 0.03 psid full-scale diaphragms. The calibration procedure for these transducers was identical to that for the straight flume experiments.

4.2.5 The Yaw Probe

Let q be the velocity vector at a point in a two-dimensional turbulent open-channel flow and ψ be the angle of deviation from a fixed reference direction. If the yaw probe is positioned in the reference direction, the total heads that will be indicated by the three tubes can be expressed as:

$$\begin{aligned} H_1 &= H_o + K_1 \frac{q^2}{2g} \\ H_2 &= H_o + K_2 \frac{q^2}{2g} \qquad (4.1) \\ H_3 &= H_o + K_3 \frac{q^2}{2g} \end{aligned}$$

where the number 2 stands for the centre tube, 3 the tube on the side of the velocity vector and 1 the remaining tube; H_o is the static head; K_1, K_2 and K_3 are calibration coefficients and functions of

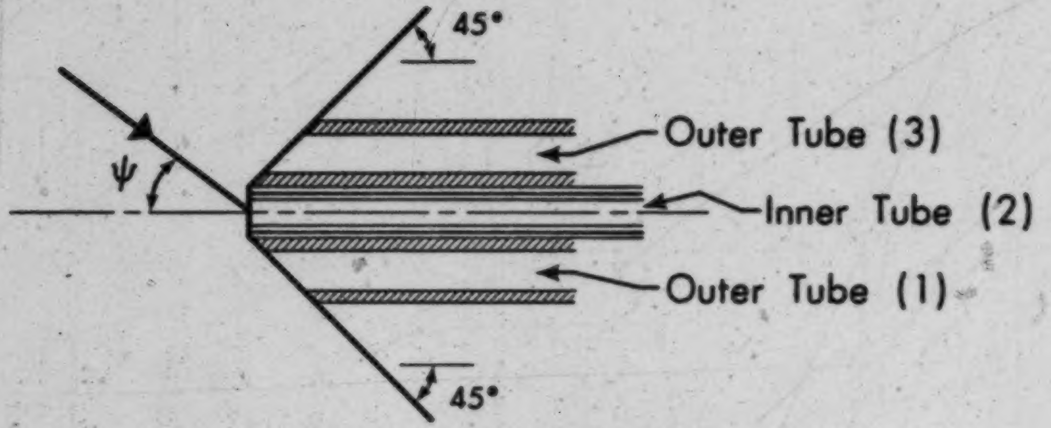
45°
Outer Tube (3)
ψ
Inner Tube (2)
Outer Tube (1)
45°

FIGURE 4.5 NOSE FORM OF YAW PROBE (NOT TO SCALE)

only ψ for a given probe if viscous effects, velocities normal to the plane of the probe and other minor correction factors are regarded as negligible.

The yaw probe was calibrated in the potential core of the plane wall jet with zero pressure gradient, produced by a deeply submerged sluice gate in a rectangular channel. The velocity in the potential core of the jet was determined by a pitot-static tube and the angle of yaw was varied from -50 to +50 degrees during the calibration. The calibration was performed for a velocity of 3.2 ft/s only. Care was taken to ensure that the plane of the tubes was horizontal.

From Equation 4.1 a fourth coefficient K_4 can be defined as:

$$K_4 = \frac{H_2 - H_3}{H_2 - H_1} = \frac{K_2 - K_3}{K_2 - K_1} \qquad (4.2)$$

K_4 is again dependent only on ψ. The calibration curve given by Rajaratnam and Muralidhar (1967), obtained for velocities ranging from 1.47 to 10.39 ft/s, was found to describe the data very well and was, therefore, adopted. This curve is shown in Figure 4.6. The negative half of the calibration curve is given by symmetry.

It is noted that the yaw probe was calibrated in a uniform velocity field away from boundary or wall effects, whereas the conditions during measurements were quite different. Near the flow bounda-

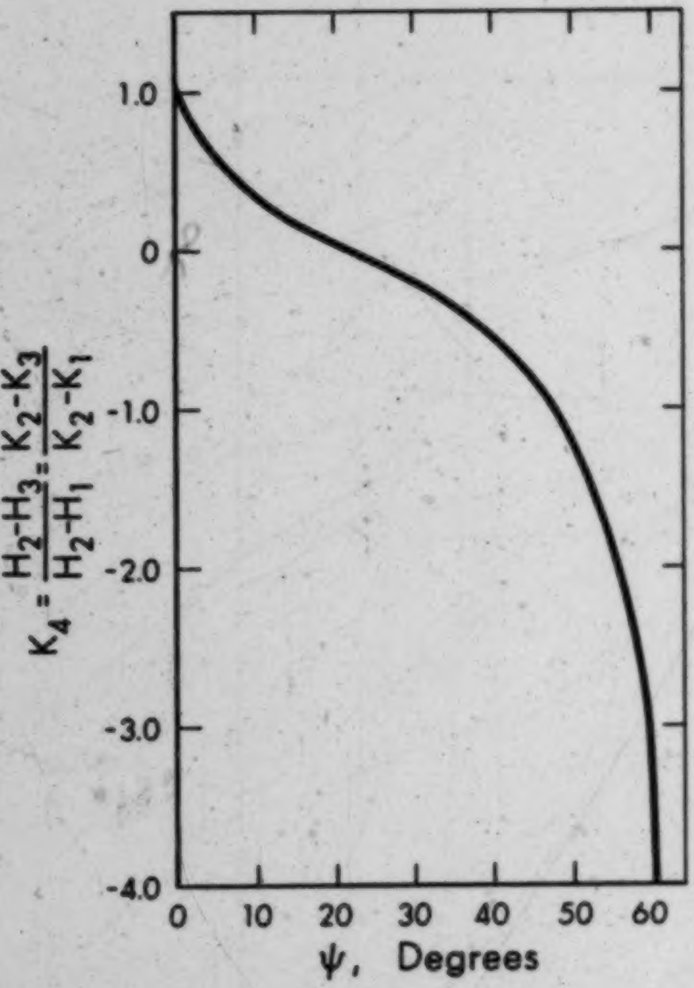

FIGURE 4.6 CALIBRATION COEFFICIENT K_4 FOR YAW PROBE

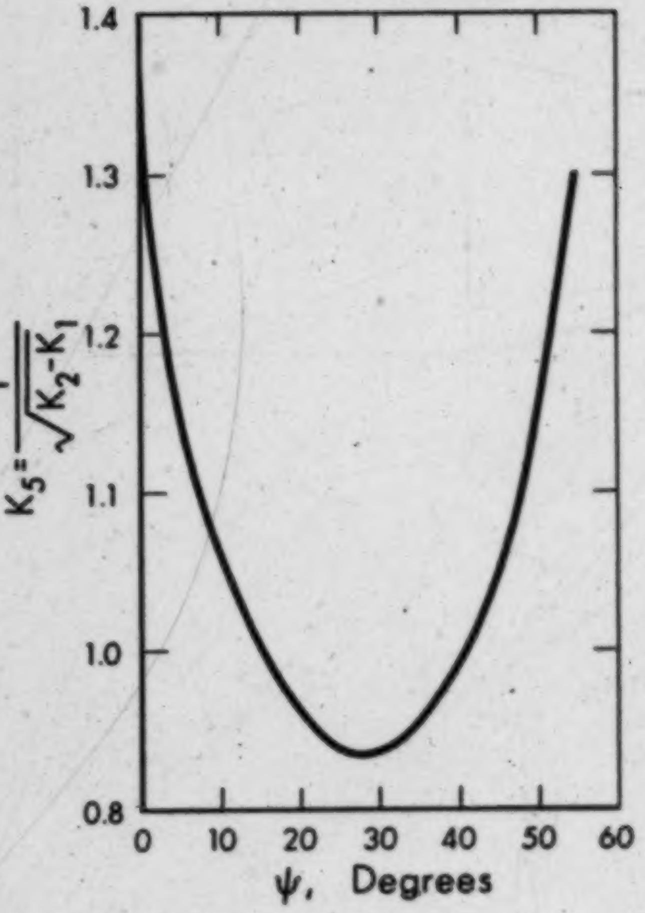

FIGURE 4.7 CURVE OF K_5 VERSUS ψ

ries viscous effects coupled with significant velocity gradients, would inevitably introduce some errors. It is possible to minimize the effect of velocity gradients by using a smaller size probe. However, such a small probe would have had a very slow response. Rajaratnam and Muralidhar (1967) conducted some measurements with the yaw probe in a wall jet and found that the uniform flow calibration curve could be used for some shear flows without serious error.

The procedure used for evaluating the velocity components u and w is outlined below. K_4 is first found from Equation 4.2 and the corresponding value of ψ is read from Figure 4.6. From Equation 4.1 it can be shown that:

$$q = \frac{\sqrt{2g(H_2 - H_1)}}{\sqrt{K_2 - K_1}} \tag{4.3a}$$

or:

$$q = K_5\sqrt{2g\Delta H} \tag{4.3b}$$

where: $K_5 = \dfrac{1}{\sqrt{K_2 - K_1}}$ and $\Delta H = H_2 - H_1$

K_5 is assumed to be a function of ψ only. A plot of K_5 versus ψ is shown in Figure 4.7. Using the known value of ψ, K_5 is found from Figure 4.7 and the magnitude of the velocity vector, q, is computed from Equation 4.3b. The two velocity components are given by:

$$u = q \cos \psi$$
$$w = q \sin \psi \qquad (4.4)$$

4.2.6 Tracer and Injection System

The general procedure for determining the rates of transverse diffusion and mixing experimentally is:

1. To introduce a tracer continuously at a steady rate into the flow at some point, and
2. Measure the tracer concentration at various cross sections downstream of the source.

The three kinds of tracers commonly used in water are salt, fluorescent dye and radioactive isotopes. Standard methods are available for measuring the concentration of all three.

The tracer used was Rhodamine WT fluorescent dye, a 20% solution having a specific gravity of approximately 1.2. Concentrations of Rhodamine WT as low as 0.1 ppb can be detected with a fluorometer by very simple procedures.

The tracer injection system was the same for both flumes. A sketch of the system is shown in Figure 4.8. The tracer was always diluted to less than 100 ppm with dechlorinated tap water and the solution stored in a 30-gallon Mariotte tank. Dechlorination was necessary because Rhodamine WT at low concentrations is found to react with residual chlorine in tap water. The dechlorination was achieved by adding about 3 ppm Sodium Thiosulphate to the water.

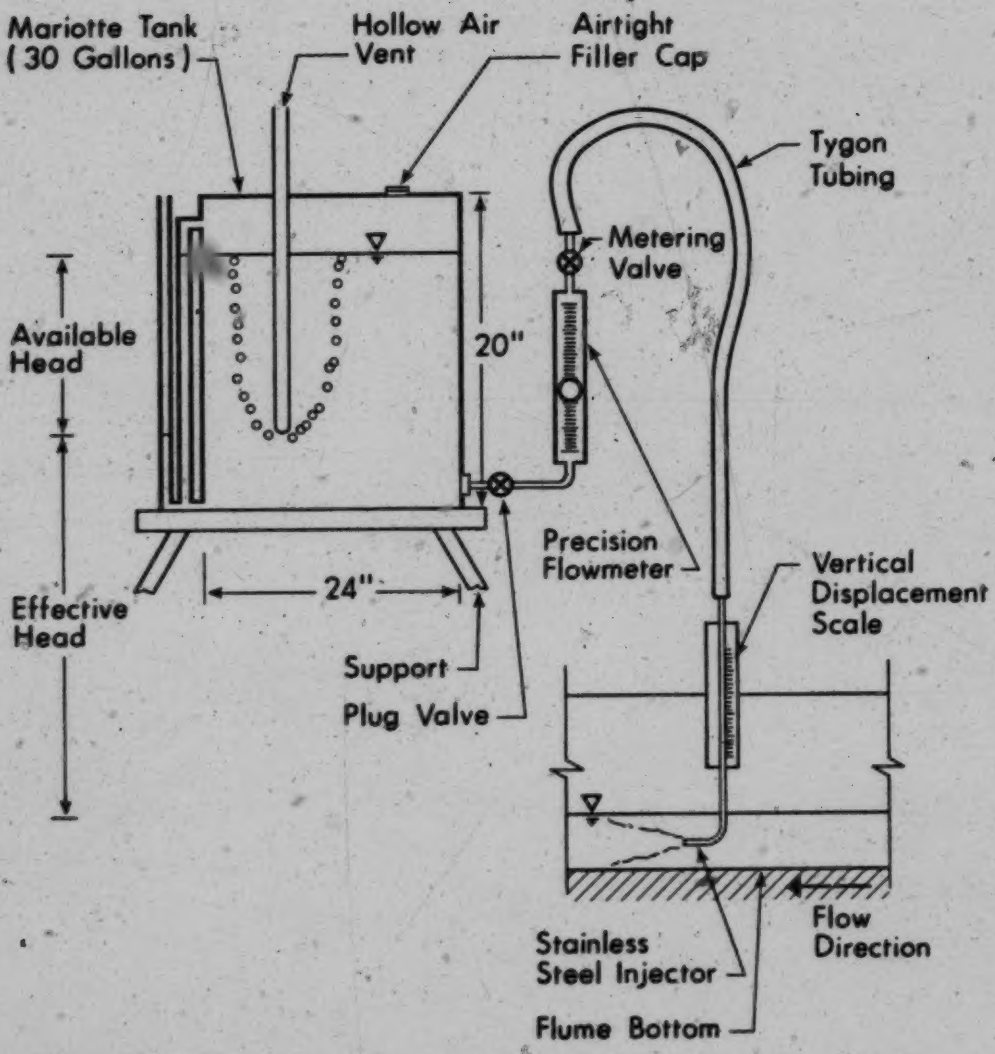
Mariotte Tank
(30 Gallons)
Hollow Air Vent
Airtight Filler Cap
Tygon Tubing
Metering Valve
Available Head
20"
Effective Head
24"
Support
Plug Valve
Precision Flowmeter
Vertical Displacement Scale
Flow Direction
Stainless Steel Injector
Flume Bottom

FIGURE 4.8 SKETCH OF TRACER INJECTION SYSTEM

A precision rotameter capable of measuring very low flows indicated the tracer flow rate. The calibration curve for the rotameter is shown in Figure 4.9. The tracer was released into the flow at a continuous and steady rate through a 1/8 inch stainless steel tube. In all experiments, the tracer was introduced at mid-depth parallel to the flow and at a velocity which approximated that of the water.

4.2.7 Concentration Measuring System

4.2.7.1 Straight Flume: The sampling probe was a 1/8 inch diameter stainless steel tube fitted into a holder mounted on an aluminium angle which was placed across the flume. The latter was provided with a scale for reading the lateral position of the sampling probe.

Samples were obtained by siphoning the flume water into 60 cc bottles and then analysed for concentration with a fluorometer (Turner Model 111). The sampling velocity was adjusted to approximate that of the mean flow velocity.

4.2.7.2 Meandering Flume: The first few tracer concentration measurements in the meandering flume were conducted utilising a system identical to that employed for the straight flume experiments. This system was later replaced by a sampling rake having 24 sampling probes made of 1/8 inch soft brass tubes. The sampling rake is shown in Figure 4.10. This rake enabled simultaneous sampling at 24 points at 0.1 ft intervals across the flume.

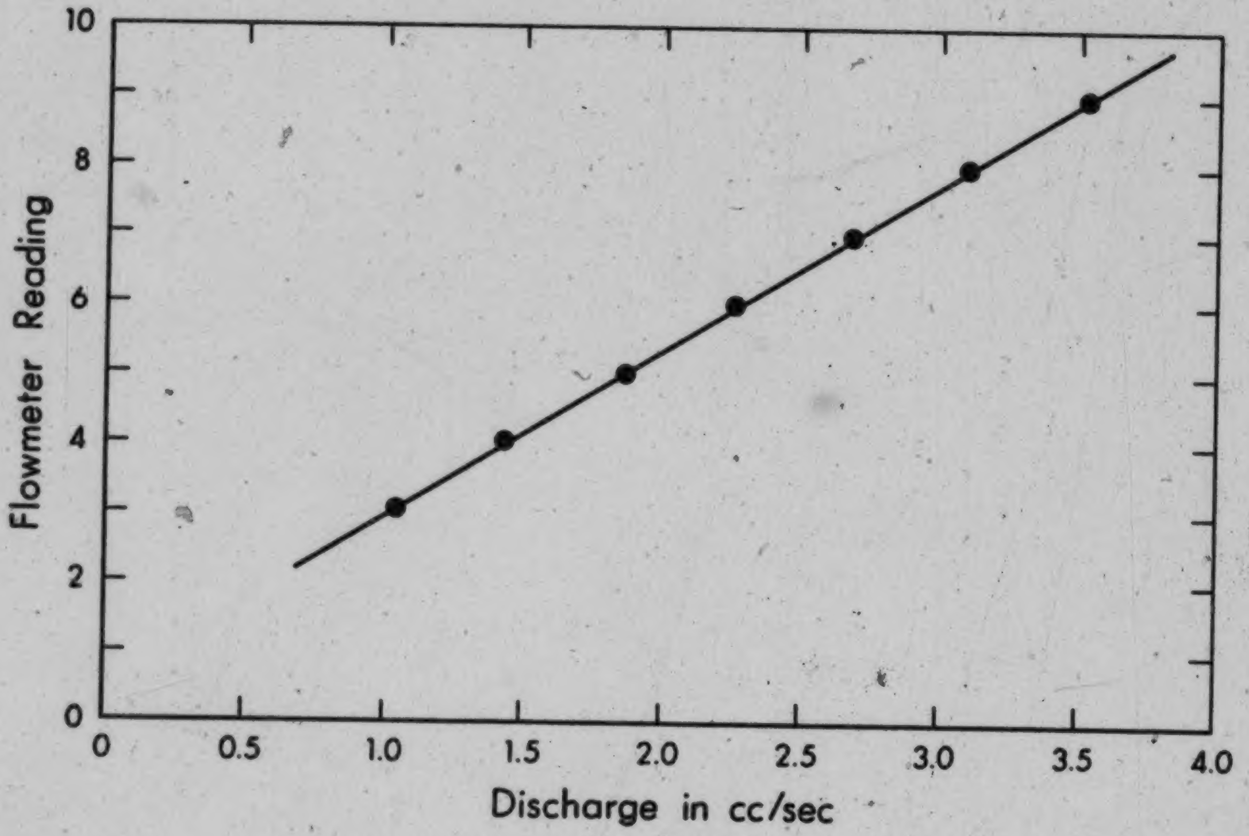

FIGURE 4.9 CALIBRATION CURVE FOR ROTAMETER

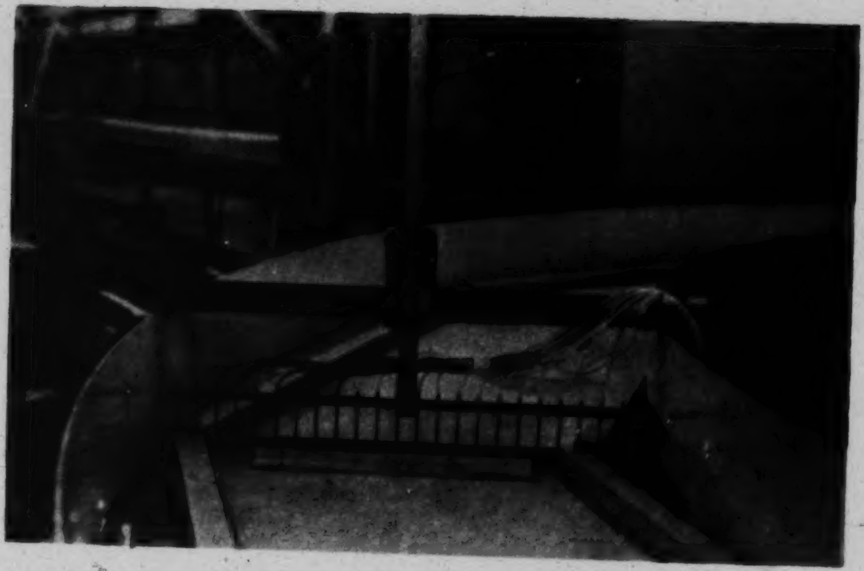

FIGURE 4.10 SAMPLING RAKE USED FOR TRACER MEASUREMENTS.

FIGURE 4.11 PHOTOGRAPH OF DATA ACQUISITION SYSTEM.

4.2.8 Coordinate Positioner

The electronic coordinate positioner was the same as that used by Hollingshead (1972) and is basically a y-z "plotter" that positions a probe at any desired location within a cross-section. The DC voltages representing the coordinates were first zeroed with reference to the flume side and bed as datum planes and then fed into the data acquisition system.

An instrument carriage for the velocity probe was mounted on both the straight and meandering flumes, with the carriage being manually positioned at any desired cross-section (x-coordinate) and the velocity probe electronically positioned within the cross-section.

4.2.9 Data Acquisition System for Velocity Measurements

The Data Acquisition System consisted of the following elements:

1. 20 Channel Scanner (VIDAR 604).
2. Integrating Digital Voltmeter (VIDAR 500).
3. Data Coupler (Control Equipment Corporation Model 310).
4. Scan Counter.
5. Teleprinter (Teletype Model ASR 33).

A photograph of this equipment is shown in Figure 4.11 and is represented schematically in Figure 4.12. All inputs for the data acquisition system were in the range zero to ten volts and each was assigned

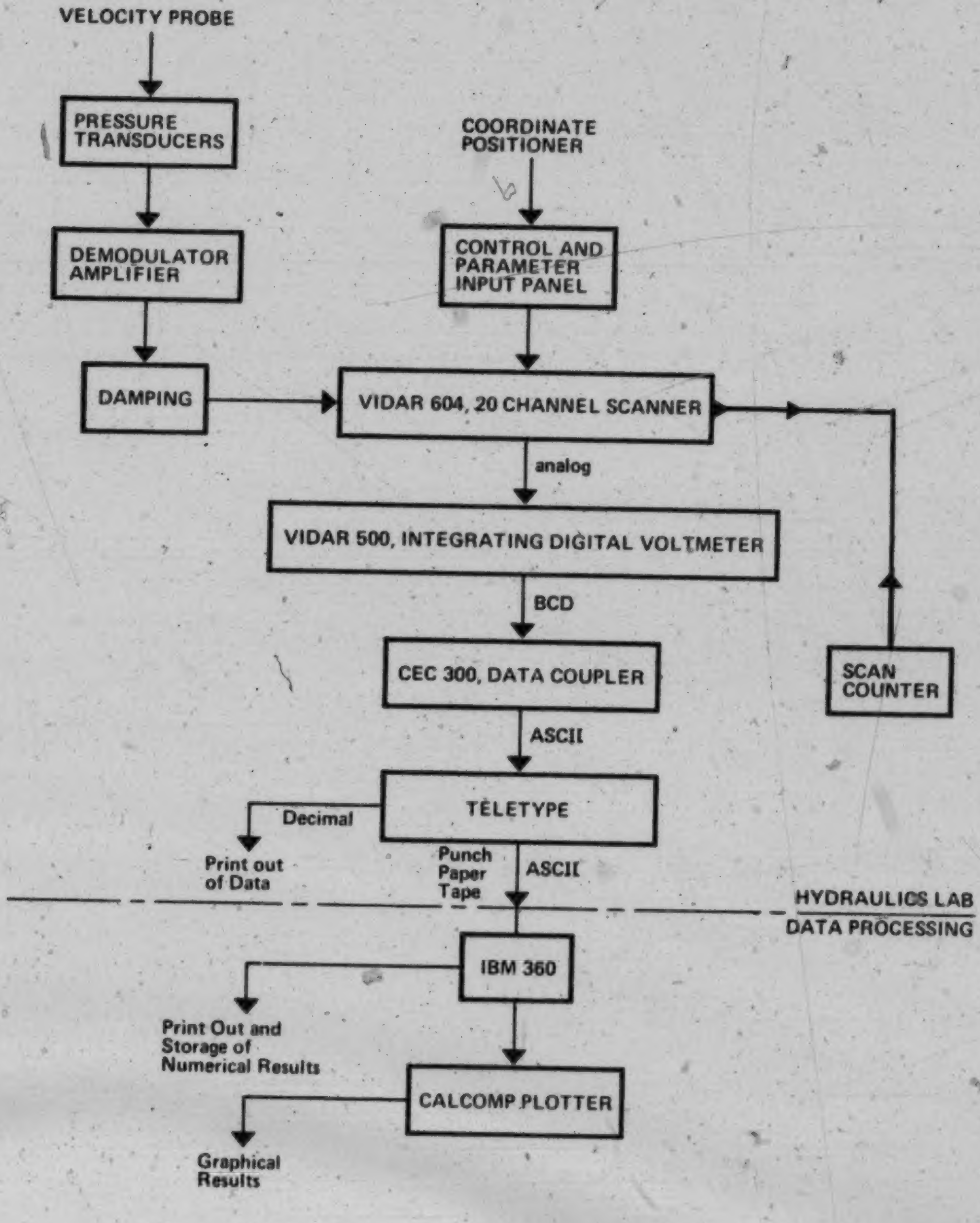
VELOCITY PROBE
PRESSURE TRANSDUCERS
DEMODULATOR AMPLIFIER
DAMPING
COORDINATE POSITIONER
CONTROL AND PARAMETER INPUT PANEL
VIDAR 604, 20 CHANNEL SCANNER
analog
VIDAR 500, INTEGRATING DIGITAL VOLTMETER
BCD
CEC 300, DATA COUPLER
ASCII
SCAN COUNTER
TELETYPE
Decimal
Print out of Data
Punch Paper Tape
ASCII
HYDRAULICS LAB
DATA PROCESSING
IBM 360
Print Out and Storage of Numerical Results
CALCOMP PLOTTER
Graphical Results

FIGURE 4.12 DATA ACQUISITION AND PROCESSING SYSTEM

to a particular channel of the Scanner. The Scanner sequentially sampled selected channels and routed the analogue signals to the Digital Voltmeter where they were digitized and converted to Binary Coded Decimal (BCD) form. The Data Coupler formated the BCD signal and directed it to the Teleprinter. The Teleprinter then punched the data on papertape in American Standard Code for Information Interchange (ASCII) and provided a decimal printout on paper. The desired number of scan cycles and the scan rate were selected on the Scan Counter and the Scanner respectively. The upper limit for the scan rate was one reading per second. This was determined by the permissible teleprinter speed of 10 characters per second.

4.3 Experimental Procedure

4.3.1 Identification Code for Flumes and Experiments

The identification code for the flumes consists of two or three letter combinations. The first letter is either S or M , S representing the straight flume and M the meandering flume. The second letter in the code indicates the type of bed roughness. R denotes a flume bottom roughened with galvanised sheet metal and S a smooth bottom. The third letter, when present, is always I and denotes the presence of an ice-cover. Thus the code MRI refers to an experiment conducted in the meandering flume with a roughened flume bed and an ice-cover.

All experiments were grouped in "series", each series being made up of a number of "Runs". The first digit of an experiment number refers to the series, the second and third digits to the run within the series. For example, run 304 stands for experiment 4 in the 300 series. Series 100 and 200 were conducted in the straight flume, series 300 and 400 in the meandering flume. Classification of the flumes and experiments is summarised in Table 4.1.

4.3.2 Description of a Typical Experiment

4.3.2.1 **Straight Flume:** The first step in all experiments was to establish uniform flow conditions by setting the flume slope and adjusting the discharge and tailgate until the desired normal depth was achieved. Uniform flow conditions were assumed to prevail when depths measured along the flume centerline were within $\pm$ 0.001 ft. of the average depth.

Velocities were measured at seven verticals located at $z/w = 0.0$, ± 0.25, ± 0.375 and ± 0.4375 and 10 points in the vertical at only one cross-section. This cross-section was located approximately half-way along the flume length.

The velocity distributions were determined as follows:

1. The y and z coordinates (coordinate positioner) and the pressure transducer were zeroed and calibrated.
2. The scan rate and the number of scan cycles were selected.
3. The velocity probe was positioned at the desired point and the counter started.

TABLE 4-1 CLASSIFICATION OF FLUMES AND EXPERIMENTS

Series	Flume	Flume Bed Roughness	Ice-Cover	Identification Code
100	Straight	Rough	No	SR
200	Straight	Rough	Yes	SRI
300	Meandering	Rough/Smooth	No	MR/MS
400	Meandering	Rough/Smooth	Yes	MRI/MSI

4. Step 3 was repeated for all selected points within the cross-section.

The pressure transducer calibration was checked after each run.

The concentration measurements in the straight flume were made after velocity measurements were completed. In all the experiments, four measuring cross-sections were used. The concentration measurements were made at three levels; y/D = 0.25, 0.50 and 0.75. Sampling began at the cross-section nearest the tracer source and proceeded downstream until all cross-sections were covered. The sampling period at each point was about 25 seconds. The total time required for sampling at the last section where the tracer cloud width was greatest was approximately 90 minutes.

Tracer measurements were carried out for both centerline and side (3 inches from side-wall) injections under identical flow conditions (for example, runs 101 and 102).

4.3.2.2 Meandering Flume: Again the tests were started with the establishment of uniform flow in the flume. For the open-channel tests uniform flow conditions were assumed to have been attained when the flow depths on the centerline were within ± 0.002 ft. of the overall average depth. The cross-sectional average flow depth for ice-cover flows was obtained by taking the average of the depths at the left bank, right bank and channel centerline. Due to the warping of the plywood "ice-cover", deviations of the cross-sectional average depth from the overall average flow depth could only be kept within ± 0.006 ft.

Velocities were determined at 5 verticals located at $z/w = 0$, ± 0.20 and ± 0.40, and 10 points in the vertical for the sections indicated in Figure 4.13. The tracer concentration measurements were made at three levels; $y/D = 0.25$, 0.50 and 0.75 for 8 to 11 sections. Three tracer source locations were used. These were at the channel centerline and at 0.05 ft. measured laterally from both the left and right banks.

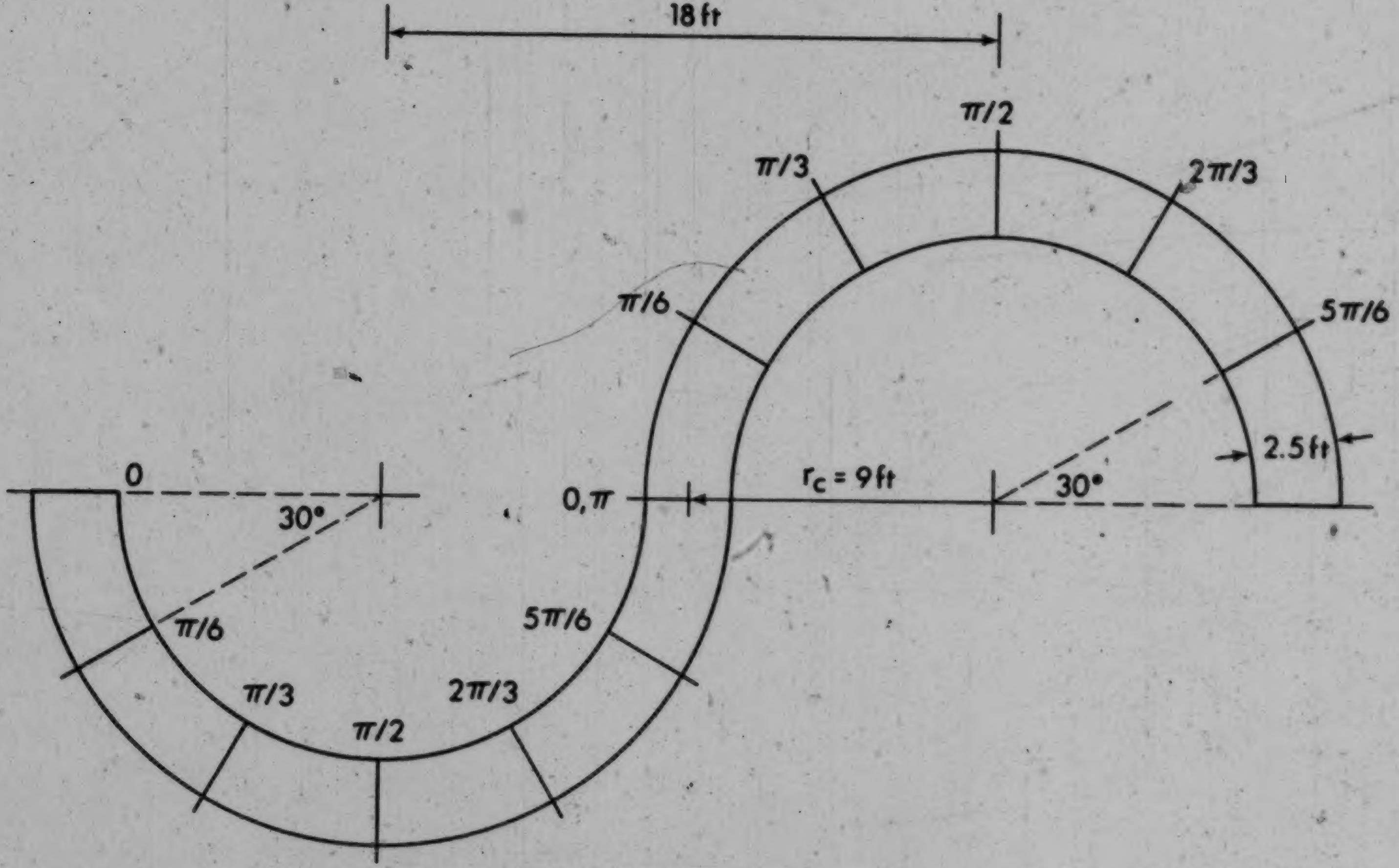
18 ft
π/2
π/3
2π/3
π/6
5π/6
2.5 ft
0
30°
0,π
r_c = 9 ft
30°
π/6
5π/6
π/3
2π/3
π/2

FIGURE 4.13 SCHEMATIC SKETCH OF MEANDERING FLUME SHOWING THE SECTIONS USED FOR VELOCITY AND CONCENTRATION MEASUREMENTS

CHAPTER 5

PRESENTATION OF VELOCITY MEASUREMENTS

5.1 Straight Flume

5.1.1 Hydraulic Data

The hydraulic conditions for all test runs are summarised in Table 5-1. Column 3 lists the uniform flow depth, d_* as measured along the channel centerline. The reference level for d_* was taken at one-half the thickness of the galvanised sheet metal (bed roughness) above the flume bed. The average shear velocity in Column 8 was evaluated from $u_* = \sqrt{gRS_f}$ where R is the hydraulic radius; S_f is the slope of the energy line and g is gravitational acceleration. The average velocity, U_o , was calculated by dividing the metered discharge, Q , by the cross-sectional area of flow.

5.1.2 Velocity Measurements

Velocity profile measurements were made at only one cross-section for each test run in order to check the metered discharge and to ascertain that the flow was two-dimensional. Velocities were determined at seven points laterally and ten points vertically. The discharge calculated from the velocity measurements was within -6% of the metered discharge. The integration of the velocity distribution near the flume walls contributed substantially to the discrepancy in

TABLE 5-1 SUMMARY OF HYDRAULIC DATA FOR STRAIGHT FLUME EXPERIMENTS

Experiment Number	Flume Identification Code	Flow Depth d_* ft.	Hydraulic Radius R ft.	Aspect Ratio W/d_*	$\frac{W}{R}$	Slope $\times 10^4$	Shear Velocity u_* ft/s	Average Velocity U_o ft/s	Friction Factor $f=8(\frac{u_*}{U_o})^2$	Reynolds Number $\frac{4U_oR}{\nu}$	Froude Number $U_o/\sqrt{gd_*}$
101 102	SR	0.155	0.144	25.8	27.8	3.0	0.0372	0.404	0.068	23,200	0.18
103 104	SR	0.213	0.193	18.8	20.7	4.3	0.0517	0.645	0.0514	49,800	0.246
105	SR	0.130	0.122	30.8	32.9	12.6	0.0704	0.865	0.053	42,200	0.424
106	SR	0.133	0.125	30.0	32.0	8.7	0.0592	0.751	0.050	37,500	0.362
201 202	SRI	0.163	0.078	24.5	51.3	6.5	0.0405	0.383	0.0895	12,500	
203 204	SRI	0.213	0.101	18.8	39.6	7.8	0.0504	0.645	0.0488	27,500	
205	SRI	0.126	0.061	31.1	65.6	24.3	0.0700	0.893	0.0492	22,500	
206	SRI	0.130	0.063	30.8	63.5	6.9	0.0570	0.770	0.0438	20,000	

the metered and calculated discharges because of the assumption of linearity between any two adjacent velocity profiles. Also the flowmeter could be read only to the nearest 0.01 cfs which could represent an average error of about ± 3% for the discharge range used.

Secondary circulation was observed in all flows and within the central 50% of the channel variations in the depth-averaged velocities of up to 12% were recorded. For the open-channel experiments the velocity profiles were found to be logarithmic; Figure 5.1 gives the velocity distribution for run 106.

The normalized mean velocity profiles near the center of the channel for all the test runs with ice cover are shown in Figure 5.2. The value of u_{max} in each run had to be taken from a plot of the velocity profile and this probably contributed to the small discrepancies in the u/u_{max} versus $\tilde{y}/D$ plots.

The mean velocity distribution is distinctly asymmetric with the point of maximum velocity located nearer the ice-cover which is the relatively smoother boundary. Velocity contours for run 203 are plotted in Figure 5.3. They show that the flow was not entirely two dimensional but is more concentrated near both side-walls.

From the logarithmic plots of the velocity profiles shown in Figure 5.4 it is evident that there is a region close to the rough wall where the velocity profile conforms with the logarithmic law. It can, therefore, be assumed that in this region the mean flow is unaffected

75

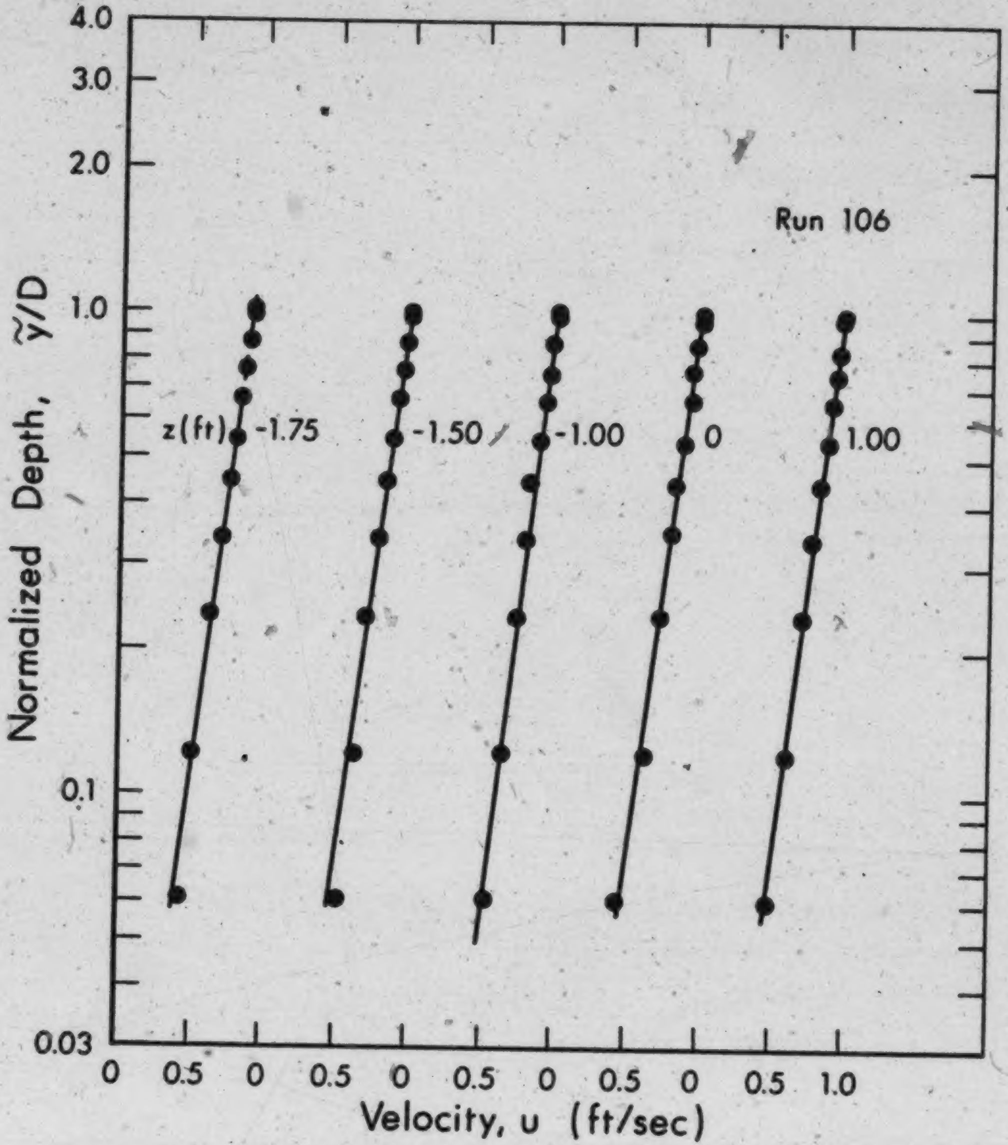

FIGURE 5.1 MEASURED VELOCITY PROFILES, RUN 106

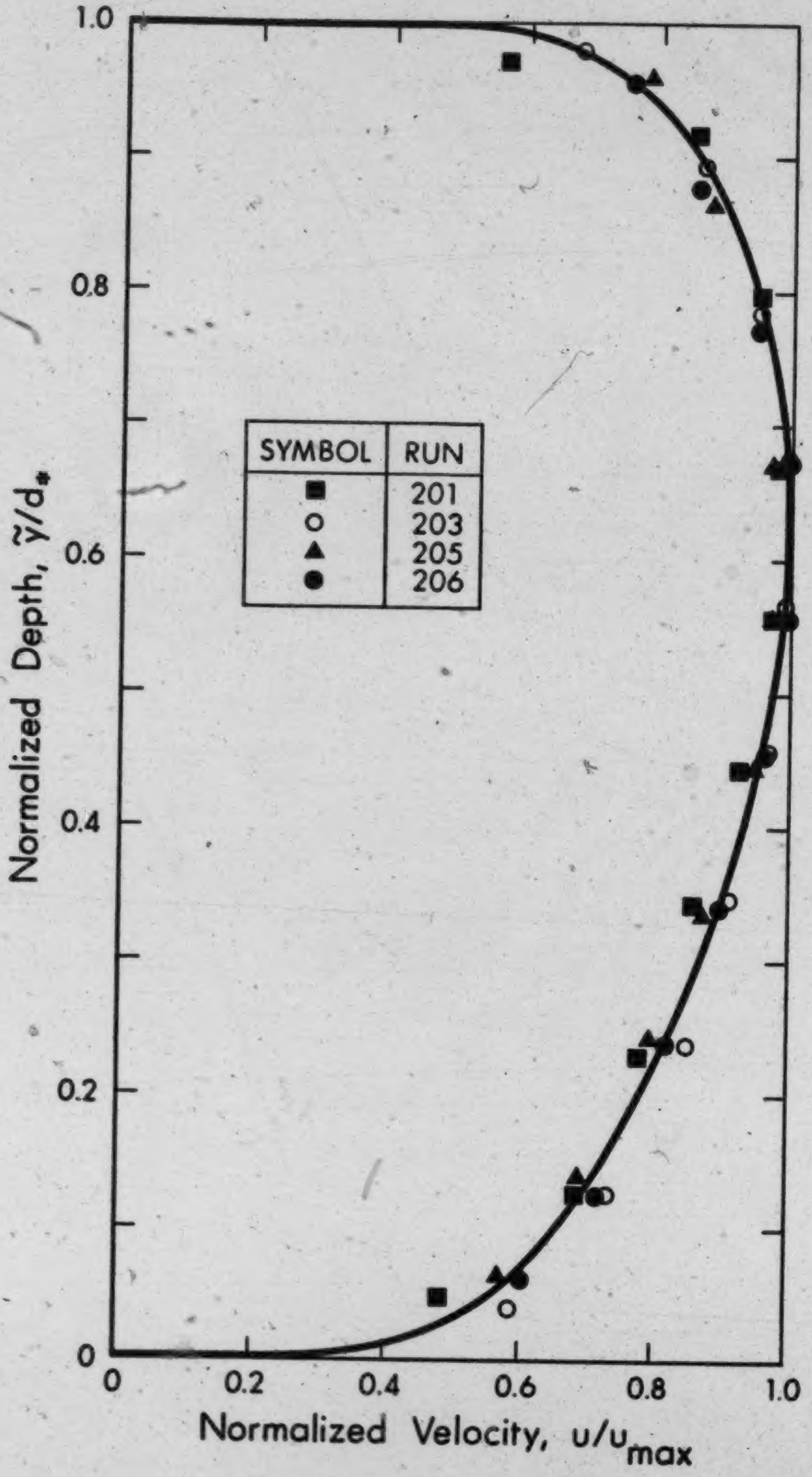

FIGURE 5.2 VELOCITY DISTRIBUTION IN ICE-COVERED CHANNEL.

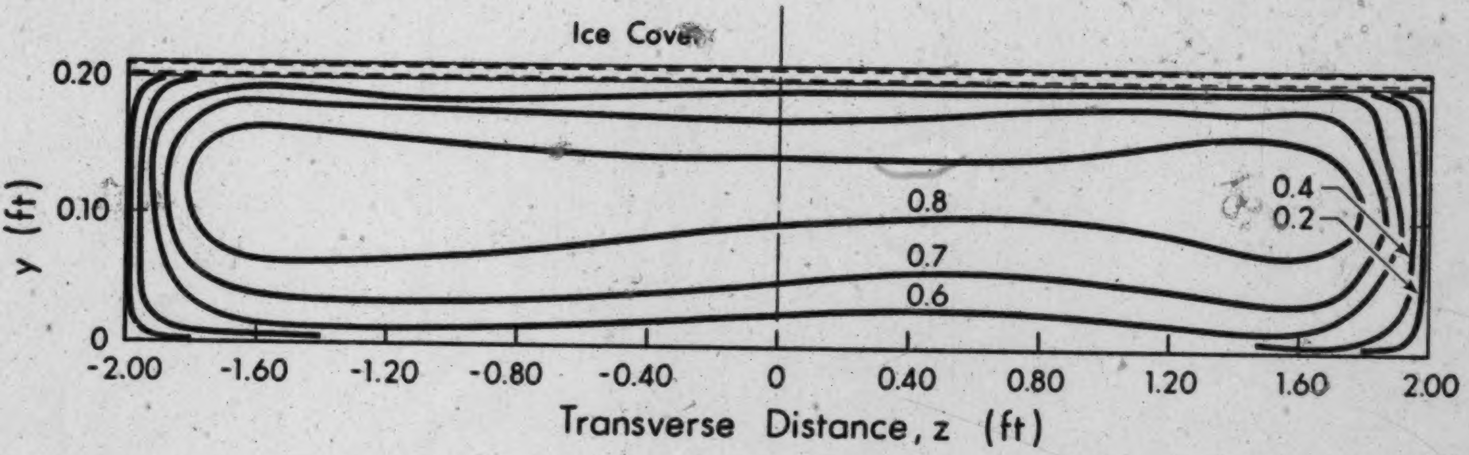

FIGURE 5.3 VELOCITY CONTOURS FOR RUN 203, VELOCITIES ON ISOVELS IN FT/SEC

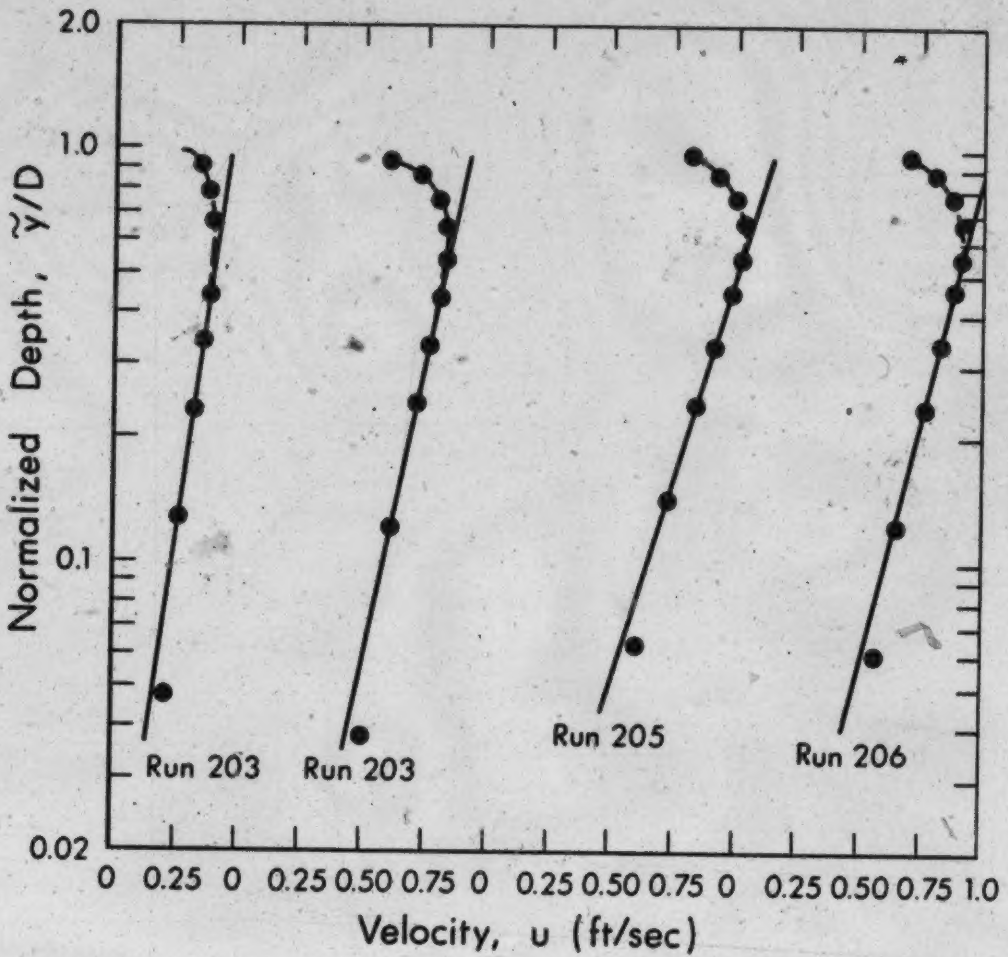

FIGURE 5.4 VELOCITY PROFILE NEAR ROUGH FLUME BED FOR ICE-COVER TESTS

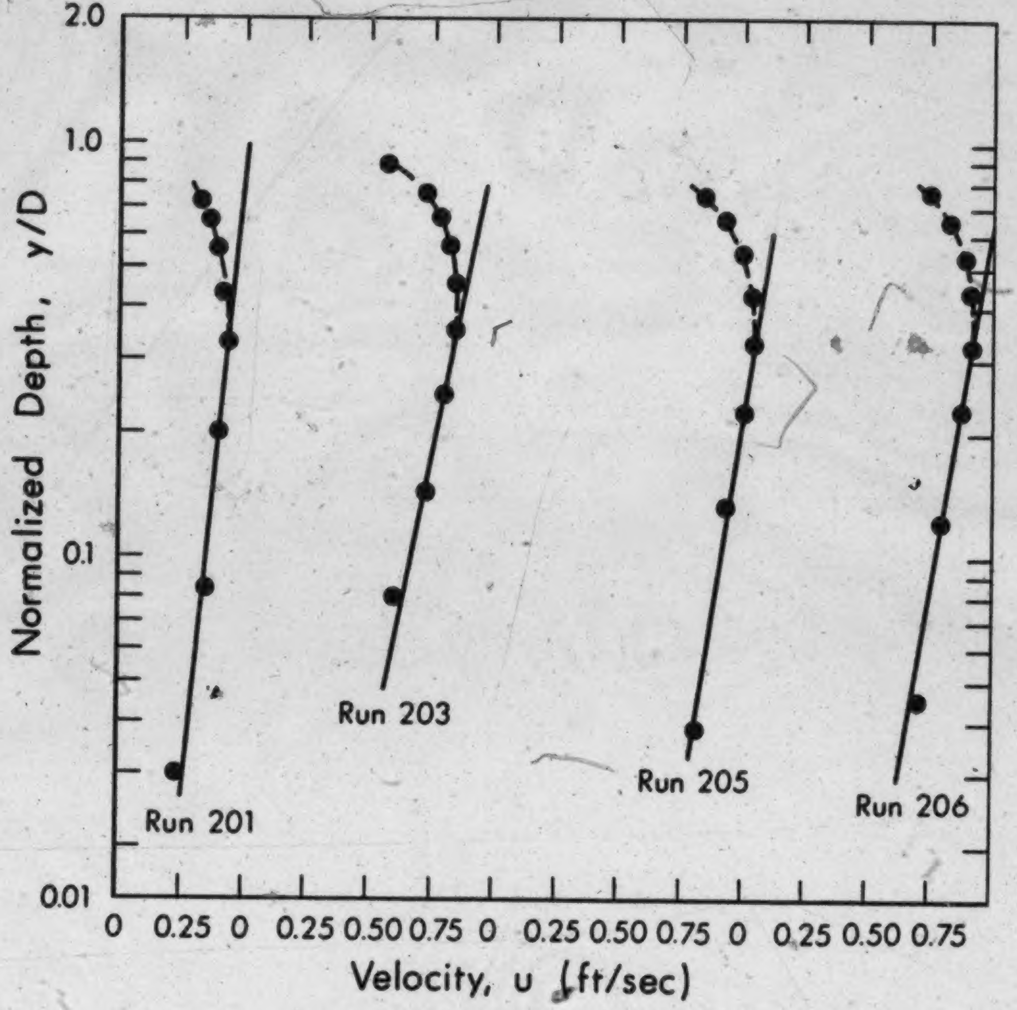

FIGURE 5.5 VELOCITY PROFILE NEAR ICE-COVER FOR RUNS 201, 203, 205 AND 206

by the ice-cover. However, farther from the rough bed the velocity distribution is seen to deviate from a logarithmic relationship. The normalized distance from the bed, $\tilde{y}/D$, at which this deviation starts is about 0.4. Figure 5.5 gives the mean velocity distribution near the ice-cover. Although insufficient velocity measurements were made close to the ice-cover the data points seem to follow a logarithmic relationship within a narrow zone. This zone is relatively smaller than that near the rough bed and extends to about $y/D = 0.2$, y being the distance measured downwards from the ice-cover.

From the above it is evident that near both the ice-cover and channel bed the mean velocity profile is unaffected by the opposite boundary. The effect of the rough wall extends farther into the flow than that of the smooth wall. Between these two regions is a transition zone wherein the velocity profile depends on the nature of both boundaries. These observations are in accord with those of Hanjalic and Launder (1968) who carried out their measurements in a wide rectangular conduit with one of the principal walls roughened.

Because the number of point velocity measurements in the vertical were insufficient it was not possible to accurately determine the location of the point of maximum velocity and to evaluate whether the Reynolds Number, R_N , has any effect on its position. However, Hanjalic and Launder observed that increasing the Reynolds number moves the maximum velocity closer to the smoother boundary. They also found a similar shift in the position of the zero-shear plane which was always nearer the smoother boundary than the point of maximum velocity.

5.2 Characteristics of Flow in Meandering Channels

5.2.1 General

Flow in meandering channels differs from that in straight channels because the presence of centrifugal forces results in the formation of transverse pressure gradients and the associated lateral circulation in the plane of a cross-section. In general, the flow structure changes in the downstream direction due to the growth, decay and reversal of this circulation or spiral motion.

In order to simulate flow conditions in natural streams the present experiments were conducted for W/d_* ratios greater than 10.0. The Froude Number was also kept low, the highest being 0.53 and the Reynolds Number was greater than 10^4 in all tests so that they were within the turbulent regime. A summary of the hydraulic data is provided in Table 5-2. For each test run, the discharge through any cross-section used for velocity and tracer measurements was calculated from the velocity measurements. This calculated discharge was found to be within ± 8% of the metered discharge. The discrepancy is attributed to the small number of vertical velocity profiles taken, measurement errors and the assumption of linearity between adjoining velocity profiles. Also, as stated previously, the magnetic flowmeter could only be read to the nearest 0.01 cfs which could cause an average error of

TABLE 5-2 SUMMARY OF HYDRAULIC DATA FOR MEANDERING FLUME EXPERIMENTS

Experiment Number	Flume Identification Code	Mean Flow Depth d_* ft.	Hydraulic Radius R ft.	Aspect Ratio	Mean Radius of Curvature to Depth Ratio r_c/d_*	Slope $\times 10^4$	Average Shear Velocity u_* ft/s	Average Velocity U_o ft/s	Friction Factor $f=8(\frac{u_*}{U_o})^2$	Reynolds Number $\frac{4U_oR}{\nu}$ $\times 10^{-4}$	Froude Number $U_o/\sqrt{gd_*}$
301 302	MR	0.231	0.195	10.8	39	6.36	0.0632	0.797	0.0503	5.65	0.292
304 305	MR	0.139	0.125	18	64.7	21.21	0.0924	1.122	0.05425	5.10	0.530
307 308	MS	0.235	0.198	10.6	38.3	4.24	0.0520	0.783	0.0353	5.64	0.285
401 402 403	MRI	0.217	0.100	11.5	41.5	12.20	0.0670	0.848	0.0437	1.673	
404 405 406	MRI	0.147	0.068	17	61.2	31.42	0.0830	1.061	0.0489	1.418	
407 408	MRI	0.245	0.111	10.2	36.7	8.48	0.0551	0.751	0.0431	1.673	

about ± 2.5% in the discharge range used here.

5.2.2 Velocity Measurements in Open Meandering Flume

Mixing in open and ice-covered channels depends greatly on the velocity distribution. The spiral motions generated by bends do not only modify the velocity distribution but also augment lateral mixing. Detailed measurements of the velocity field are, therefore, necessary for an understanding of the mixing process.

5.2.2.1 Longitudinal Velocity Component: Typical plots of longitudinal velocity measurements using the data from run 301 is presented in Figures 5.6a, b and c. The corresponding measurements for runs 303 and 307 are shown in Figures A.1 and A.2 of Appendix A. A study of the measurements reveals that close to both the inner and outer banks, the maximum longitudinal velocity does not in general occur at the surface but is displaced downwards. This is caused by the spiral motion which transfers low momentum fluid from the bottom layers to the water surface near the inside bank, while near the outer bank it supplies high-momentum fluid from the surface downwards. Also, the formation of a circulation cell with an opposite sense of rotation to the main spiral motion at the upper corner of either the outside or inside of the bend could shift the maximum longitudinal velocity downwards. The reduction in velocity near the free surface at the outer bank appears to be smaller than that near the inner bank.

The transverse distribution of the depth-averaged longitudinal

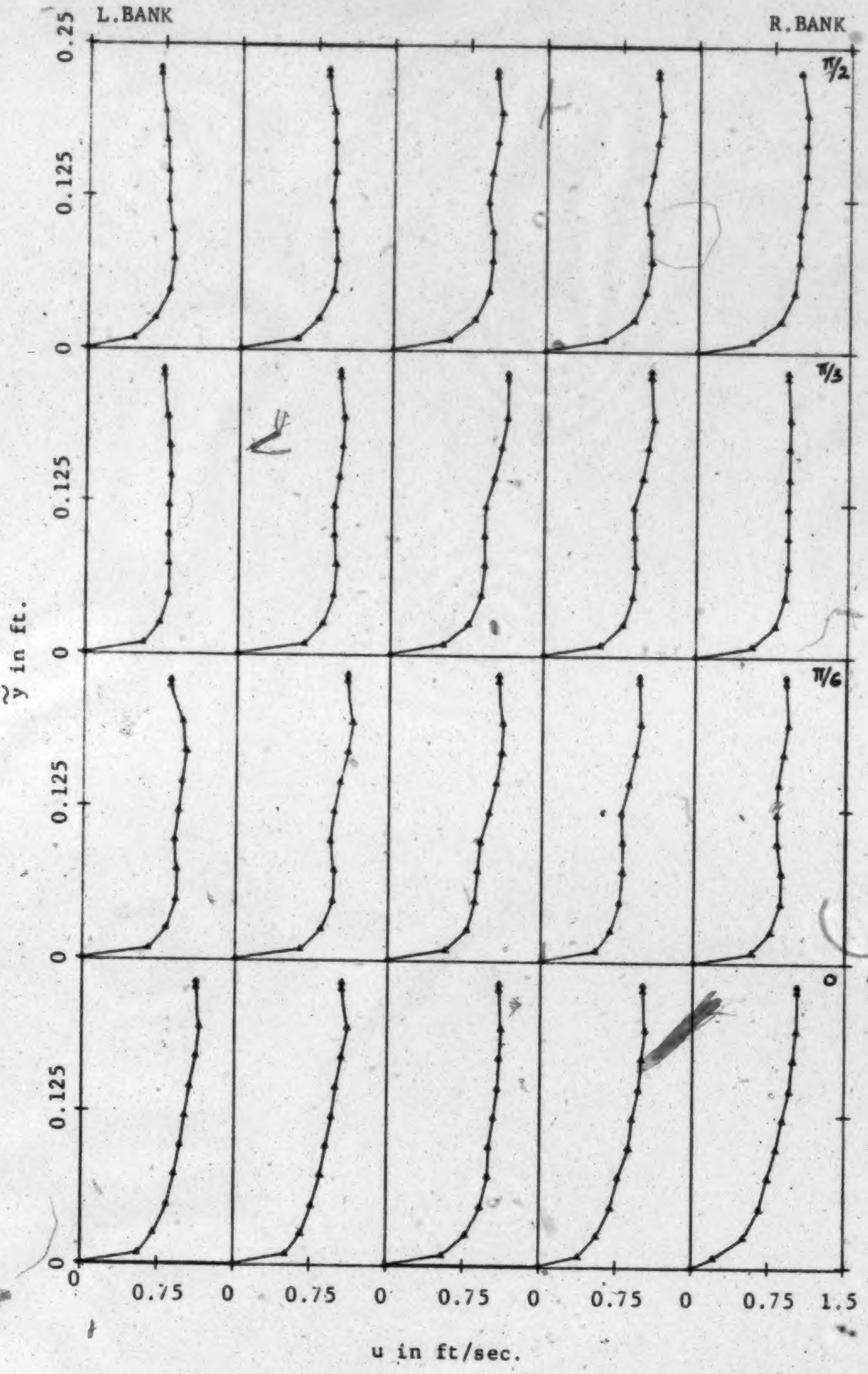

FIGURE 5.6a VERTICAL DISTRIBUTIONS OF LONGITUDINAL VELOCITY, RUNS 301/2/3, SECTIONS $\theta_1 = 0$ TO $\pi/2$.

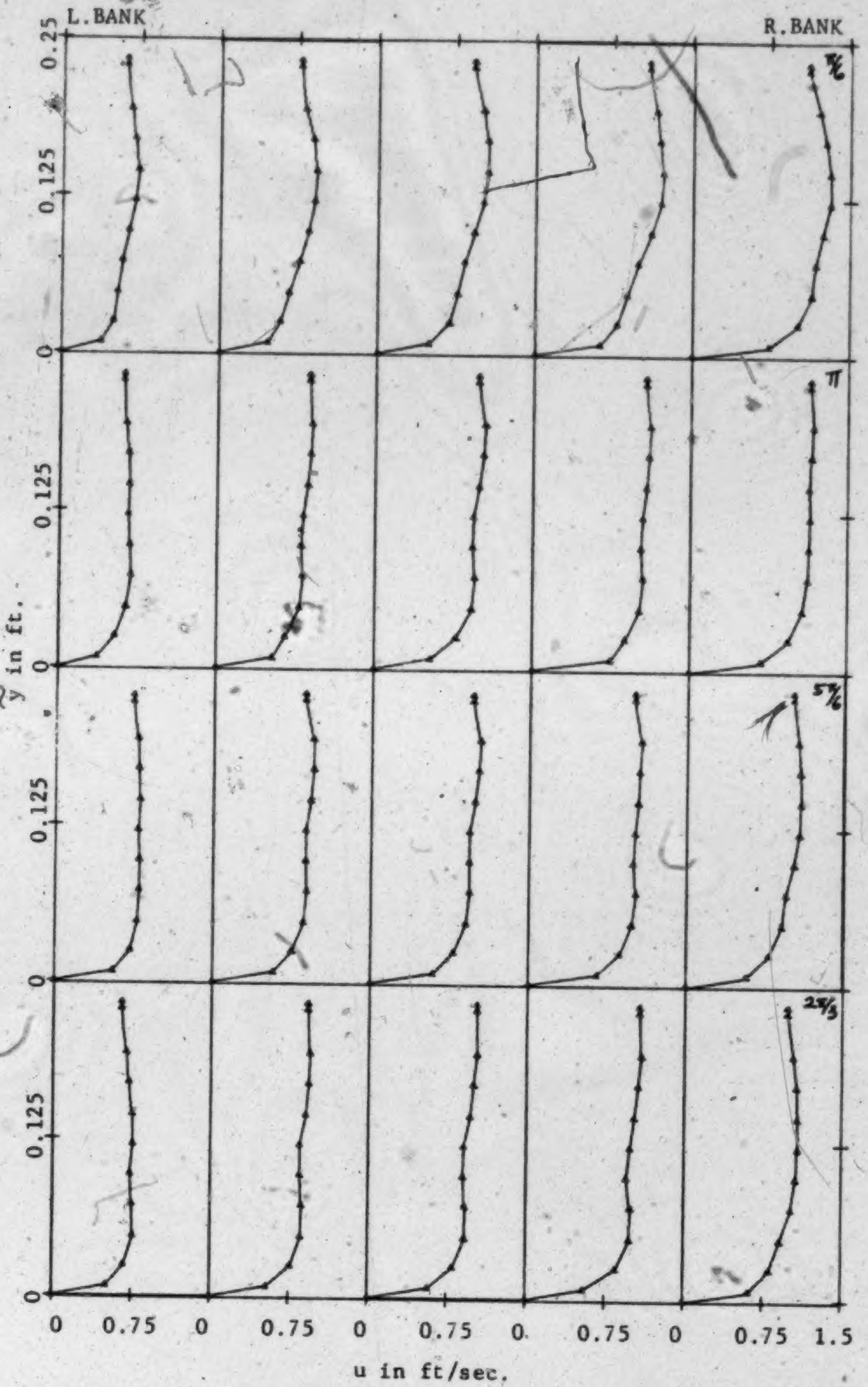

FIGURE 5.6b VERTICAL DISTRIBUTIONS OF LONGITUDINAL VELOCITY RUNS 301/2/3, SECTIONS $\theta_1 = 2\pi/3$ TO $\theta_2 = \pi/6$

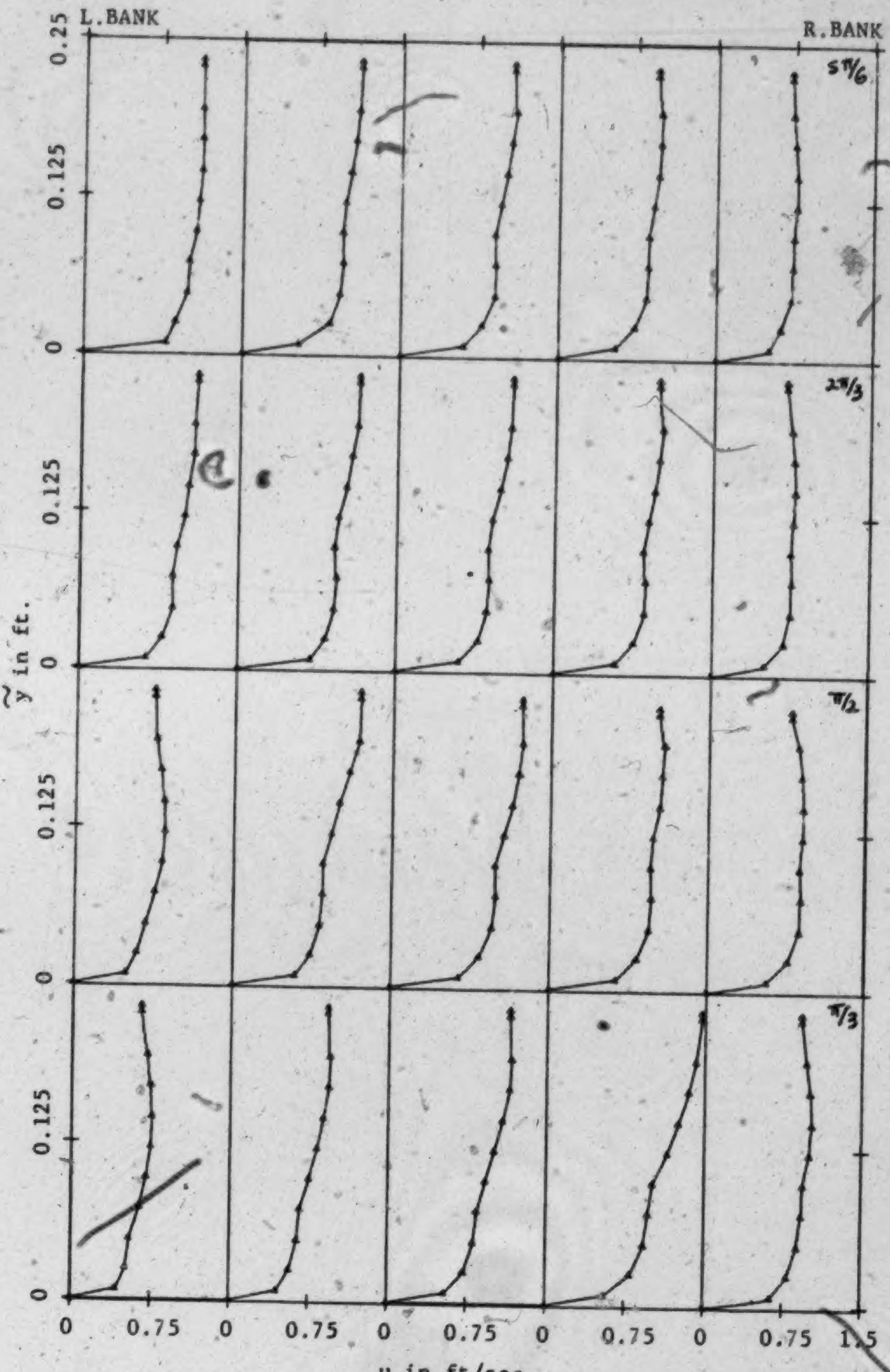

FIGURE 5.6c VERTICAL DISTRIBUTIONS OF LONGITUDINAL VELOCITY RUNS 301/2/3, SECTIONS $\theta_2 = \pi/3$ TO $5\pi/6$.

velocity, $\bar{u}$, are given in Figures 5.7a, b, c. It is evident from these figures that the higher velocities occur near the inside of the first bend at the beginning of the bend. This observation is in agreement with potential flow theory for flow around a bend which predicts a free vortex type of motion with $\bar{u} \sim 1/r$. The high velocity zone starts to shift towards the channel centerline after angle, θ_1 , from the beginning of the bend exceeds about $\pi/6$.

Downstream from $\theta_1 = \pi/6$ the zone of maximum velocity gradually moves away from the inside bank and at $\theta_1 = 2\pi/3$ it is near the outer bank. On emerging from the first bend the zone of high velocity flow is located near the inside of the second bend. This produces a marked non-uniformity in the lateral distribution of $\bar{u}$ which persists in the second bend until $\theta_2 = \pi/3$, where θ_2 is the angle in the second bend. From this section downstream the high velocity filament again moves across to the outside bend. If this series of bends were continued, odd-numbered bends for example, will exhibit similar depth-averaged longitudinal velocity profiles at corresponding sections.

The experiments also indicate that the displacement of the high velocity flow region from the inside to the outside of a bend is accomplished over a relatively shorter distance for flows over rough beds compared with that over the smooth bed. The cause of this is not very clear but is believed to be related to the non-uniform distribution of bed resistance.

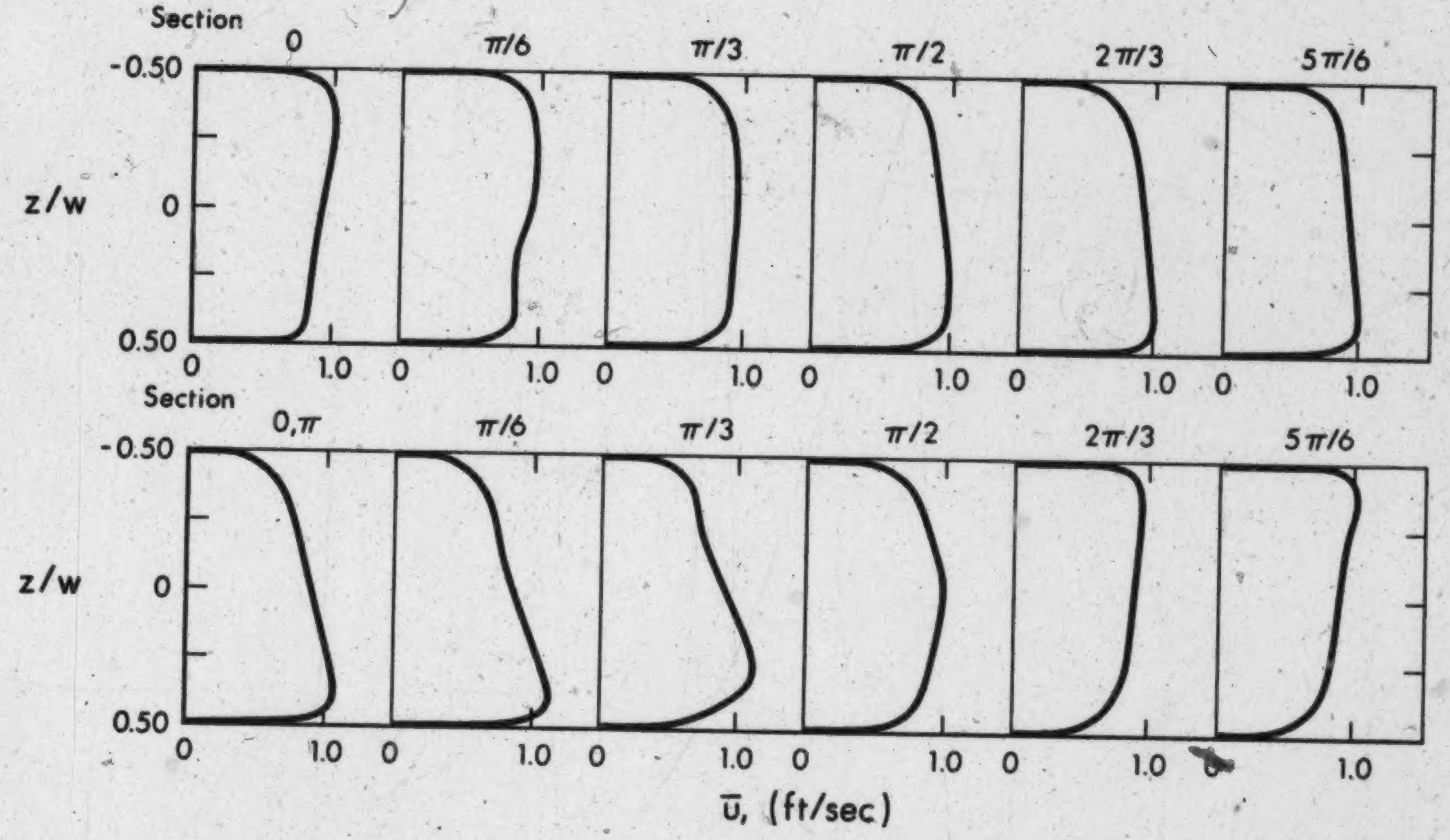

FIGURE 5.7a LATERAL DISTRIBUTIONS OF DEPTH-AVERAGED LONGITUDINAL VELOCITY, RUN 301/2/3

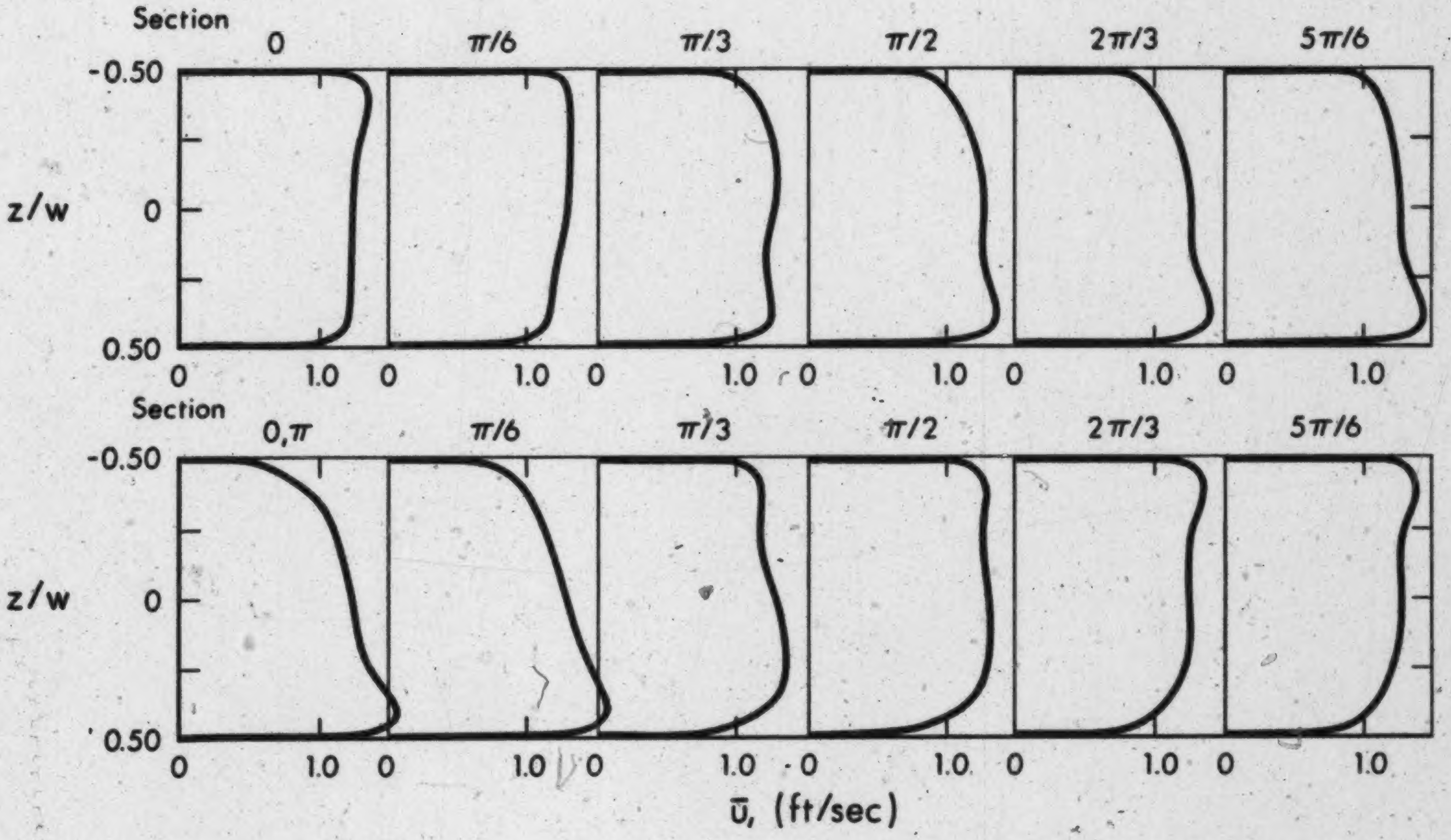

FIGURE 5.7b LATERAL DISTRIBUTIONS OF DEPTH-AVERAGED LONGITUDINAL VELOCITY, RUN 304/5/6

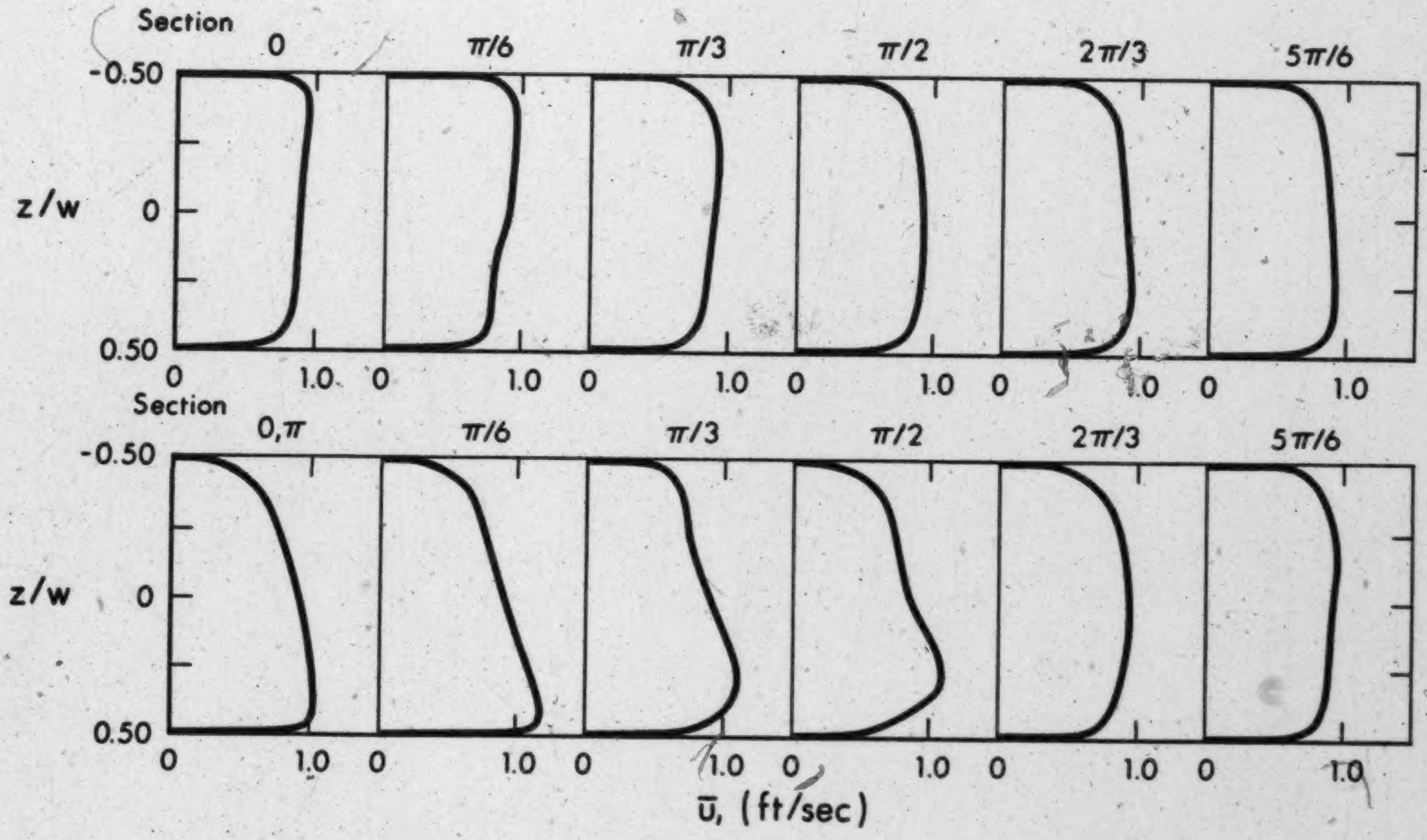

FIGURE 5.7c LATERAL DISTRIBUTIONS OF DEPTH-AVERAGED LONGITUDINAL VELOCITY, RUN 307/8

A parameter which can be used to describe the non-uniform distribution of velocity is the dimensionless mean square velocity deviation, δ , defined as:

$$\delta = \frac{1}{W} \frac{\int_{-W/2}^{+W/2} (\bar{u} - U_o)^2 dz}{U_o^2}$$

where W is the channel width and U_o is mean velocity. The longitudinal variation of δ for all tests is shown in Figure 5.8. The contributions to δ are due only to velocity variations in the lateral direction. It is seen from Figure 5.8 that high values of δ occur between $\theta_1 = 2\pi/3$ and $\theta_2 = \pi/3$ and in run 307, where the channel bed was smooth, δ retains a high value even at $\theta_2 = \pi/2$ because the high velocity zone was still located within the inside half of the bend at that section. The degree of non-uniformity in the velocity field was observed to be relatively low within the first bend.

5.2.2.2 Transverse Velocity Components: Measurements of the transverse velocity component from the data of run 301 are shown plotted in Figures 5.9a, b and c. The corresponding measurements for runs 304 and 307 are given in Figures A.3 and A.4 of Appendix A. The plots clearly show the growth and decay of transverse circulation or spiral motion in the two bends. Following Yen (1972), the strength of the spiral motion, S , can be defined as:

$$S = \int_o^D |w| dy$$

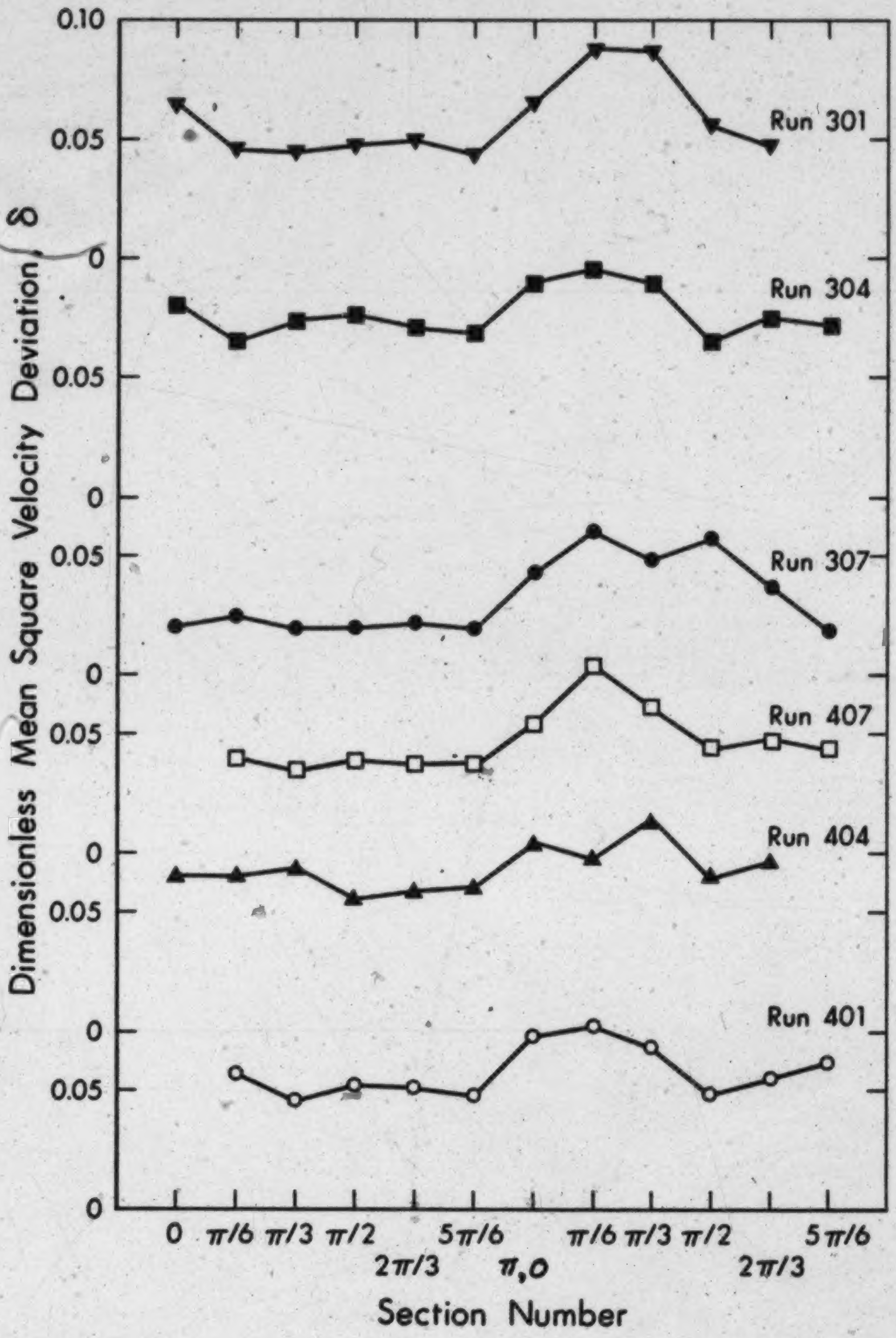

FIGURE 5.8 LONGITUDINAL VARIATION OF THE DIMENSIONLESS MEAN SQUARE VELOCITY DEVIATION, δ.

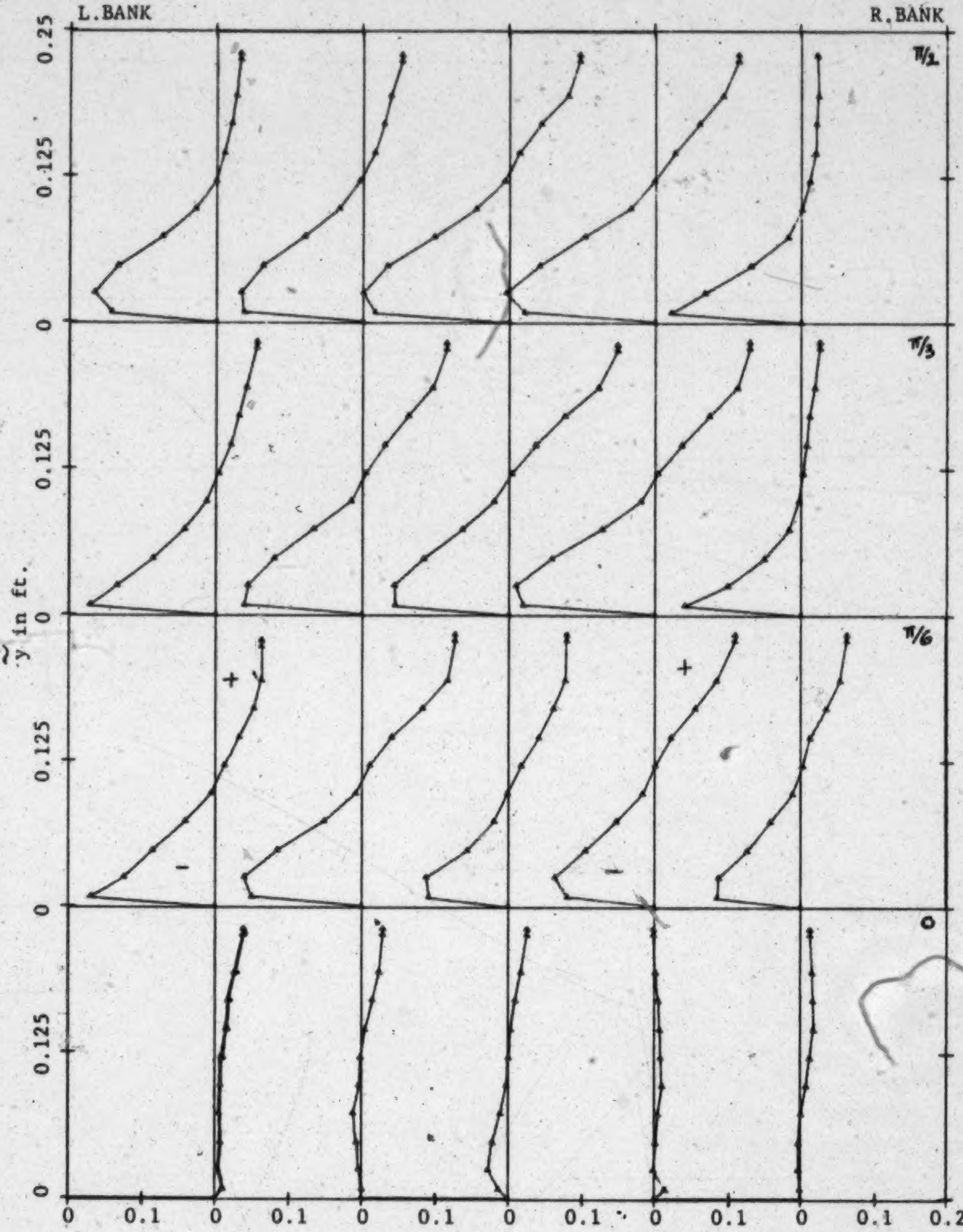

FIGURE 5.9a VERTICAL DISTRIBUTIONS OF TRANSVERSE VELOCITY, RUNS301/2/3, SECTIONS θ_1 = 0 TO π/2.

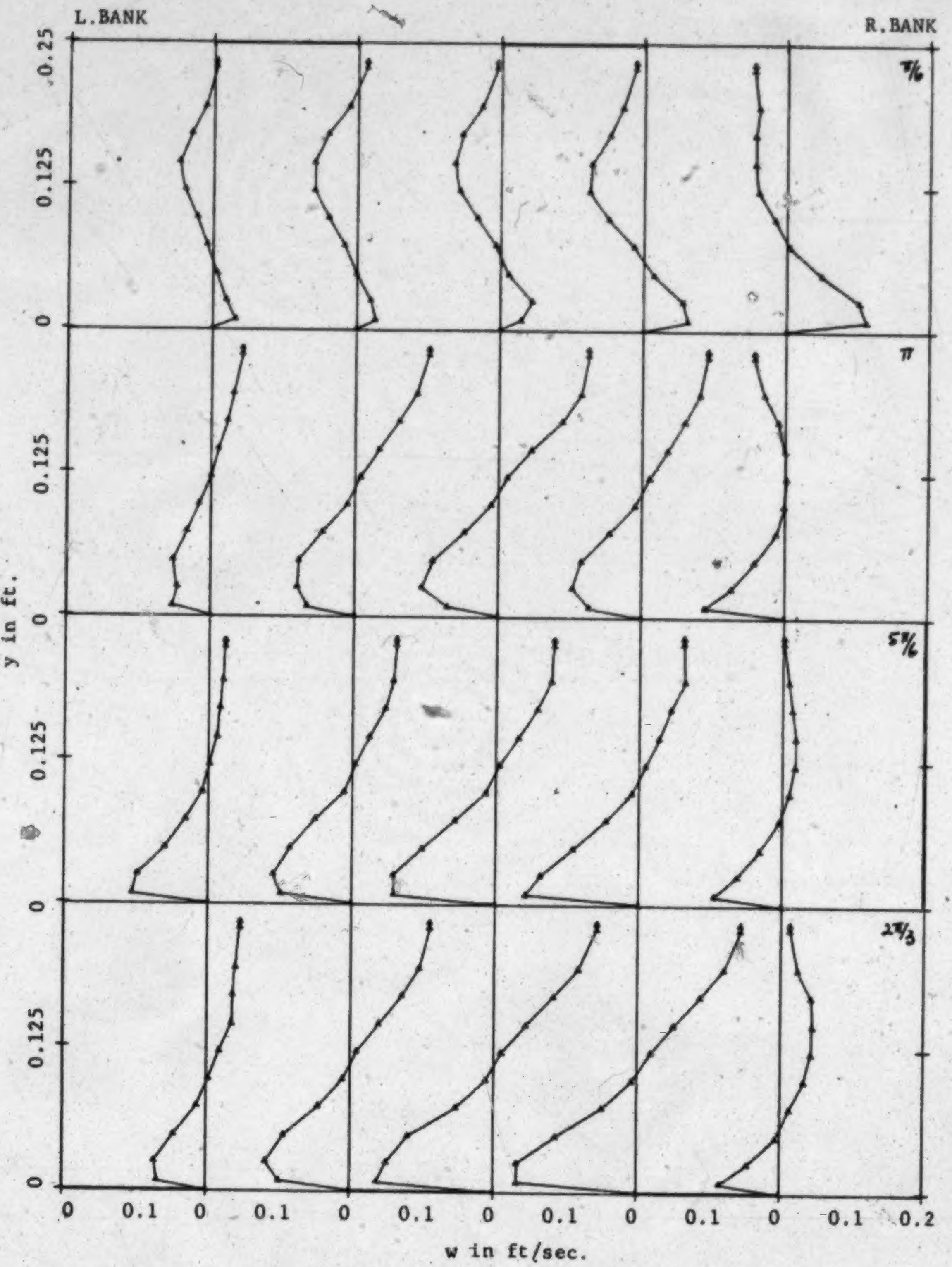

FIGURE 5.9b VERTICAL DISTRIBUTIONS OF TRANSVERSE VELOCITY,
RUNS 301/2/3, SECTIONS $\theta_1 = 2\pi/3$ TO $\theta_2 = \pi/6$

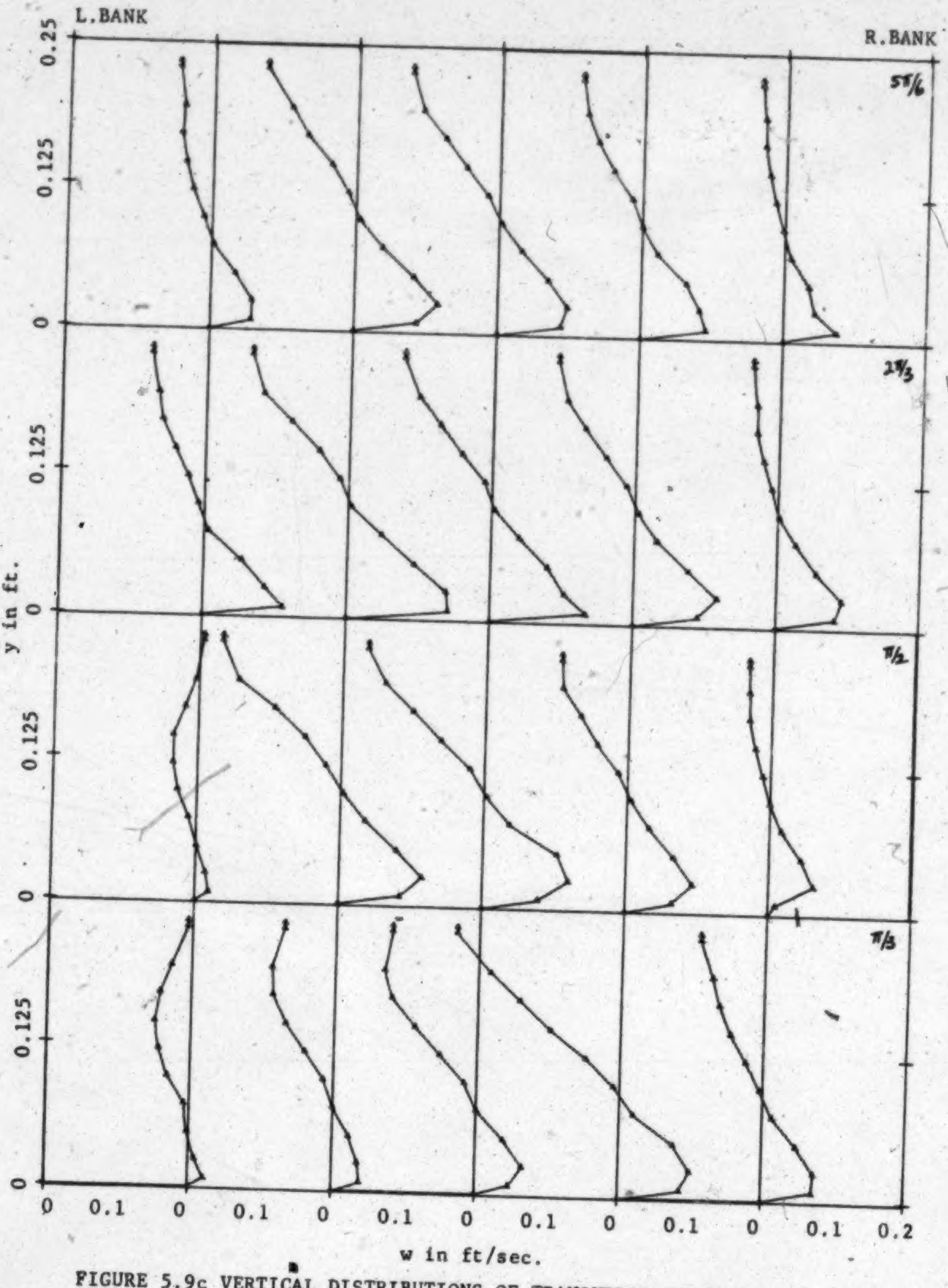

FIGURE 5.9c VERTICAL DISTRIBUTIONS OF TRANSVERSE VELOCITY, RUNS 301/2/3, SECTIONS $\theta_2 = \pi/3$ TO $5\pi/6$.

S therefore denotes the sum of the inward and outward unit lateral discharges and is very convenient for computational purposes. The longitudinal variation of S is presented in Figure 5.10, where the solid lines describe the centerline variation of S and the plotted points represent the variation of S within the central 40% of the flume.

Since the sense of rotation of the spiral motion reverses in the second bend the spiral motion strength, S , in this bend should be represented differently from that in the first bend. However, because the number of lateral point velocity measurements was small it was not possible to account properly for the residual spiral motion from the first bend in the second bend. Therefore, in Figure 5.10 S is plotted with the same sign for both bends. The stream function cannot be used as an alternative parameter because the flows are three-dimensional.

The strength of the spiral motion varied laterally in all cross-sections as illustrated in Figure 5.11 for run 407. When this figure is compared with Figure 5.14c it is seen that the shift of the region of highest spiral motion strength from one bank to the other generally follows a pattern which is similar to that of the maximum velocity filament.

It is evident, from Figure 5.7 and from the fact that there was neither a section with zero lateral discharge nor any flow parameters independent of x , that the fully developed bend flow condition was not attained in any of the test runs.

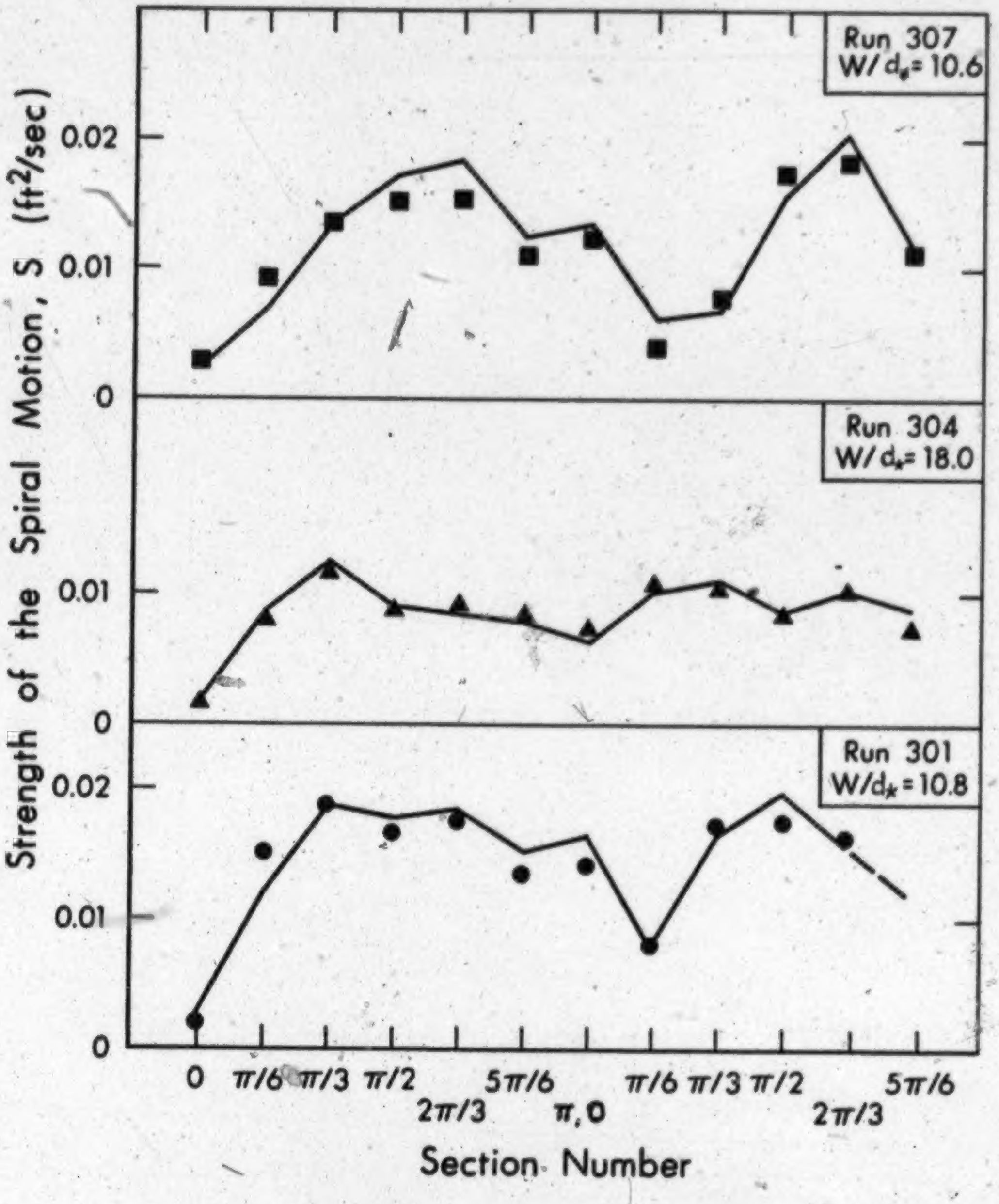

FIGURE 5.10 LONGITUDINAL VARIATION OF THE STRENGTH OF SPIRAL MOTION NEAR CHANNEL CENTERLINE FOR OPEN CHANNEL EXPERIMENTS

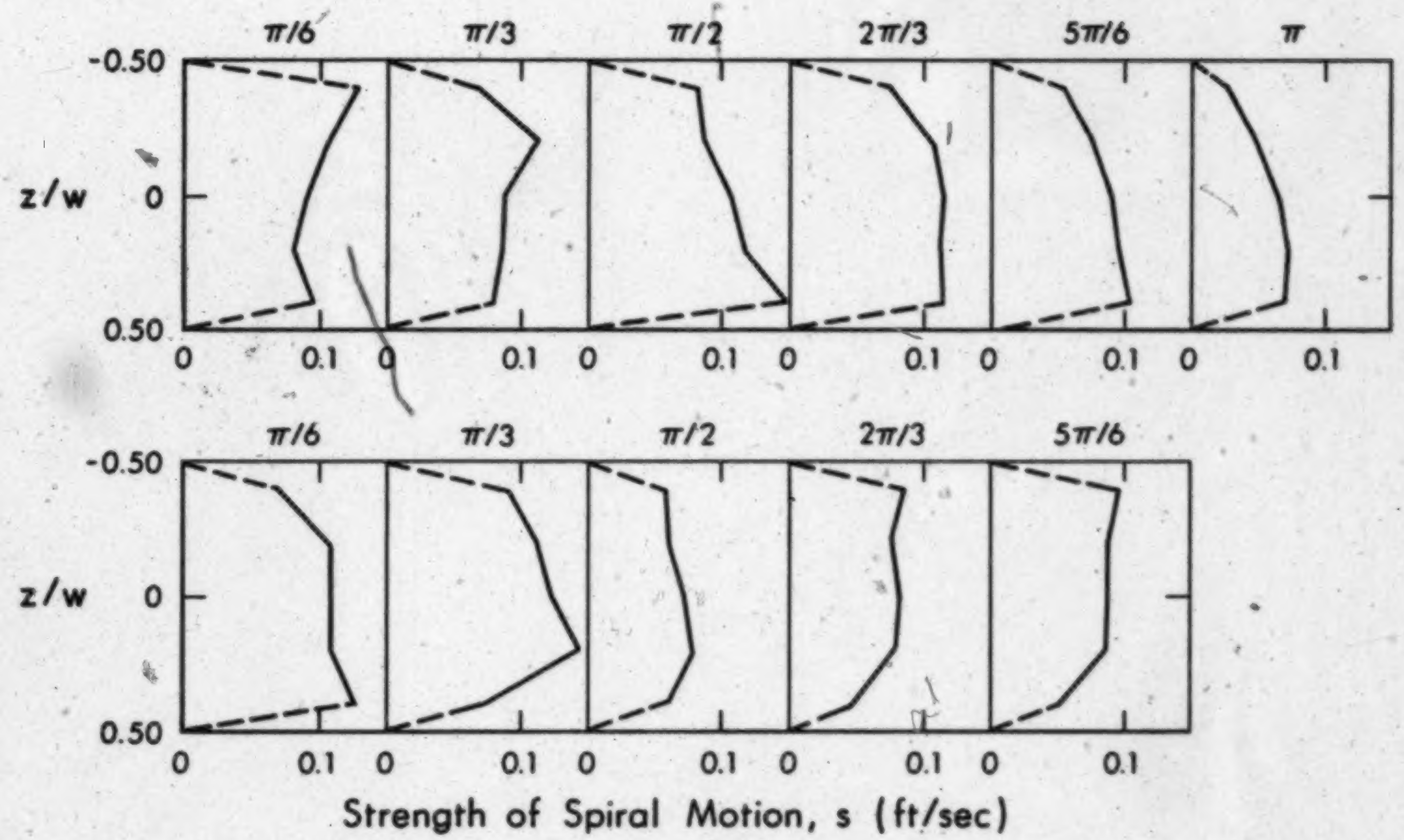

FIGURE 5.11 TRANSVERSE AND LONGITUDINAL VARIATION OF STRENGTH OF SPIRAL MOTION, RUN 407

All the test runs indicate the presence of transverse circulation at the beginning of the first bend and the spiral motion develops relatively faster in the rough bed experiments, runs 301 and 304, compared with the smooth bed experiment, run 307. It attained its peak near $\theta_1 = \pi/3$ for the rough bed experiments and at $\theta_1 = 2\pi/3$ for the smooth bed test. Further downstream, but still in the first bend, the spiral motion gradually starts to weaken. Yet at $\theta_1 = \pi$ or $\theta_2 = 0$ it still retained considerable intensity. Minimum values of S, the strength of the spiral motion, were recorded between $\theta_2 = 0$ and $\theta_2 = \pi/6$.

Downstream of $\theta_2 = 0$ the helical motion due to the second bend begins to grow and occupy an increasing area of the flow cross-section (see Figure 5.9 and Figures A.3 and A.4 of Appendix A). At the same time it displaces the residual spiral motion from the first bend towards the outside of the bend removing it completely between $\theta_2 = \pi/3$ and $\theta_2 = 2\pi/3$.

The results tend to show that the decay of residual circulation from the first bend is controlled by the roughness and width-to-depth ratio. The residual spiral motion persisted over a longer reach for the smooth bed flow than for the rough bed flows. It was also observed that the residual circulation decays relatively faster for large W/d_* ratios. These observations are in agreement with the findings of Yen (1965). The helical motion due to the second bend did not reach its peak strength until after the residual spiral motion had decayed completely. It then decays towards the bend exit because of the presence of the tail-gate.

Maximum observed transverse velocities near the bed were slightly larger in the first bend than in the second bend. On the other hand the transverse velocities near the free surface were approximately the same for both bends except in run 307 where higher transverse surface velocities were recorded in the second bend. Most vertical profiles indicated the reduction in the transverse velocity near the bed beginning further from the bed for the rough bed flows (runs 301 and 304) than for the smooth bed flow (run 307). As could be anticipated, the transverse velocities are smaller near the side-walls than within the central portions of the flow. Near the walls the vertical velocity components become important and continuity considerations require that the w-component decrease.

5.2.2.3 Angle of Deviation of the Velocity Vector: The variation of the horizontal angle of deviation of the velocity vector, ψ , in the vertical and lateral directions is presented in Figure 5.12 and Figures A.5 and A.6 of Appendix A. The angle ψ can be regarded as an indicator or measure of the spiral motion since $\psi = \tan^{-1}(w/u)$. The maximum inward angle occurred near the channel bed and the maximum outward angle near the free surface. In general $|\psi_{\tilde{y}=o}| > |\psi_{\tilde{y}=D}|$ for most verticals. The zero angle of deviation in a vertical was located in the lower half of the depth for practically all verticals.

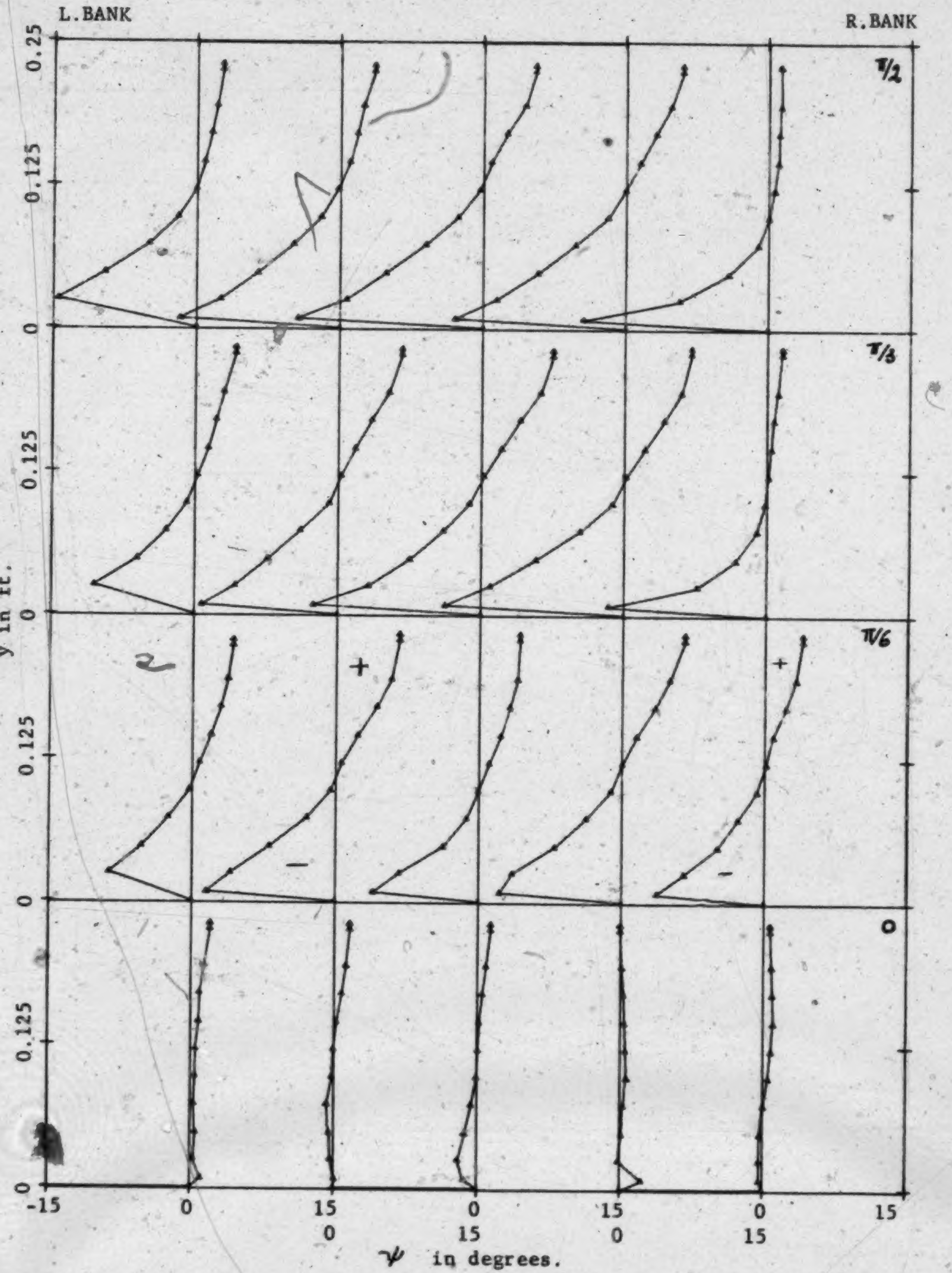

FIGURE 5.12a VERTICAL DISTRIBUTIONS OF HORIZONTAL ANGLE OF VELOCITY VECTOR, RUNS 301/2/3. SECTIONS $\theta_1 = 0$ TO $\pi/2$

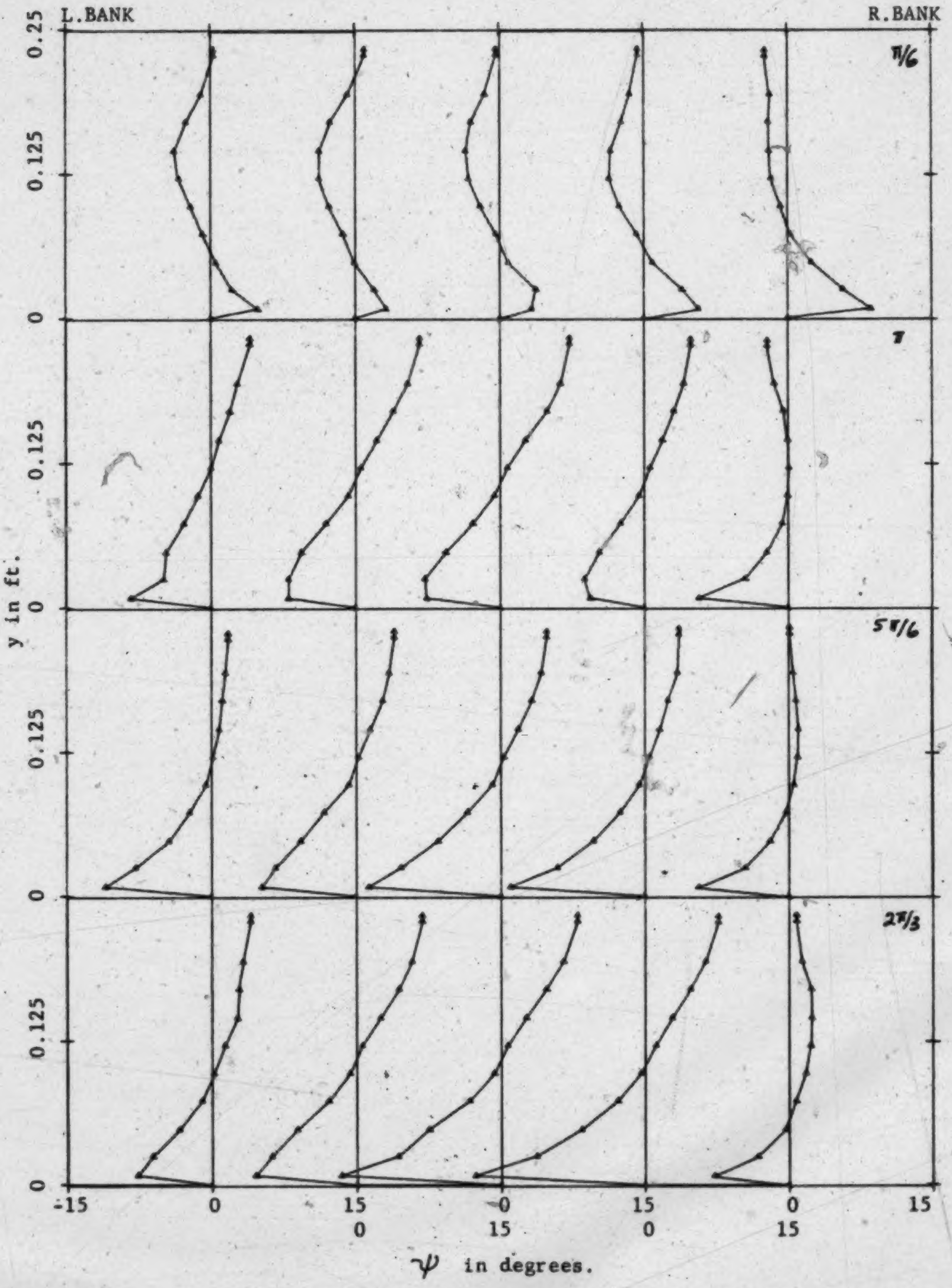

FIGURE 5.12b VERTICAL DISTRIBUTIONS OF HORIZONTAL ANGLE OF VELOCITY VECTOR, RUNS 301/2/3, SECTIONS $\theta_1 = 2\pi/3$ TO $\theta_2 = \pi/6$.

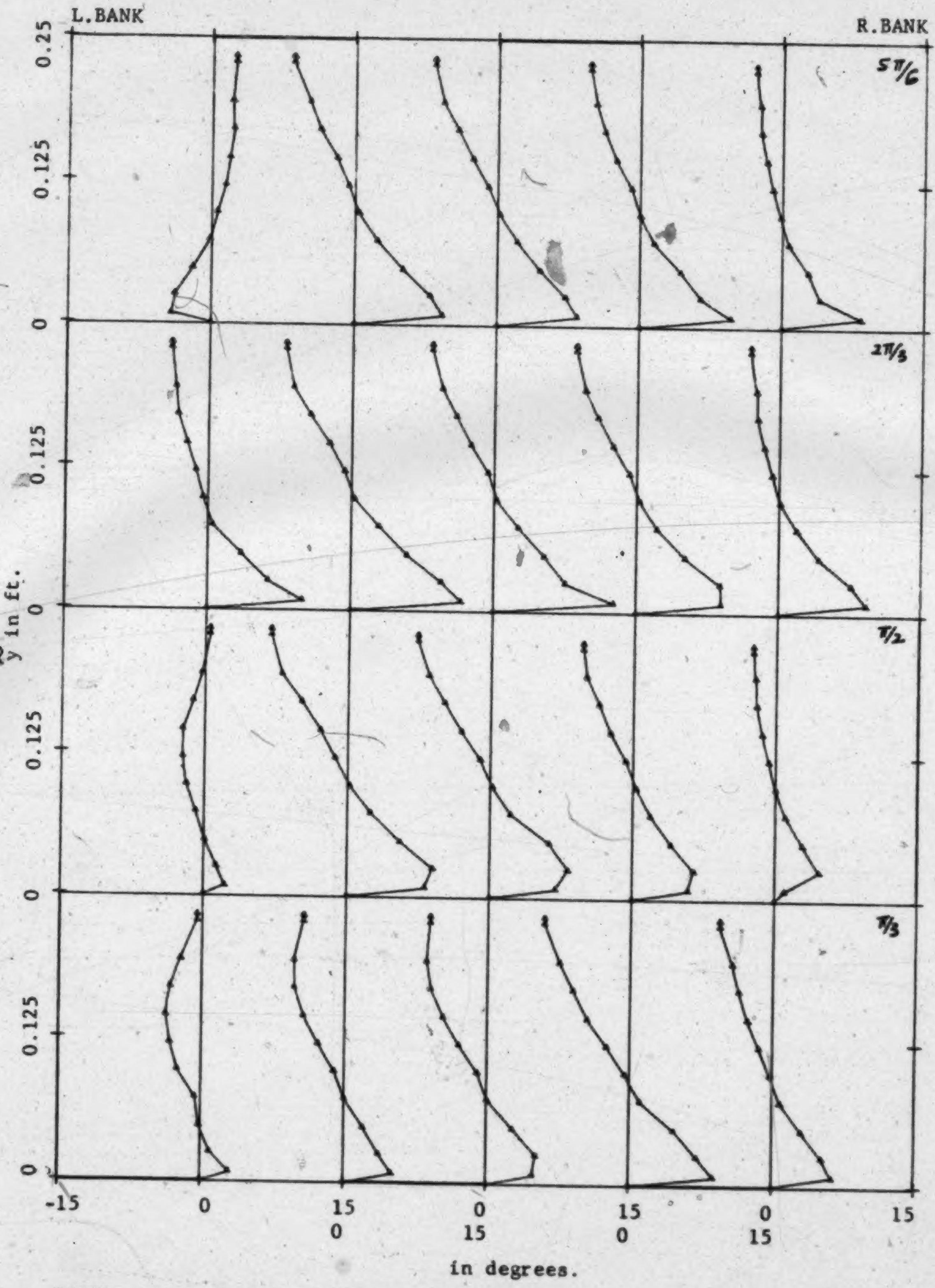

FIGURE 5.12c VERTICAL DISTRIBUTIONS OF HORIZONTAL ANGLE OF VELOCITY VECTOR, RUNS 301/2/3, SECTIONS $\theta_2 = \pi/3$ TO $5\pi/6$.

According to Yen (1972) and Rozovskii (1963) tan ($|\psi_{\tilde{y}\approx o}|$) varies approximately with the product $\frac{d_*}{r_c}\,\frac{1}{\kappa^2}$ (where κ is von Karman's constant). Rozovskii recommends that for both smooth and rough channel beds tan ψ near the bed be approximated by (10-12) d_*/r for fully developed bed flow. The observed maximum values of $\psi_{\tilde{y}\approx o}$ are compared with Rozovskii's approximation in Table 5-3.

TABLE 5-3 COMPARISON OF OBSERVED AND COMPUTED $\psi_{y\approx o}$ VALUES

Run Number	d_*/r_c	$\psi_{\tilde{y}\approx o} = \tan^{-1}[(10-12)\frac{d_*}{r_c}]$	Experimental $\psi_{\tilde{y}\approx o}$	Remarks
301	1/39	14.4° - 17.1°	19.3°	Rough bed
304	1/64.7	8.8° - 10.5°	13.6°	Rough bed
307	1/38.3	14.6° - 17.4°	16.3°	Smooth bed

The values of $\psi_{\tilde{y}\approx o}$ observed in this study are of the same order of magnitude as those given by Rozovskii's relation. However, the observed ψ values contain measurement errors due to inaccuracy of the yaw probe in steep velocity gradients. Also it is noted that the width to depth ratio does not appear in Rozovskii's approximation for $\psi_{\tilde{y}\approx o}$ and yet experimental evidence (Rozovskii, 1963) indicates that it has a significant influence on the development and decay of the spiral motion and also on $\psi_{\tilde{y}\approx o}$.

5.2.3 Velocity Measurements in Ice-Covered Meandering Flume

One characteristic difference between flows in ice-covered and open channel bends is the formation of a double transverse circulation or spiral motion in ice-covered bends due to the presence now of velocity gradients at both the bed and the ice-cover. In this section some properties of flow under ice-cover conditions are described and compared with those observed for open water conditions.

5.2.3.1 Longitudinal Velocity Component: The longitudinal velocity measurements are presented graphically in Figure 5.13a, b, c for run 404. The velocity data for other test runs in series 400 are given in Figures A.7 and A.8 of Appendix A. Near the outside of the bend there is transport of high momentum fluid from the central portions of the flow to the top and bottom layers. This is expected to produce a fairly uniform distribution of the longitudinal velocity over a substantial portion of the depth on this side of the bend. The same effect on the longitudinal velocity distribution near the inside of the bend is anticipated by the transfer of low momentum fluid from the top and bottom layers to the central portion of the flow. The above observations were found to be valid for many cross-sections especially near the inside bend for runs 401 and 407 but not for run 404. In this run, the transverse velocities were much less than the longitudinal velocities and consequently the transport of low momentum fluid by the spiral motion to the central portion of the flow did not cause any noticeable change in the longitudinal velocity profile near the inside of the bend.

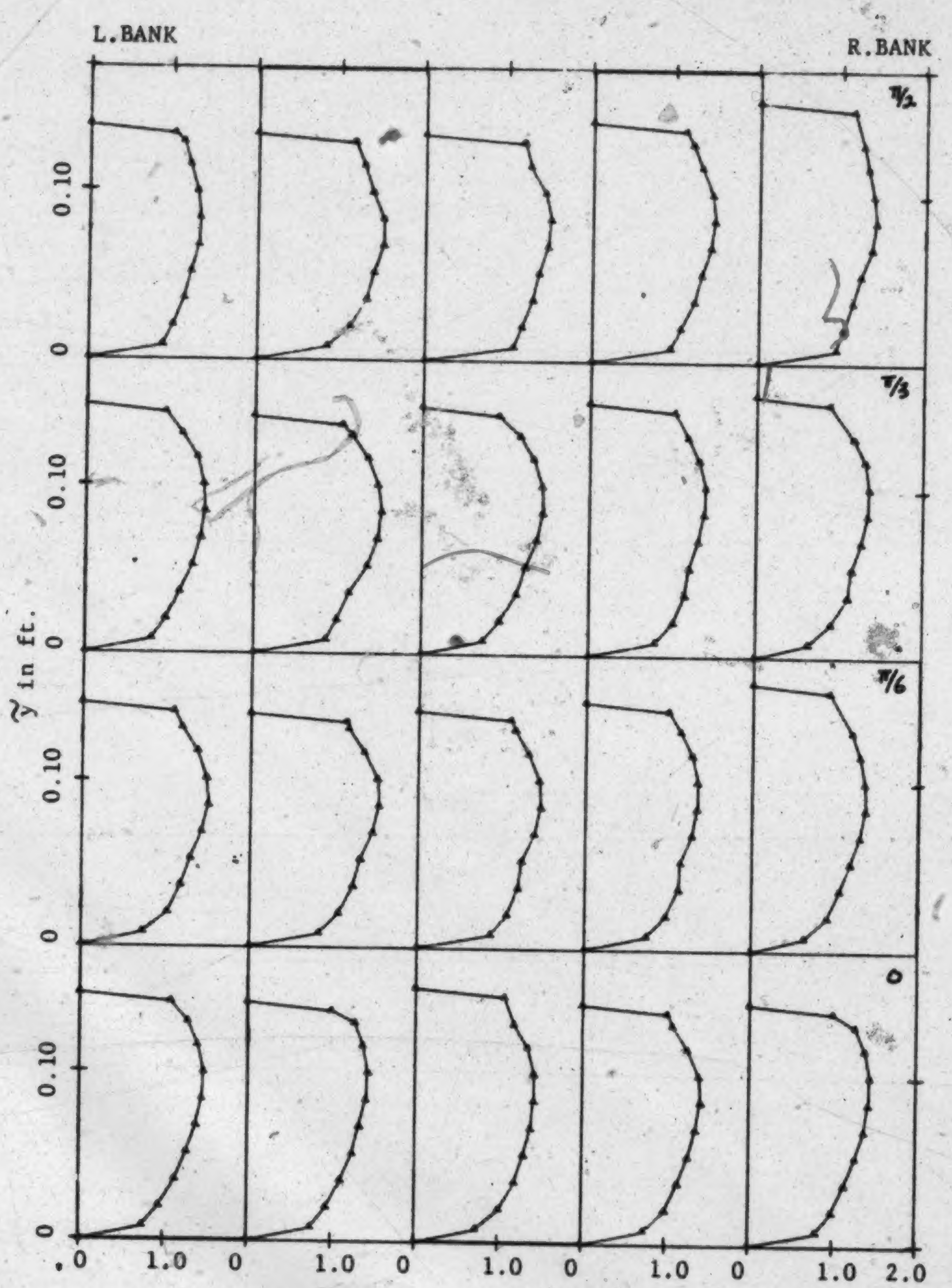

FIGURE 5.13a VERTICAL DISTRIBUTIONS OF LONGITUDINAL VELOCITY

Runs 404/5/6. SECTIONS θ_1 = 0 TO π/2

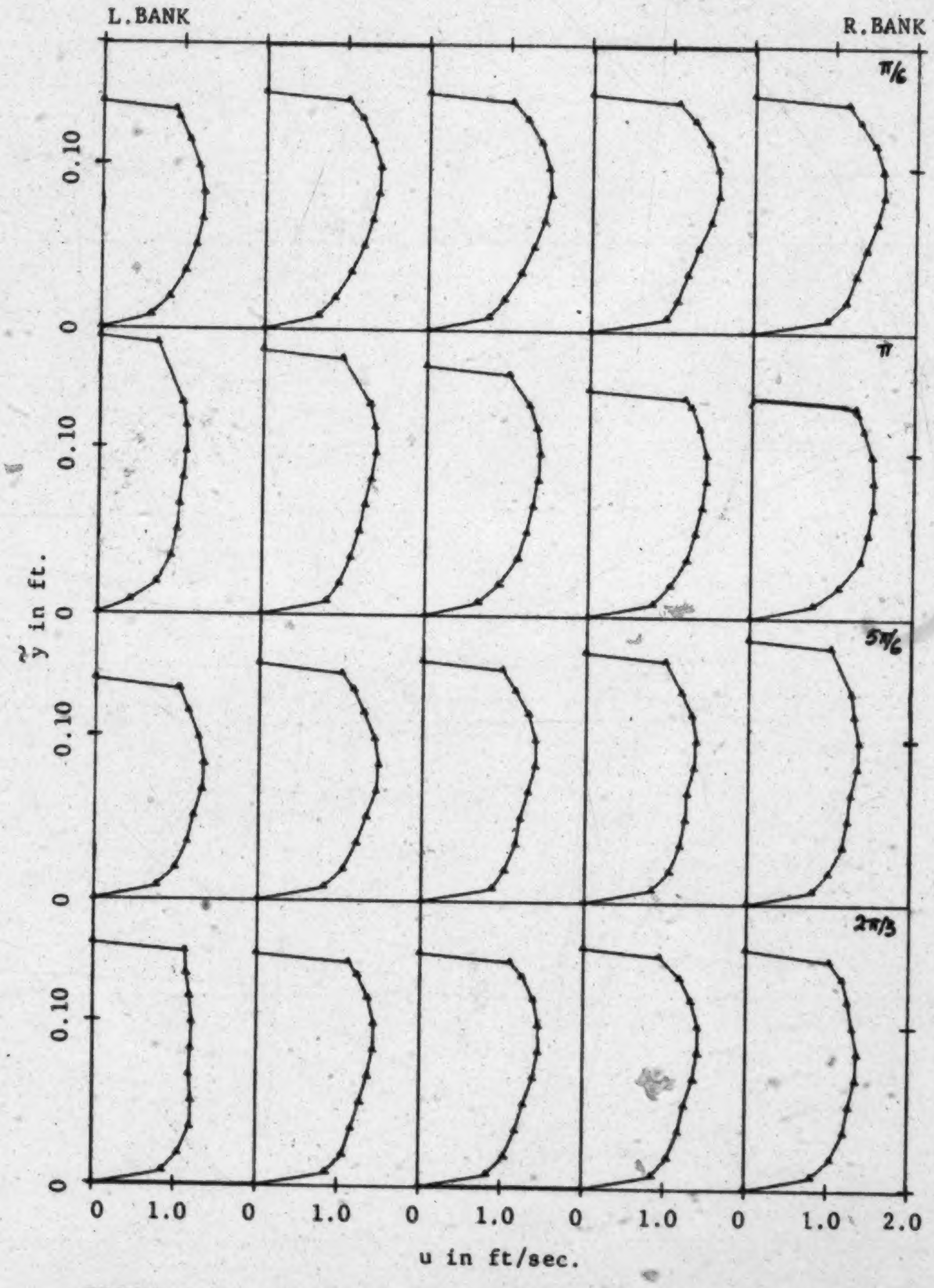

FIGURE 5.13b VERTICAL DISTRIBUTIONS OF LONGITUDINAL VELOCITY Runs 404/5/6. SECTIONS $\theta_1 = 2\pi/3$ TO $\theta_2 = \pi/6$

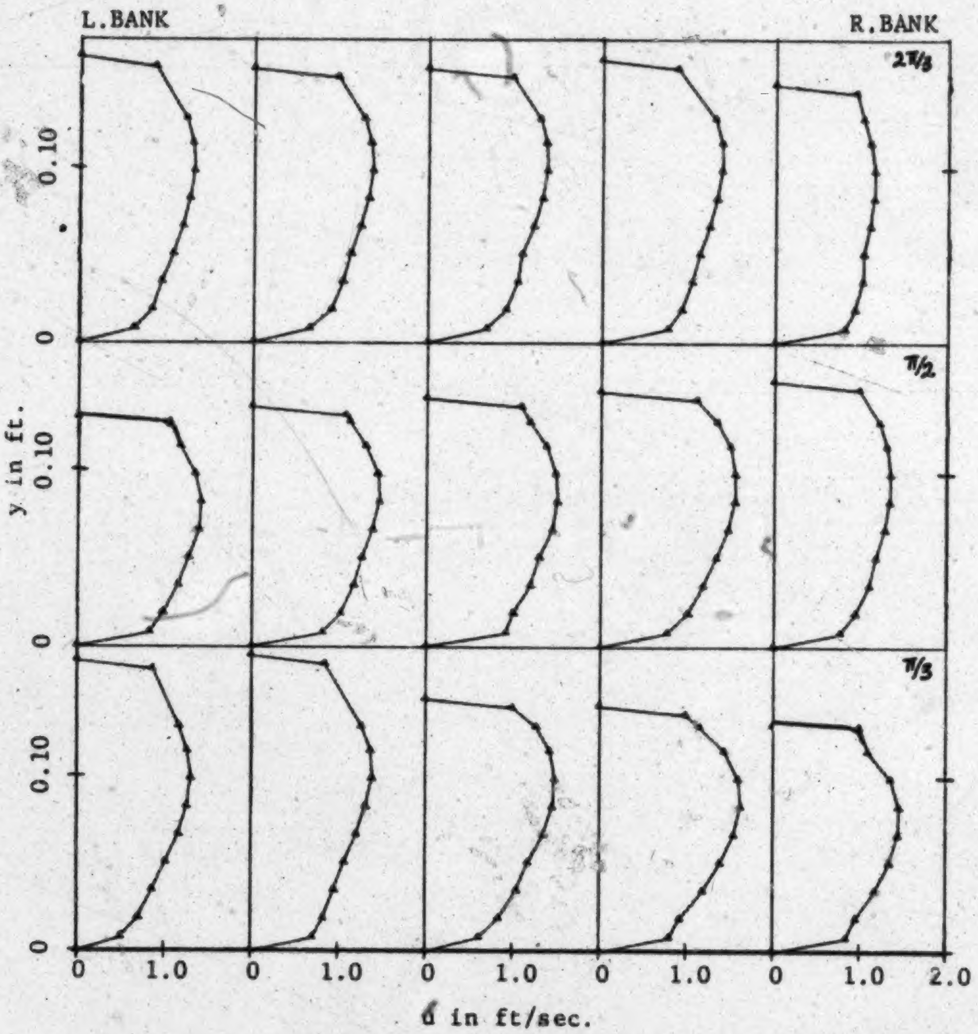

FIGURE 5.13c VERTICAL DISTRIBUTIONS OF LONGITUDINAL VELOCITY, Runs 404/5/6. SECTIONS $\theta_2 = \pi/3$ to $2\pi/3$

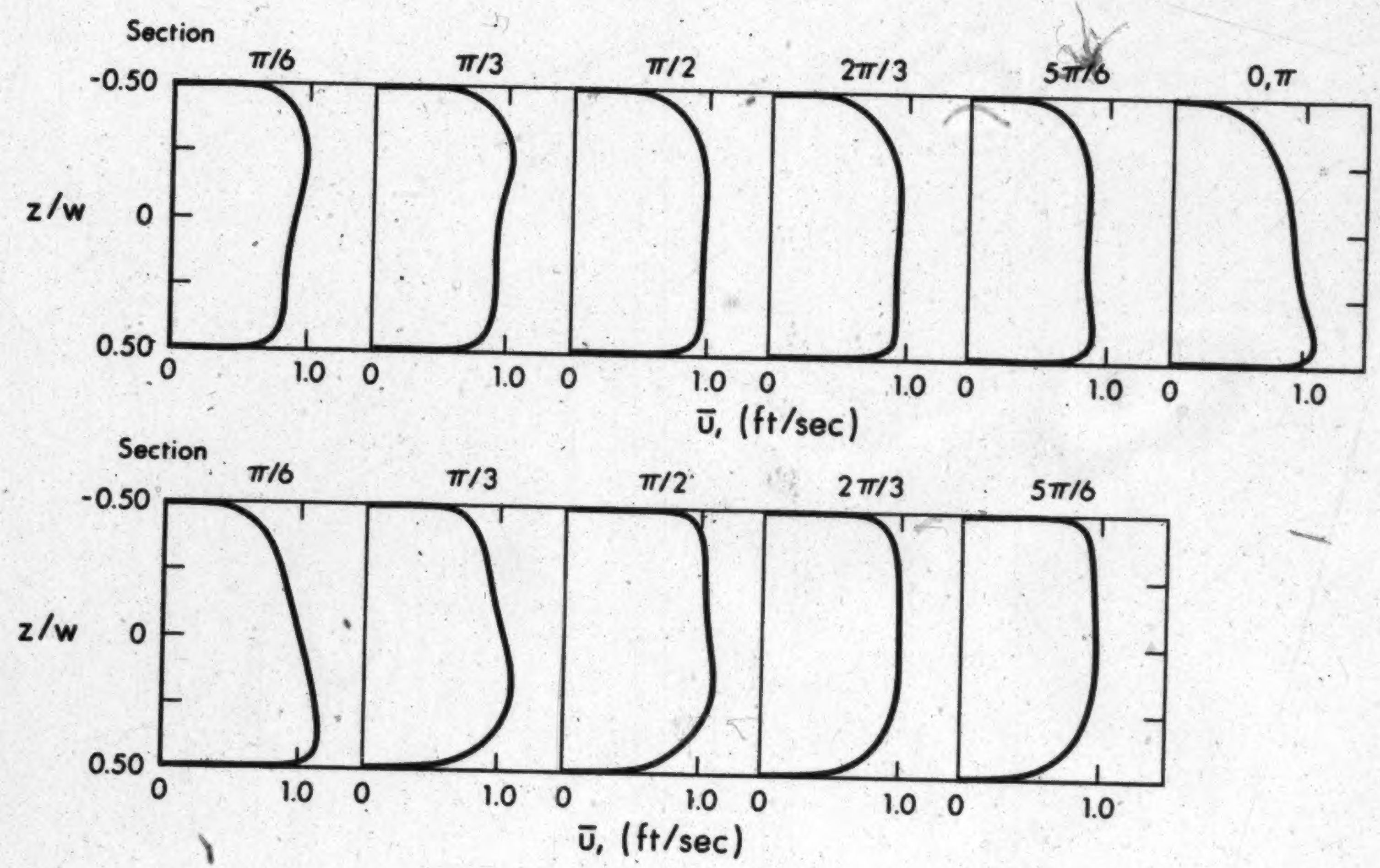

FIGURE 5.14a LATERAL DISTRIBUTIONS OF DEPTH-AVERAGED LONGITUDINAL VELOCITY RUNS 401/2/3

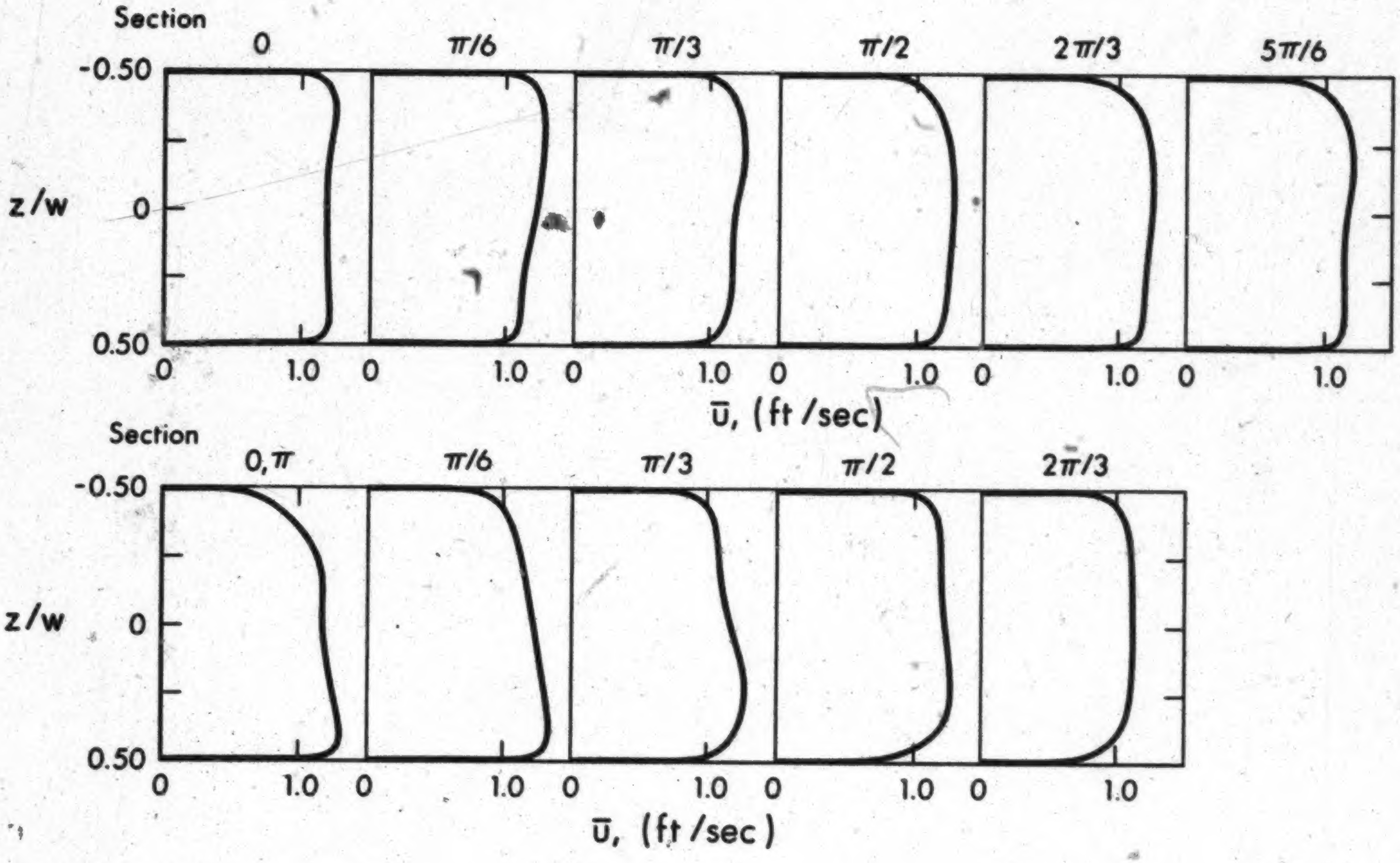

FIGURE 5.14b LATERAL DISTRIBUTIONS OF DEPTH-AVERAGED LONGITUDINAL VELOCITY RUNS 404/5/6

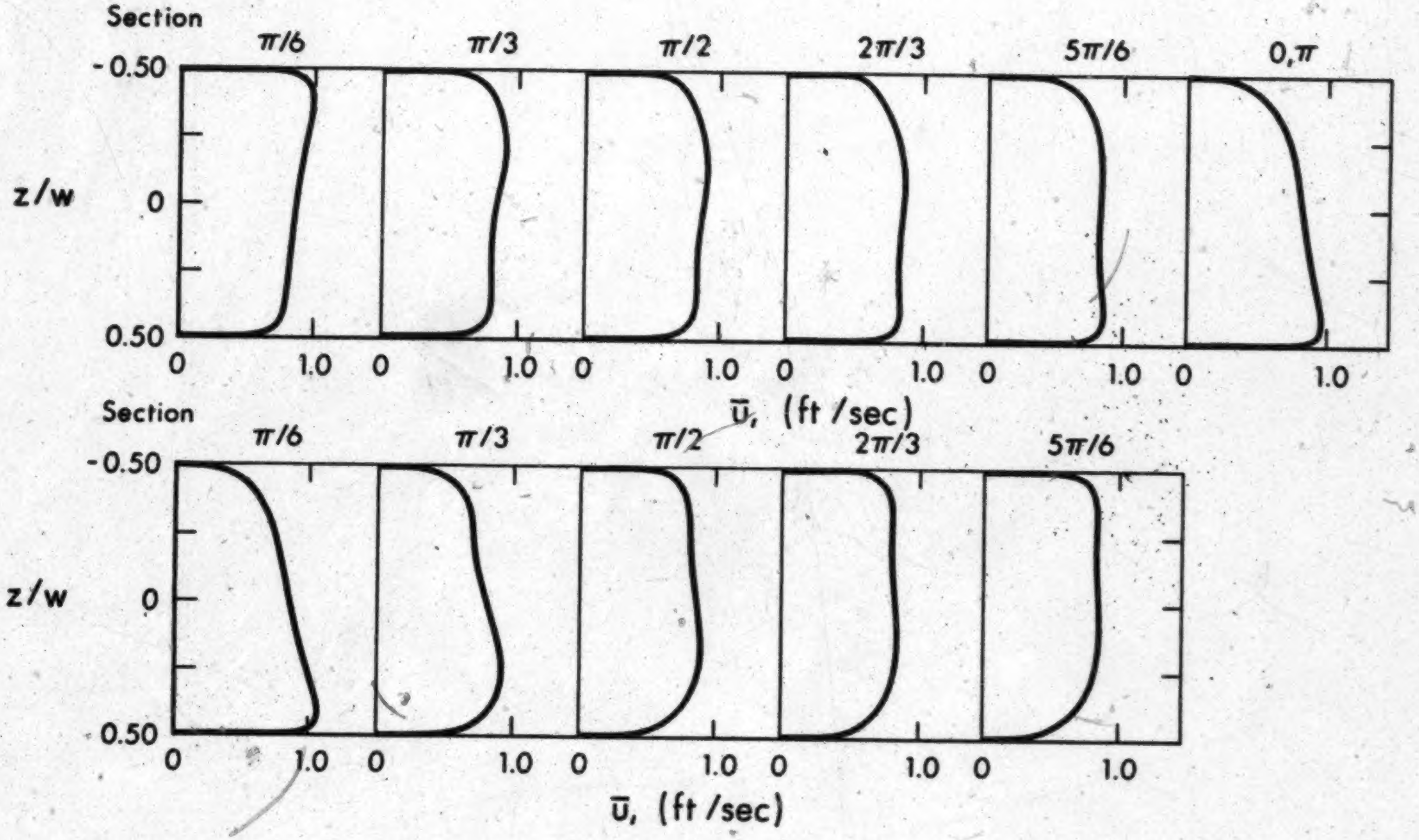

FIGURE 5.14c LATERAL DISTRIBUTIONS OF DEPTH-AVERAGED LONGITUDINAL VELOCITY RUNS 407/8

For the rough bed experiments, that is runs 401 and 404, the maximum velocity was generally located between 0.50 to 0.70 of the local depth from the channel bottom. With a smooth bed it was close to mid-depth (Figure A.8).

The lateral distribution of depth-averaged longitudinal velocity along the two bends is given in Figure 5.14a, b, c. The high velocity portion of the flow is again initially located near the inside bend but starts to depart from it after $\theta_1 = \pi/6$. On emerging from the first bend the fluid near the inside of the second bend is further accelerated and this results in a pronounced non-uniformity in the lateral distribution of $\overline{u}$ similar to that observed for the open channel tests. Downstream of $\theta_2 = \pi/3$ the high velocity filament again gradually crosses over to the outer bend. The displacement of the high velocity area from one side of the bend to the other was observed to be relatively more gradual with an ice-cover than the corresponding open channel tests and is probably due to increased resistance to the flow.

The variation of the dimensionless mean square velocity deviation, δ, is presented in Figure 5.8. In general, the longitudinal variation of δ was similar to that observed for the open channel tests especially within the second bend. Also the average value of δ for run 401 (rough bed) was higher than that for run 407 (smooth bed). Both runs had approximately the same W/d_* and U_o. The same was observed for runs 301 and 307 in the open channel tests. This phenomenon is probably caused by the combined effects of the spiral motion and the non-uniform distribution of ice-cover and bed shear. The non-uniformity of the transverse depth-averaged longitudinal velocity profile increased with width-depth ratio for both ice-cover and open water experiments but the variation was smaller for ice-cover flows.

5.2.3.2 Lateral Velocity Component: The measured local lateral velocity components are shown in Figure 5.15a, b, c for run 404 and Figures A.9 and A.10 of Appendix A for runs 401 and 407. They illustrate clearly the growth and decay of the spiral motion. Two spiral motions with opposite sense of rotation were observed for most cross-sections. The bottom spiral motion generally occupied more than one-half the flow depth for the rough bed experiments. In the smooth bed experiments, run 407, each spiral motion was confined to approximately one-half the flow depth. The longitudinal variation of the strength of the spiral motion, S , is presented in Figure 5.16. The S-values for the ice-cover experiments include the effects due to the warping of the plywood used as the ice-cover. Substantial warping was noticed in some sections of the ice-cover. At $\theta_2 = \pi/2$ of run 404, for example, (see Figure 5.15) the greatest depth of flow was located on the inside instead of the outside bend as would have been expected.

Transverse circulation was present at $\theta_1 = 0$ and is obviously a manifestation of the lateral pressure gradient associated with the curvilinear nature of the flow. The spiral motions attained peak strength between $\theta_1 = \pi/6$ and $\theta_1 = \pi/3$ in runs 401 and 404. However, for run 407 (smooth bed) the spiral motions did not reach maximum strength within

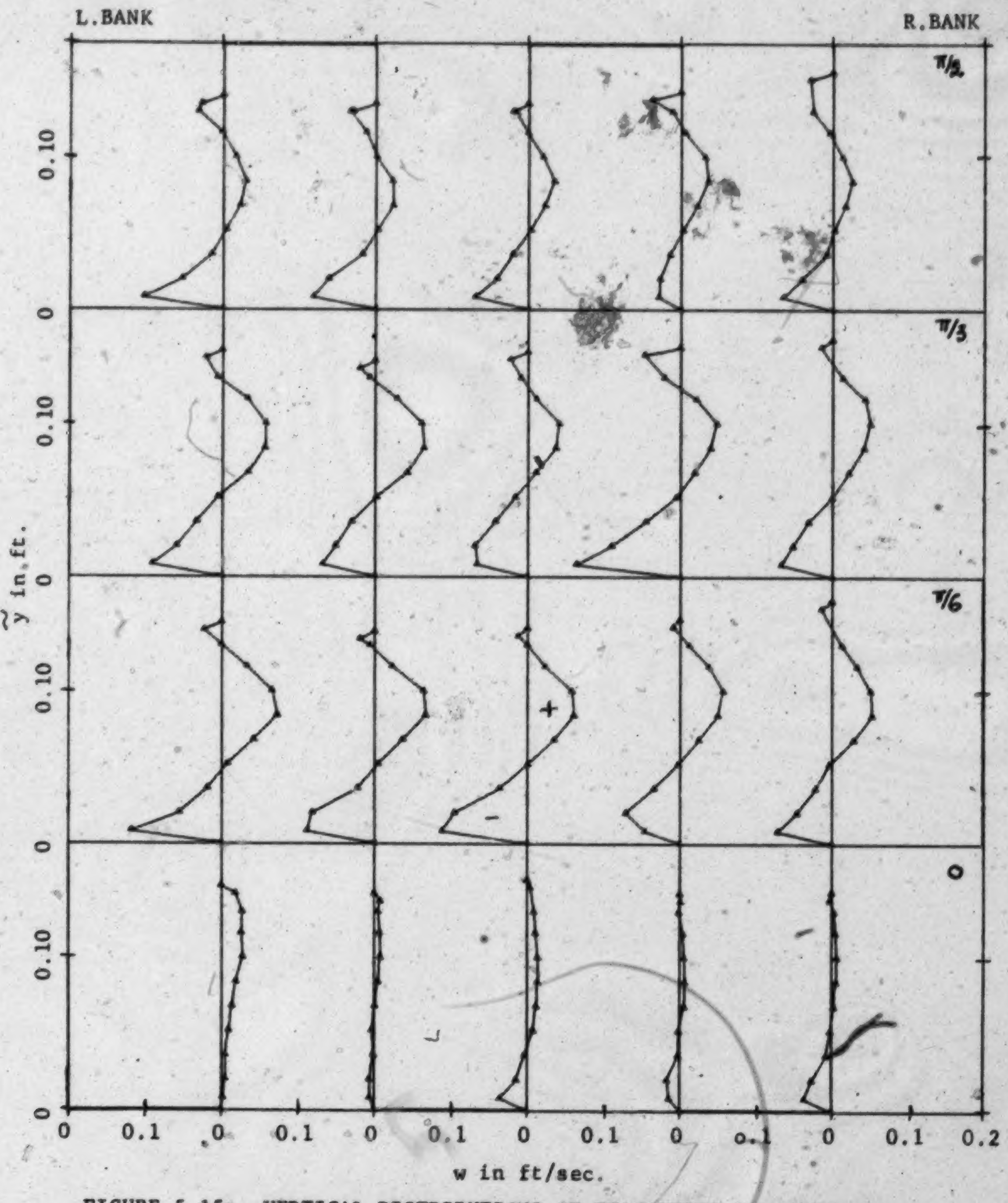

FIGURE 5.15a VERTICAL DISTRIBUTIONS OF TRANSVERSE VELOCITY, Runs 404/5/6. SECTIONS θ₁ = 0 to π/2.

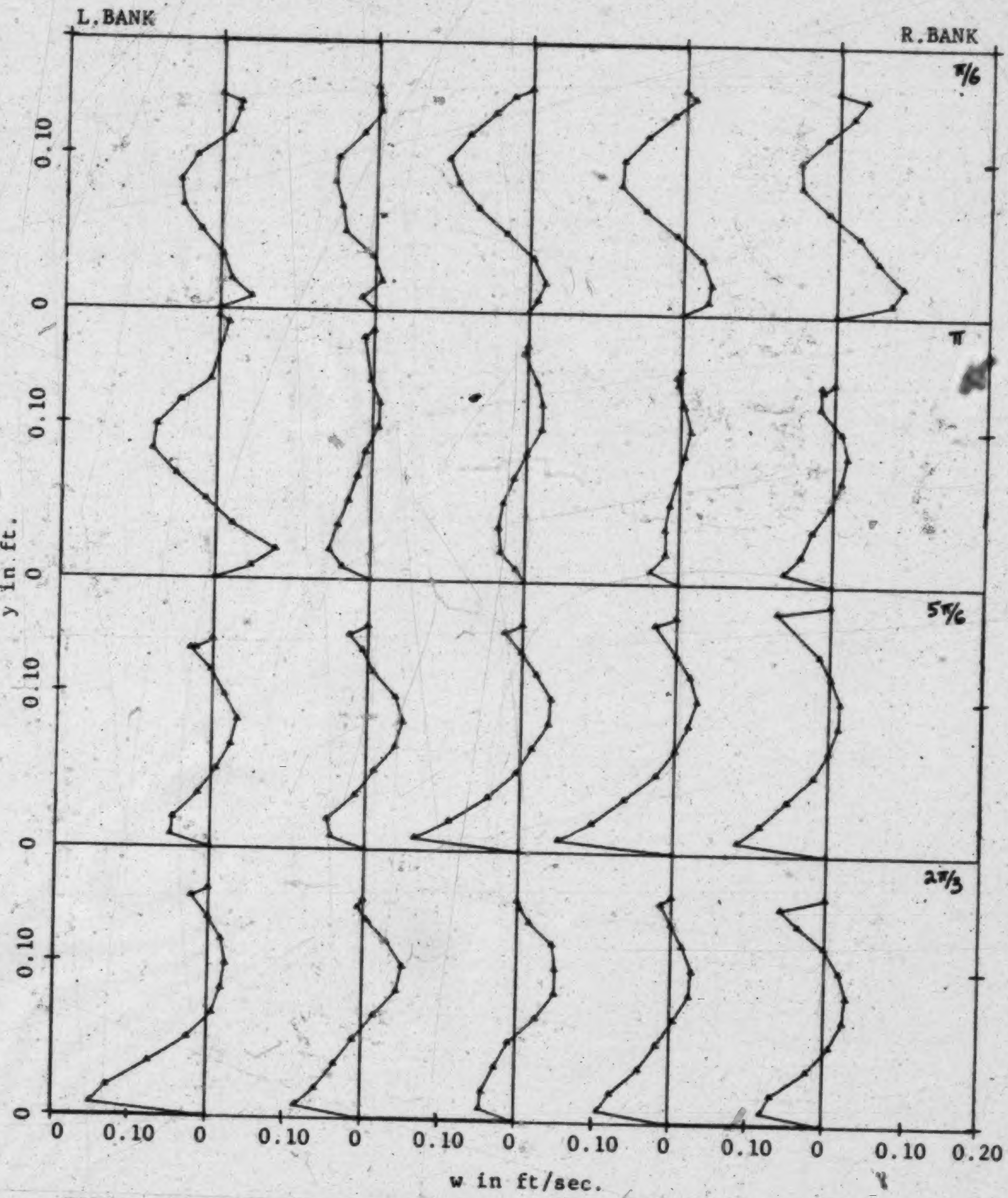

FIGURE 5.15b VERTICAL DISTRIBUTIONS OF TRANSVERSE VELOCITY, Runs 404/5/6. SECTIONS $\theta_1 = 2\pi/3$ TO $\theta_2 = \pi/6$.

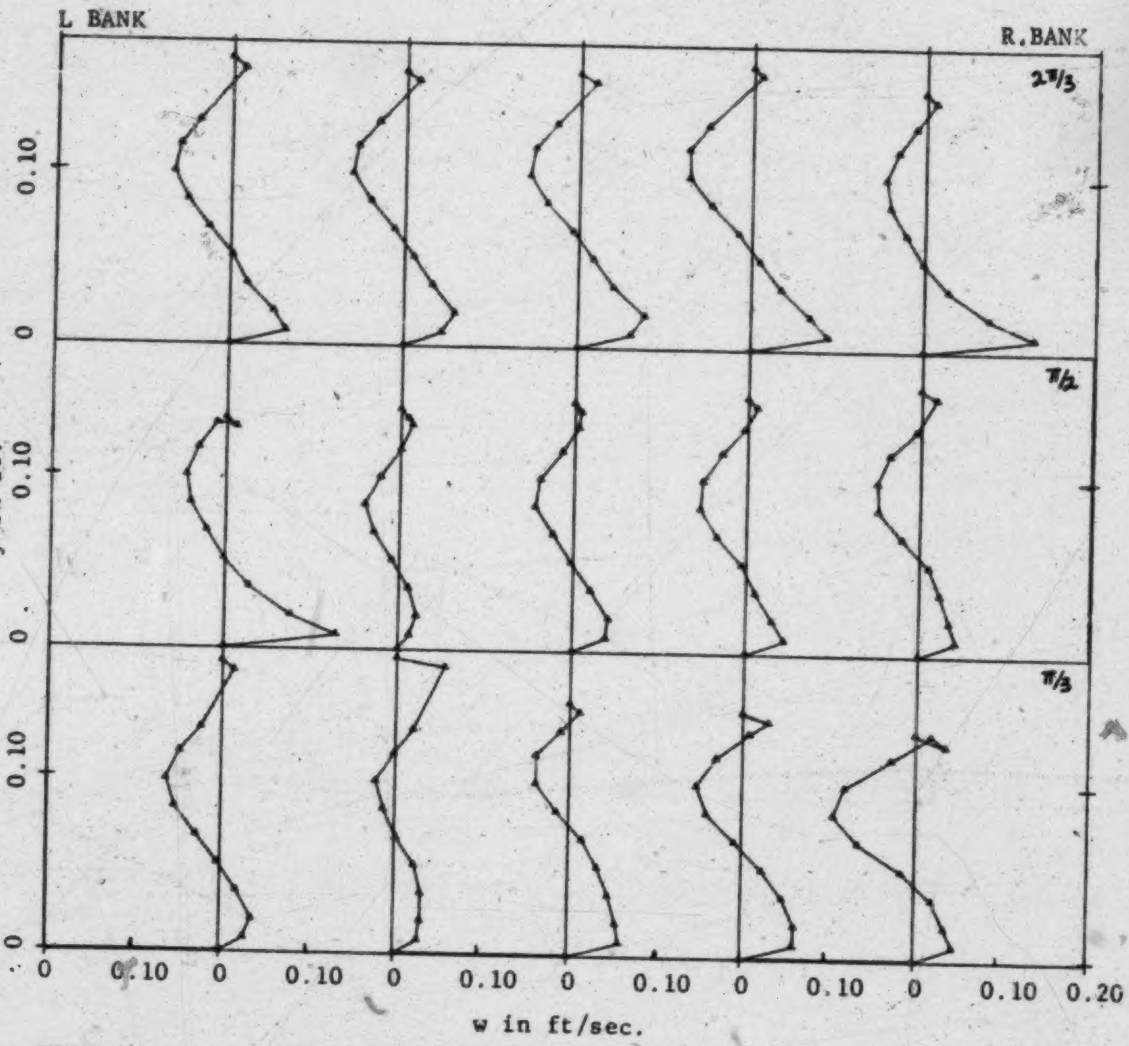

FIGURE 5.15c VERTICAL DISTRIBUTIONS OF TRANSVERSE VELOCITY, Runs 404/5/6. SECTIONS θ_2 = π/3 TO 2π/3.

the first bend until $\theta_1 = 2\pi/3$. The variation of S for run 404 was rather erratic and is believed to have been caused by the warping of the ice-cover which had a marked effect on this run because of the small depth of flow.

The spiral motions diminished downstream of the section of maximum S to a minimum value at $\theta_1 = \pi$ or $\theta_2 = 0$ for all test runs. The gradual reduction in S within the middle of the first bend in run 401 (Figure 5.16) is probably caused by increased resistance to flow because of the presence of the ice-cover while the further drop in S at the exit of the first bend, for all test runs, is due to the presence of the second bend. In contrast to the open channel tests the spiral motions due to the second bend were observed to have penetrated the entire flow width at $\theta_2 = \pi/6$. This actually is not surprising because the average value of S within the first bend for the ice-cover experiments were about one-half the value for the corresponding open channel tests. Note that any two corresponding tests have the same experimental number in their respective series, e.g., runs 301 and 401. The new spiral motions in the second bend develop rapidly and peak between $\theta_2 = \pi/6$ and $\theta_2 = \pi/3$. They, however, decay near the bend exit because of the presence of a tail-gate at the end of this bend. By taking the average value of S for the two bends it is concluded that, for the W/d_* ratios used in the tests, the strength of the spiral motion is greater if the width to depth ratio is smaller. This conclusion was also found to be valid for the open channel experiments.

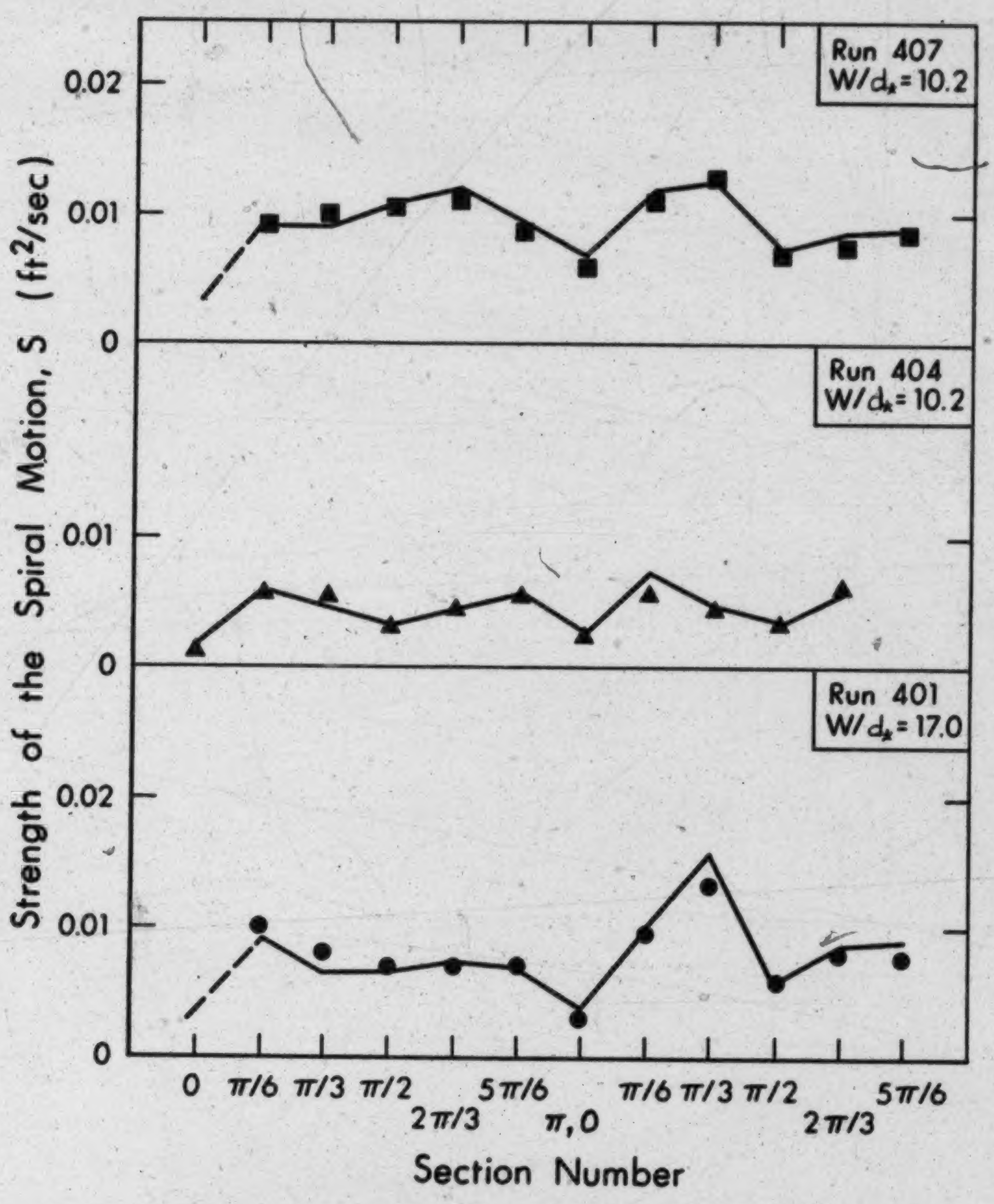

FIGURE 5.16 LONGITUDINAL VARIATION OF THE STRENGTH OF SPIRAL MOTION, S , NEAR CHANNEL CENTERLINE FOR ICE-COVER EXPERIMENTS

5.2.3.3 Horizontal Angle of Deviation of Velocity Vector:

Measurements of the local horizontal angle of deviation of the velocity vector, ψ , are given in Figures 5.17 for run 404 and Figures A.11 and A.12 of Appendix A for runs 401 and 407. The largest angle of deviation occurred near the channel bed. For runs 401 and 407 the observed $|\psi_{y\approx 0}|$ was 12° while that in run 404 was about 10°. These values are less than those observed for open channel tests and indicate that the strength of the spiral motion is comparatively less for ice-covered flows.

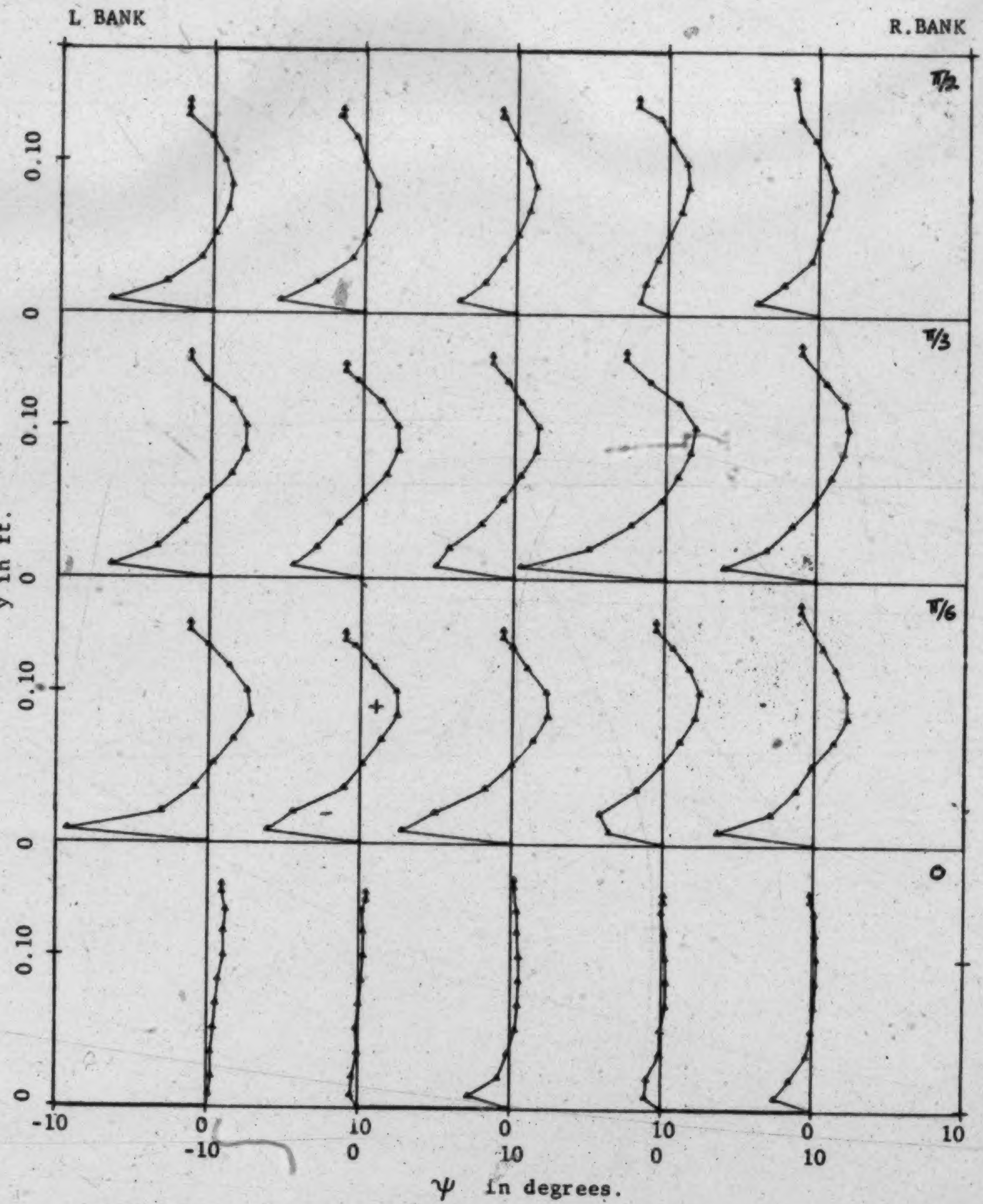

FIGURE 5.17a VERTICAL DISTRIBUTIONS OF HORIZONTAL ANGLE OF DEVIATION OF THE VELOCITY VECTOR, ψ, Runs 404/5/6. SECTIONS $\theta_1 = 0$ TO $\pi/2$.

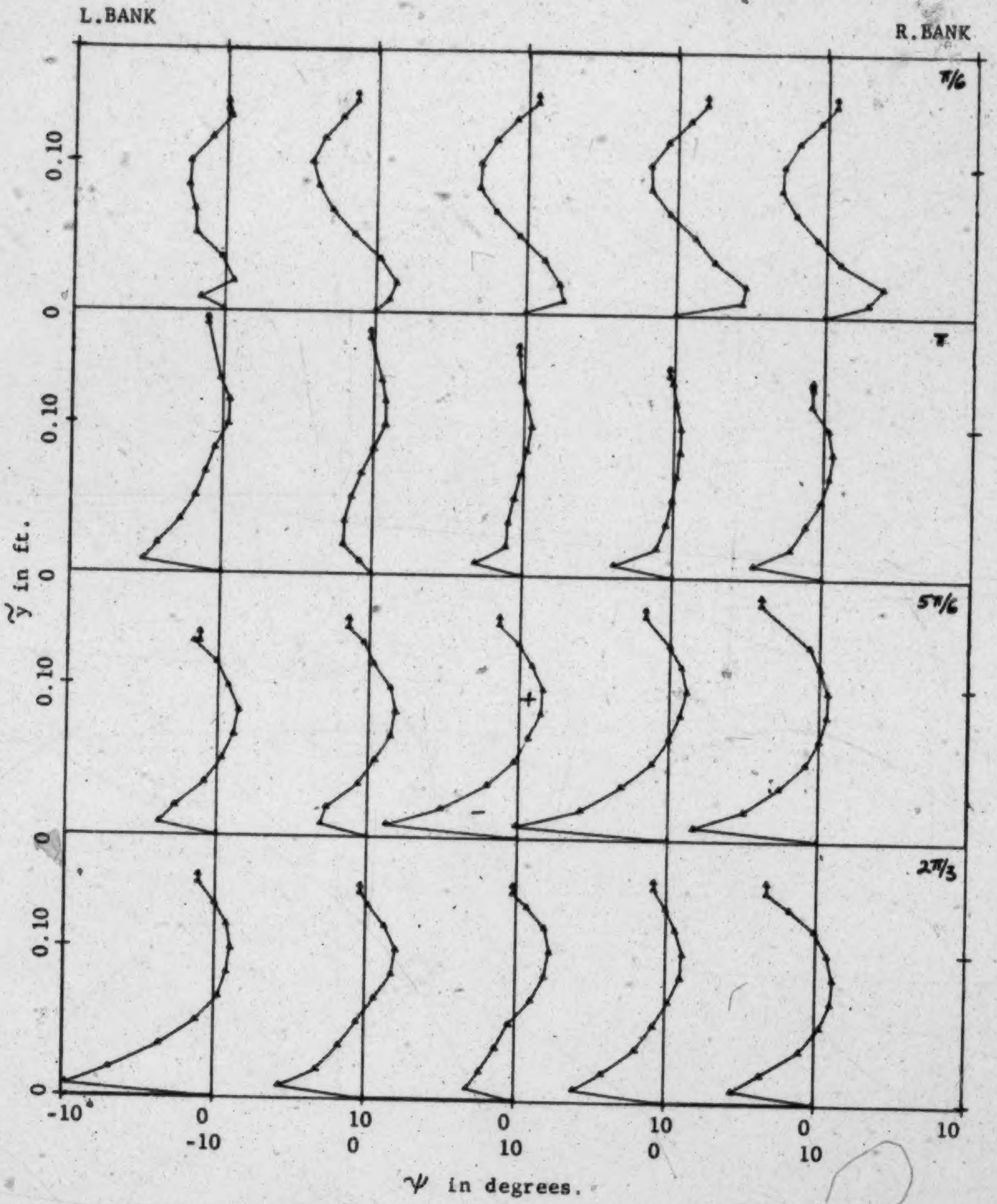

FIGURE 5.17b VERTICAL DISTRIBUTIONS OF HORIZONTAL ANGLE OF DEVIATION OF THE VELOCITY VECTOR, ψ. Runs 404/5/6. SECTIONS $\theta_1 : 2\pi/3$ TO $\theta_2 = \pi/6$

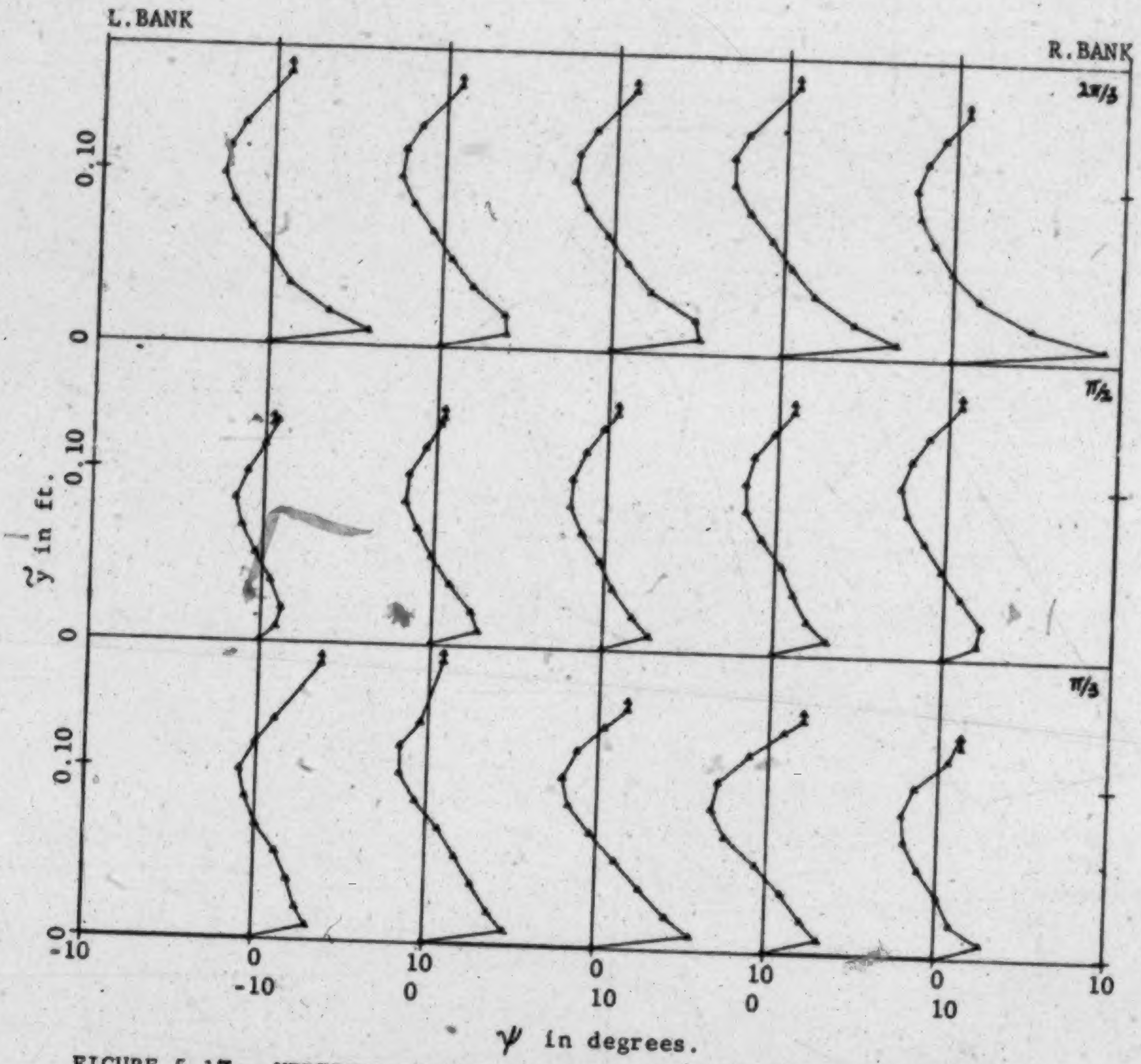

FIGURE 5.17c VERTICAL DISTRIBUTIONS OF HORIZONTAL ANGLE OF DEVIATION OF THE VELOCITY VECTOR, ψ, Runs 404/5/6. SECTIONS $\theta_2 = \pi/3$ TO $2\pi/3$.

CHAPTER 6

PRESENTATION OF CONCENTRATION MEASUREMENTS AND DISCUSSION OF RESULTS

In this chapter the experimental results relating to tracer concentration distribution in the straight and meandering flumes are presented and discussed.

6.1 Straight Flume

6.1.1 Transverse Distribution of Tracer Concentration

Typical transverse tracer concentration profiles at the four measuring sections are shown in Figures 6.1a to d. The measured tracer concentration was normalized with the concentration for fully mixed conditions and no tracer losses, C_o , and then plotted against the normalised transverse distance z/W for various x-values. With source at the channel centerline, the data indicate displacement of the centroid of the concentration profile from the channel centerline at some sections. No explanation can be offered for this because velocity measurements were made at only one section but it is speculated that this feature is probably caused by a tendency for the flow to meander along the channel. The shift in the centroid of the concentration distribution can also be seen for ice-covered flows and is more pronounced in these flows probably because of the warping of the plywood used to simulate the ice cover.

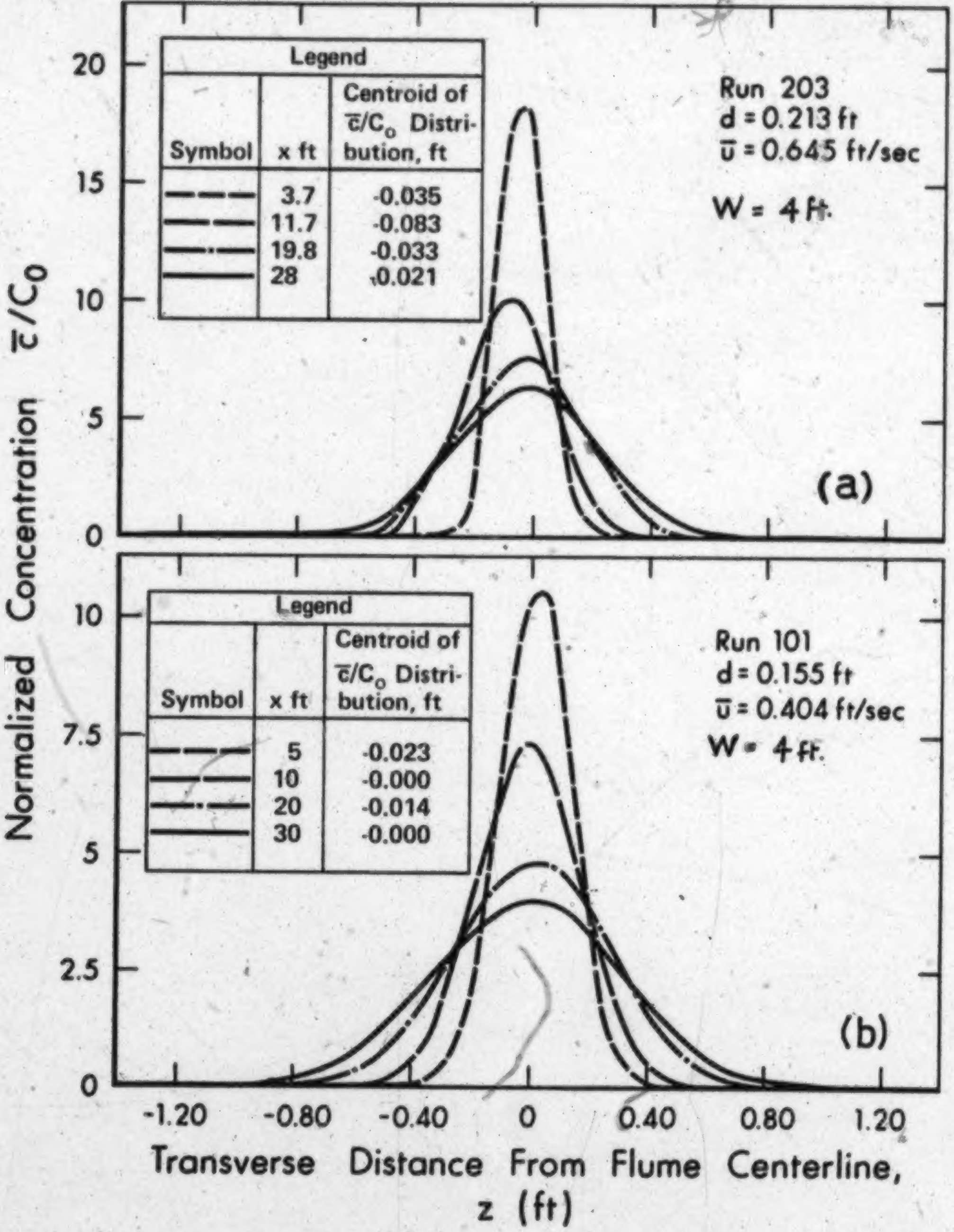

FIGURE 6.1 LATERAL DISTRIBUTIONS OF DEPTH-AVERAGED CONCENTRATION AT VARIOUS DISTANCES DOWNSTREAM OF SOURCE FOR CENTERLINE INJECTION

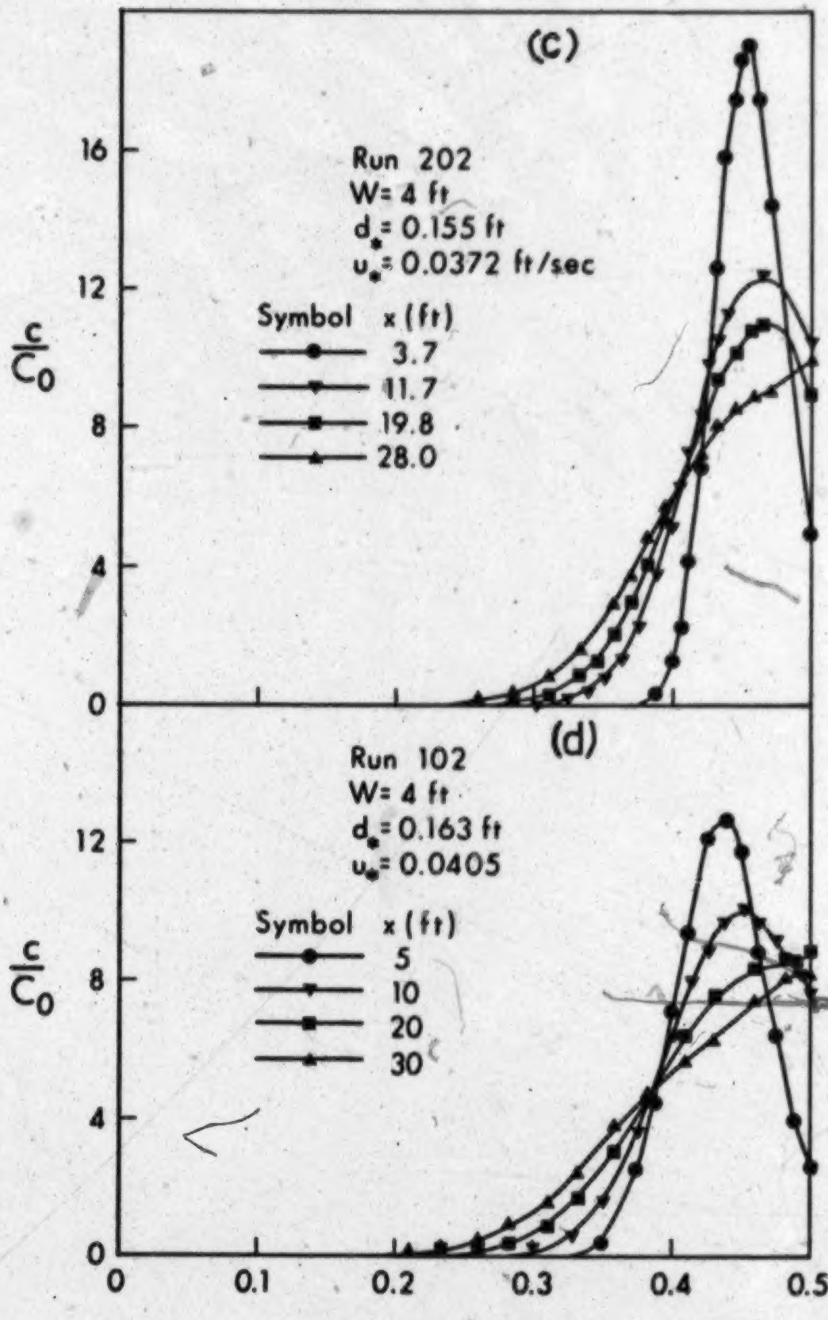

FIGURE 6.1 LATERAL DISTRIBUTIONS OF DEPTH-AVERAGED CONCENTRATION AT VARIOUS DISTANCES DOWNSTREAM OF SOURCE FOR SIDE INJECTION

When tracer is released near the side the peak depth-averaged concentration is observed to shift to the wall with longitudinal distance (see Figures 6.1c and d). This feature can be explained by the reflection or image source technique (Sayre and Chang, 1968) in which the portion of the concentration distribution falling beyond the side is folded back and added to the portion falling inside the channel. It has been established that for uniform turbulent flow in a wide rectangular channel away from the side-wall boundary layers, the lateral concentration distribution within a tracer cloud follows the Gaussian distribution. This is confirmed in Figure 6.2 where the normalized tracer concentrations are compared with Equation 3.18, that is:

$$\frac{C_1}{C_{1m}} = f(\alpha) = e^{-\frac{U_1 A_2{}^2 \alpha^2}{4k}} \qquad (3.18)$$

This equation may be rewritten as:

$$\frac{C_1}{C_{1m}} = \frac{\bar{c}}{\bar{c}_m} = f(\tfrac{z}{b}) = e^{-\frac{U_o b^2}{4E_z x}\left(\frac{z}{b}\right)^2} \qquad (6.1)$$

where $\bar{c}_m$ is maximum depth-averaged concentration and b represents half the transverse distance between the verticals on which $\bar{c} = 0.5\bar{c}_m$. In plotting these curves, transverse distances were measured from the vertical of maximum depth-averaged concentration. In Figure 6.2 the data points are plotted together with the Gaussian distributions obtained from Equation 6.1 using the measured values of U_o and E_z. It

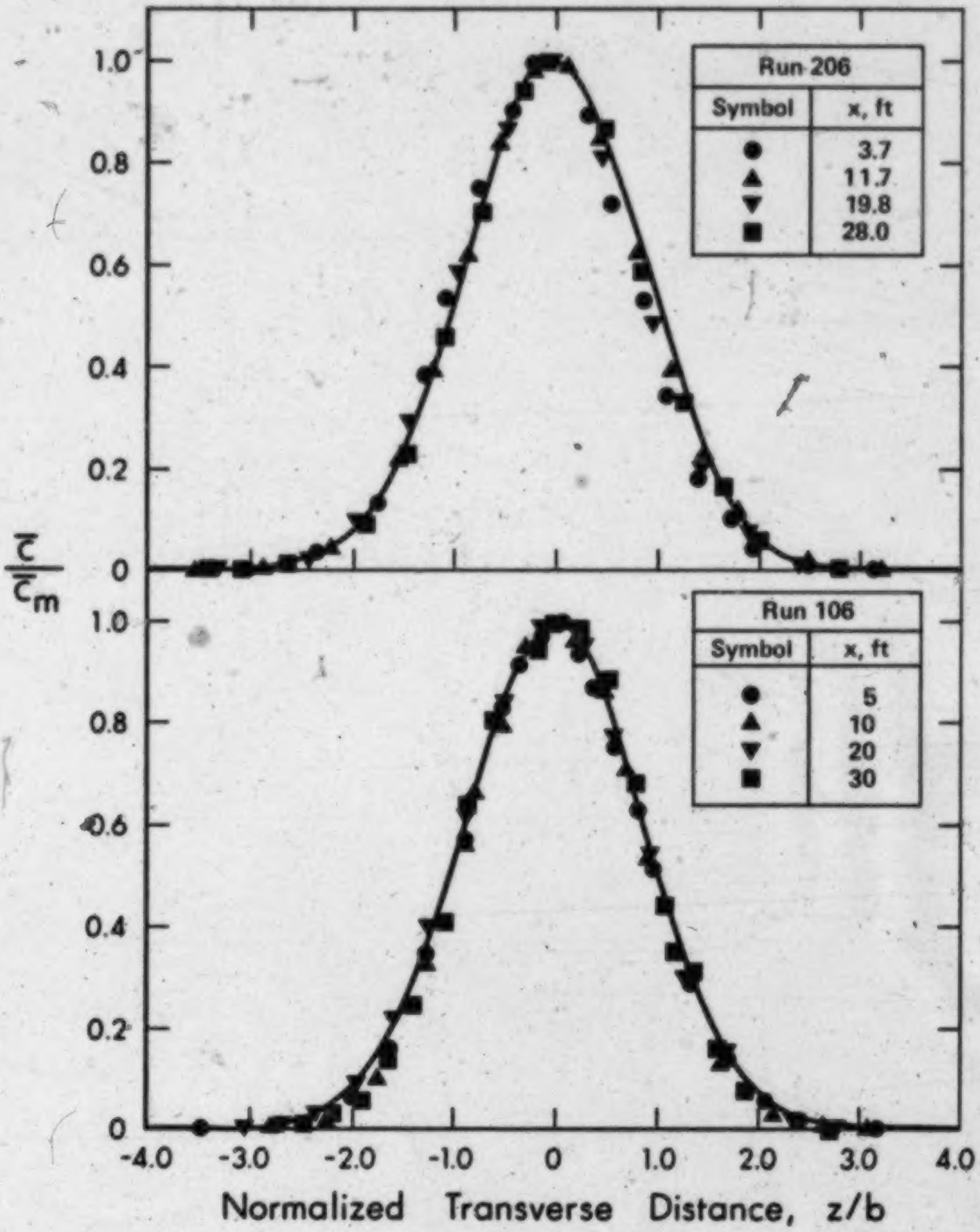

FIGURE 6.2 GRAPH OF NORMALISED CONCENTRATION AGAINST NORMALISED DISTANCE: RUNS 106 AND 206

is evident that the fit is good for both open and ice-covered channels.

6.1.2 Moments of the Transverse Tracer Flux Distribution

6.1.2.1 Calculation of Moments: Lateral variation in the depth-averaged longitudinal velocity, $\bar{u}$, of up to 12% across the width of the tracer cloud was observed in all test runs. To allow for this variation of $\bar{u}$ the measured concentration values were discharge weighted so that the moments were actually calculated from the tracer flux ($D\,\bar{u}\,\bar{c}$) distribution instead of the usual concentration distribution. The second moments about the point of tracer release, $M_2(x)$, were calculated numerically by:

$$M_2(x) = \left(\sum_{i=1}^{N} M'_{2i} \Big/ \sum_{i=1}^{N} M'_{oi} \right) \tag{6.2}$$

in which M'_{oi} and M'_{2i} are the zeroth and second moments, respectively, of the tracer flux between any two successive data points about the point of tracer release. M'_{oi} and M'_{2i} are defined as follows:

$$M'_{oi} = \frac{D}{2}\left[\bar{u}(\eta_{i+1})\bar{c}(x,\eta_{i+1}) + \bar{u}(\eta_i)\bar{c}(x,\eta_i)\right](\eta_{i+1} - \eta_i) \tag{6.3a}$$

and:

$$M'_{2i} = \frac{D}{2}\left[\bar{u}(\eta_{i+1})\bar{c}(x,\eta_{i+1}) + \bar{u}(\eta_i)\bar{c}(x,\eta_i)\right]$$

$$\left[\left\{(\eta_{i+1} + \eta_i) / 2\right\}^2\right](\eta_{i+1} - \eta_i) \tag{6.3b}$$

where η_{i+1} and η_i are the transverse distances of any two successive data points from z_o, the point of tracer release. The moments calculated by the above procedure are given in Table 6-1.

6.1.2.2 Growth of the Second Moments with Longitudinal Distance: Figures 6.3 and 6.4 show the growth of the second moments of the tracer flux with longitudinal distance downstream of the tracer source for centerline introduction of tracer. The plots indicate a linear growth rate of the second moments except close to the source. Since the centroid of the tracer flux distribution at various sections was found to be located very close to the channel centerline, the variance of the tracer flux distribution $\sigma^2_{fz}(x)$ was assumed equal to $M_2(x)$.

The linear growth rate of $\sigma^2_{fz}(x)$ extends nearly back to the source. This suggests that the lateral diffusion process converges to the one-dimensional diffusion model fairly rapidly. The deviation from linearity close to the source is primarily due to the non-uniform vertical distribution of tracer concentration as shown, for example, in Figure 6.5 and to the fact that the tracer cloud might be too small for gradient-type diffusion to be truly applicable.

From Equation 6.1 which was derived with the assumption of uniform velocity of flow across the channel, we can express the variance of the tracer concentration distribution, $\sigma^2_z(x)$, as follows:

TABLE 6-1 NUMERICAL VALUES OF X, $M_2(X)$ AND A IN EQUATION 6.5

Run	X ft	$M_2(X)$ ft^2	A ft/s	Run	X ft	$M_2(X)$ ft^2	A ft/s
101	5	0.0155	0.0502	201	3.7	0.0066	0.427
(CL)*	10	0.0339	0.0503	(CL)	11.7	0.0207	0.430
	20	0.0698	0.0504		19.8	0.0422	0.428
	30	0.1050	0.0505		28	0.0623	0.428
103	5	0.0213	0.0762	203	3.7	0.0068	0.679
(CL)	10	0.044	0.0765	(CL)	11.7	0.0237	0.684
	20	0.088	0.0769		19.8	0.421	0.684
	30	0.130	0.0771		28	0.594	0.685
105	5	0.0143	0.0931	205	3.7	0.0057	0.917
(CL)	10	0.0275	0.0933	(CL)	11.7	0.0166	0.919
	20	0.0569	0.0937		19.8	0.0341	0.924
	30	0.0873	0.0937		28	0.0490	0.927
106	5	0.0145	0.895	206	3.7	0.0063	0.755
(CL)	10	0.0302	0.897	(CL)	11.7	0.0191	0.760
	20	0.0608	0.899		19.8	0.0353	0.760
	30	0.0932	0.901		28	0.0506	0.758
102	5	0.0146	0.496	202	3.7	0.0113	0.427
(B)†	10	0.0233	0.788	(B)	11.7	0.0185	0.748
	20	0.0502	1.235		19.8	0.0284	0.960
	30	0.0759	1.589		28	0.0424	1.279
104	5	0.0154	0.862	204	3.7	0.0097	.724
(B)	10	0.0285	1.324	(B)	11.7	0.0240	1.360
	20	0.0503	1.996		19.8	0.0292	1.525
	30	0.0652	2.165		28	0.0430	1.850

Notes:

* CL refers to centerline injection.
† B refers to near-bank injection.

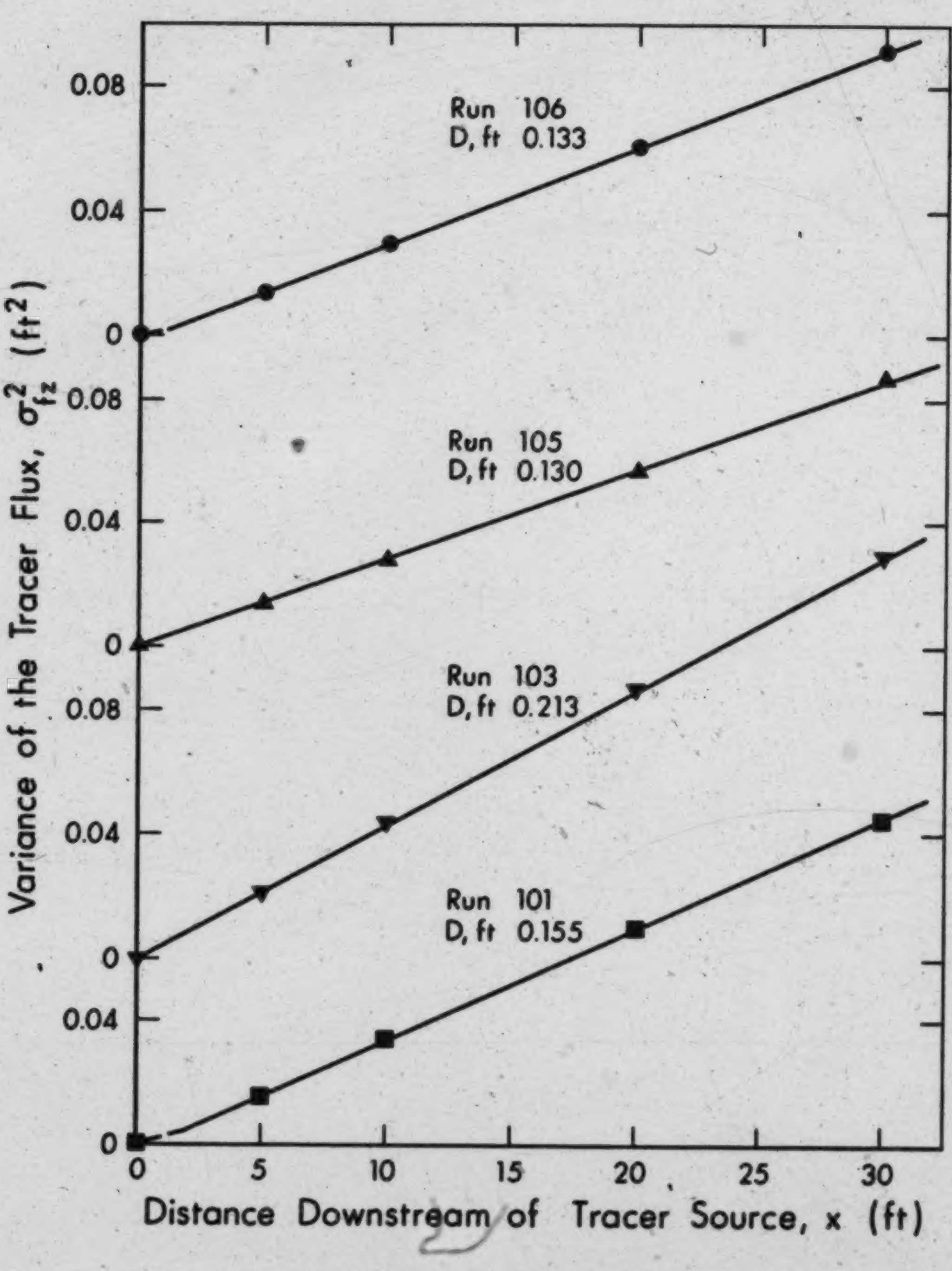

FIGURE 6.3 GROWTH OF VARIANCE OF TRACER FLUX WITH DISTANCE DOWNSTREAM OF SOURCE FOR OPEN CHANNEL TESTS

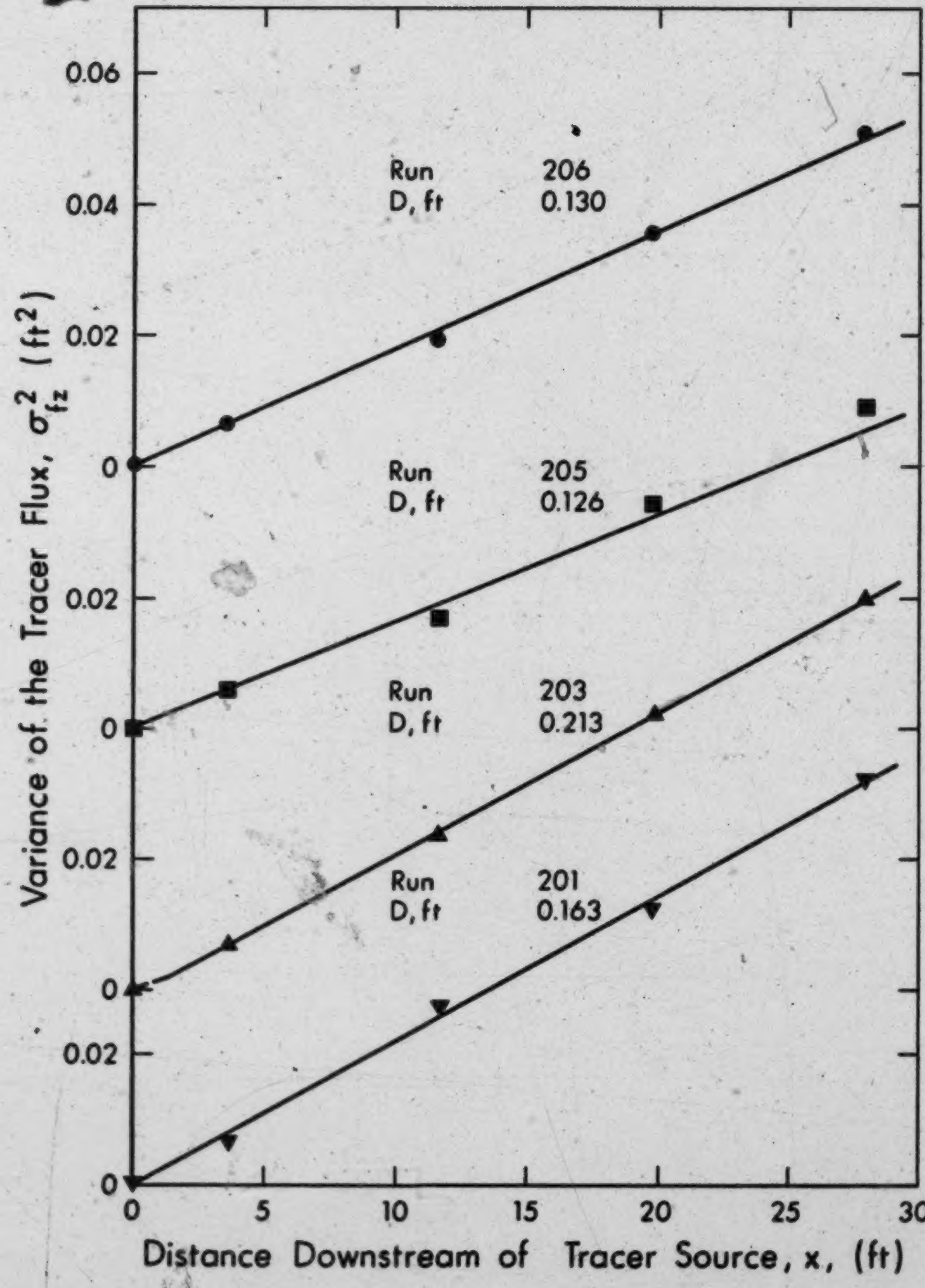

FIGURE 6.4 GROWTH OF VARIANCE OF TRACER FLUX WITH DISTANCE DOWNSTREAM OF SOURCE

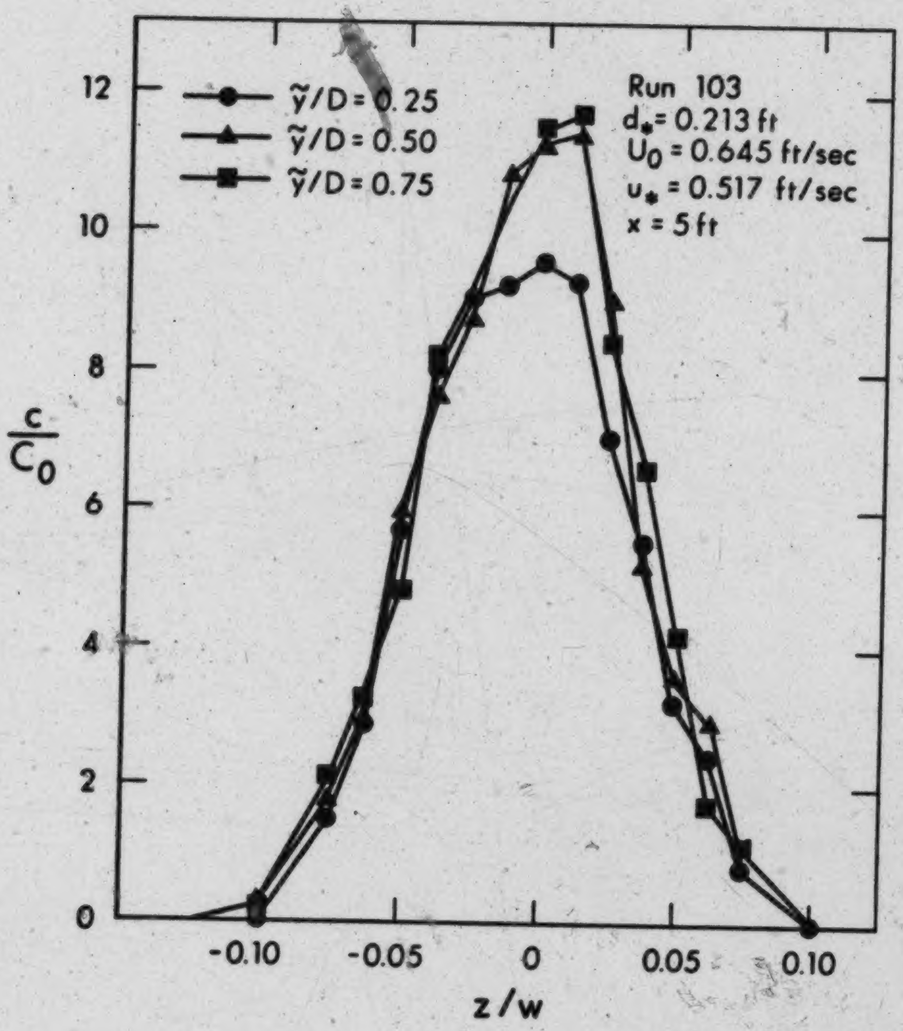

FIGURE 6.5 TRANSVERSE CONCENTRATION PROFILES AT DIFFERENT LEVELS FOR FIRST SECTION OF TRACER MEASUREMENT

$$\sigma_z^2(x) = \frac{2E_z x}{U_o} \qquad (6.4)$$

We can conclude from Equation 6.4 and Equation 3.16 that $b^2 \propto \sigma_z^2(x)$ and as b is a characteristic dimension of the tracer cloud width, that the cloud width grows parabolically with longitudinal distance.

For tracer releases near the side-wall, the plots of $M_2(x)$ versus x given in Figure 6.6, do not clearly show a linear growth rate of $M_2(x)$ with x over the test reach. There is an initial reach over which $M_2(x)$ shows a fairly rapid growth rate, and this is probably due to the fact that the tracer was injected about 3 inches from the side and, therefore, it spreads laterally in two directions until no concentration gradients exist in one of these directions. As the tracer cloud spreads and occupies more of the uniform flow region, the growth rate of the second moments should approach the same rate as observed for centerline injection of tracer. It is not very clear from the data how quickly the linear growth rate of $M_2(x)$ is established in this case.

6.1.3 The Transverse Exchange Coefficient

6.1.3.1 Determined by the Method of Moments: It was shown in Section 3.3.1 that for tracer released from an arbitrary point within a cross-section, the average transverse exchange coefficient within a reach can be calculated using Equation 3.31, that is:

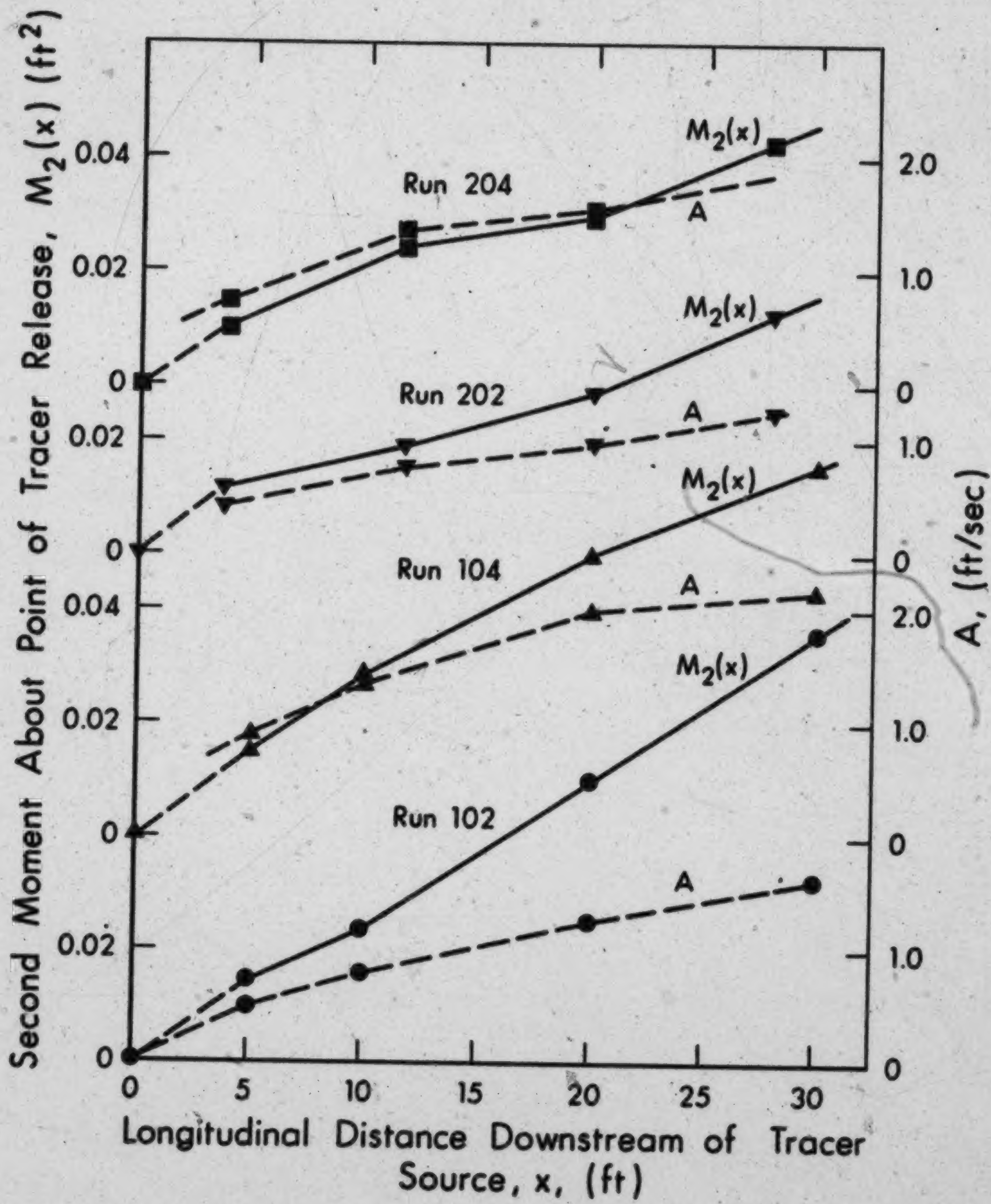

FIGURE 6.6 LONGITUDINAL VARIATION OF $M_2(X)$ AND A FOR NEAR SIDE TRACER INJECTION

$$E_z = \frac{1}{2} \frac{d}{dx}\left[\int_{W_1}^{W_2} \bar{u}\,\bar{c}\,\eta^2 d\eta\right] \Bigg/ \left[\int_{W_1}^{W_2} \left\{\bar{c} - \frac{\partial}{\partial\eta}(\bar{c}\eta)\right\} d\eta\right] \tag{3.31}$$

This equation can be rewritten as:

$$E_z = \frac{A}{2} \frac{dM_2(x)}{dx} \tag{6.5}$$

where $M_2(x) = \left[\int_{W_1}^{W_2} \bar{u}\,\bar{c}\,\eta^2 d\eta\right] \Bigg/ \left[\int_{W_1}^{W_2} \bar{u}\,\bar{c}\, d\eta\right]$

and $A = \left[\int_{W_1}^{W_2} \bar{u}\,\bar{c}\, d\eta\right] \Bigg/ \left[\int_{W_1}^{W_2} \left\{\bar{c} - \frac{\partial}{\partial\eta}(\bar{c}\eta)\right\} d\eta\right]$

$M_2(x)$, A and x are tabulated in Table 6.1.

The results pertaining to centerline release of tracer are first considered. As expected A was essentially constant for a particular test run with a variation not exceeding ± 0.7% from the mean for the four measuring sections. Since E_z and A are constant $M_2(x)$ must grow linearly with x as observed in Section 6.1.2.2. Straight lines were, therefore, fitted to the $M_2(x)$ versus x plots and their slopes determined. Equation 6.5 was then used to calculate E_z.

For near-bank release of tracer, A is no longer a constant but a function of x. The variation of A for runs 102, 104, 202 and

204 are shown in Figure 6.6 together with that of the second moments, $M_2(x)$. Equation 6.5 was used to determine average values of E_z between any two adjacent cross-sections. This average E_z is plotted at the downstream section as indicated in Figure 6.7. The broken lines in Figure 6.7 are the E_z values obtained for centerline introduction of tracer. The average E_z between the tracer source and the first section of tracer measurement is lower than the average for each of the runs. Very close to the source only the small size eddies contribute to the diffusion of the tracer. As x increases and the tracer cloud expands, the average eddy size capable of making a contribution to the spreading of the tracer also increases resulting in a higher rate of diffusion. Since the largest eddy size is controlled by the flow dimensions and is partially dependent on the proximity of the side walls the rate of diffusion cannot increase indefinitely but should approach a limiting value. The smaller values of E_z observed between the source and the first section of tracer measurement are, therefore, reasonable.

The functional forms of A and $M_2(x)$ are not known and errors are inevitably introduced by assuming a linear variation of both variables between any two successive cross-sections to evaluate E_z. However, the technique used by Holley et al (1972) could be applied here by integrating Equation 6.5 once with respect to x to give:

$$M_2(x) = 2E_z \quad I(x) + \text{constant} \qquad (6.6)$$

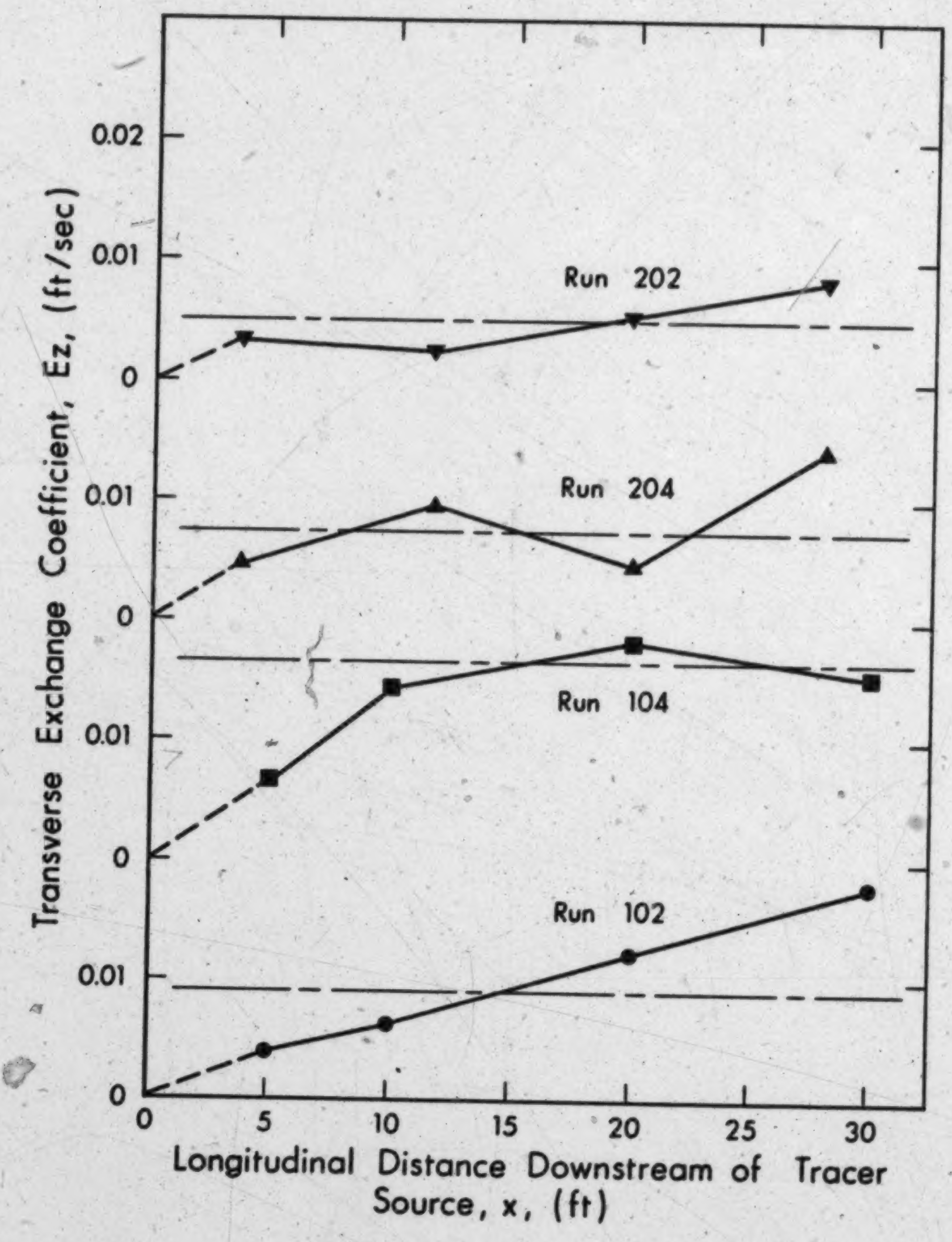

FIGURE 6.7 LONGITUDINAL VARIATION OF THE TRANSVERSE EXCHANGE COEFFICIENT, E_z

where $I(x) = \int \frac{dx}{A}$. It is to be noted that a plot of $M_2(x)$ versus $I(x)$ must yield a straight line with a slope of $2E_z$. Some of the data for side release of tracer were analysed using Equation 6.6 but curves were obtained when $M_2(x)$ was plotted against $I(x)$. This could be caused by variable transverse diffusion coefficient near the side walls and the large distance between sections of tracer measurement.

6.1.3.2 Determined by the Similarity Analysis: On the asumption of similarity, which is confirmed in Figure 6.2, the distribution of C_1/C_{1m} or $\overline{c}/\overline{c}_m$ was shown to be Gaussian in Section 3.1 and the exchange or diffusion coefficient was derived as:

$$E_z = \frac{b^2 U_o}{4x\ln 2} \qquad (3.20)$$

It is to be noted that this equation does not apply in situations with side-wall effects. Equation 3.20 was also used to evaluate the average exchange coefficient over a reach of length x, where U_o is now the mean velocity across the tracer cloud width. Only one measurement of the transverse tracer concentration profile is required to determine b in Equation 3.20. In this study the concentration profile obtained at the last measuring section was used to determine b and hence E_z. The E_z values so obtained together with those determined by the method of moments are listed in Table 6-2. The table also gives the percentage difference between the two E_z values based on the E_z values calculated by the method of moments. The difference between the E_z values

TABLE 6-2 COMPARISON OF E_z VALUES AS DETERMINED BY THE METHOD OF MOMENTS AND SIMILARITY ANALYSIS

Run Number	Transverse Exchange Coefficient E_z , ft^2/s		% Difference $t^\dagger$
	1*	2*	
101	0.00092	0.00094	+ 2.2
103	0.00167	0.00174	+ 4.2
105	0.00134	0.00137	+ 2.2
106	0.00142	0.00149	+ 4.9
201	0.00050	0.00051	+ 2.0
203	0.00075	0.00076	+ 1.3
205	0.00074	0.00083	+ 12.1
206	0.00067	0.00071	+ 6.0
Average			+ 4.5

Notes:

1* E_z as determined by Method of Moments

2* E_z as determined by Similarity Analysis

† $$t = \frac{E_z(\text{Similarity}) - E_z(\text{Moments})}{E_z(\text{Moments})} \times 100\%$$

was within 12%. In general, the differences were much smaller for open-water conditions than for ice-cover conditions. These differences can partly be traced to the assumption of constant uniform velocity across the tracer cloud width. This simplification was not fully satisfied in all the runs. Another cause of the differences is experimental errors. The average absolute difference between the E_z values was about 4.5%. This indicates that Equation 3.20 is a satisfactory method for evaluating E_z.

6.1.4 Effect of a Smooth Ice-Cover on the Exchange Coefficient

In order to evaluate the influence of an ice-cover on the diffusion process, experiments were conducted in both open and ice-covered channels. The results from the open-water experiments served as the basis for this evaluation. The flow depth and discharge were kept approximately the same for any two corresponding experiments (see Table 5-3). To facilitate comparison, any two corresponding experiments are given the same experiment number in their respective series. For example, run 201 corresponds to run 101.

It is evident from the summary of data in Table 6-3 that the diffusion capacity of ice-covered flows, as measured by E_z, is substantially reduced. An average reduction of approximately 50% was observed in all the experiments. The presence of an ice-cover reduces the significant size scale of the eddies and as a consequence there is

TABLE 6-3 SUMMARY OF MEASURED EXCHANGE COEFFICIENTS AND RELATED PARAMETERS

Run	Flume Code	Avg. Flow Depth d_* ft	Hydraulic Radius R ft	Aspect Ratio W/d_*	W/R	Discharge Velocity U_o ft/s	Shear Velocity u_* ft/s	Transverse Exchange Coefficient E_z, ft^2/s		Normalized† Coefficient	
								1*	2*	E_z/u_*d_*	E_z/u_*R
101	SR	0.155	0.144	25.8	27.8	0.404	0.0372	0.00092	0.00094	0.1595	0.172
103	SR	0.213	0.193	18.8	20.7	0.645	0.0517	0.00167	0.00174	0.1516	0.167
105	SR	0.130	0.122	30.8	32.9	0.865	0.0704	0.00134	0.00137	0.1460	0.156
106	SR	0.133	0.125	30.0	32.0	0.751	0.0592	0.00142	0.00149	0.1800	0.192
201	SRI	0.163	0.078	24.5	51.3	0.383	0.0405	0.00050	0.00051	0.0757	0.158
203	SRI	0.213	0.101	18.8	39.6	0.645	0.0504	0.00075	0.00076	0.0700	0.147
205	SRI	0.126	0.061	31.1	65.6	0.893	0.0700	0.00074	0.00083	0.0842	0.174
206	SRI	0.130	0.063	30.8	63.5	0.770	0.0570	0.00067	0.00071	0.0908	0.187

Notes:

1* Transverse exchange coefficient as determined by Method of Moments.

2* Transverse exchange coefficient as determined by Similarity Analysis.

† Normalized exchange coefficients as determined using E_z values obtained by Method of Moments.

a reduction in diffusion potential. An obvious consequence of this is that the attenuation of peak concentration, which is indicative of the rate of spreading of the tracer cloud, is reduced in ice-covered flows compared with open-water flows. This also means that the channel reach required to achieve the same degree of mixing will be much longer for ice-covered flows than for the open-water case. These aspects of diffusion will be discussed later.

6.1.5 Factors Affecting the Normalised Exchange Coefficient

Turbulence in channel flows is generated by shear originating at the channel boundaries and this turbulence provides an efficient mechanism for mixing. Two features of turbulence relevant to diffusion are the turbulence intensity and the average size of the turbulence eddies. Laufer (1951) has shown that the r.m.s. value of the transverse velocity fluctuations is proportional to the shear velocity, u_* , in a 2-dimensional flow in a wind tunnel. The size of eddies in a turbulent channel flow is limited by the average flow depth, d_* , and the flow width, W. The above observations suggest normalising the exchange or diffusion coefficient with the product u_*d_*. The length scale, d_* , should be regarded only as reflecting the average size of the dominant eddies producing the maximum mixing.

Transverse velocities resulting from changes in channel geometry with longitudinal distance can affect E_z , however, only rectangular channels are considered here.

Bulk properties of a uniform turbulent flow in a straight rectangular channel (e.g., the average transverse exchange or diffusion coefficient, E_z , friction factor, f , mean velocity, U_o , etc.) depend on the following variables: d_* , average flow depth; W , channel width; ν , kinematic viscosity; k_s , equivalent sand roughness; g , gravitational acceleration; S_o , bed slope. The dependence of E_z on the other variables can be expressed as:

$$E_z = \Lambda_1[d_*, W, \nu, g, S_o, k_s] \tag{6.6}$$

Without loss of generality, Equation 6.6 can be rewritten as:

$$E_z = \Lambda_2[d_*, W, \nu, k_s, u_*, g] \tag{6.7}$$

where $u_* = \sqrt{gRS_o}$ and R is the hydraulic radius. It is noted that for rectangular channels, the hydraulic radius, R , is defined if d_* and W are specified. Dimensional analysis then gives:

$$\frac{E_z}{u_* d_*} = \Lambda_3\left[\frac{W}{d_*}, \frac{k_s}{d_*}, \frac{u_* d_*}{\nu}, \frac{u_*}{\sqrt{gd_*}}\right] \tag{6.8}$$

It can also be shown that:

$$f = \Lambda_4 \left[\frac{W}{d_*}, \frac{k_s}{d_*}, \frac{u_* d_*}{\nu}, \frac{u_*}{\sqrt{g d_*}} \right] \tag{6.9}$$

where $f = 8(u_*/U_o)^2$ and $u_*/\sqrt{gd_*}$ is a form of Froude Number. For fully rough turbulent flows, the friction Reynolds Number, $u_* d_*/\nu$ has a minimal effect on $E_z/u_* d_*$ and f, and $u_*/\sqrt{gd_*}$ does not play a significant role in subcritical open channel flows and in ice-covered flows is not pertinent. Equation 6.8 and 6.9 reduce to:

$$\frac{E_z}{u_* d_*} = \Lambda_5 \left[\frac{W}{d_*}, \frac{k_s}{d_*} \right] \tag{6.10}$$

and:

$$f = \Lambda_6 \left[\frac{W}{d_*}, \frac{k_s}{d_*} \right] \tag{6.11}$$

Combining Equation 6.10 and 6.11 also gives:

$$\frac{E_z}{u_* d_*} = \Lambda_7 \left[\frac{W}{d_*}, f \right] \tag{6.12}$$

The normalised transverse diffusion coefficient, therefore, depends on the aspect ratio, W/d_* , and the relative roughness, k_s/d_* (or friction factor, f), for fully rough turbulent flows.

If the relative roughness k_s/d_* remains unchanged then E_z/u_*d_* should approach a constant value for small aspect ratios. For very large W/d_*, the width ceases to be an important parameter and should no longer influence the average size of the eddies. It follows, therefore, that if k_s/d_* is held constant, E_z/u_*d_* should approach a limiting value for large W/d_* and for fully rough turbulent conditions. In subsequent discussions, Equation 6.12 will be referred to instead of Equation 6.11 because the friction factor, f, is given for most of the available data.

All the available laboratory data have been summarised in Table 2.1 and with the present experimental results, are shown plotted plotted in Figure 6.8. The plot reveals some apparent dependence of E_z/u_*d_* on W/d_* as reported by Okoye (1970). However, it is evident that the normalised diffusion coefficient varies over a wide range at small W/d_* and this is due to varying f. That this is true can be seen from the data of Miller and Richardson for which there was a 400% variation in the friction factor, f. Values of the normalised diffusion coefficient for $W/d_* > 30$ are sparse and the available data for this range are due to Okoye. Okoye's data for $W/d_* > 30$ were obtained for smooth bed conditions only. Since f did not remain constant in all the reported data it will be erroneous to conclude that E_z/u_*d_* depends solely on the aspect ratio W/d_*. It is believed that the variations observed in Figure 6.7 are primarily caused by varying f

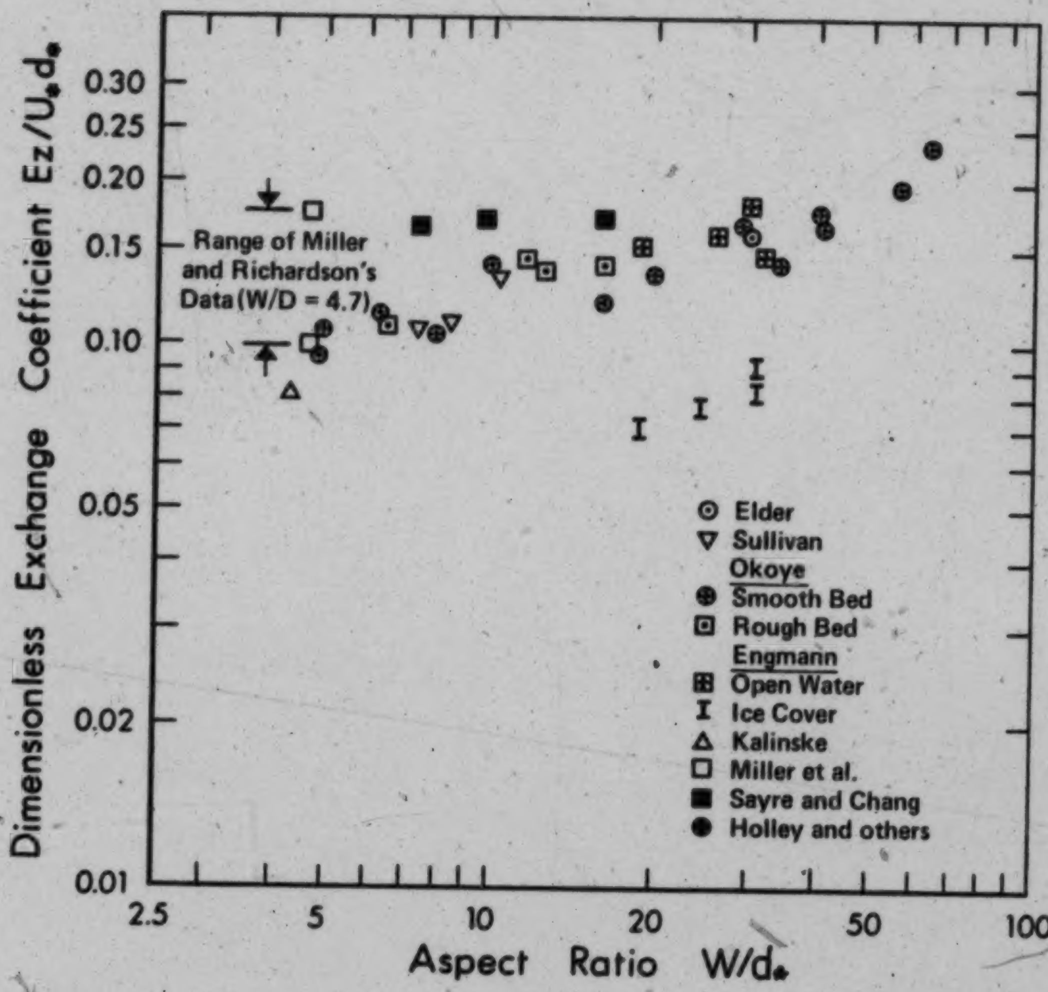

FIGURE 6.8 VARIATION OF THE NORMALISED EXCHANGE (DIFFUSION) COEFFICIENT, $E_z/u_* d_*$ WITH ASPECT RATIO W/d_*

and u_*d_*/ν values. The hydraulic radius, R, is commonly used to describe channel geometry and thus it facilitates comparison of results from rectangular and non-rectangular prismatic channels. One could, therefore, replace d_* with R in Equation 6.12 to obtain:

$$\frac{E_z}{u_*R} = \Lambda_{12}[\frac{W}{R}, f] \qquad (6.13)$$

It must be remembered that Equation 6.13 is valid for fully rough turbulent flows only. A plot of E_z/u_*R against W/R for all the available data is presented in Figure 6.9. The effects of the friction factor, f, and the modified aspect ratio W/R cannot be separated since both parameters varied over a wide range in all the reported data. The only exception is the data of Miller and Richardson (1974). Their experiments were performed for a constant W/R and fully rough turbulent flow conditions. Their data can, therefore, be described by the relation:

$$\frac{E_z}{u_*R} = \Lambda_{13}[f] \qquad (6.14)$$

The plot of E_z/u_*R against f for the data of Miller and Richardson is given in Figure 6.10. It is seen that the normalised diffusion coefficient increases with an increase in the friction factor f when W/R is held constant and the flow is fully rough turbulent.

The results of the ice-cover experiments do not fit the trend

147

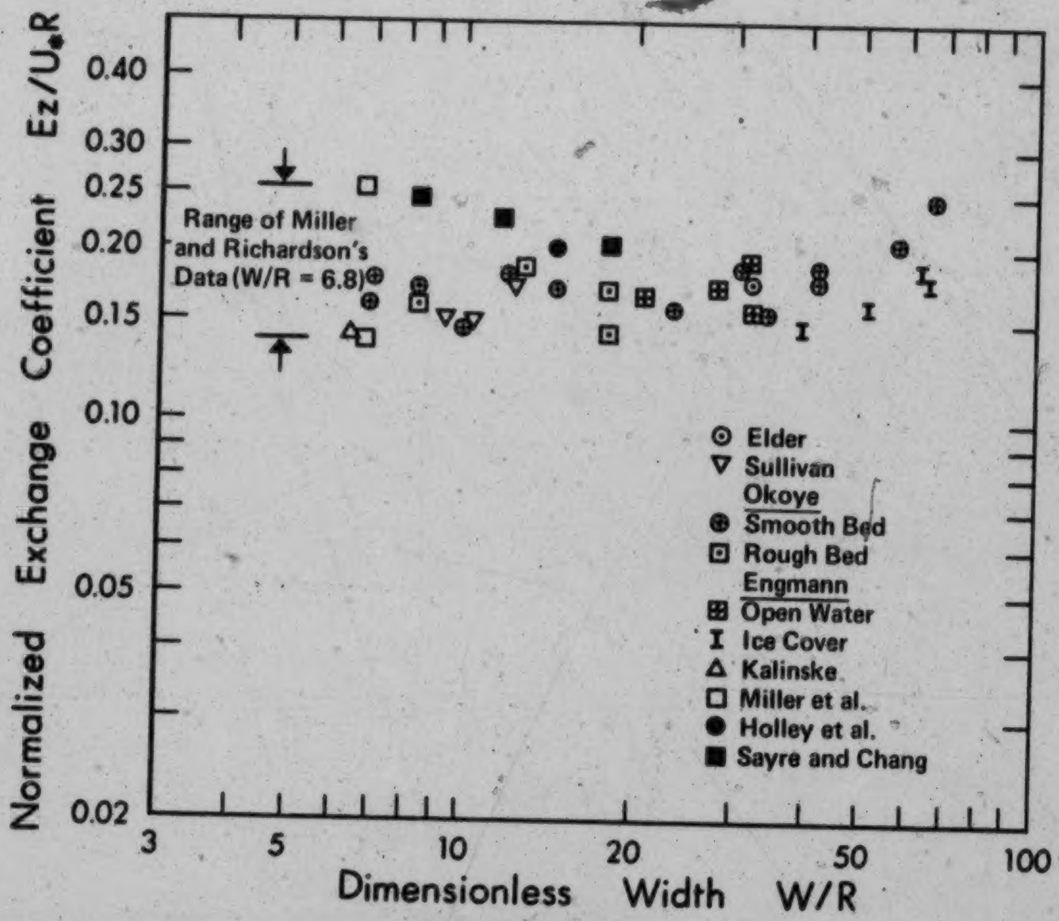

FIGURE 6.9 VARIATION OF THE NORMALISED EXCHANGE (DIFFUSION) COEFFICIENT, E_z/u_*R , WITH DIMENSIONLESS WIDTH, W/R

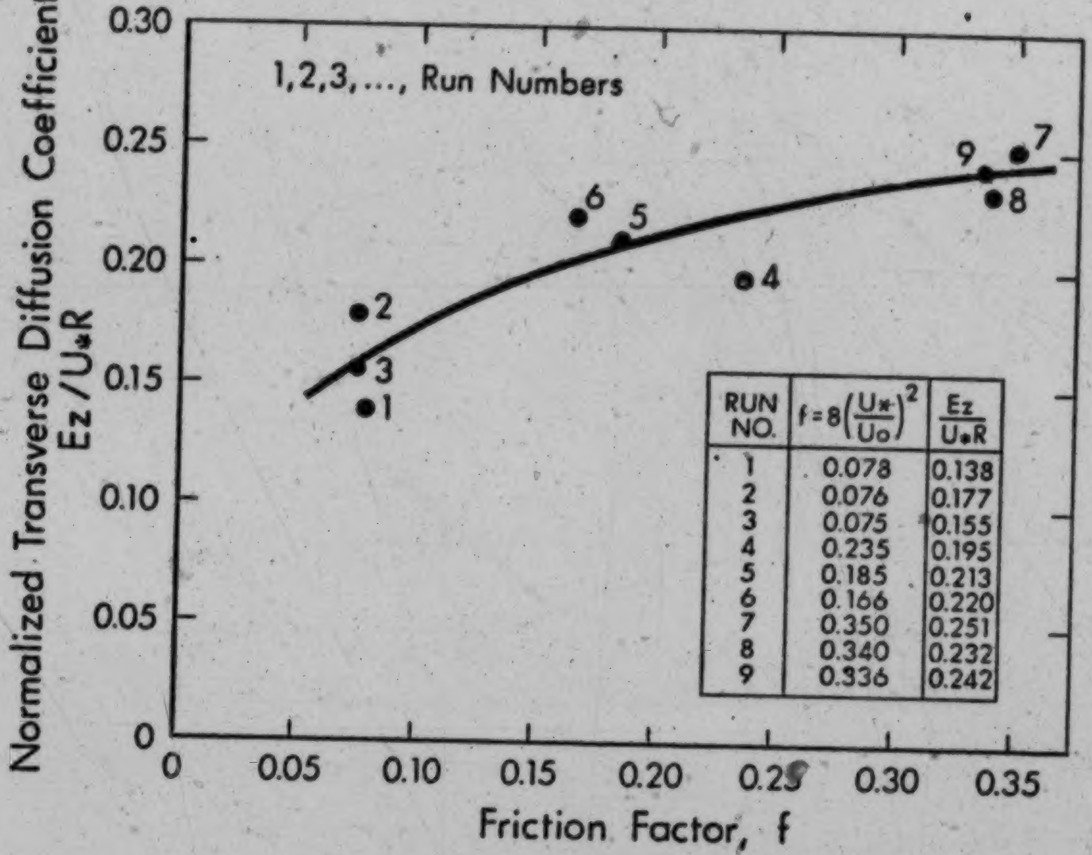

RUN NO.	$f=8\left(\frac{U_*}{U_o}\right)^2$	$\frac{E_z}{U_*R}$
1	0.078	0.138
2	0.076	0.177
3	0.075	0.155
4	0.235	0.195
5	0.185	0.213
6	0.166	0.220
7	0.350	0.251
8	0.340	0.232
9	0.336	0.242

FIGURE 6.10 VARIATION OF THE NORMALISED TRANSVERSE DIFFUSION COEFFICIENT, E_z/u_*R, WITH FRICTION FACTOR, f, USING MILLER AND RICHARDSON'S (1974) DATA.

of the other data when E_z/u_*d_* is plotted against W/d_* (see Figure 6.7) but they fit in well with the general trend of the open channel data when E_z/u_*R is plotted against W/R. It is evident from Table 6-3 that the normalised diffusion coefficient, E_z/u_*R, for ice-cover conditions is, in general, only slightly less than the corresponding coefficient for open-water conditions.

6.1.6 Attenuation of Peak Concentration

Very close to the tracer source the tracer concentration at various flow levels will exhibit different decay rates along the axis of the tracer cloud depending on the position of the source in the vertical. For the case where the tracer is well mixed in the vertical it was shown in Section 3.1 that the decay rate of the depth-averaged peak concentration is given by:

$$C_{1m} = A_1 X_1^{p} \tag{3.15}$$

where p is an exponent with a theoretical value of -0.50; C_{1m} is the depth-averaged peak concentration relative to the concentration for fully mixed conditions, and X_1 ($= X/d_*$) is dimensionless distance in the longitudinal direction.

Figure 6.11 shows plots of C_{1m} versus X_1 for Runs 103, 105, 201 and 205. The slope of each of the straight line plots is equal to the exponent p in Equation 3.15. A summary of the P values is

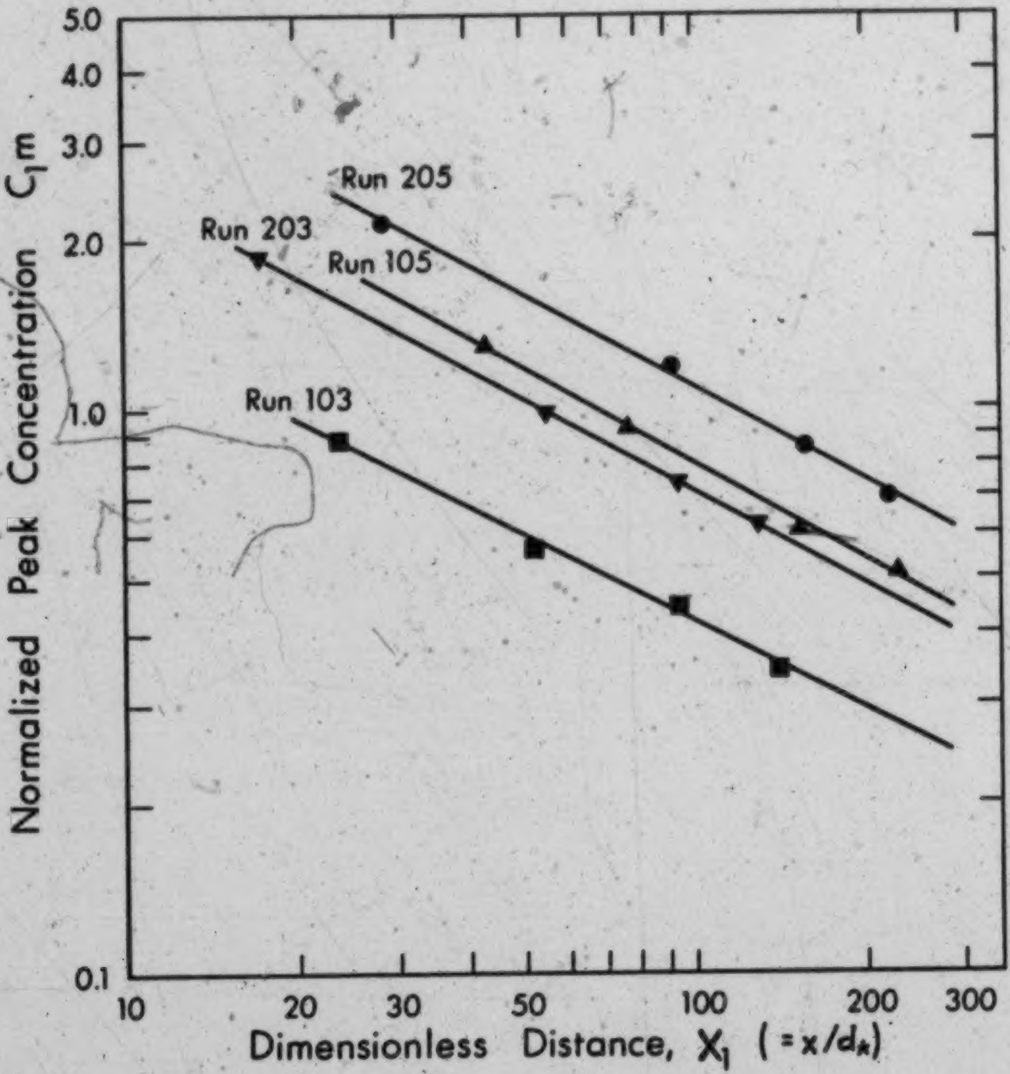

FIGURE 6.11 DECAY OF NORMALISED PEAK CONCENTRATION, C_{1m} , WITH DIMENSIONLESS WIDTH, X_1

TABLE 6-4 SUMMARY OF DECAY EXPONENTS FOR THE ATTENUATION OF DEPTH-AVERAGED PEAK CONCENTRATION

Run	Flume Code	Flow Depth ft	Decay Exponent P	Run	Flume Code	Flow Depth ft	Decay Exponent P
101	SR	0.155	-0.547	201	SRI	0.163	-0.565
103	SR	0.213	-0.520	203	SRI	0.213	-0.546
105	SR	0.130	-0.562	205	SRI	0.126	-0.543
106	SR	0.133	-0.548	206	SRI	0.130	-0.512
Average			-0.544	Average			-0.542

given in Table 6-4. The results do not exhibit any definite trend regarding the dependence of p on any particular hydraulic parameter, because of the comparatively limited range of the parameters in these experiments.

The plots, nevertheless, clearly show that for any two experiments performed at the same flow depth and discharge but with one having an ice-cover and the other a free water surface, e.g., Runs 203 and 103, a longer distance is required to achieve the same value of C_{1m}. This is in agreement with the earlier findings which established a substantial reduction in E_z due to the presence of an ice-cover.

The average values of the decay exponent were found to be -0.544 and -0.542 respectively for open and ice-cover flows. These values indicate an attenuation rate which is slightly greater than the predicted value of $p = -0.50$ for one-dimensional transverse diffusion. The reason for this is that the vertical distribution of tracer concentration along the channel axis is not strictly uniform until after an initial reach length which must depend on the flow depth. Within this reach the attenuation of maximum concentration is caused by both transverse and vertical diffusion. It can be shown, Czernuszenko (1973), that in a stream of large depth where the influence of the water-level and the boundaries on the tracer spreading are not marked the variation of C_{1m} with X_1 assuming Gaussian distributions in both the y and z directions is given by:

$$C_{1m} \propto (E_z E_y)^{-0.50} X_1^{-1.0} \tag{6.15}$$

where E_y is the vertical diffusion coefficient. The diffusion in the y and z directions separately cause C_{1m} to decay at a rate proportional to $X_1^{-0.50}$. The fact that the average value obtained for p was close to the predicted value indicates that downstream of the first section of tracer measurement the effect of vertical diffusion near the axis of the tracer cloud was not very pronounced.

6.2 Meandering Flume

6.2.1 Concentration Measurements

Transverse distributions of the normalised depth-averaged concentration, $\bar{c}/C_o$, for some test runs are presented in Figures 6.12a to f. C_o represents the tracer concentration when fully mixed with no tracer losses and is related to the tracer flux across any section by:

$$C_o Q = \frac{1}{1-a} \int_{W_1}^{W_2} D \, \bar{u} \, \bar{c} \, d z = \left[\sum_{j=1}^{N} D_j \, \bar{u}_j \, \bar{c}_j \, \Delta z \right] / [1-a]$$

where $\bar{c}$ and $\bar{u}$ are depth-averaged concentration and velocity respectively; Q is total discharge; D is local depth; a is fraction of tracer which is lost and N = 26.

As could be expected, the data show that the tracer spreads much faster for centerline release of tracer than for side release. Figures 6.12a and f indicate a distinct displacement of the zone of peak depth-averaged concentration from the channel centerline. This displacement could be caused partly by the movement of the high velocity filament from the inside to the outside bank, and partly by the spiral motions. It is observed, for example, to be much larger in run 401 than in run 404 and this seems reasonable because the strength of the spiral motion is greater in run 401 than in run 404 (see Figure 5.16). A similar shift of the zone of maximum depth-averaged concentration can be seen in the transverse concentration distributions for run 302 (left-bank injection).

The normalised concentration distributions in general appear to be smooth. For open channel tests patches of water having a high tracer concentration interspersed with patches having a low or even zero concentration were visible to the naked eye for some distance downstream of the source. However, the fact that a reasonably smooth distribution was always obtained at the first section of tracer measurement demonstrates that the sampling period used was long enough to smooth out most of the concentration fluctuations.

Typical transverse concentration profiles in the first bend of the ice-covered channel at different levels and for various source locations are shown in Figure 6.13a. The plots indicate that for left-bank releases of tracer, the concentration distribution over a vertical

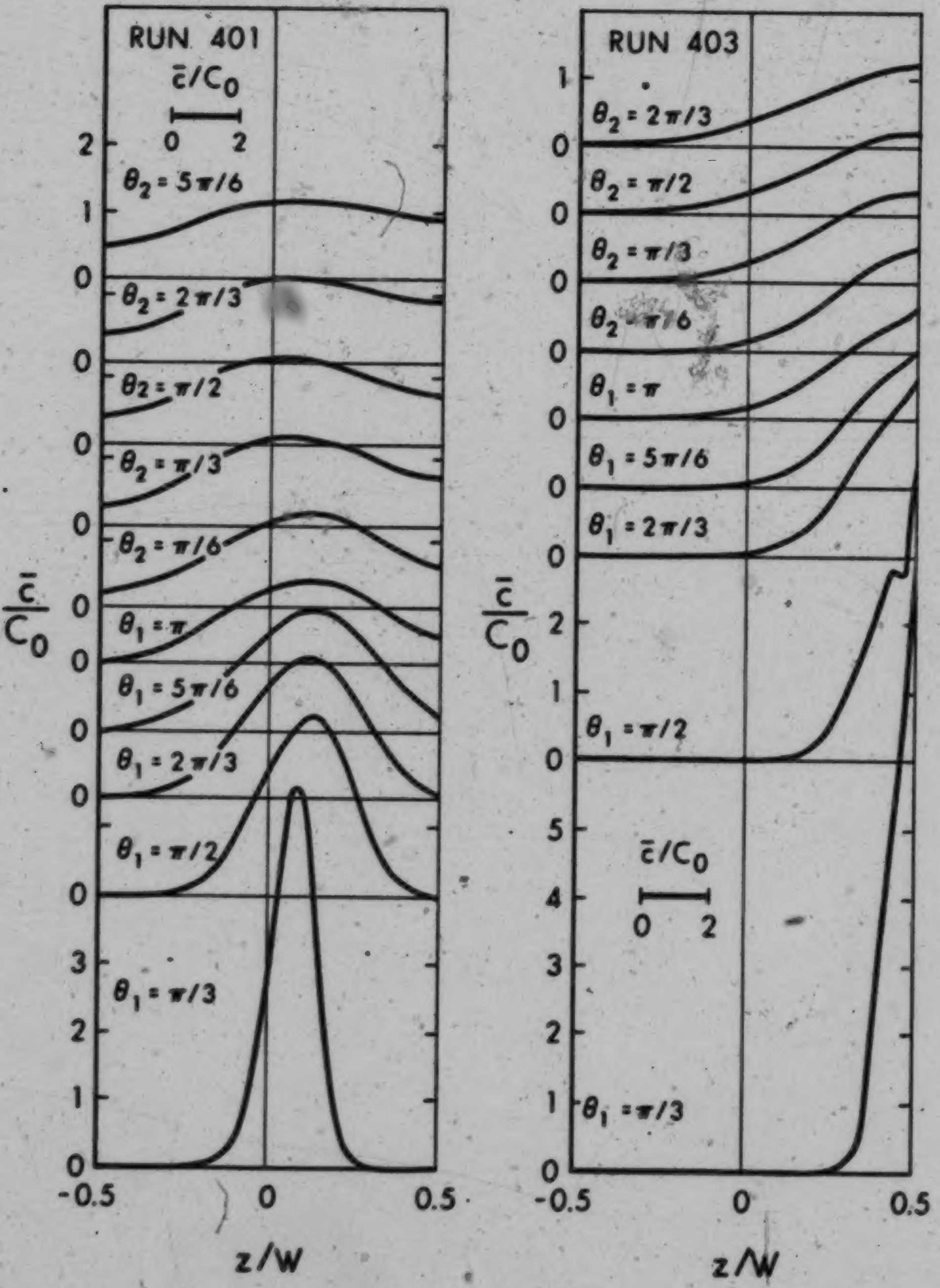

(a) (b)

FIGURE 6.12 TRANSVERSE DISTRIBUTIONS OF DEPTH-AVERAGED TRACER CONCENTRATION AT VARIOUS SECTIONS DOWNSTREAM OF SOURCE

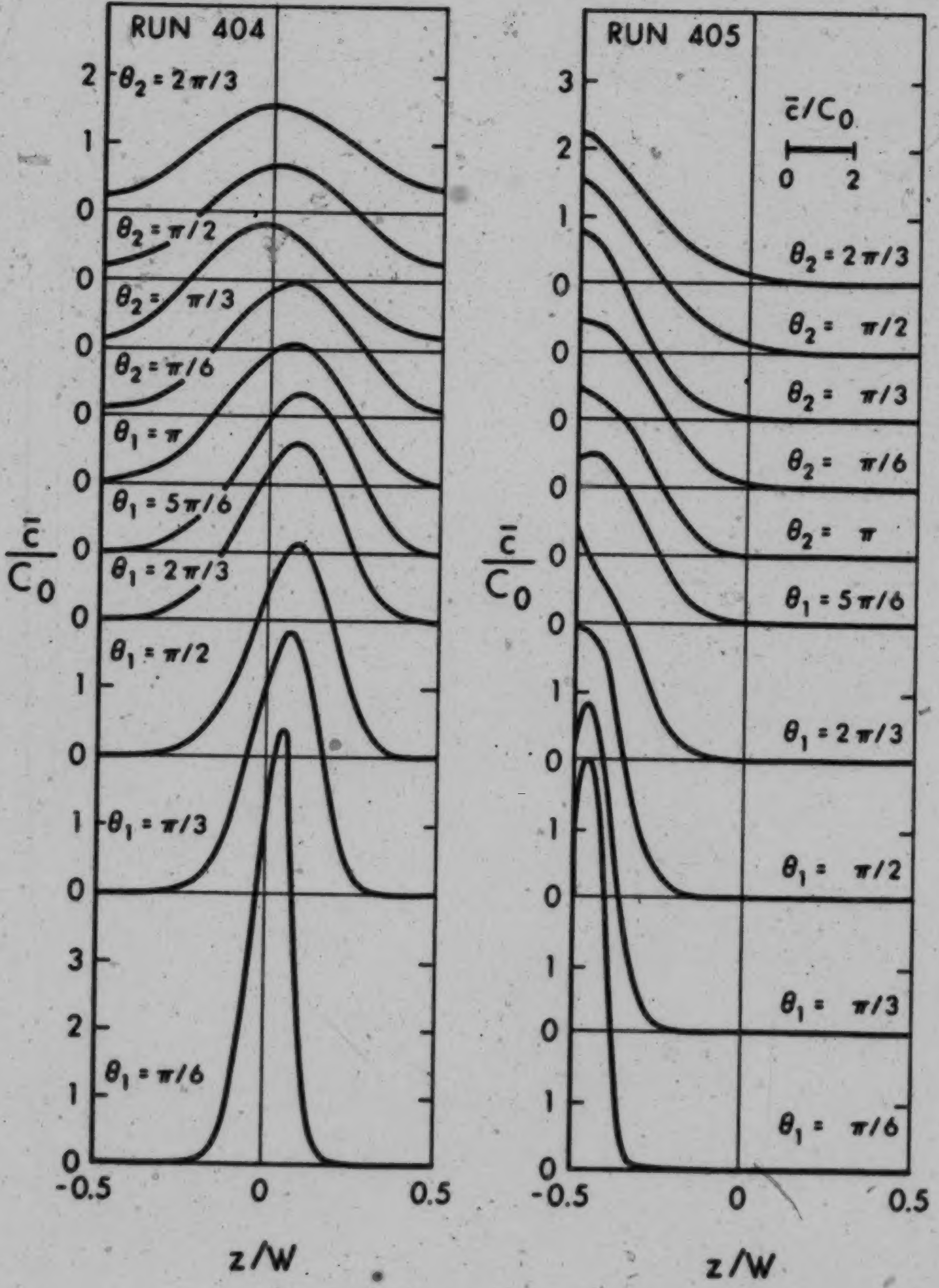

(c)

(d)

FIGURE 6.12 TRANSVERSE DISTRIBUTIONS OF DEPTH-AVERAGED TRACER CONCENTRATION AT VARIOUS SECTIONS DOWNSTREAM OF SOURCE

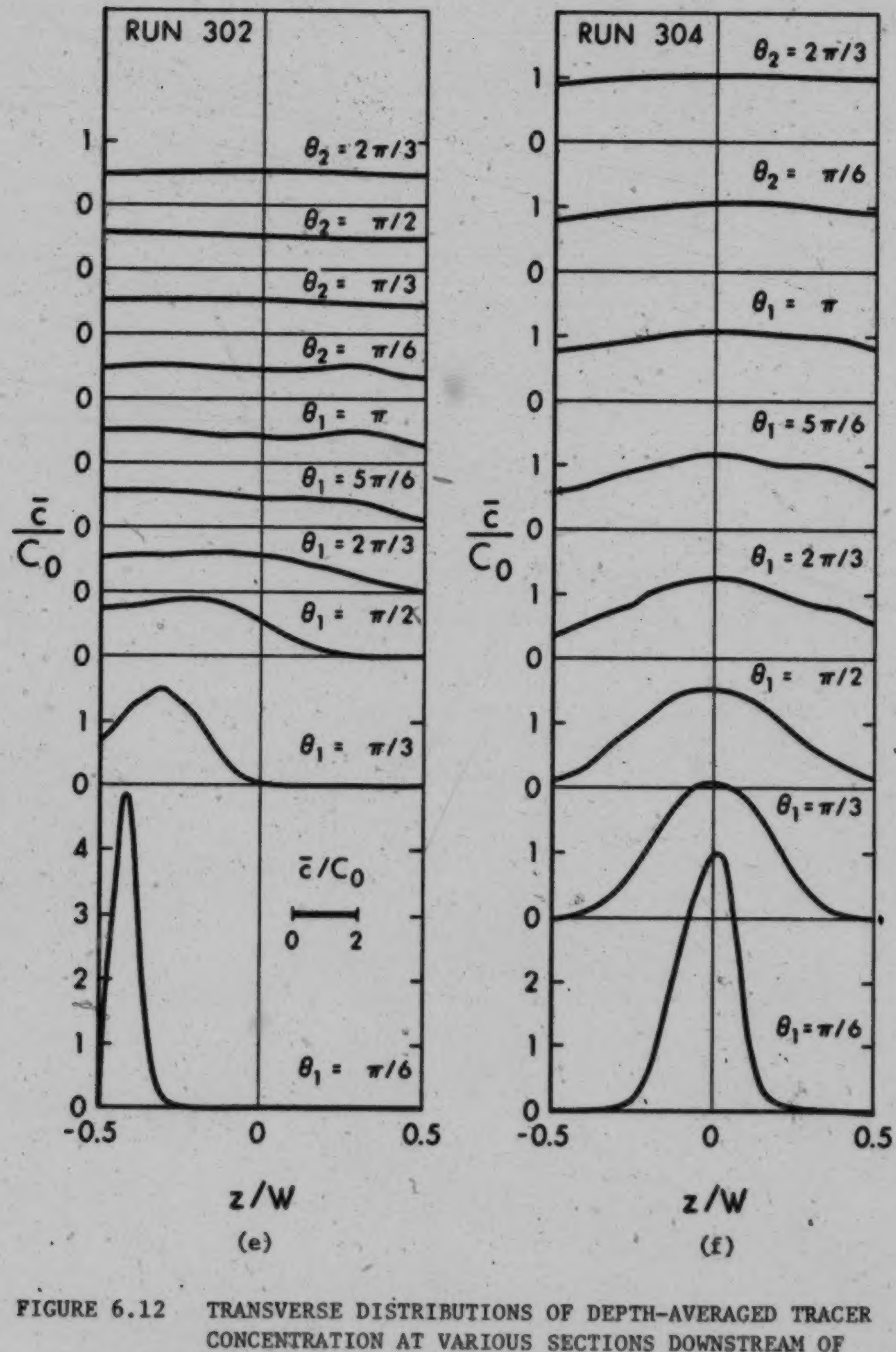

FIGURE 6.12 TRANSVERSE DISTRIBUTIONS OF DEPTH-AVERAGED TRACER CONCENTRATION AT VARIOUS SECTIONS DOWNSTREAM OF SOURCE

follows the pattern of transverse velocities in the vertical, the high concentration fluid being located near mid-depth in a vertical.

The distributions for right bank and central releases of tracer are also consistent with what would be expected to result from the pattern of transverse velocities. This means that tracer is not uniformly mixed in the vertical as is usually assumed and that distances required to achieve vertical mixing are comparatively longer in the presence of transverse velocities. The observed lateral displacement of the tracer cloud in run 401 is attributable to the fact that the tracer was released at $\theta_1 = \pi/6$ for this particular run and it is evident from Figure A9a that significant transverse velocities exist at this section. These velocities could initially shift the entire tracer cloud laterally.

Corresponding transverse concentration distributions at various levels and for different source locations are presented in Figure 6.13b for some open channel tests. Again the concentration distributions are consistent with the measured transverse velocity distributions. Run 302 indicated rather large differences in concentration over a vertical and a marked lateral displacement of the zone of high concentration. It is noted that the average velocity for this run is 0.80 ft/sec and the maximum observed transverse velocity near the water surface between $\theta_1 = 0$ and $\pi/2$ is about 0.13 ft/sec. If a vertical line source is imagined to be located at the left bank then in the absence of turbulence the observed maximum w would cause a lateral

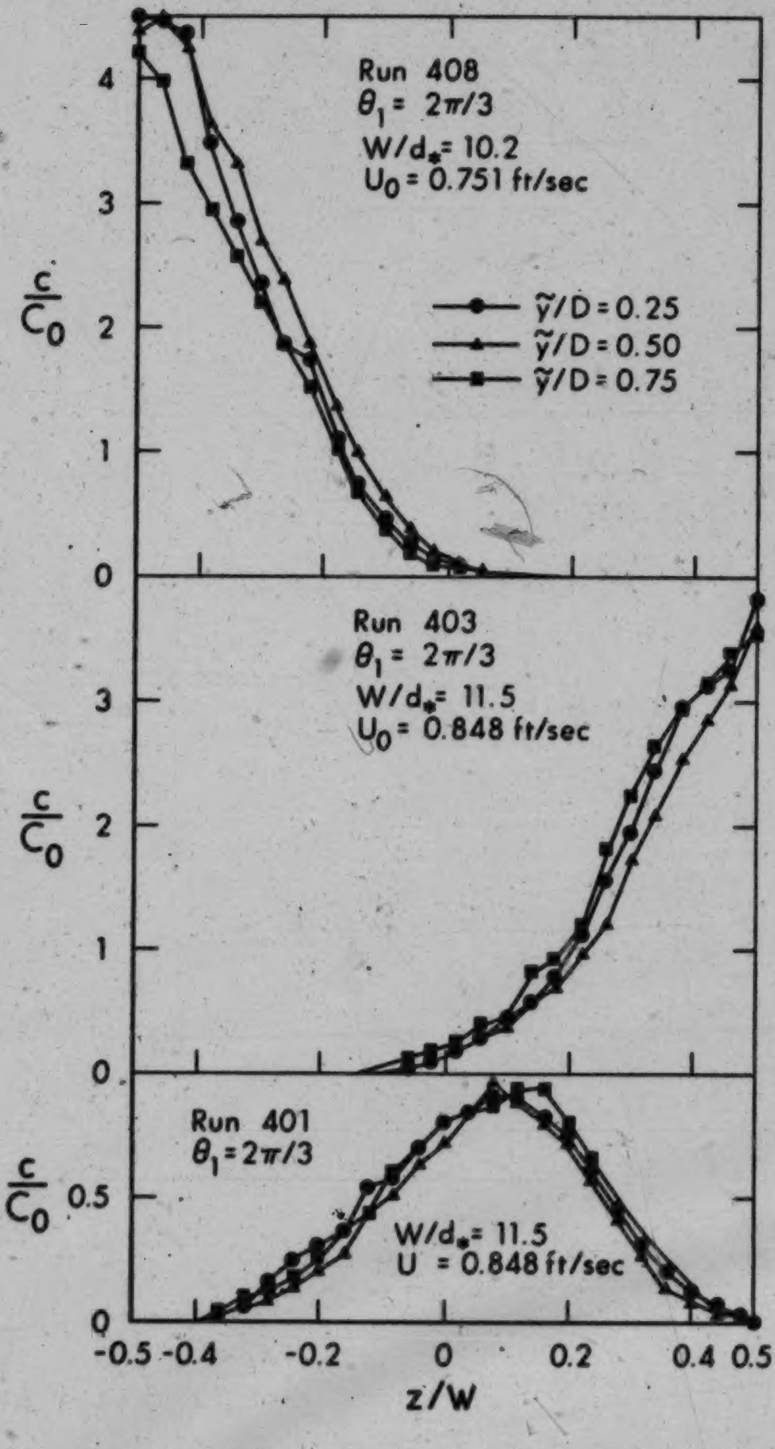

FIGURE 6.13a TRANSVERSE CONCENTRATION PROFILES AT VARIOUS FLOW LEVELS AND AT SECTION $\theta_1 = 2\pi/3$

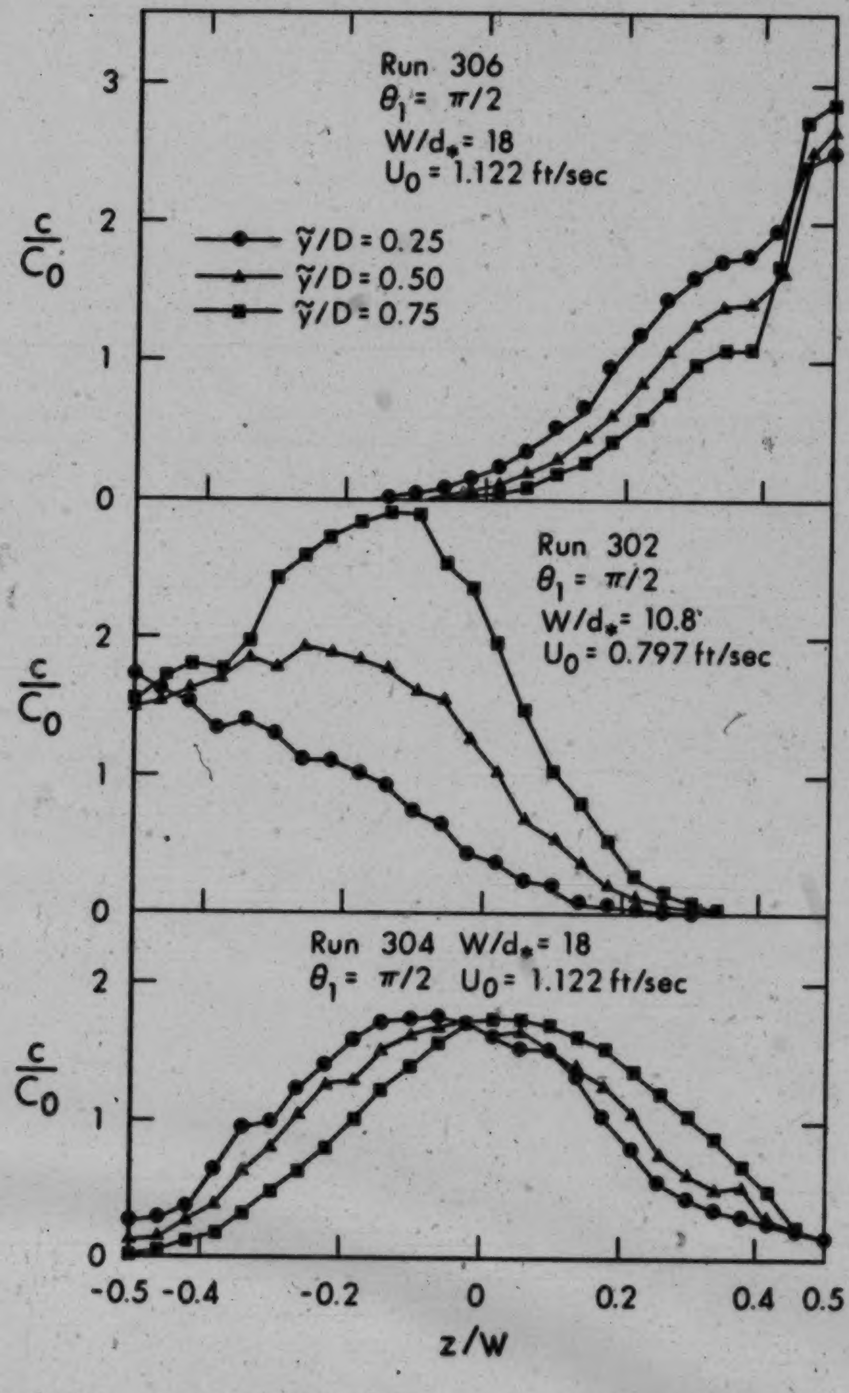

FIGURE 6.13b TRANSVERSE CONCENTRATION PROFILES AT VARIOUS FLOW LEVELS AND AT SECTION $\theta_1 = \pi/2$

spread of tracer of about 2.25 ft (or $z/w = 0.9$) at $\theta_i = \pi/2$. This lateral spread appears to be comparable to the observed spread at $\tilde{y}/D = 0.75$. Again in the absence of turbulence there will be no lateral spread in the lower half of the flow due to the effects of transverse velocities. The effect of turbulence is to even out any vertical differences in concentration, however, the large differences observed in run 302 are probably due to the fact that vertical mixing takes place over a relatively large depth. The differences for runs 304 and 306, Figure 6.11b, are seen to be less because of the smaller depth of flow.

Turbulence causes the observed vertical differences in concentration to diminish with distance downstream. However, if these differences are still large when the flow enters the second bend the subsequent reversal of the spiral motions will result in a gradual modification of the vertical concentration profiles.

The root mean square concentration deviation, C_v, often termed the coefficient of variation, of the depth-averaged transverse concentration distribution can be defined as:

$$C_v = \frac{\left\{\frac{1}{N}\sum_{j=1}^{N}[\bar{c}_j - C_o]^2\right\}^{1/2}}{C_o} .$$

C_v is a good indicator of the degree of transverse mixing and is analogous to the non-uniformity coefficient, δ, used in Chapter 5. Figures 6.14a and b give the longitudinal variation of $\bar{C}_v$ for all test

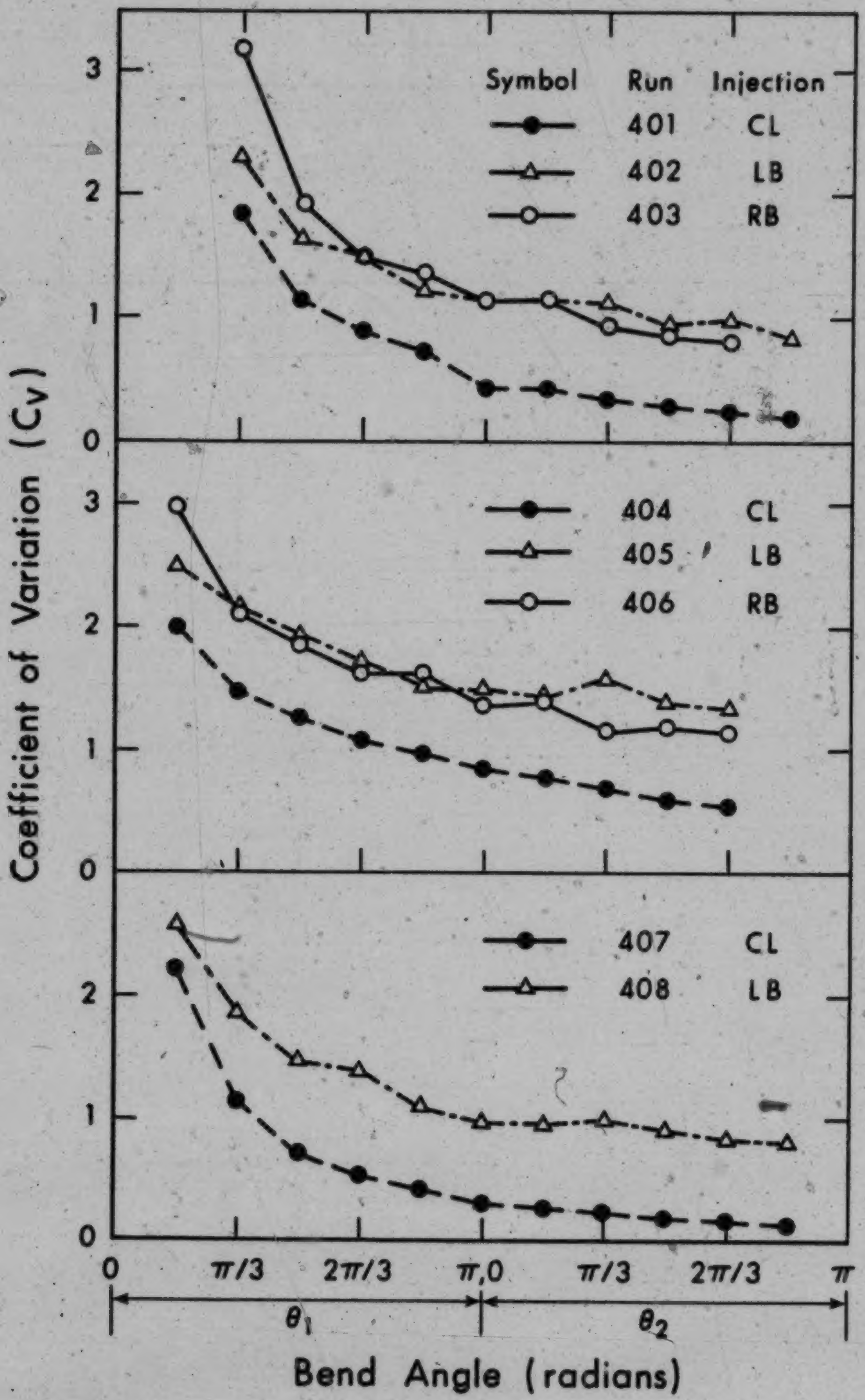

FIGURE 6.14a COEFFICIENT OF VARIATION CURVES FOR ICE-COVER TESTS

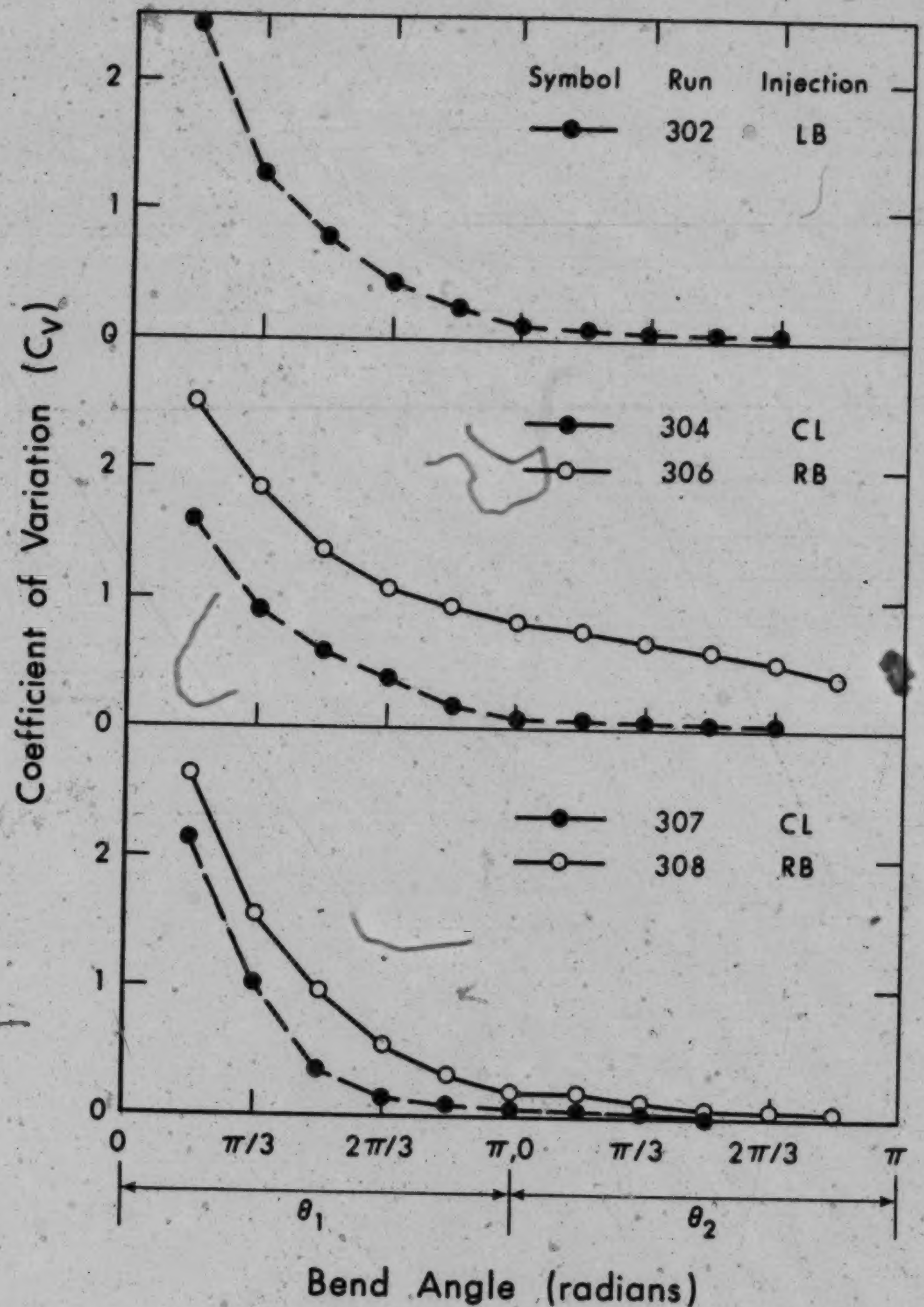

FIGURE 6.14b COEFFICIENT OF VARIATION CURVES FOR OPEN CHANNEL TESTS

runs.

It is to be noted that low values of C_v imply a high degree of mixing. As expected, much better mixing was always obtained for tracer introduced on the channel centerline compared with the side release of tracer for the same flow conditions. The diagrams also reveal a tendency for the rate of mixing to have an anomalous decrease at the beginning of the second bend ($\theta_2 = 0$ to $\theta_2 = \pi/3$). This is clearly demonstrated in runs 405 and 408, the former even indicating an increase in C_v. This phenomenon is presumably associated with the decay and reversal of the spiral motion from the first bend.

There is evidence from Figures 6.14a and b that the tracer undergoes different rates of mixing within the same bend depending on the the source position. This is consistent with previous observations in Chapter 5 that the spiral motion varied both laterally and longitudinally.

It is appropriate here to compare some of the above results with that of a straight flume. If it is assumed that $E_z/u_* d_* = 0.20$ for straight open channels, then according to the procedure of Ward (1973) the distance, X_m , required to achieve a given percentage degree of mixing (defined as $[1 - C_v] \times 100\%$) is given by $X_m/W = T_1/0.20 \cdot U_o/u_* \cdot W/d_*$. T_1 is a variable which depends on the source position and the specified degree of mixing. Run 304, for example, achieved approximately 95% mixing at $\theta_2 = \pi/3$. According to Ward's method an equivalent straight channel with the same W, d_*, U_o and u_* as in run

304 would require at least 6 times this distance to achieve the same degree of mixing.

6.2.2 Evaluation of Transverse Exchange Coefficient

6.2.2.1 Method of Moments: From the theoretical considerations of Chapter 3, the following equation was derived for evaluation of E_z':

$$\frac{d}{dx}\left[\frac{\int_{W_1}^{W_2} D(\bar{u}\,\bar{c} + \overline{u'c'})\,\eta^2 d\eta}{\int_{W_1}^{W_2} D\,\bar{u}\,\bar{c}\,d\eta}\right] - \frac{2\int_{W_1}^{W_2} D\eta\left(1 \pm \frac{\eta + z_o}{r_c}\right)(\bar{w}\,\bar{c} + \overline{w'c'})\,d\eta}{\int_{W_1}^{W_2} D\,\bar{u}\,\bar{c}\,d\eta}$$

$$= 2E_z' \left[\frac{\int_{W_1}^{W_2} \phi D\bar{c}\left(1 \pm \frac{2\eta + z_o}{r_c}\right) d\eta + \int_{W_1}^{W_2} \phi\bar{c}\eta\left(1 \pm \frac{\eta + z_o}{r_c}\right)\frac{\partial D}{\partial \eta}\,d\eta}{\int_{W_1}^{W_2} D\,\bar{u}\,\bar{c}\,d\eta}\right]$$

$$- 2E_z' \left[\frac{\int_{W_1}^{W_2} \phi\,\frac{\partial}{\partial \eta}\left\{D\bar{c}\eta\left(1 \pm \frac{\eta + z_o}{r_c}\right)\right\} d\eta}{\int_{W_1}^{W_2} D\,\bar{u}\,\bar{c}\,d\eta}\right] \qquad (3.27)$$

To assess the importance of the dispersion term $\overline{u'c'}$ a straight line was fitted by least squares to the concentration data in a vertical and the c' values were determined although the vertical concentration profiles were sometimes far from linear. The velocity distributions over verticals with concentration data were determined by interpolation and the u' values computed. The $\overline{u'c'}$ values were then evaluated by numerical integration. It was found that $\overline{u'c'}$ was in general about two orders of magnitude smaller than $\bar{u}\,\bar{c}$ and, therefore could be neglected.

By a suitable choice of coordinate system it is generally possible to make the depth-averaged transverse velocity, $\bar{w}$, negligibly small and for this situation the convective term $\bar{w}\,\bar{c}$ becomes unimportant. Such a coordinate system was employed by Yotsukura and Cobb (1972) who used the cumulative discharge, q_*, as an alternative transverse coordinate. This system of coordinates will be utilised in Chapter 7 to analyse the field data and it is shown there that this method gives practically the same value of E_{zw} as that obtained by using the meandering coordinate system. This indicates that $\bar{w}\,\bar{c}$ is of secondary importance compared with $\overline{w'c'}$. In the laboratory, the magnitude of $\bar{w}$ was of the same order as the error in measurement of w hence $\bar{w}\,\bar{c}$ could not be accurately determined. However, because of its apparent unimportance in the more extreme field situation it was assumed so in the laboratory.

The major effects of curvature on the mixing, therefore, must be caused by the dispersion term $\overline{w'c'}$. A general comparison of the relative importance of $\overline{w'c'}$ and transverse diffusion can be made using, for example, the data from run 401 (centerline injection). It is noted that the average velocity for this run is 0.85 ft/sec and the average relative transverse velocity between tracer particles located in the central and either the upper or lower layers of the flow is about 0.085 ft/sec. The transverse displacement rate due to this relative transverse velocity would be $\frac{0.085}{0.85} = 0.1$ ft per foot of channel length. An estimate of the diffusion rate can be obtained by assuming that the concentration distribution due to diffusion alone is Gaussian and that $E_z/u_* d_* = 0.10$. If it is noted that in run 401 $U_o/u_* = 12.65$, the above assumptions indicate that the standard deviation:

$$\sigma_z \left(= \left[\frac{2E_z}{u_* d_*} \cdot \frac{u_*}{U_o} d_* x \right]^{1/2} \right)$$

would grow at a rate of about 0.029 ft per foot length of channel. The displacement rate due to transverse velocities is, therefore, much greater than that caused by diffusion. The same was observed to be true for the open channel tests. It is clear from the above illustration that the transverse spreading of tracer could be reduced appreciably in regions where the pattern of transverse velocities reverses.

The function ϕ generally varies in an unknown manner. In the present analysis it is assumed equal to unity. For this situation $E'_z = E_z$ and since $\overline{u'c'} \ll \overline{u}\,\overline{c}$ Equation 3.27 can be simplified to:

$$\frac{dM_2(X)}{dX} - G(X) = E_z \cdot B(X) \tag{6.16}$$

in which:

$$M_2(X) = \left[\int_{W_1}^{W_2} D\,\bar{u}\,\bar{c}\,\eta^2 d\eta\right] \Bigg/ \left[\int_{W_1}^{W_2} D\,\bar{u}\,\bar{c}\,d\,\eta\right] \tag{6.17}$$

and represents the second moments of the tracer flux about point of tracer release:

$$G(X) = \frac{2\displaystyle\int_{W_1}^{W_2} D\eta\left(1 \pm \frac{\eta + z_o}{r_c}\right)\left(\bar{w}\,\bar{c} + \overline{w'c'}\right)d\eta}{\displaystyle\int_{W_1}^{W_2} D\,\bar{u}\,\bar{c}\,d\,\eta} \tag{6.18}$$

and:

$$B(X) = 2\left[\frac{\displaystyle\int_{W_1}^{W_2} D\bar{c}\left(1 \pm \frac{2\eta + z_o}{r_c}\right)d\eta + \int_{W_1}^{W_2} \bar{c}\eta\left(1 \pm \frac{\eta + z_o}{r_c}\right)\frac{\partial D}{\partial \eta}\,d\eta}{\displaystyle\int_{W_1}^{W_2} D\,\bar{u}\,\bar{c}\,d\,\eta}\right]$$

$$- 2\left[\frac{\displaystyle\int_{W_1}^{W_2} \frac{\partial}{\partial \eta}\left\{D\bar{c}\eta\left(1 \pm \frac{\eta + z_o}{r_c}\right)\right\}d\eta}{\displaystyle\int_{W_1}^{W_2} D\,\bar{u}\,\bar{c}\,d\,\eta}\right] \tag{6.19}$$

Equation 6.16 simply states that the change in second moments of the tracer flux results from the spreading of tracer caused by transverse velocities and diffusion. The transverse exchange (or diffusion) coefficient E_z can be determined using Equation 6.16 provided the variations of $M_2(X)$, $G(X)$ and $B(X)$ are known.

In practical situations we are more often interested in the overall mixing due to both turbulence and transverse velocities and it is convenient to define an exchange coefficient which accounts for these two factors. It was shown in Chapter 3 that the relevant equation for the above situation is Equation 3.29. Again, if ϕ_w is regarded as equal to unity and therefore $E'_{zw} = E_{zw}$ then since $\bar{u}\,\bar{c} >> \overline{u'c'}$ Equation 3.29 can be simplified to:

$$\frac{dM_2(X)}{dX} = E_{zw} \cdot B(X) \tag{6.20}$$

The variation of the second moments of the tracer flux, $M_2(X)$, with longitudinal distance, X, are presented in Figures 6.15a and b, for some test runs. In general $M_2(X)$ varied non-linearly with X and this non-linearity is believed to be related to the growth, decay and reversal of the spiral motions. Some of the plots indicate a flattening out and even a decrease of $M_2(X)$ between $\theta_2 = 0$ and $\pi/3$.

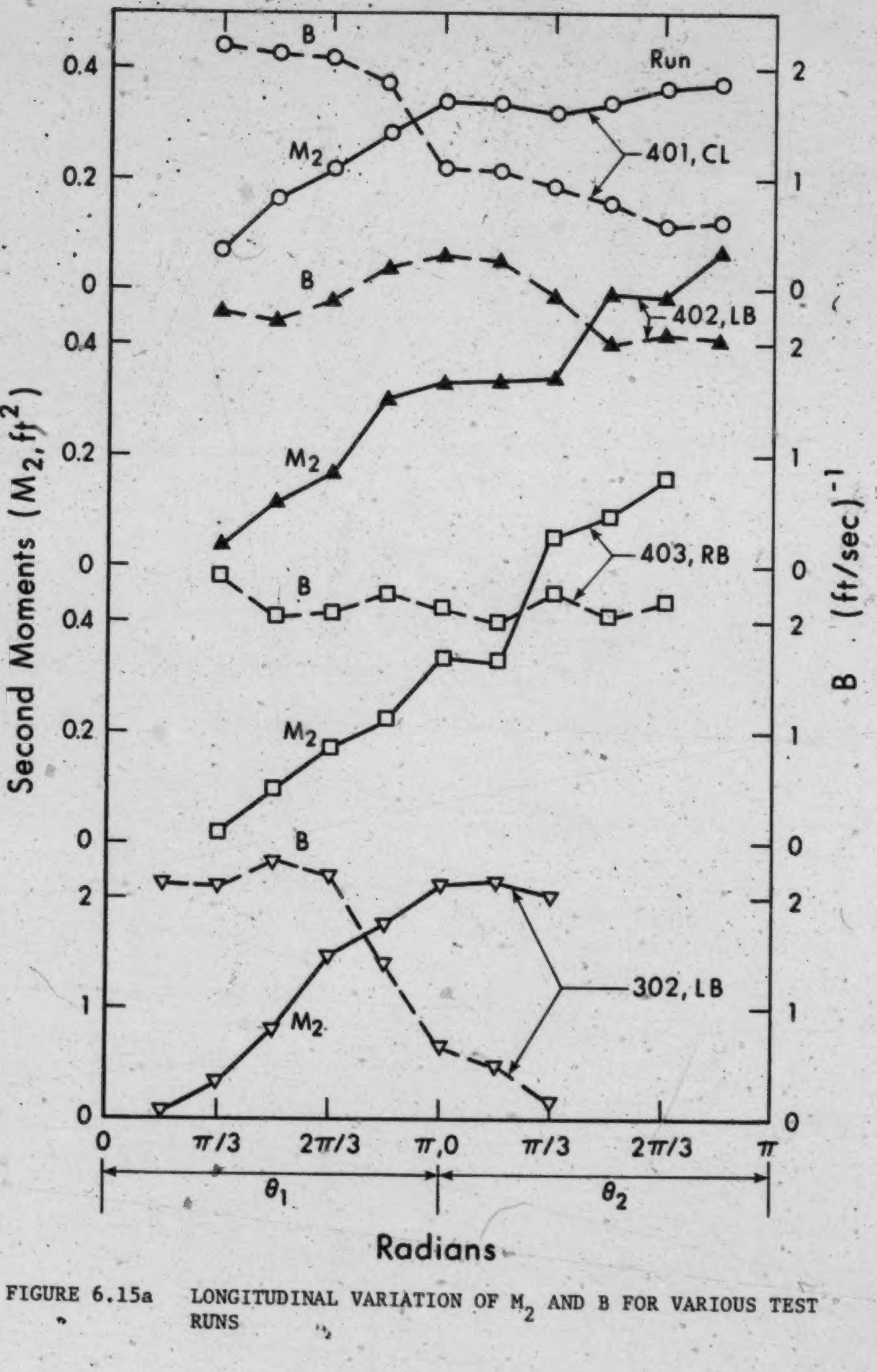

FIGURE 6.15a LONGITUDINAL VARIATION OF M_2 AND B FOR VARIOUS TEST RUNS

173

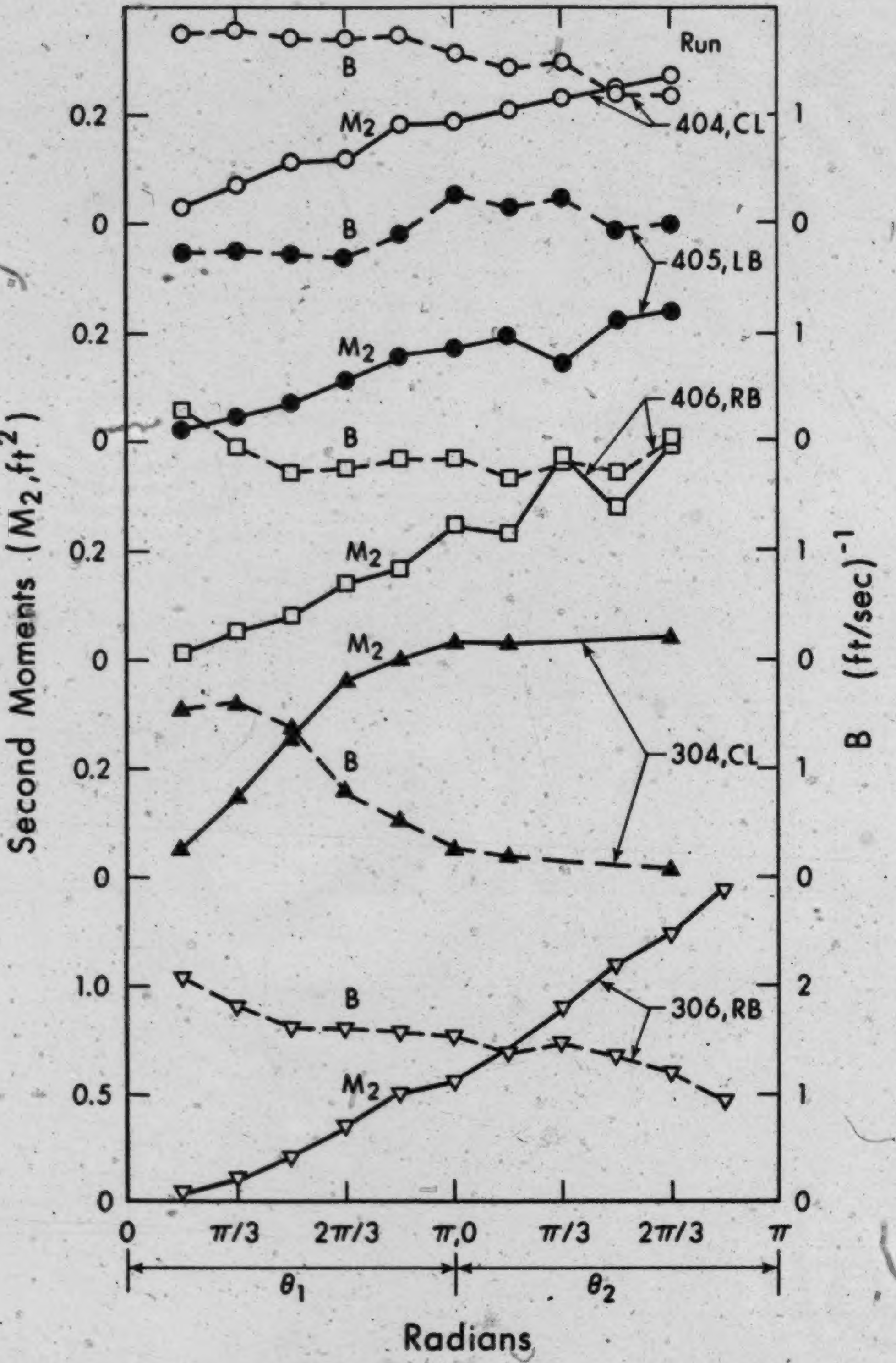

FIGURE 6.15b LONGITUDINAL VARIATION OF M_2 AND B FOR VARIOUS TEST RUNS

There is a significant dip in $M_2(X)$ for run 406 at $\theta_2 = \pi/2$. A study of velocity profiles for this run in Figures 5.13 reveals that the warping of the plywood (ice-cover) caused the maximum flow depth to occur at the inside of the bend instead of the outside as could be anticipated. The change in cross-sectional shape between $\theta_2 = \pi/3$ and $\pi/2$ could cause a net transverse flow towards the right bank and thus inhibit the spreading of the tracer to the left bank. This will manifest itself by a reduction in the observed value of $M_2(X)$ and probably by a slight increase in C_v (see Figure 6.14a). If the above physical reasoning is correct then there must be a corresponding increase in $M_2(X)$ at $\theta_2 = \pi/2$ for left-bank release of tracer under the same flow conditions. This is confirmed by the variation of $M_2(X)$ for run 405 in Figure 6.15b.

As the tracer concentration becomes more uniform across the channel, the second moments of the tracer flux, $M_2(X)$, should approach a constant value. This is illustrated by runs 304 and 401 in Figure 6.15a, b. From Equation 6.19, the following functions can be defined for $\phi_w = 1.0$:

$$B_1(X) = 2\left[\int_{W_1}^{W_2} D\bar{c}\left(1 \pm \frac{2\eta + z_o}{r_c}\right)d\eta\right] \Bigg/ \left[\int_{W_1}^{W_2} D\,\bar{u}\,\bar{c}\,d\eta\right] \qquad (6.21)$$

$$B_2(X) = 2\left[\int_{W_1}^{W_2} \bar{c}\eta\left(1 \pm \frac{\eta + z_o}{r_c}\right) \frac{\partial D}{\partial \eta}\, d\eta\right] \Bigg/ \left[\int_{W_1}^{W_2} D\, \bar{u}\, \bar{c}\, d\, \eta\right] \qquad (6.22)$$

$$B_3(X) = 2\left[\int_{W_1}^{W_2} \frac{\partial}{\partial \eta} \left\{D\bar{c}\eta\left(1 \pm \frac{\eta + z_o}{r_c}\right)\right\} d\eta\right] \Bigg/ \left[\int_{W_1}^{W_2} D\, \bar{u}\, \bar{c}\, d\, \eta\right] \qquad (6.23)$$

so that:

$$B(X) = B_1(X) + B_2(X) - B_3(X) \qquad (6.24)$$

The longitudinal variation of B_1, B_2, B_3 and B are given in Figures 6.16a, b and c for some test runs. It is evident from these plots that for centerline release B_1 remained reasonably constant over the length of the test reach. However, for injection at the right bank, B_1 was initially high but decreased to a fairly steady value downstream. When tracer is introduced near the left bank B_1 increases to a maximum before dropping to a near constant value. These differences in the observed B_1 distributions for the various source locations can be explained by imagining a vertical line source of unit width and uniform concentration C_s with its centroid located at z_o. It is to be noted that $r_c = 9$ ft and that within the first bend:

$$B_1 = \left[\int_{W_1}^{W_2} D\bar{c}\left(1 + \frac{2\eta + z_o}{r_c}\right) d\eta \right] \Big/ Q_s$$

where Q_s is the tracer flux. The following relations can be obtained for B_1 at the section of tracer release (X = 0) for the various source locations:

Source at left bank, $z_o = -1.20$ $\quad B_1(0) = 0.867\ DC_s/Q_s$

Source at centerline, $z_o = 0$ $\quad B_1(0) = 1.0\ DC_s/Q_s$

Source at right bank, $z_o = 1.20$ $\quad B_1(0) = 1.133\ DC_s/Q_s$

The above relations predict an initially high B_1 value for injection at the right bank and a low value at the left bank. These differences in B_1 values therefore appear to be largely due to the system of coordinates used here.

B_2 expresses the importance of depth variations within a cross-section on the mixing. Such variations in the laboratory experiments result from superelevation and unevenness of flume bed and ice-cover. It is evident from Figure 6.16 that variations in depth were generally insignificant in the laboratory tests.

B_3 does not influence or affect the computed value of E_{zw} until a significant portion of tracer encounters both banks. For the

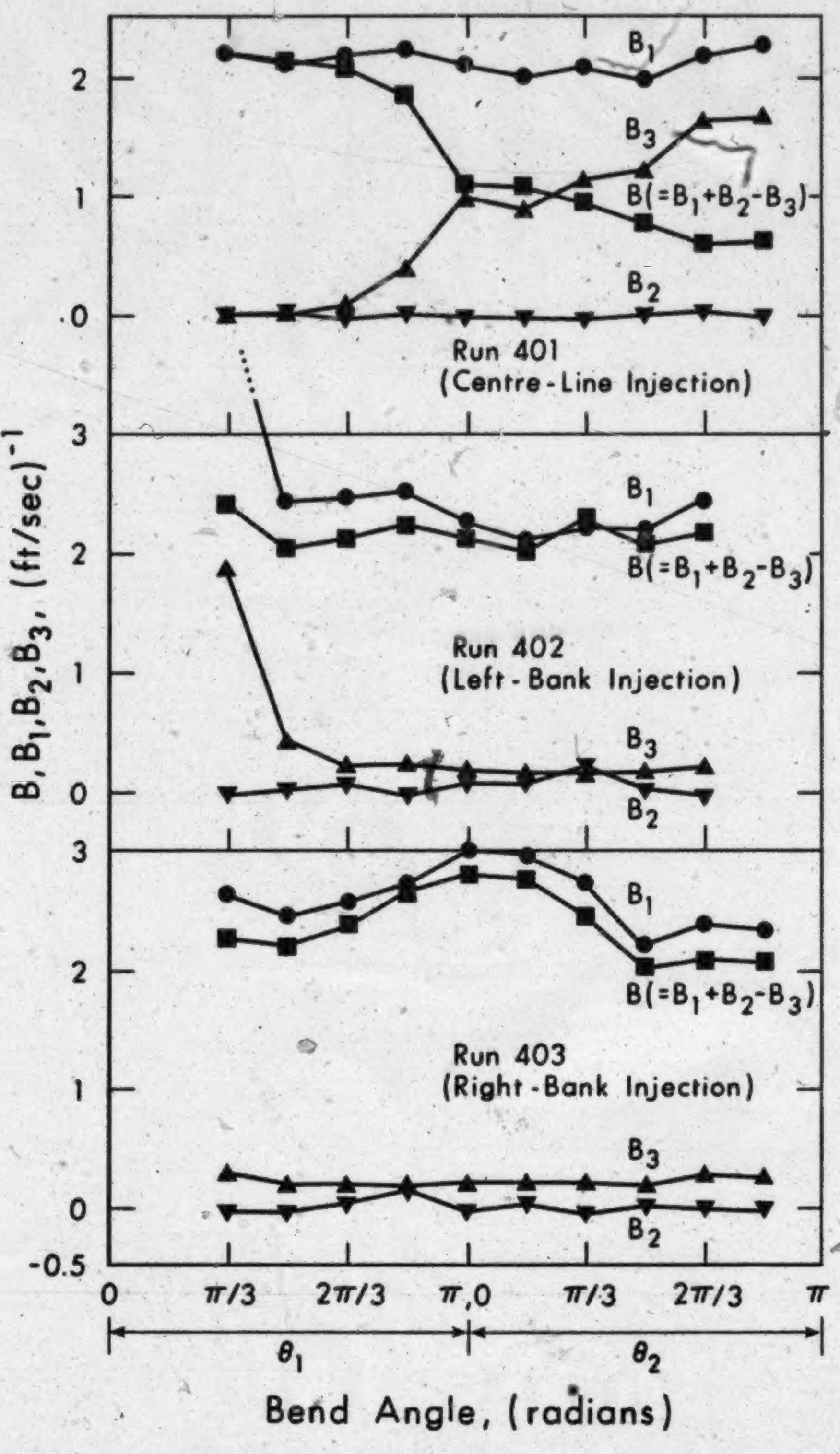

FIGURE 6.16a LONGITUDINAL VARIATION OF B_1, B_2, B_3 AND B

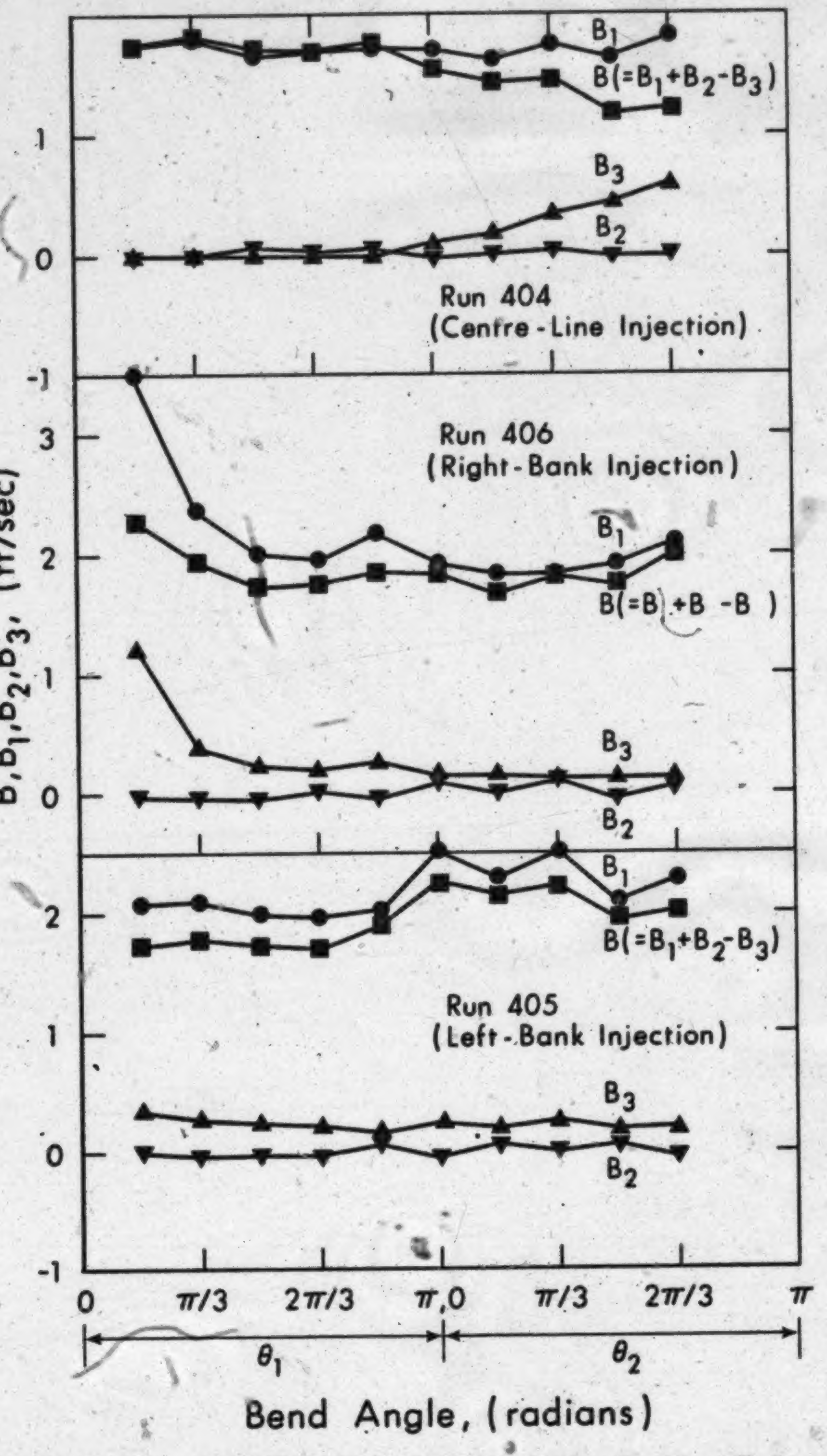

FIGURE 6.16b LONGITUDINAL VARIATION OF B_1, B_2, B_3 AND B

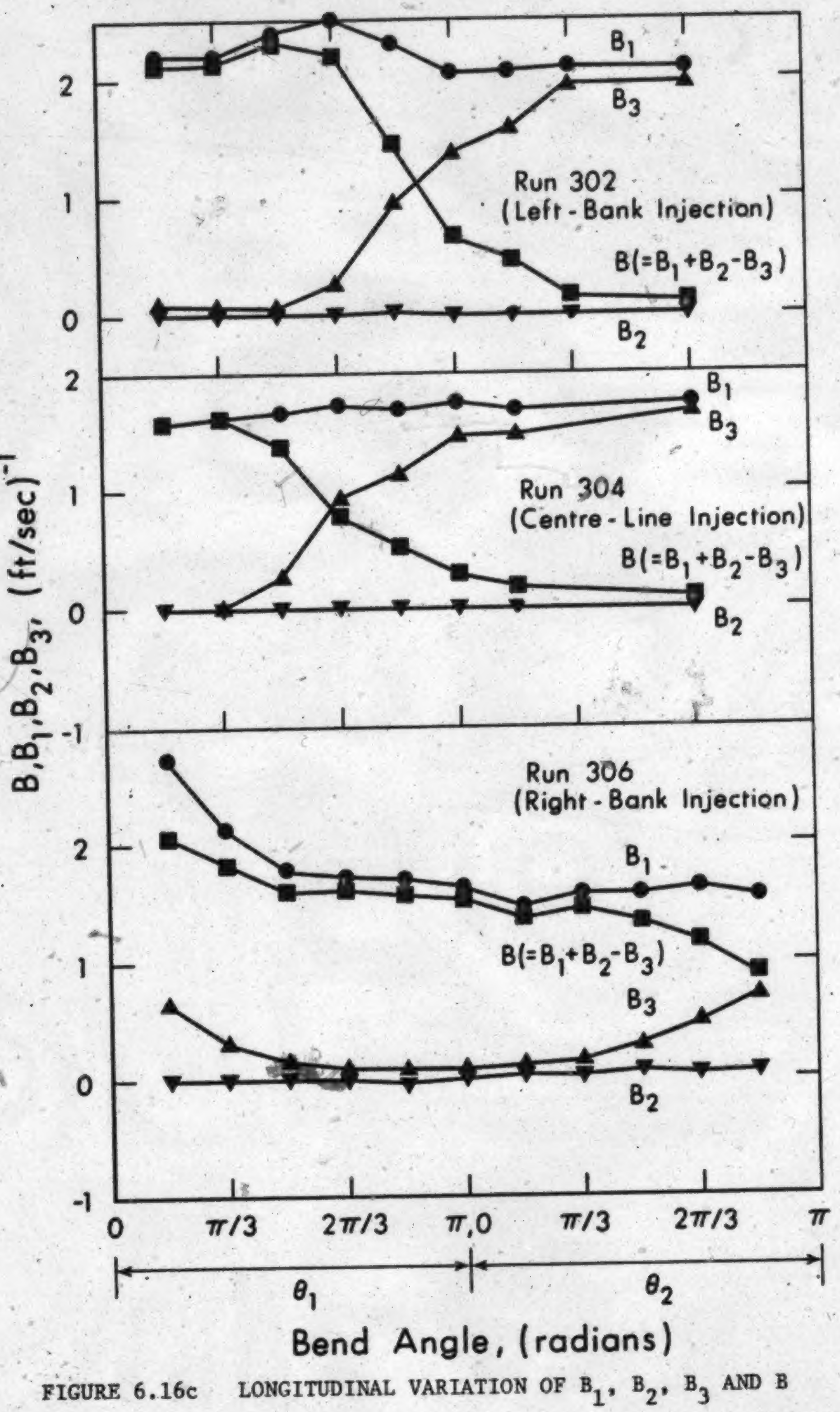

FIGURE 6.16c LONGITUDINAL VARIATION OF B_1, B_2, B_3 AND B

179

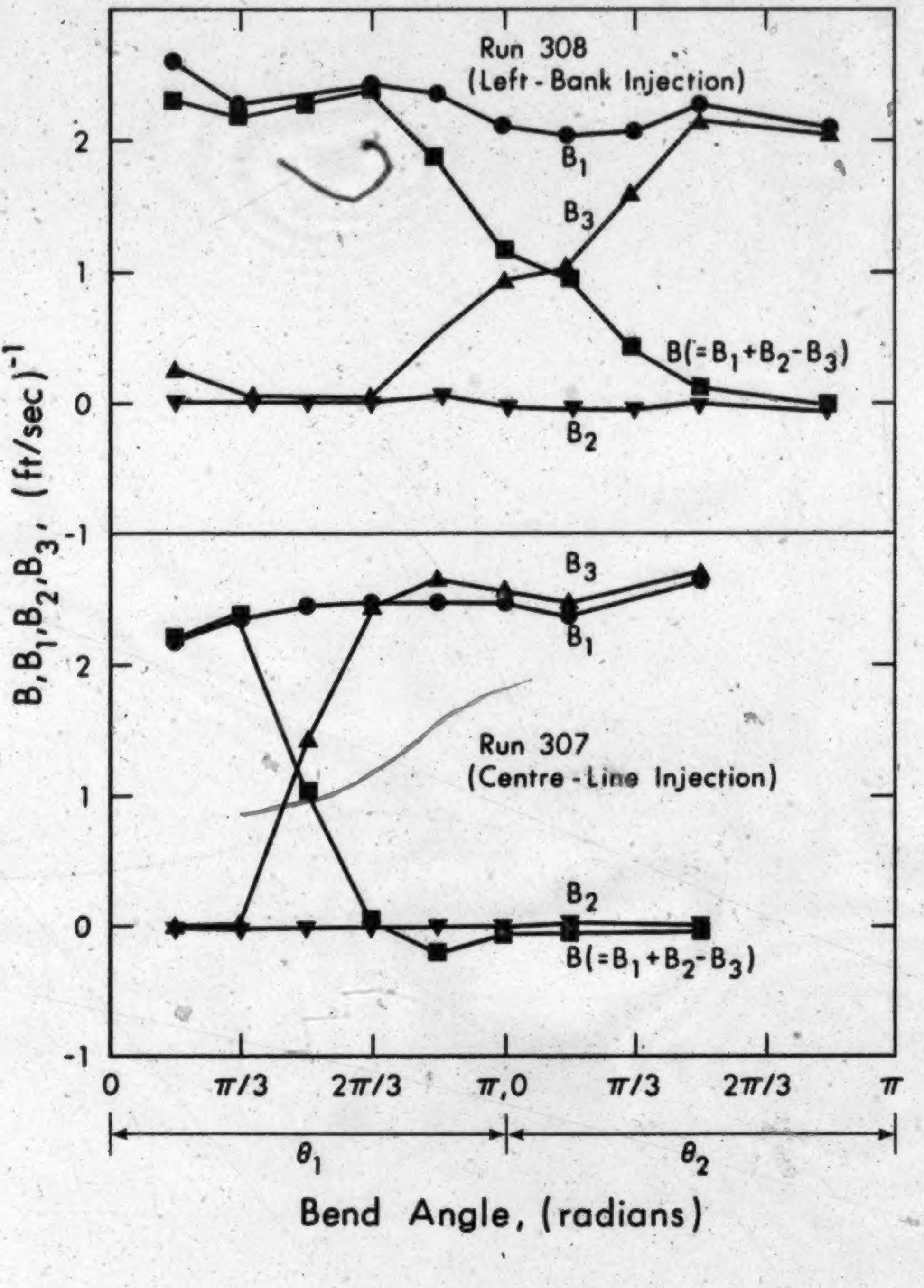

FIGURE 6.16d LONGITUDINAL VARIATION OF B_1, B_2, B_3 AND B

situation where the source position is near the side, B_3 is expected to decrease slightly with distance downstream because of the decay of concentration along the bank on which the source is located. However, as more tracer encounters the opposite bank B_3 might increase and approach a constant value which is attained when the tracer becomes uniformly mixed laterally (see Figure 6.16c and runs 302 and 306). Strong variations in B_3 were observed for right bank injection compared with left bank tracer release. Figures 6.12b and e, for example, reveal that the concentrations at the right bank are much higher when tracer is released near this bank compared with the corresponding case of left bank injection. For source located at the channel center B_3 will be zero until the tracer reaches the sides and then will increase until tracer is uniformly mixed.

From the above discussions B $(= B_1 + B_2 - B_3)$ is expected to decrease gradually with distance downstream of the source and to approach zero as the tracer becomes fully mixed. This trend can be seen in Figures 6.16 for some of the test runs. Some test runs, for example 403 and 406, do not exhibit this expected variation in B and this is attributed to the fact that these runs did not achieve any appreciable degree of mixing even at $\theta_2 = 2\pi/3$.

The longitudinal variation of $B(X)$ is presented in Figures 6.15a and b together with that of $M_2(X)$ for some test runs. Numerical values of $M_2(X)$, $B(X)$ and E_{zw} for all test runs are summarised in Table 6.5. To facilitate comparison of ice-cover experiments (series

400) with those having free water-surface (series 300), tests performed under similar flow conditions are given the same number in their respective series. Comparison of the E_{zw} values for the open channel and ice-cover tests will be given later.

6.2.2.2 Integral Method: The integral method is used not only to evaluate the average transverse mixing coefficient over a channel reach but also the variation of E_{zw} over transverse portions of the same reach. It is to be noted that E_{zw} in this case represents the average transverse mixing coefficient for either the whole or part of the reach. From the theoretical considerations in Chapter 3 it was shown that:

$$\int_{W_1}^{z} \left[\frac{d}{dx} \int_{W_1}^{z} D(\bar{u}\,\bar{c} + \overline{u'c'})dz \right] dz =$$

$$E_{zw} \left[\left\{ Dh_1\bar{c} \right\}_{W_1}^{z} - \int_{W_1}^{z} \bar{c}\, \frac{\partial (Dh_1)}{\partial z}\, dz \right] \qquad (3.36)$$

The integrals in the above equation were determined numerically by performing the integration from the bank of tracer release for progressively increasing or decreasing values of z until the entire width of the tracer cloud was covered. The value of the term in square brackets on the RHS of Equation 3.36 was evaluated by averaging the corresponding values at the beginning and end of a reach. The cross-channel variation of E_{zw} within a reach is shown plotted at the downstream section of the same reach in Figures 6.17a to d for some test runs. It is mentioned that the observed lateral and longitudinal variations in E_{zw} are actually due to variations in the depth-averaged transverse mixing coefficient $\bar{\varepsilon}_{zw}$ since E_{zw} is considered to represent the average of the generally variable $\bar{\varepsilon}_{zw}$.

As the integrations in Equation 3.36 proceed from one bank to the other the effect of small variations in $\bar{\varepsilon}_{zw}$ on E_{zw} are not discernible from the plots and appreciable changes in $\bar{\varepsilon}_{zw}$ only cause a slight change in E_{zw} especially when the integration covers a large percentage of the channel width.

Figure 6.17 shows that negative values of E_{zw} occur near the left bank when the source is located close to this bank. This can be seen in both ice-cover and open channel tests and for some distance downstream of the source. This feature is not unreasonable because the spiral motions could initially displace the zone of maximum depth-averaged concentration away from the left bank (see Figures 6.12d and e) and at the same time transport low depth-averaged concentration fluid from the sides against the concentration gradient to regions of high depth-averaged concentration consequently causing a negative E_{zw}. As expected, this does not occur for tracer released near the right bank. The plots also indicate low and even negative E_{zw} values at the beginning of the second bend and this accords with the results from the moments method.

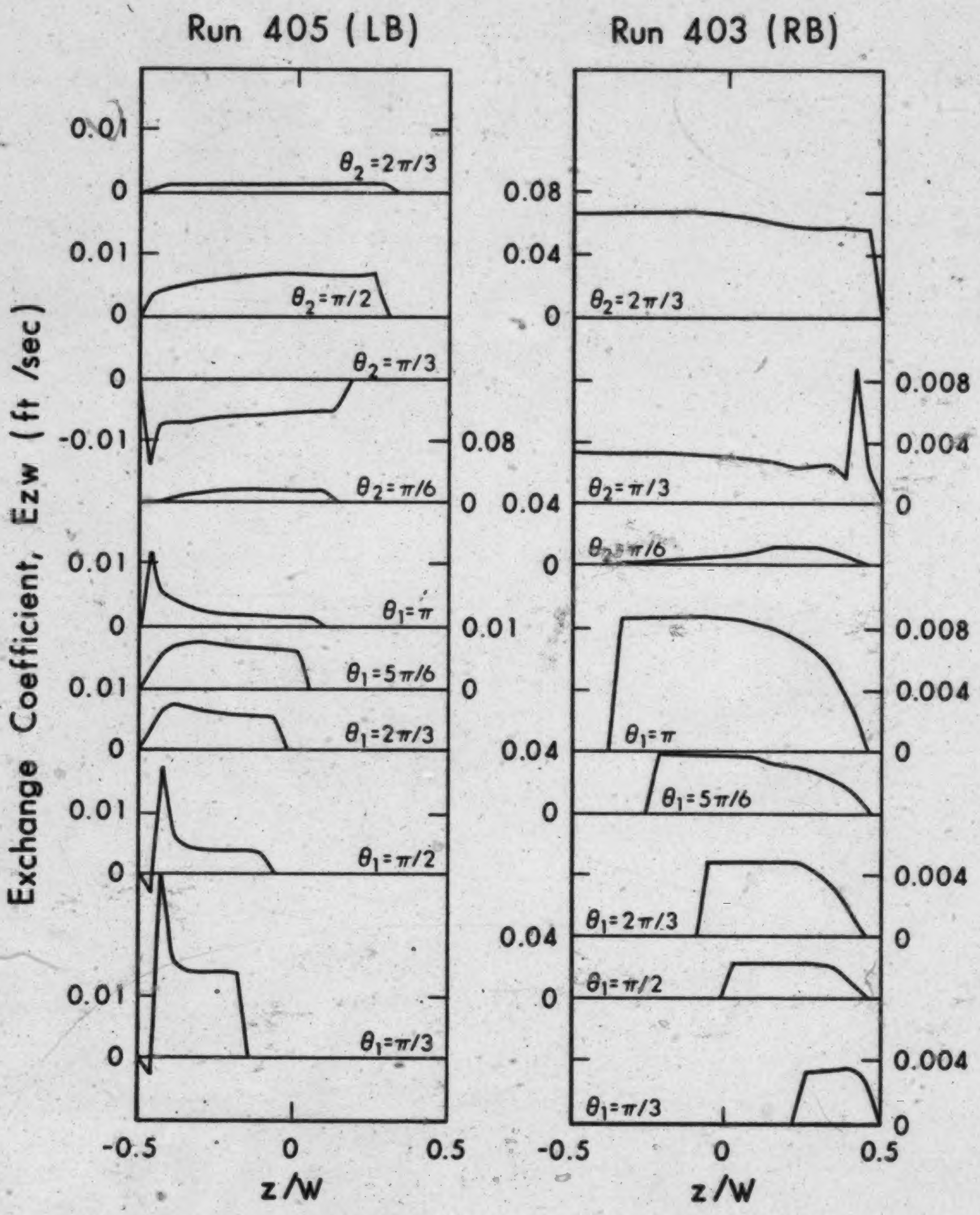

(a)

(b)

FIGURE 6.17 LONGITUDINAL AND LATERAL VARIATION OS THE MIXING COEFFICIENT E_{zw}

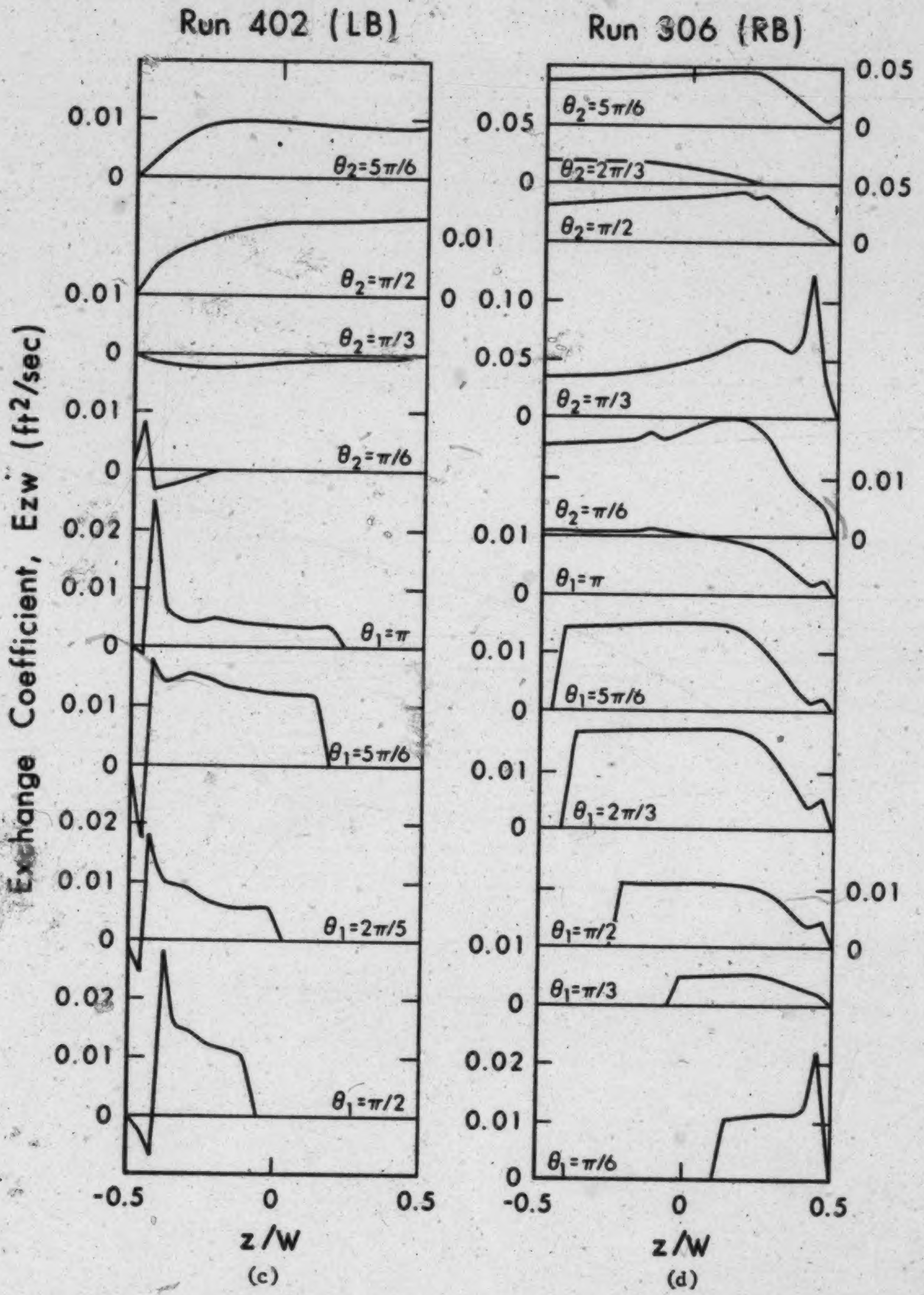

(c) (d)

FIGURE 6.17 LONGITUDINAL AND LATERAL VARIATIONS OF THE MIXING COEFFICIENT E_{zw}

For situations where source is located at the right bank E_{zw}, or more correctly $\bar{\varepsilon}_{zw}$, is again seen to exhibit marked variations near this bank in both bends. Figures 6.17 show that there are similarities in the general pattern of variation of E_{zw} for the same source position but different flow conditions. This is dramatically illustrated by runs 306 and 403. Both runs indicated a high E_{zw} value near the right bank between $\theta_2 = \pi/6$ and $\pi/3$ although the pattern of spiral motions was different in both runs. No explanation can be offered for this behaviour in E_{zw} but it is speculated that it might be due to some strong disturbance within the flow in the neighbourhood of the right bank between $\theta_2 = \pi/6$ and $\pi/3$.

It is evident from Figures 6.17 that the depth-averaged transverse mixing coefficient varied both along and across the channel. The variation of E_{zw} for the various test runs is listed in Table 6.5 together with the values obtained by the method of moments.

The integral method was found not to work for situations where the source was located at the channel centerline. It yielded values of E_{zw} which were on the average an order of magnitude greater than those given by the method of moments.

It is evident from Table 6.5 that for similar conditions of discharge and flow depth and for the same source position the mixing capacity as measured by E_{zw} was of the order 3 to 6 times greater for open channel flows than for ice-covered flows. The straight flume

TABLE 6-5 SUMMARY OF NUMERICAL VALUES OF $M_2(X)$, B(X) AND E_{zw}

RUN	406 RB				306 RB			
Section	$M_2(X)$ ft^2	B(X) $(ft/s)^{-1}$	E_{zw} (M)* ft^2s^{-1}	E_{zw} (I)* ft^2s^{-1}	$M_2(X)$ ft^2	B(X) $(ft/s)^{-1}$	E_{zw} (M) ft^2s^{-1}	E_{zw} (I) ft^2s^{-1}
θ_1 0	0	2.460			0	2.250		
			0.00226	0.00322			0.00479	0.00824
π/6	0.0144	2.460			0.0321	2.250		
			0.00348	0.00180			0.00804	0.00394
π/3	0.0516	2.357			0.0976	2.114		
			0.00332	0.00227			0.01338	0.00866
π/2	0.0836	2.037			0.2127	1.768		
			0.00639	0.00508			0.01903	0.01439
2π/3	0.1404	2.022			0.3569	1.676		
			0.00341	0.00106			0.01685	0.01364
5π/6	0.1665	1.872			0.4834	1.566		
			0.00910	0.00764			0.00785	0.01050
θ_2 ~~0~~ π	0.2430	1.711			0.5671	1.588		
			-0.00281	-0.00231			0.01389	0.01606
π/6	0.2284	1.544			0.6962	1.444		
			0.01878	0.02072			0.02644	0.03617
π/3	0.3718	1.761			0.8918	1.551		
			-0.00453	-0.00588			0.02924	0.03292
π/2	0.3372	1.638			1.0907	1.449		
			0.00679	0.00738			0.02150	0.01868
2π/3	0.3899	1.945			1.2328	1.273		
							0.03590	0.03891
5π/6					1.4431	0.954		

* M- METHOD OF MOMENTS I-INTEGRAL METHOD

TABLE 6-5 (Cont'd) SUMMARY OF NUMERICAL VALUES OF $M_2(X)$, $B(X)$ AND E_{zw}

RUN	402 LB				302 LB			
Section	$M_2(X)$ ft^2	$B(X)$ $(ft/s)^{-1}$	E_{zw} (M)* ft^2s^{-1}	E_{zw} (I)* ft^2s^{-1}	$M_2(X)$ ft^2	$B(X)$ $(ft/s)^{-1}$	E_{zw} (M) ft^2s^{-1}	E_{zw} (I) ft^2s^{-1}
θ_1 0					0	2.131		
							0.00464	0.07459
π/6	0	2.4158			0.0448	2.131		
			0.00281	0.00326			0.02707	0.07253
π/3	0.0189	2.4158			0.3265	2.124		
			0.00771	0.00244			0.04552	0.07765
π/2	0.0944	2.0485			0.8063	2.329		
			0.00859	0.00492			0.06004	0.08535
2π/3	0.1684	2.1113			1.4667	2.207		
			0.00552	0.00387			0.03397	0.04157
5π/6	0.2219	2.2414			1.7393	1.394		
			0.01112	0.00865			0.08262	0.11766
θ_2 0 π	0.3300	2.1190			2.1334	0.652		
			-0.00061	0.00024			0.01559	0.02718
π/6	0.3285	2.0088			2.1627	0.483		
			0.02339	0.02828			-0.09818	-0.14942
π/3	0.5510	2.2692			2.0115	0.144		
			0.00382	0.00333				
π/2	0.5925	2.0529						
			0.00713	0.00671				
2π/3	0.6613	2.1809						
5π/6								

* M-METHOD OF MOMENTS I-INTEGRAL METHOD

TABLE 6-5 (Cont'd) SUMMARY OF NUMERICAL VALUES OF $M_2(X)$, $B(X)$ AND E_{zw}

RUN	308 LB				408 LB			
Section	$M_2(X)$ ft^2	$B(X)$ $(ft/s)^{-1}$	E_{zw} (M) ft^2s^{-1}	E_{zw} (I) ft^2s^{-1}	$M_2(X)$ ft^2	$B(X)$ $(ft/s)^{-1}$	E_{zw} (M) ft^2s^{-1}	E_{zw} (I) ft^2s^{-1}
θ_1 0	0	2.316			0	2.356		
			0.00227	0.01951			0.00214	0.01159
π/6	0.0213	2.316			0.0184	2.356		
			0.01435	0.02711			0.00561	0.00722
π/3	0.1692	2.184			0.0759	2.428		
			0.03808	0.07239			0.00836	0.01144
π/2	0.5659	2.270			0.1675	2.386		
			0.05987	0.10805			0.00536	0.00589
2π/3	1.2273	2.373			0.2218	2.587		
			0.04251	0.06696			0.01456	0.01410
5π/6	1.6326	1.866			0.3977	2.688		
			0.05250	0.08517			0.01059	0.01112
θ_2 0\π	2.0111	1.155			0.5316	2.886		
			0.01443	0.01967			0.00176	0.00133
π/6	2.0529	0.952			0.5538	2.972		
			-0.01262	-0.01680			-0.00265	-0.00410
π/3	2.0278	0.393			0.5201	2.869		
			-0.02636	-0.07470			0.00437	0.00382
π/2	2.0039	0.111			0.5753	2.553		
							0.00704	0.00532
2π/3					0.6561	2.402		
							0.00173	0.00348
5π/6					0.6714	2.176		

M-METHOD OF MOMENTS I-INTEGRAL METHOD

TABLE 6-5 (Cont'd) SUMMARY OF NUMERICAL VALUES OF $M_2(X)$, B(X) AND E_{zw}

RUN	403 RB				405 LB			
Section	$M_2(X)$ ft^2	B(X) $(ft/s)^{-1}$	E_{zw} (M) ft^2s^{-1}	E_{zw} (I) ft^2s^{-1}	$M_2(X)$ ft^2	B(X) $(ft/s)^{-1}$	E_{zw} (M) ft^2s^{-1}	E_{zw} (I) ft^2s^{-1}
θ_1 0					0	1.736		
							0.00323	0.01671
π/6	0	1.753			0.0218	1.736		
			0.00229	0.00253			0.00301	0.00356
π/3	0.0189	1.753			0.0427	1.778		
			0.00644	0.00191			0.00316	0.00350
π/2	0.0944	1.994			0.0672	1.736		
			0.00666	0.00403			0.00526	0.00529
2π/3	0.1684	2.132			0.1063	1.705		
			0.00512	0.00353			0.00623	0.00604
5π/6	0.2219	2.044			0.1573	1.894		
			0.01142	0.00914			0.00121	0.00152
θ_2 0/π	0.3300	1.853			0.1691	2.227		
			-0.00065	0.00027			0.00282	0.00223
π/6	0.3285	1.770			0.1924	2.147		
			-0.02420	0.02690			-0.00555	-0.00546
π/3	0.5510	2.107			0.1407	2.236		
			0.00386	0.00353			0.00871	0.00693
π/2	0.5925	1.932			0.2199	1.952		
			0.00712	0.00707			0.00180	0.00129
2π/3	0.6613	2.084			0.2390	2.023		

M-METHOD OF MOMENTS I-INTEGRAL METHOD

experiments indicated that the diffusion coefficient, E_z , for open channel flows was in general twice as large as that observed for ice-covered flows for correspondingly similar flow conditions. It is not unreasonable to assume that this observation is also true for the flows in the meandering flume because the flume bed and ice-cover roughnesses were the same as in the straight flume tests. Since the mixing coefficient, E_{zw} , represents the rate of mixing due to both turbulence and bend-generated transverse velocities the further increase in E_{zw} (1.0 to 4 times, relative to E_{zw} for ice-covered channel flows) for the open channel tests can be attributed to additional mixing caused by transverse velocities. That this is true can be seen by comparing Figures 5.6 and 5.10. The average values of the strength of spiral motion, S , for open water tests are observed to be about 1.5 to 2.0 times greater than the corresponding ice-cover tests. The comparatively high values of E_{zw} for open channel tests, therefore, seem to be reasonable. One factor which must be noted is that the curved flow could modify the structure of the turbulence field, but there is no information available on this modification.

6.2.3 The Normalised Transverse Mixing Coefficient

A summary of the normalised transverse mixing coefficient k ($= E_{zw}/u_*R$) for all test runs is given in Table 6-6. The values of k were computed using the overall average hydraulic radius, R , and the average shear velocity, u_* , and are shown plotted against X in

TABLE 6-6 SUMMARY OF RESULTS

Test Run	Flow Condition			a) Source Location	b) Method of Analysing Data	E_{zw}/u_*R											
	$\frac{W}{d_*}$	$f \times 10^2$	$\frac{r_c}{d_*}$			$\theta_1 \rightarrow$ 0	$\frac{\pi}{6}$	$\frac{\pi}{3}$	$\frac{\pi}{2}$	$\frac{2\pi}{3}$	$\frac{5\pi}{6}$	$\theta_2 \rightarrow$ 0	$\frac{\pi}{6}$	$\frac{\pi}{3}$	$\frac{\pi}{2}$	$\frac{2\pi}{3}$	$\frac{5\pi}{6}$
302	10.8	5.03	39	$\theta_1=0$, LB	M		0.38	2.20	3.69	4.87	2.76	6.70	1.27				
					I		6.06	5.89	6.30	6.78	3.37	9.55	2.21				
304	18	5.43	64.8	$\theta_1=0$, CL	M		0.59	1.17	1.35	1.63	1.29	1.30	0.29				
306				, RB	M		0.41	0.70	1.16	1.65	1.46	0.68	1.20	2.29	2.53	1.86	3.11
					I		0.71	0.34	0.75	1.25	1.18	0.91	1.39	3.13	2.85	1.62	3.37
307	10.6	3.53	38.3	$\theta_1=0$, CL	M		0.24	1.43	2.80	1.44	-1.45	1.84					
308				, LB	M		0.21	0.55	0.81	0.52	1.41	1.03	0.17	-0.26	0.42	0.68	0.17
					I		1.12	0.70	1.11	0.57	1.37	1.08	0.13	-0.40	0.37	0.52	0.03
401	11.5	4.98	41.5	$\theta_1=\frac{\pi}{6}$, CL	M			0.93	1.47	0.72	1.06	1.26	-0.16	-0.32	0.65	1.42	0.16
402				, LB	M			0.53	1.25	0.75	1.71	0.52	0.03	0.01	2.28	0.04	1.26
					I			2.49	1.69	0.83	1.78	0.54	-0.03	-0.16	1.91	-0.32	1.28
403				, RB	M			0.34	0.96	0.99	0.76	1.70	-0.10	3.61	0.58	1.06	
					I			0.38	0.28	0.60	0.53	1.37	0.04	4.01	0.53	1.06	
404	17	4.89	61.2	$\theta_1=0$, CL	M		0.58	0.95	0.84	0.15	1.37	0.12	0.61	0.45	0.62	0.56	
405				, LB	M		0.57	0.53	0.56	0.93	1.10	0.21	0.50	-0.98	1.54	0.32	
					I		2.96	0.63	0.62	0.94	1.07	0.27	0.40	-0.97	1.23	0.23	
406				, RB	M		0.40	0.62	0.59	1.13	0.60	1.61	-0.50	3.33	-0.80	1.20	
					I		0.57	0.32	0.40	0.90	0.20	1.35	-0.41	3.67	-1.04	1.31	
407	10.2	4.31	36.7	$\theta_1=0$, CL	M		0.31	1.38	1.84	0.97	1.08	0.82	0.63	0.14	0.91	1.44	0.76
408				, LB	M		0.35	0.92	1.37	0.88	2.38	1.73	0.29	-0.43	0.71	1.15	0.28
					I		1.90	1.18	1.87	0.96	2.31	1.82	0.22	-0.67	0.63	0.87	0.06

Notes: b) M - Moments Method. I - Integral Method

a) CL, LB and RB indicate centerline, left bank and right bank respectively. For bank injections source is located 0.05 ft from bank.

Figures 6.18a and b. There is a tendency for the Integral method to give higher values of k in the first bend especially at the first section downstream of the source and lower k-values in the second compared with the moments method, when tracer is released from the left bank. The reverse tendency is seen to be true for the case where source is located on the right bank. In general, the values of k obtained by both methods are remarkably close and both methods exhibit similar patterns in the longitudinal variation of k.

The discussions which follow are based on results obtained by the method of moments but the same general comments also apply to results obtained by the integral method except for situations where tracer was released from the channel centerline.

It is evident from Figures 6.18 that the longitudinal variation of k is influenced by the source position and probably reflects the role of transverse velocities in the mixing. As could be expected the normalised transverse mixing coefficient for centerline release of tracer was observed to be greater within the first half of the first bend. k reaches maximum values for different source positions between $\theta_1 = \pi/2$ and π of the first bend while minimum k-values occurred at the beginning of the second bend. It is of interest to note that the decay and reversal of the spiral motions also occurred, in general, between $\theta_2 = 0$ and $\pi/3$.

High k-values were observed in the second bend when tracer

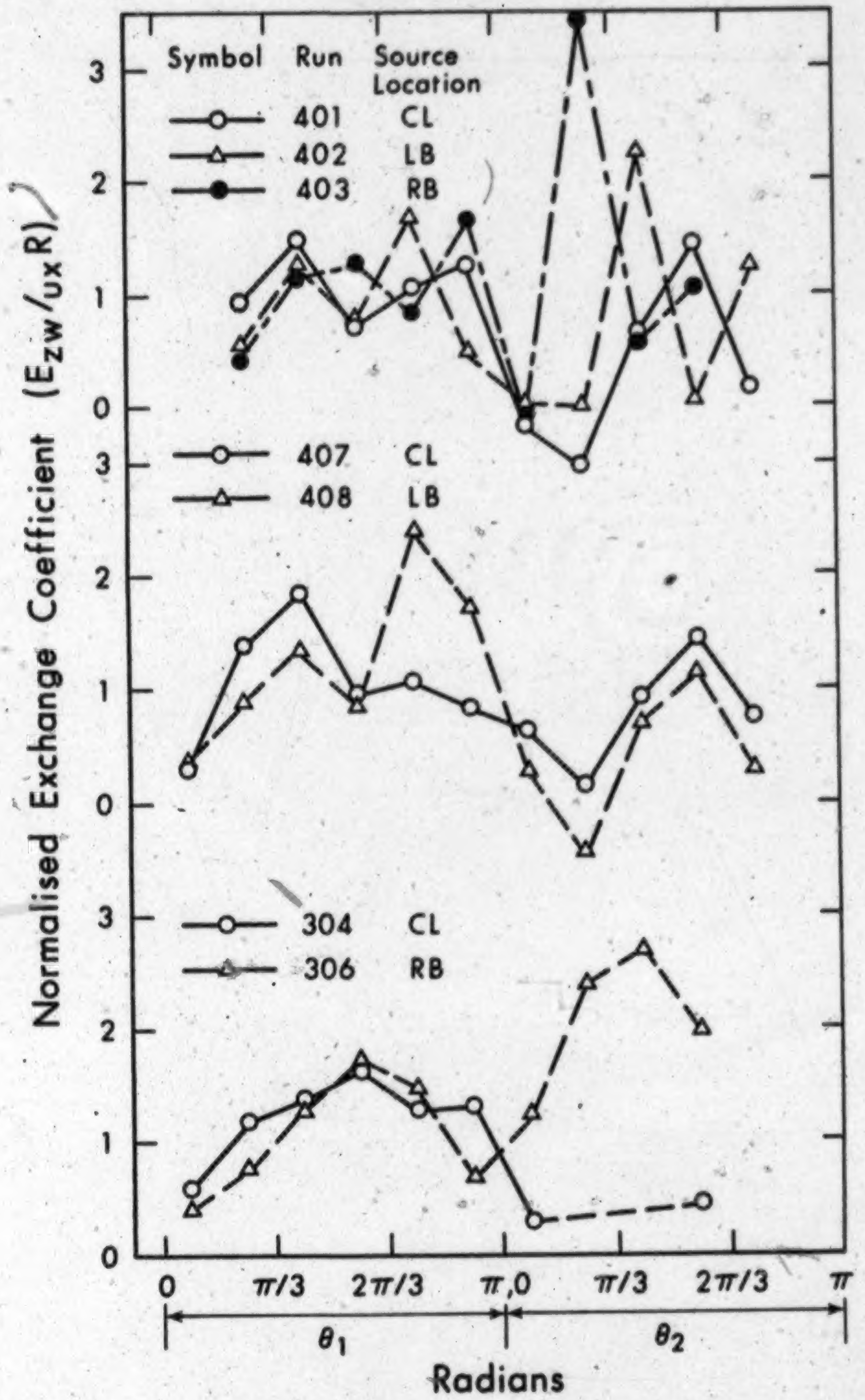

FIGURE 6.18a LONGITUDINAL VARIATION OF THE NORMALISED TRANSVERSE EXCHANGE (MIXING) COEFFICIENT

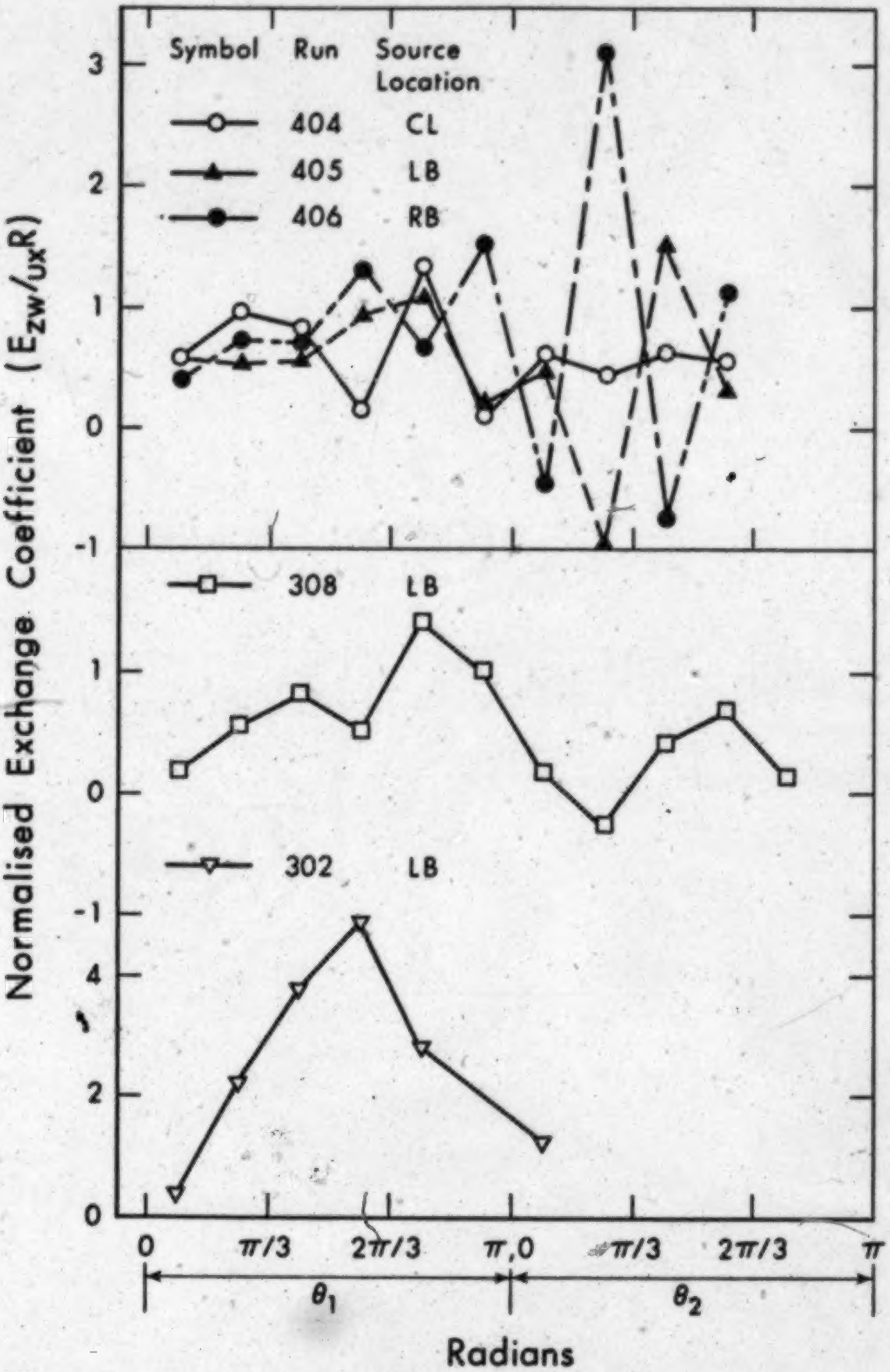

FIGURE 6.18b LONGITUDINAL VARIATION OF THE NORMALISED TRANSVERSE EXCHANGE (MIXING)COEFFICIENT

was introduced at the right bank. This is probably due to the fact that when the source is located at this bank the spiral motions in the first bend appear to inhibit spreading of tracer in that bend while in the second bend they seem, initially, to enhance the spreading of tracer. Evidence for this is seen, for example, in Figures 6.15 and runs 403 and 406. Both runs indicated a sharp increase in second moments between $\theta_2 = \pi/6$ and $\pi/3$.

Negative values of the normalised transverse mixing coefficient occurred for some test runs at the beginning of the second bend. This is not unexpected. Although this violates the concept of gradient-type mixing it is realised that the gradient-type mixing concept is an approximation and cannot be expected to apply to all flow situations. It is possible to obtain negative k-values in regions of curvature reversal as this is initially accompanied by a net lateral discharge towards the outside bank. This net flow can inhibit spreading of tracer released from the outside bank and produce a negative k-value. A similar situation applies when longitudinal changes in cross-sectional shape cause significant transverse velocities, for example, run 406 and between $\theta_2 = \pi/3$ and $\pi/2$ (Figures 5.13 and Figure 6.18b).

Further downstream in the second bend the normalised transverse mixing coefficient is again seen to increase to a maximum in the middle third of this bend before decreasing again towards the bend exit. The longitudinal variation of k for some ice-cover tests was rather erratic and is probably caused by the warping of the plywood (ice-cover). This was more pronounced in runs 404/5/6. It is noted that the flow depth for these runs was comparatively small and consequently the results were more affected by the warping of the ice-cover.

The tracer was observed to be almost fully mixed at $\theta_2 = \pi/6$ for run 302 which indicated high values of k in the first bend. The k-values evaluated for subsequent reaches beyond $\theta_2 = \pi/6$ for this run were found to be unreasonably large and this could only be traced to measurement errors. As discussed previously when tracer becomes more uniformly distributed laterally the variable B(X) tends to zero. Any errors in the measurements of velocity and concentration, therefore, can result in very unrealistic values of k.

The values of k averaged for different source positions but for the same flow conditions are shown plotted against X in Figure 6.19. It is evident from this figure that maximum values of the normalised transverse mixing coefficient occur in the middle third of both bends and minimum values occur at the beginning ($\theta_2 = 0$ and $\pi/3$) of the second bend. When the k variation in Figure 6.19 is compared with the variation of spiral motion strength in Figures 5.6 and 5.10, it is evident that k seems to be strongly related to the growth-decay-reversal cycle of the spiral motion. With only two bends it was not possible to relate the probable cyclic variations of k to that of S.

Table 6-7 shows a comparison between the normalised mixing coefficients obtained over the same reach for the same source position

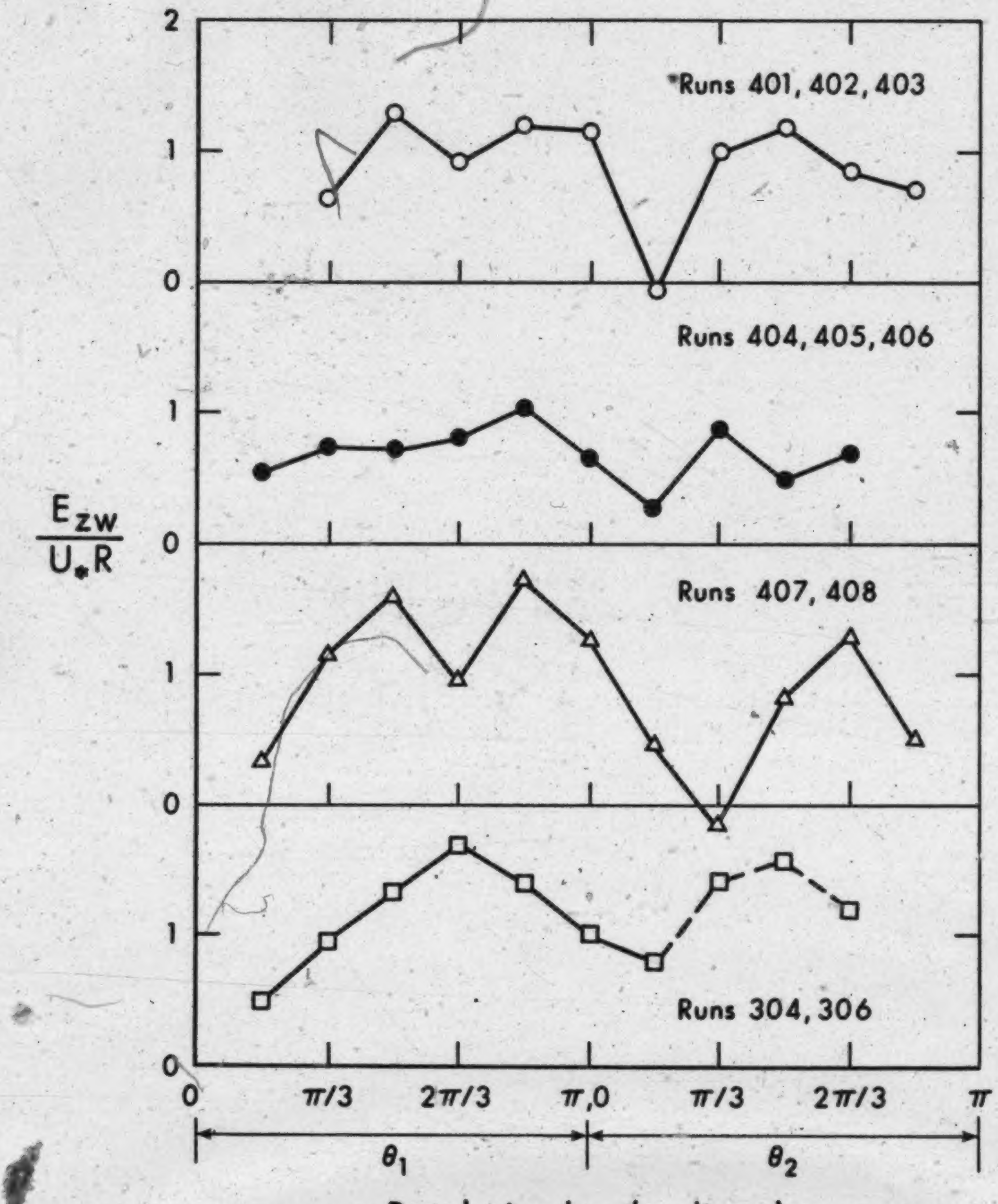

FIGURE 6.19 LONGITUDINAL VARIATION OF THE AVERAGED NORMALISED TRANSVERSE MIXING COEFFICIENT FOR DIFFERENT FLOW CONDITIONS

TABLE 6-7 COMPARISON OF E_{zw}/u_*R FOR THE SAME REACH AND SOURCE POSITION AND SIMILAR FLOW CONDITIONS

Ice-Cover Tests		Open Channel Tests	
Run	$\frac{E_{zw}}{u_*R}$	Run	$\frac{E_{zw}}{u_*R}$
402	0.88	302	3.14
404	0.63	304	0.89
406	0.71	306	1.44
408	0.88	308	2.00

and similar flow condition in the open and ice-covered channel tests. The magnitude of k is seen to be considerably greater for open-water than for ice-covered conditions. Since an ice-cover also reduces the product u_*R by a factor of approximately $2\sqrt{2}$, if depth remains constant, the results again indicate that an ice-cover can reduce the mixing capacity in channel flows substantially.

6.2.4 Parameters Controlling E_{zw}/u_*R

In turbulent meandering channel flows, the dependence of bulk flow properties such as the mixing coefficient, E_{zw}, average velocity, U_o, and friction factor, f, on other parameters may be expressed as:

$$E_{zw} = \pi_1(R, W, \nu, k_s, g, S_o, r_c, L) \qquad (6.25)$$

where the variables have their usual meaning and L represents the overall bend length (measured along the channel centerline).

Dimensional analysis can be used to give:

$$\frac{E_{zw}}{u_*R} = \pi_2\left(\frac{W}{R}, \frac{k_s}{R}, \frac{u_*R}{\nu}, \frac{u_*}{\sqrt{gR}}, \frac{r_c}{R}, \frac{L}{r_c}\right) \qquad (6.26)$$

where $u_*/\sqrt{gR}$ is a form of Froude Number.

Again for fully rough turbulent flows the friction Reynolds number u_*R/ν has a minimal effect on E_{zw}/u_*R and the Froude number, $u_*/\sqrt{gR}$, does not play a significant role in subcritical open channel flows and in ice-covered flows is not pertinent. For these conditions Equation 6.26 simplifies to:

$$\frac{E_{zw}}{u_*R} = \pi_3\left(\frac{W}{R}, \frac{k_s}{R}, \frac{r_c}{R}, \frac{L}{r_c}\right) \tag{6.27}$$

or:

$$\frac{E_{zw}}{u_*R} = \pi_4\left(\frac{W}{R}, f, \frac{r_c}{R}, \frac{L}{r_c}\right) \tag{6.28}$$

The present data cannot be used to explore the importance of all the various parameters in Equation 6.27 or 6.28 because of the limited range of these parameters in the experiments. Nevertheless, the ice-cover data can be used to gain some insight into the dependence of E_{zw}/u_*R on the other four parameters. The values of the parameters in Equation 6.28 are summarised in Table 6-8.

TABLE 6-8 NUMERICAL VALUES OF VARIABLES IN EQUATION 6.27

Run	$\frac{E_{zw}}{u_*R}$	$\frac{W}{R}$	f	$\frac{r_c}{R}$	$\frac{L}{r_c}$	Flume Bed
401/2/3	0.865	25	0.0498	90	5.23	Rough
404/5/6	0.658	36.8	0.0489	132	5.23	Rough
407/8	0.904	22.5	0.0431	81	5.76	Smooth

It is evident that there is a tendency for k to decrease with increasing r_c/R and W/R. The effect of roughness is not too clear because the data is insufficient.

Fischer (1969) investigated the effect of bend generated spiral motions on transverse mixing. He obtained an expression for the additional mixing caused by transverse velocities, that is $\overline{w'c'}$, based on Rozovskii's transverse velocity distribution in the vertical for fully developed turbulent open channel bend flow. By further assuming that $\overline{w'c'} = -\varepsilon_d\, \partial\bar{c}/\partial z$, where ε_d is the transverse dispersion coefficient, Fischer obtained:

$$\frac{\varepsilon_d}{u_* d_*} = -\left(\frac{U_o}{u_*}\right)^2 \left(\frac{d_*}{r_c}\right)^2 \frac{I}{\kappa^5} \qquad (6.29)$$

in which κ is von Karman's constant and values of the function I are given by Fischer. Fischer recognized the limitations of the above equation and suggested that it should be used for order of magnitude estimates only. Equation 6.29 can be rewritten as:

$$\frac{\varepsilon_d}{u_* R} \propto \left(\frac{U_o}{u_*}\right)^2 \left(\frac{R}{r_c}\right)^2 \qquad (6.30)$$

According to Fischer's predictions, therefore, ε_d/u_*R should decrease with roughness. This appears to be consistent with earlier observations that the strength of the spiral motion decreases with roughness for similar conditions of depth and discharge. Also ε_d/u_*R should decrease with increasing r_c/R ratio. If it is assumed that r_c/R does not affect the diffusion coefficient there is some evidence in Table 6-8 to support this prediction. It is noted that because of the assumptions inherent in the derivation of Equation 6.29 the aspect ratio, W/d_*, does not appear in this equation. The importance of the various parameters in Equation 6.28 will be discussed further in Chapter 7.

CHAPTER 7

FIELD INVESTIGATIONS

Velocity and tracer measurements were made in the Lesser Slave River (Alberta) in August 1972 and February 1973, and these measurements are described and discussed in this chapter.

7.1 Description of the Test Reach

The field tests were conducted on the Lesser Slave River (Alberta), approximately eight miles downstream of Lesser Slave Lake. This site was selected because discharge from this large lake remains constant over prolonged periods, the water quality is suitable for dye tracing, reasonable depths of flow can be obtained under ice-covered conditions, and there are no tributaries within the study reach of 12,000 ft. length. During the winter test the river width varied between 90 and 160 ft and the average depth was between 5.5 ft and 8.0 ft. The maximum depth was found to be less than 14 ft during both winter and summer tests. The river has an irregular, but marked meander pattern with a sinuosity of about 1.8. The bed material is predominantly fine sand with a median size of 0.20 mm. The hydrologic and geomorphic characteristics of a nearby, similar reach of the Lesser Slave River are listed by Kellerhals, Neill, and Bray (1972). The Water Survey of Canada maintains a gauging station approximately six miles downstream of the study reach. A plan of the study reach is shown in Figure 7.1.

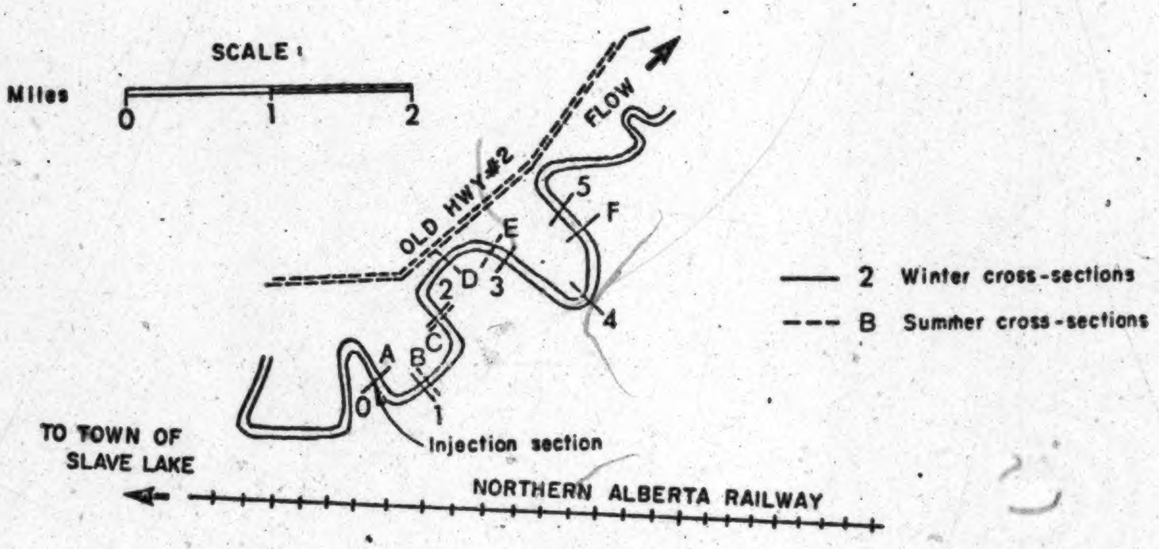
SCALE:
Miles
0
1
2
OLD HWY #2
FLOW
5
F
E
D
3
2
C
B
A
0
1
4
Injection section
TO TOWN OF SLAVE LAKE
NORTHERN ALBERTA RAILWAY
2 Winter cross-sections
B Summer cross-sections

FIGURE 7.1 PLAN OF STUDY REACH

7.2 Experimental Procedure

7.2.1 Velocity Measurements

For the velocity and tracer measurements under ice-cover, holes were drilled through the ice at the six numbered cross-sections shown on Figure 7.1. Velocity measurements were taken at 1 ft intervals in the vertical and at 20 ft intervals across the river. A few more detailed vertical velocity profiles (0.5 ft intervals) were also obtained. Under open water conditions, velocities were only measured at 0.2 and 0.8 of the local depth, D, along verticals spaced at 10 ft intervals at Sections A, C, and F shown in Figure 7.1.

7.2.2 Tracer Measurements

Rhodamine WT dye diluted with stream water to about 2% by weight was used as tracer. For the winter tests it was injected at a constant rate of 13.5 $cm^3 s^{-1}$ just below the underside of the ice at a point approximately 60 ft from the left-bank of the river at Section 0. About 90 minutes elapsed after commencement of injection until a steady state concentration distribution was established at Section 1. After this time, sampling was begun at Section 1 and progressed gradually downstream to Section 5 where it was completed 6 hours after the start of the experiment.

A sampler, capable of taking 60 cc samples simultaneously at various depths up to 8 ft, was used. Samples were collected at 3 ft, 5 ft and 7 ft below the free water surface, which corresponds to depths of approximately 1.5 ft, 3.5 ft and 5.5 ft below the underside of the ice, and at 10 ft intervals across the channel for each section.

For the open-water test, the tracer was injected 15 ft from the left bank at Section A, and samples were taken at Sections B, C, D, and E at depths of 1 ft and 4 ft using a 10 ft spacing across the channel.

7.3 Experimental Results

7.3.1 Ice Cover

Ice-thickness was found to vary between 1.0 and 3 ft, being greatest near the banks except where the zone of maximum velocity was close to the bank (Figure 7.3). Three slabs were cut from the ice cover and turned over to reveal the relief on the ice underside (Figure 7.2). A surprisingly regular dune-like pattern is evident in Figure 7.2(a). The ridges are perpendicular to the main flow direction. Figure 7.2(b) shows a complex, wavy and irregular pattern, while Figure 7.2(c) shows a relatively smooth underside. With only three samples, no firm conclusions concerning the spatial distribution of the 3 patterns can be drawn but a general smoothing of the ice underside in the downstream direction was indicated.

7.3.2 Hydraulic Data

The hydraulic data for the winter test are summarized in

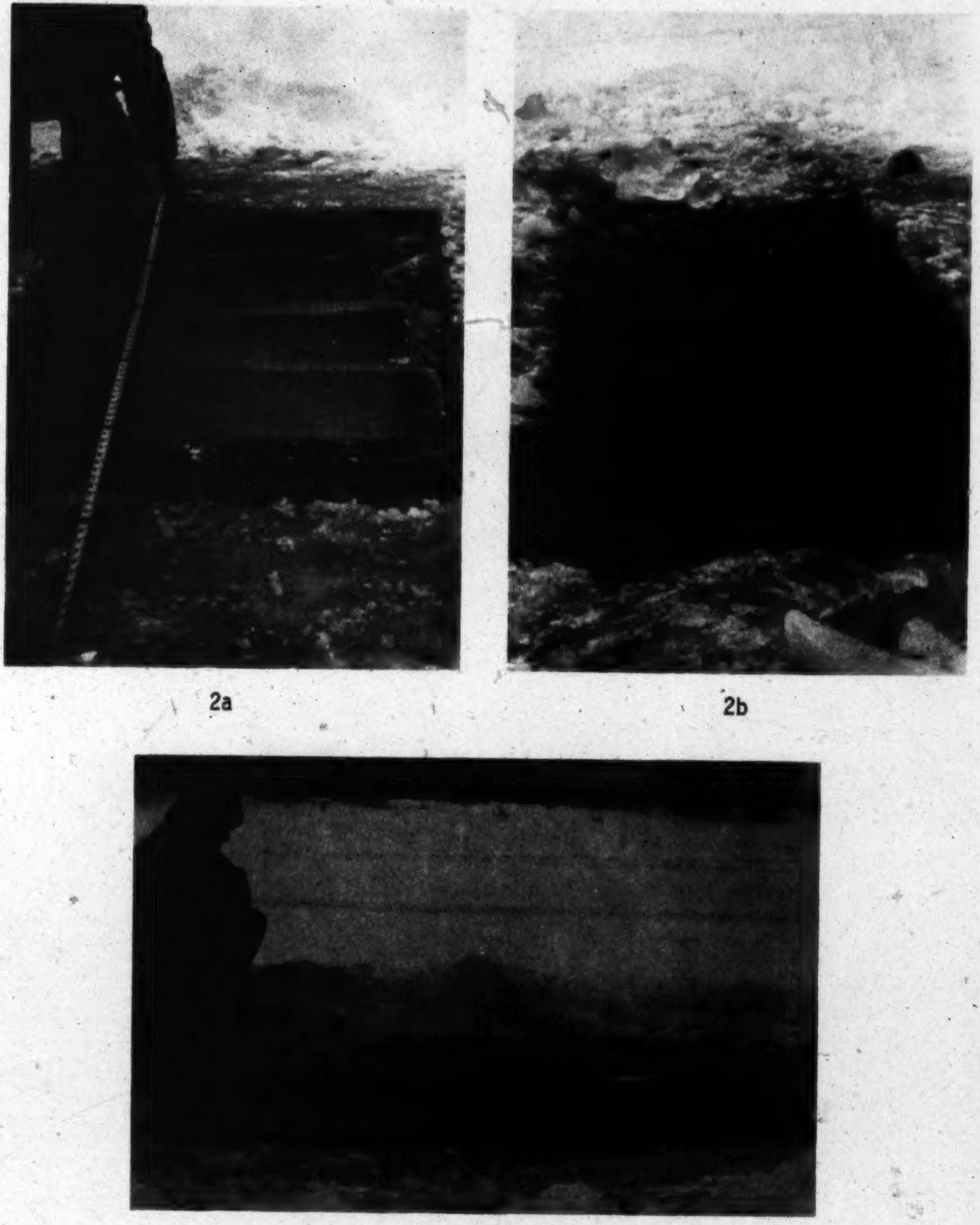

2a

2b

2c

FIGURE7.2. RELIEF ON ICE UNDERSIDE

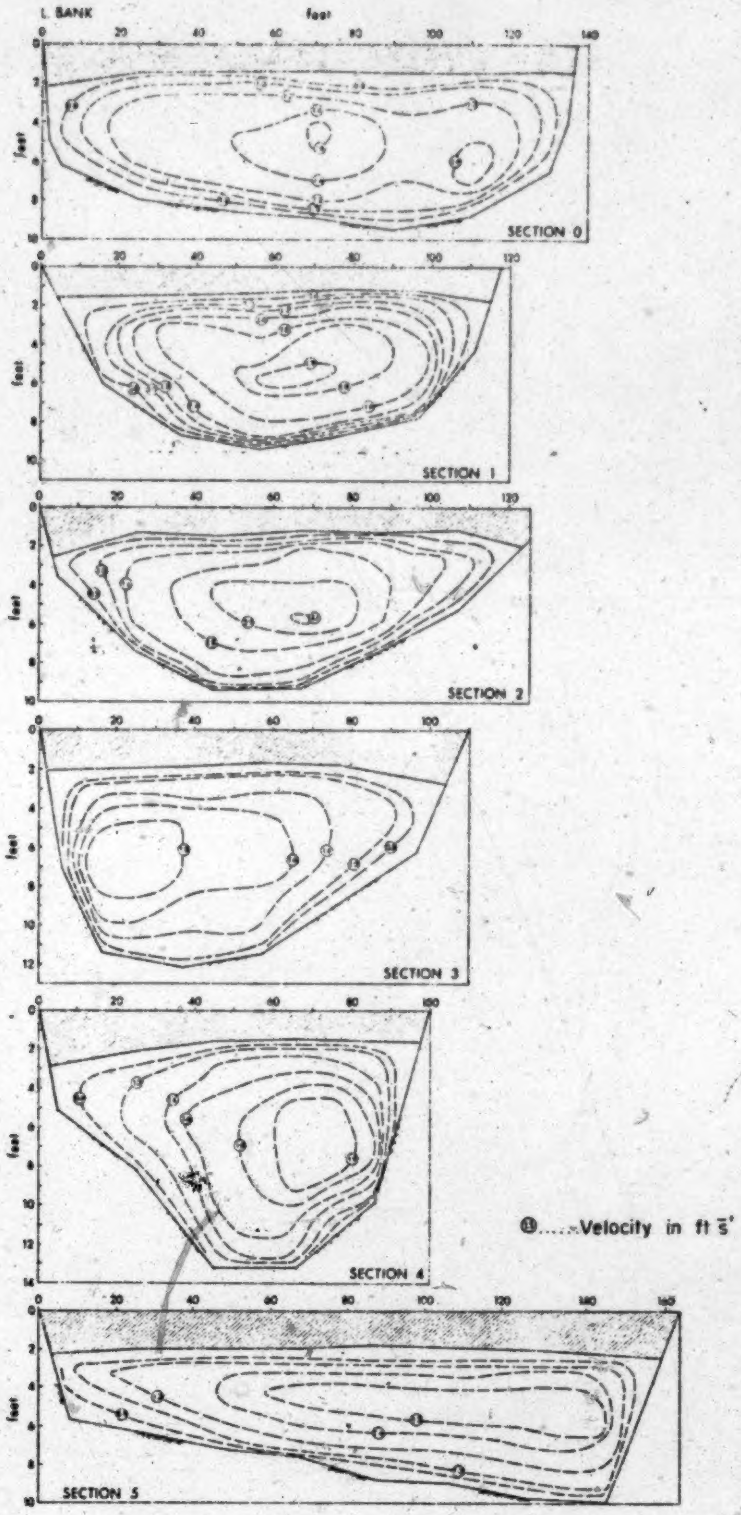

FIGURE 7.3 VELOCITY CONTOURS

Table 7-1 and velocity contours for the six cross-sections are presented in Figure 7.3. The point of maximum velocity was observed to be located anywhere between 0.2D and 0.7D, measured from below the underside of the ice cover. However, it generally occurred within the upper half of the flow. The vertical location of this point of maximum velocity is controlled by two main factors: (i) the relative roughnesses of ice-cover and river-bed and (ii) the spiral motions induced by the bends. Some of the velocity contours of Figure 7.3 indicate the presence of secondary current cells but the exact number and extent of the cells is generally not clear. The variation in discharge over the three days on which velocities were measured is probably caused by differing wind conditions in the region of open water at the outlet of Lesser Slave Lake.

The hydraulic data for the corresponding summer test are listed in Table 7-2 and two observed lateral distributions of mean velocity (for a vertical) are shown on Figure 7.4. Exact correspondence between summer and winter cannot be achieved because winter flows are generally lower than summer flows, and at equal flow, winter stages are considerably higher.

The slope of the free water surface, S_o, was observed to be 0.095×10^{-3} under winter conditions, and this should correspond closely to the slope of the energy line and to the open-water slope. It is close to the value of 0.11×10^{-3} listed in Kellerhals, Neill and Bray (1972) for the nearby reach of river.

TABLE 7-1 HYDRAULIC DATA FOR WINTER CONDITIONS

Cross-section No.	Date of velocity measurement[1]	Thalweg distance (ft)	Maximum flow width (ft)	Range of ice-thickness (ft)	Flow area (ft^2)	Discharge ($ft^3\ s^{-1}$)	Mean depth (ft)	Mean velocity ($ft\ s^{-1}$)
0	Feb. 27, 1973	0	132	1.4 - 2.2	924	960	7.04	1.04
1	Feb. 28	1,150	115	1.2 - 1.8	688	879	5.98	1.27
2	Feb. 28	3,450	116.5	1.2 - 2.5	651	893	5.59	1.37
3	March 1	7,000	102	1.7 - 2.8	768	957	7.53	1.25
4	March 1	9,400	92.5	1.5 - 2.8	737	953	7.97	1.29
5	March 1	11,800	157	1.[illegible] - 2.4	904	998	5.76	1.10

[1] The tracer test took place on March 1, 1973.

Cross-section No.	Date of velocity measurement[1] Q	Thalweg distance (ft)	Water surface width (ft)	Flow area (ft^2)	Discharge ($ft^3\ s^{-1}$)	Mean depth (ft)	Mean velocity ($ft\ s^{-1}$)
A	Aug. 30, 1972	0	145	1188	2080	8.2	1.75
B		1300	135	885		6.6	
C	Aug. 30, 1972	3800	140	980	2140	7.0	2.18
D		5200	135	1040		7.7	
E		6280	141	1130		8.0	
F	Aug. 30, 1972	11000	134	1025	1920	7.7	1.87

1) Tracer measurements took place on August 17th., when the discharge was 2500 $ft^3 s^{-1}$ according to preliminary records of the Water Survey of Canada. Mean velocity and mean depth were adjusted according to the Manning formula and checked against the stage-discharge rating curve.

TABLE 7.2. HYDRAULIC DATA FOR OPEN WATER CONDITIONS

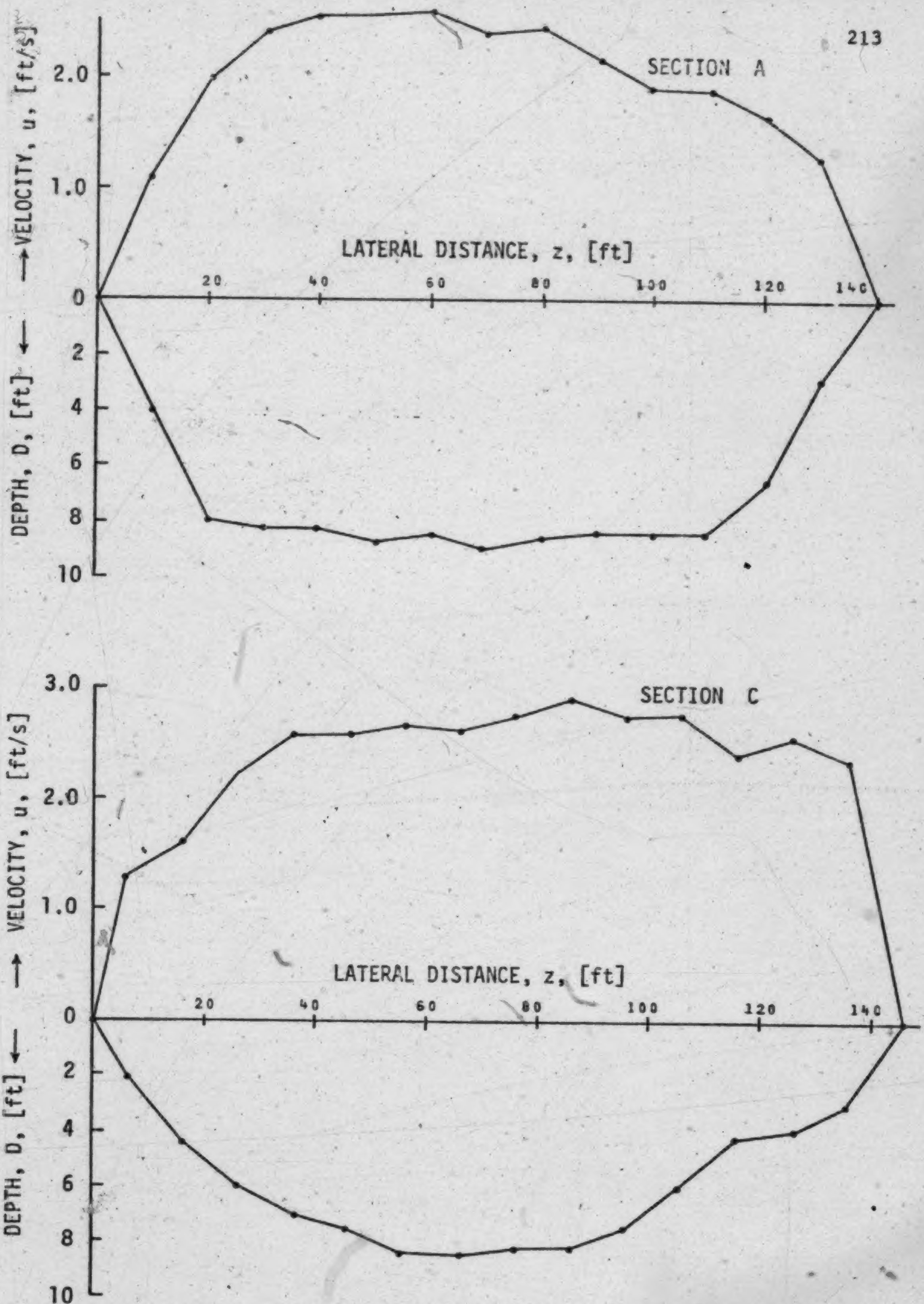

FIGURE 7.4 TRANSVERSE PROFILES OF VELOCITY AND DEPTH AT SECTIONS A AND C (OPEN-WATER)

The average values of R and u_* are 3.22 ft and 0.10 ft s^{-1} for ice-covered conditions and 8.3 ft and 0.16 ft s^{-1} for open-water conditions.

7.3.3 Tracer Distributions

The observed transverse tracer distributions are shown in Figures 7.5a and b for winter and summer respectively. It is to be noted that C_o is the concentration for fully mixed conditions with no tracer losses. The effects of secondary currents due to bends are noticeable in both winter and summer data. The winter data in particular show the zone of highest concentration moving downwards (between Sections 1 and 3) and then upwards (Sections 3 to 5). The displacement of the zone of maximum concentration with the shifting thalweg can be observed between Sections 2 and 4. The distances needed for vertical and transverse mixing under ice-cover conditions appear to be of the same order of magnitude in the Lesser Slave River. This differs from the case of reasonably straight broad channels, where the distance for vertical mixing is much shorter than the distance for transverse mixing.

7.4 Computation of the Transverse Mixing Coefficient, E_{zw}

No direct field measurements of the transverse velocities, w , were made in this investigation and their effects must, therefore, be included in a modified exchange coefficient, $\overline{\varepsilon}_{zw}$, defined in

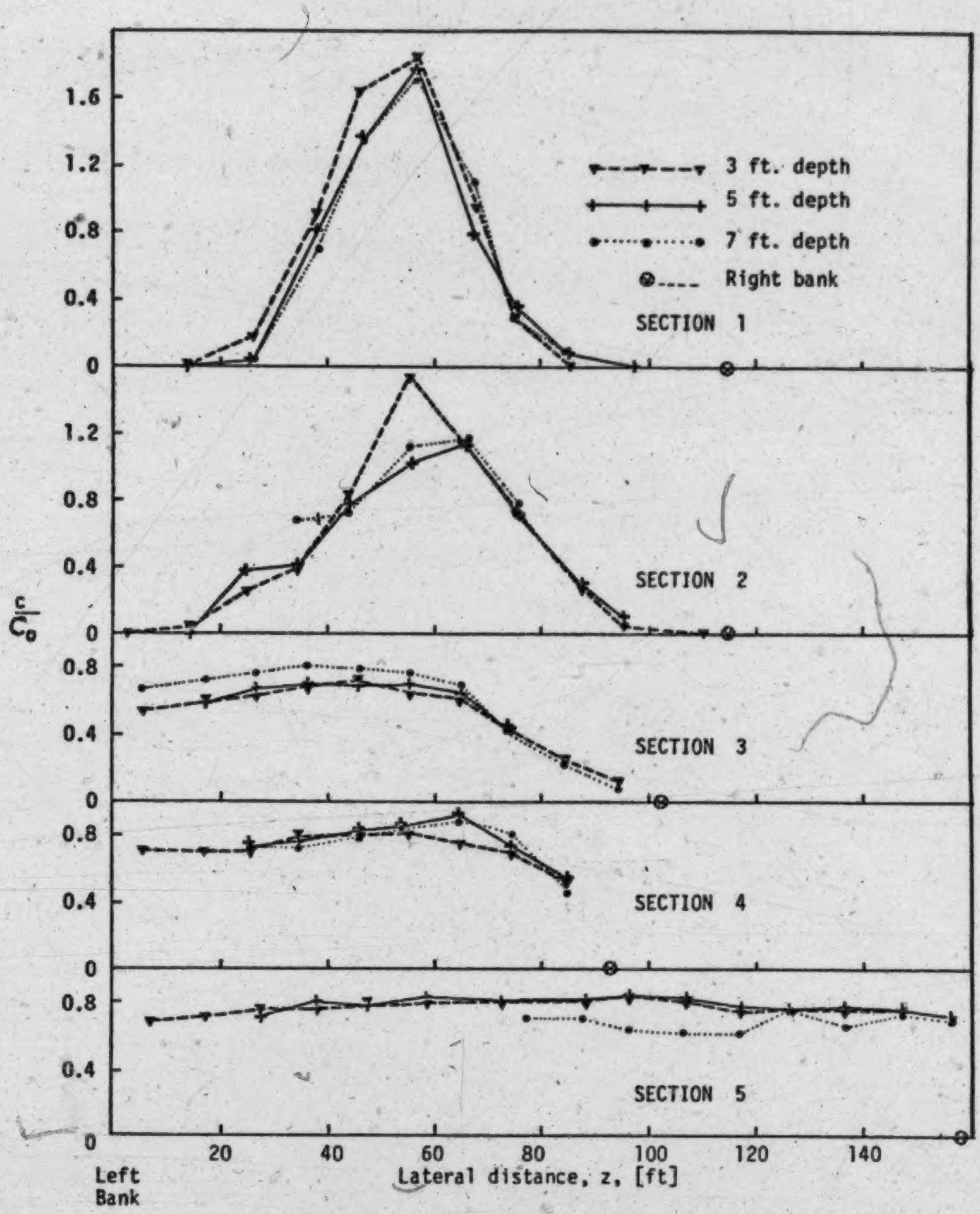

FIGURE 7.5a TRACER DISTRIBUTIONS, WINTER .

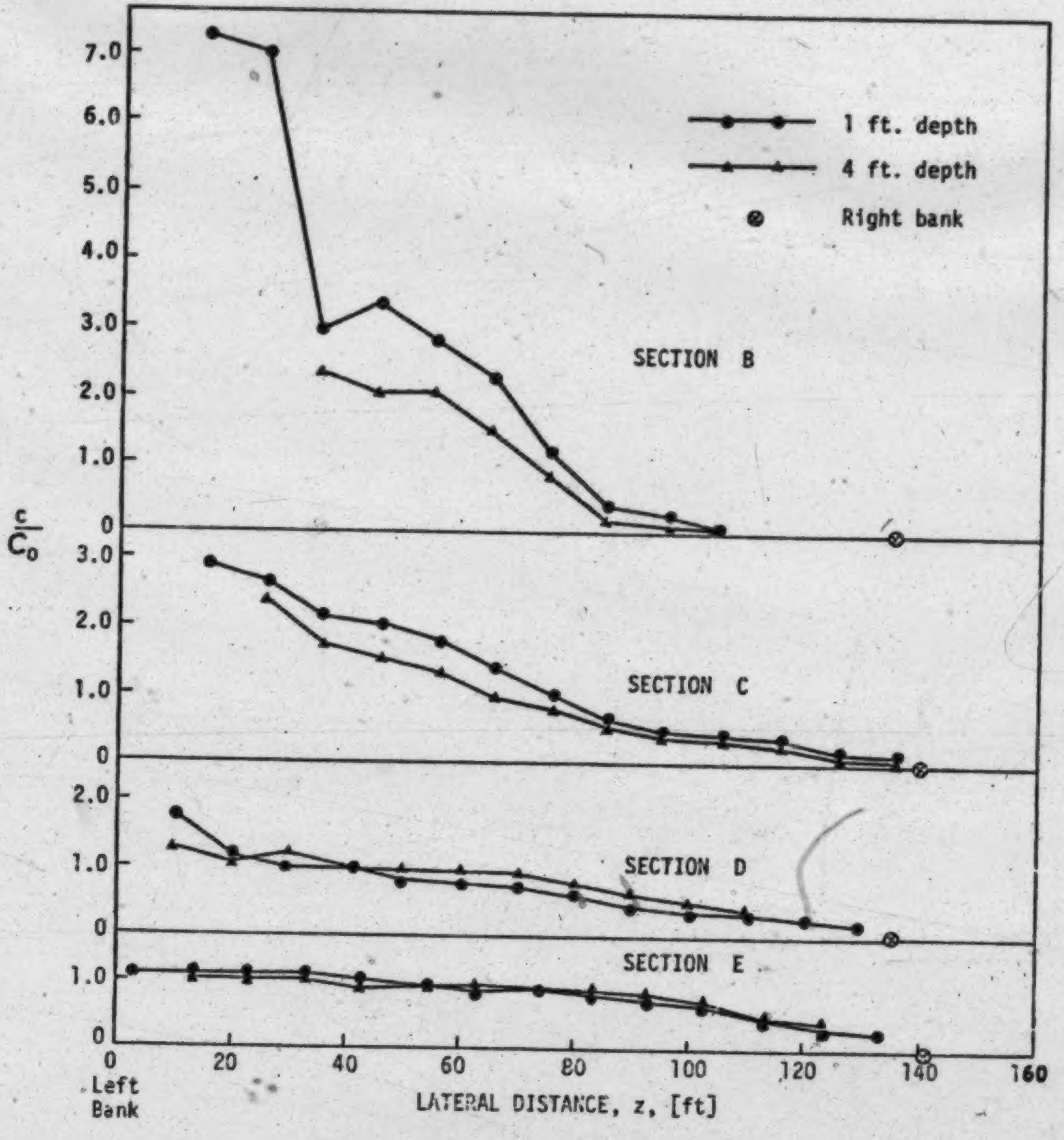

FIGURE 7.5b TRACER DISTRIBUTIONS, SUMMER.

Section 3.3.1 as:

$$\overline{\varepsilon}_{zw} \frac{\partial \bar{c}}{\partial z} = E'_{zw} \, \phi_w \, (x, z) \tag{3.28}$$

The relevant equation for evaluating E'_{zw} is Equation 3.30 and it is to be remembered that this equation is valid only for rivers with zero depth at the banks. Again, ϕ_w is assumed equal to 1.0 so that Equation 3.30 simplifies to:

$$\frac{d}{dx} \left[\frac{\int_{W_1}^{W_2} D(\bar{u}\,\bar{c} + \overline{u'c'})\eta^2 d\eta}{\int_{W_1}^{W_2} D\,\bar{u}\,\bar{c}\; d\,\eta} \right] =$$

$$\frac{2E_{zw} \int_{W_1}^{W_2} \left[D\bar{c}\left(1 \pm \frac{2\eta + z_o}{r_c}\right) + \bar{c}\eta\left(1 \pm \frac{\eta + z_o}{r_c}\right) \frac{\partial D}{\partial \eta} \right] d\eta}{\int_{W_1}^{W_2} D\,\bar{u}\,\bar{c}\; d\,\eta} \tag{7.5}$$

if it is noted that for $\phi_w = 1$, $E'_{zw} = E_{zw}$.

To compare the magnitude of $\overline{u'c'}$ to $\bar{u}\;\bar{c}$, a straight line was fitted by least squares to the concentration measurements in a vertical and the c' values were determined for the points where u' was known. The velocity distribution over verticals on which no velocities were measured were found from the velocity contours. The values of $\overline{u'c'}$ exceeded 3% of the corresponding $\bar{u}\,\bar{c}$ value on only 3 verticals out of 65 and these were located near the tails of the transverse tracer distributions where the $\bar{u}\,\bar{c}$ values are themselves small. For practical purposes $\overline{u'c'}$ can, therefore, be dropped from Equation 7.5. This does not mean that the vertical concentration gradients are unimportant, since their major effect would appear in the term $\overline{w'c'}$ which has been included in E_{zw}. Equation 7.5 now reduces to:

$$\frac{d}{dx}\left[\frac{\int_{W_1}^{W_2} D\,\bar{u}\,\bar{c}\,\eta^2 d\eta}{\int_{W_1}^{W_2} D\,\bar{u}\,\bar{c}\,d\eta}\right] =$$

$$\frac{2E_{zw}\int_{W_1}^{W_2}\left[D\bar{c}\left(1 \pm \frac{2\eta + z_o}{r_c}\right) + \bar{c}\eta\left(1 \pm \frac{\eta + z_o}{r_c}\right)\frac{\partial D}{\partial \eta}\right] d\eta}{\int_{W_1}^{W_2} D\,\bar{u}\,\bar{c}\,d\eta} \qquad (7.6)$$

which is now written as:

218

$$\frac{dM_2(X)}{dX} = E_{zw} \quad B(X) \tag{7.7}$$

The definitions of $M_2(X)$ and $B(X)$ can be obtained by comparing Equations 7.6 and 7.7. Since the width of the river varied over a wide range, the calculated second moments had to be adjusted to allow for this variation. The formula used was (Fischer, 1967):

$$(M_2)_c = (M_2)_a \left(\frac{W_{sm}}{W_s}\right)^2 \tag{7.8}$$

in which $(M_2)_c$ is the corrected second moment; $(M_2)_a$ is the actual or calculated second moment; W_s is the maximum width at a cross-section and W_{sm} the average maximum width for the test reach. The adjustment of $M_2(X)$ as suggested by Fischer is not entirely unreasonable because convergence or divergence of the flow does not necessarily imply reduced or increased mixing. The values of $(M_2)_a$, $(M_2)_c$, B and E_{zw} are tabulated in Table 7-3 and in Figure 7.6, plots of $(M_2)_c$ and B against X are presented. It is evident that the decrease in B with longitudinal distance, X , follows the same trend as was observed for the laboratory experiments which were conducted at approximately constant depth. Possible lateral variations of the two terms:

$$D\bar{c}\left(1 \pm \frac{2\eta + z_o}{r_c}\right) \quad \text{denoted by } F_1$$

and:

$$\bar{c}\eta\left(1 \pm \frac{\eta + z_o}{r_c}\right)\frac{\partial D}{\partial \eta} \quad \text{denoted by } F_2$$

TABLE 7.3 NUMERICAL VALUES OF SOME VARIABLES IN EQUATIONS 7.7 and 7.8

Cross-Section Number.	$(M_2)a$ ft.^{2}	$(M_2)c$ ft.^{2}	B $(ft/s)^{-1}$	E_{zw} ft^2/s	$\frac{E_{zw}}{u_*R}$
WINTER					
0	0	0			
			1.22	0.1865	0.58
1	238	256			
			1.02	0.0207	0.06
2	289	303			
			0.70	0.1307	0.41
3	506	691			
			0.46	-0.0045	-0.01
4	379	630			
			0.34	0.3168	0.98
5	1608	927			
SUMMER					
A	0	0			
			1.48	0.442	0.33
B	1575	1717			
			1.05	0.509	0.38
C	3625	3288			
			0.62	0.134	0.10
D	3150	3433			
			0.48	0.634	0.48
E	3800	3800			

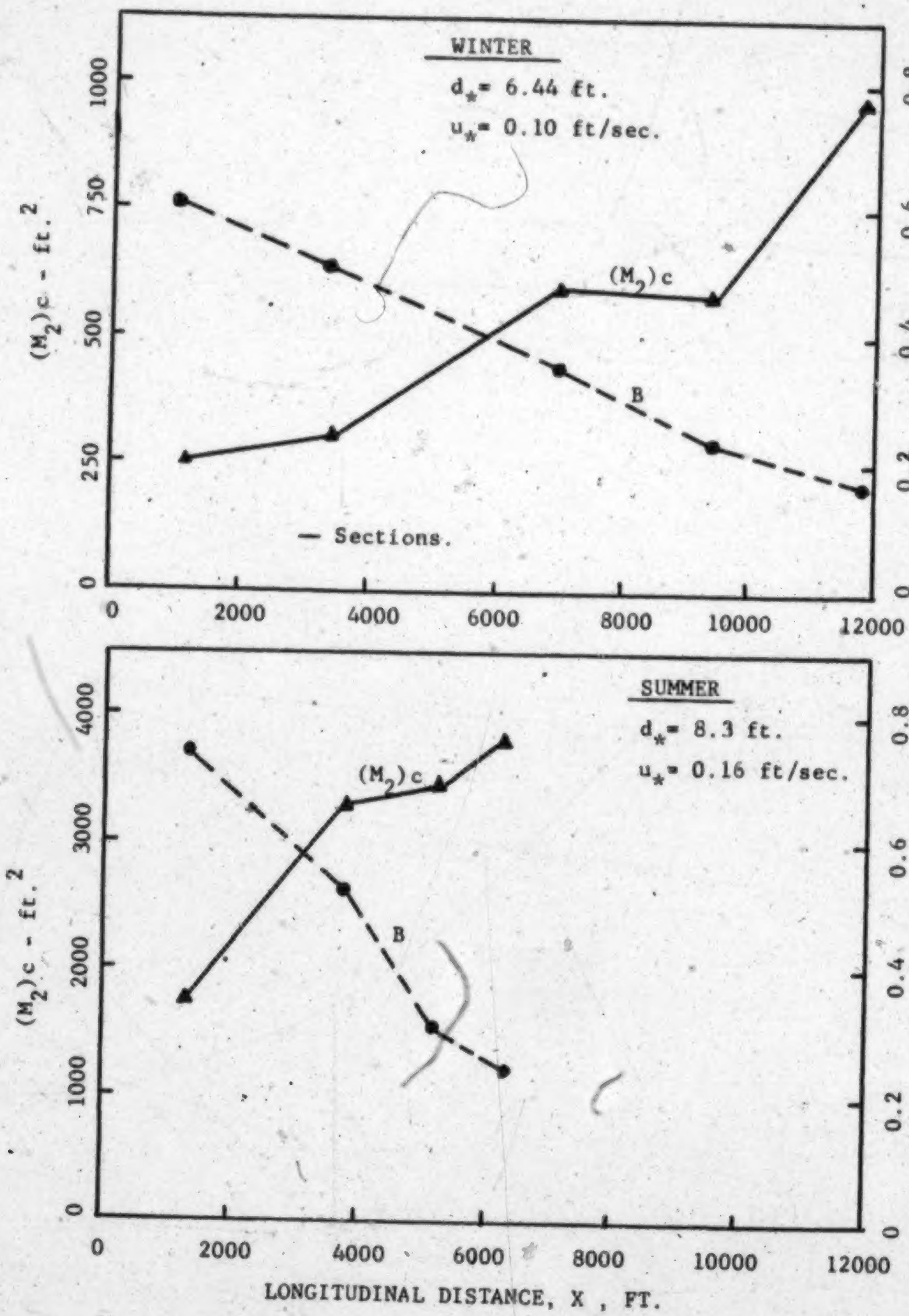

FIGURE 7.6 VARIATIONS OF $(M_2)c$ AND B WITH X FOR SUMMER AND WINTER TESTS.

are illustrated in Figure 7.7. It is evident that depth variations modify the distributions of F_1 and F_2 but when F_1 and F_2 are integrated over the cross-section, the effects of depth variations on B and consequently on the normalised mixing coefficient, k , are less obvious. Nevertheless, some understanding of the importance of depth variations on the mixing may be gained by comparing the results from channels of non-uniform cross-section with those from equivalent rectangular channels. This aspect of the mixing is discussed later.

The average value for the transverse mixing coefficient, E_{zw} , over the length of the test reach is 0.113 ft^2s^{-1} for the winter test and the normalised mixing coefficient, k , is 0.36. The open water values are $E_{zw} = 0.433\ ft^2s^{-1}$ and $k = 0.33$. Although this k-value is only slightly less than the winter value, strict comparison between the summer and winter k-values cannot be made for two reasons. Firstly, the point of tracer release was different for summer and winter. Secondly, the lateral mixing process depends strongly on bend induced spiral motions and the intensity of these motions together with the size of the dominant turbulent eddies vary laterally. Consequently tracer experiences different rates of mixing depending on the source position. Another factor which should be mentioned is that, in the laboratory, comparison of E_{zw} or k values from ice-cover and open water tests were made for corresponding flows having approximately the same depth and discharge but different slopes. The summer test was performed at a higher depth and discharge compared to the winter

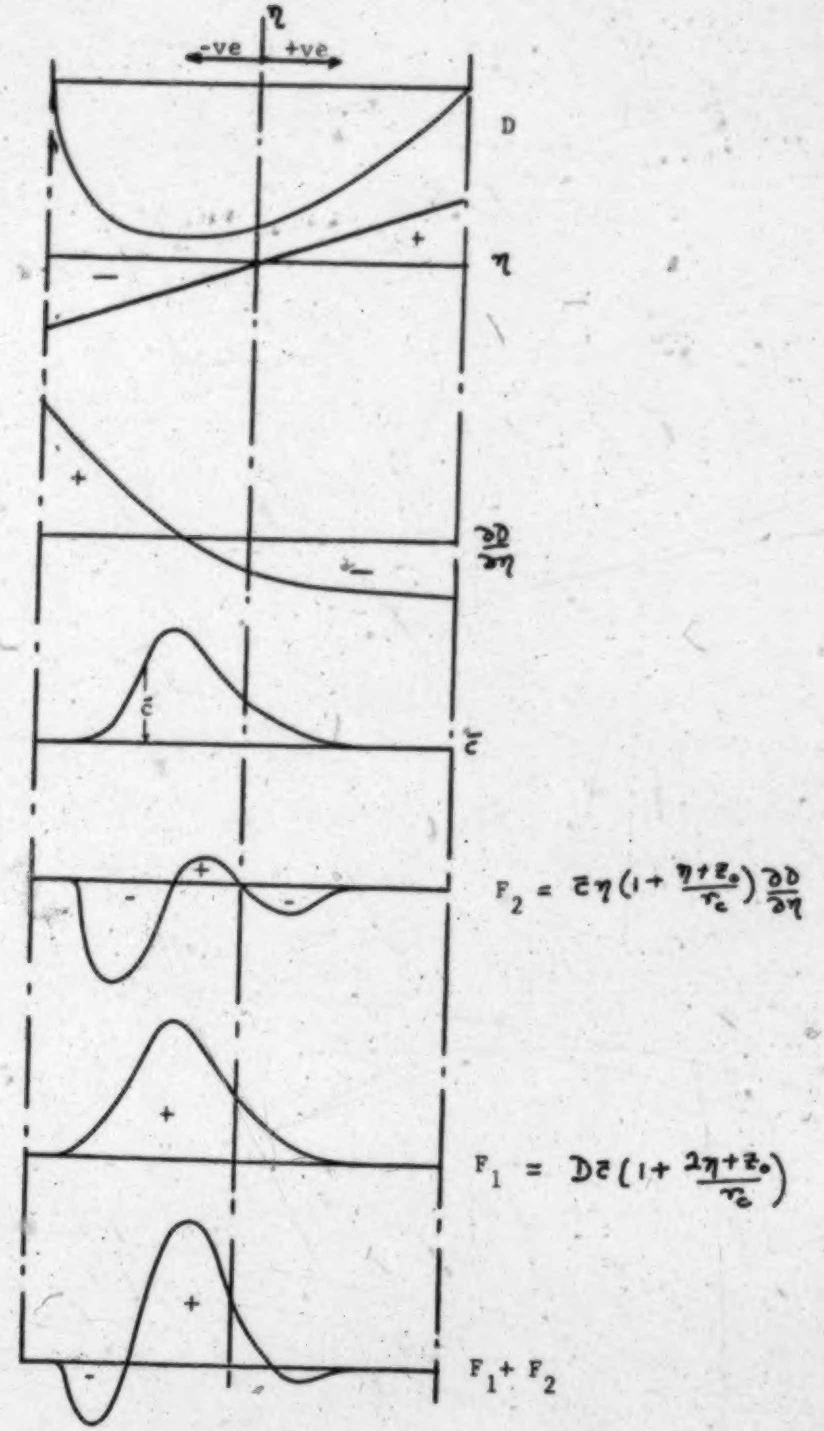
η
-ve
+ve
D
+
−
η
+
$\frac{\partial D}{\partial \eta}$
−
$\bar{c}$
$\bar{c}$
+
-
-
$F_2 = \bar{c}\eta\left(1+\frac{\eta+z_0}{r_c}\right)\frac{\partial D}{\partial \eta}$
+
$F_1 = D\bar{c}\left(1+\frac{2\eta+z_0}{r_c}\right)$
+
-
$F_1 + F_2$

FIGURE 7.7 LATERAL VARIATION OF TERMS IN B(X).

test although the slope during both tests is not significantly different.

In spite of the above limitations, some rough comparisons can be made between the winter and summer results. The mixing potential of the river as measured by E_{zw} for the initial reach length of about 7000 ft is more than four times greater in summer than in winter. This can be seen by comparing the concentration distributions (Figures 7.5a and b) at Sections 3 (winter) and E (summer) which are located closely together and indicate a similar degree of mixing, even though in summer the tracer was injected near the left bank, while injection was near the channel centerline in winter. The low value of E_{zw} for winter is reasonable and is probably caused by the reduction in both diffusion capacity and strength of spiral motions as discussed previously in Chapter 6.

It is important to remember that E_{zw} is considered to be representative of the reach average of the generally variable $\bar{\varepsilon}_{zw}$ (depth-averaged transverse mixing coefficient). It was emphasized in Chapter 3 that if ϕ_w (or $\bar{\varepsilon}_{zw}$) does vary in a particular flow situation, different values of E_{zw} or k will be obtained depending on the point (z_o) about which the moments are taken. It is to be noted that both laboratory and field data were analysed with z_o taken as the transverse co-ordinate of source position. It is of particular interest, therefore, to test the sensitivity of k to moments taken about different z_o. Table 7-4 summarises the variation of the normalised exchange ocefficient, k, for $z_o = 0.0$ and -6.0.

Also shown in Table 7-4 are the k-values obtained by taking moments about the centroid of the tracer flux distribution as suggested by Holley and Abrahams (1972) for centerline release of tracer.

It is important to mention that the winter test achieved 90% mixing over the test reach with the tracer cloud occuping the entire river cross-section. Table 7.4 indicates significant differences in the computed values of k for the various reaches but the distance weighted average k for the entire reach resulting from taking moments about $z = 0$ and $z = -6.0$ are practically the same. The reason for this is probably due to the fact that the cumulative effects of variations in $\bar{\varepsilon}_{zw}$ (or ϕ_w) which were not accounted for in Equation 7.7 average out when the mixing is considered over a series of alternating bends and when a very high degree of mixing has been achieved.

Table 7-4 also indicates that approximately the same average k-value is obtained when moments are taken about the centroid of the tracer flux distribution. This seems fortuitous because the locus of the centroid of the tracer flux distribution at the various sections is neither concentric with or parallel to the channel axis which is taken either as an arc of a circle or a straight line.

Figure 7.8 indicates that the longitudinal variation of the normalised transverse mixing coefficient for the winter test follows a trend which is quite similar to that observed in the laboratory tests with the maximum k occurring around the middle of a bend and

TABLE 7.4 DEPENDENCE OF E_{zw}/u_*R ON POINT ABOUT WHICH MOMENTS OF TRACER FLUX ARE TAKEN OR VALUE OF CUMULATIVE DISCHARGE ABOUT WHICH MOMENTS OF TRACER CONCENTRATION ARE TAKEN.

Cross-Section Number.	E_{zw}/u_*R +			E_{zw}/u_*R ++	
	Moments About $z=0$	Moments About $z=-6$	Moments About z_c *	Moments About $q_*=0.44Q$	Moments About $q_*=0.55Q$
0					
	0.58	0.39	0.33	0.91	0.94
1					
	0.06	0.17	0.14	0.20	-0.02
2					
	0.41	0.24	0.20	0.22	0.30
3					
	-0.01	0.64	0.06	0.16	0.06
4					
	0.98	0.50	1.16	0.54	0.81
5					
Distance Weighted Averaged.	0.35	0.37	0.36	0.34	0.36

NOTES.

+ E_{zw}/u_*R obtained from moments of tracer flux distribution with respect to z.

++ E_{zw}/u_*R obtained from moments of tracer concentration distribution with respect to q_o

* z_c is transverse coordinate of centroid of tracer flux distribution.

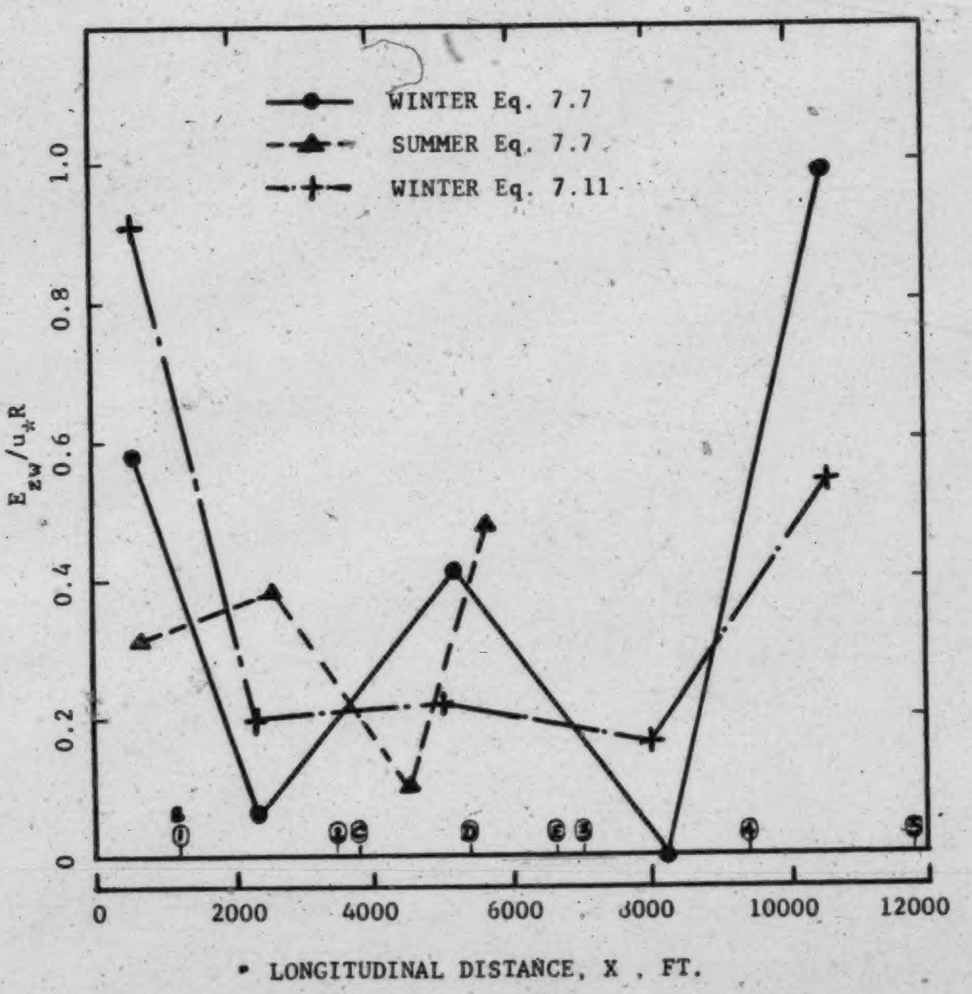

FIGURE 7.8 LONGITUDINAL VARIATION OF THE NORMALISED TRANSVERSE MIXING COEFFICIENT, E_{zw}/u_*R.

the minimum at the beginning of a bend.

The open water tests indicated some reduction in the value of normalised mixing coefficient, k, between sections C and D. This could be expected again because the transverse velocities would tend to move the tracer back toward the left bank and thus inhibit the spreading of tracer which was injected from the left bank. It is noted that the open water results are not as reliable as those for the winter test.

Yotsukura and Cobb's (1972) method for describing the tracer concentration distribution as a function of the normalised cumulative discharge, that is, $\bar{c} = \bar{c}\ (q_*/Q)$, appears to be more suitable for non-uniform meandering channels such as the Lesser Slave River. It is to be noted that q_* is the cumulative discharge and Q is the total discharge. The cumulative discharge, q_*, is defined as:

$$q_* = \int_0^z \bar{u} D dz$$

where $z = 0$ is taken at one bank.

Representing the concentration distribution as $\bar{c} = \bar{c}\ (q_*/Q)$ instead of $\bar{c} = \bar{c}\ (z/w)$ describes the mixing process in the context of fluid mixing rather than spatial transport. By using q_* as an alternative transverse coordinate in place of z, Yotsukura and Cobb showed that the steady state convective-diffusion equation averaged over depth could be transformed to:

$$\frac{\partial \bar{c}}{\partial x} = \frac{\partial}{\partial q_*} (\bar{\varepsilon}_{zw} \, \bar{u}D^2 \frac{\partial \bar{c}}{\partial q_*})$$

or:

$$\frac{\partial \bar{c}}{\partial x} = E'_{zw} \frac{\partial}{\partial q_*} (\phi_w \, \bar{u}D^2 \frac{\partial \bar{c}}{\partial q_*}) \qquad (7.9)$$

It is noted that $\phi_w = \phi_w(x, q_*)$ and as mentioned previously, it defines the variation of the depth-averaged transverse mixing coefficient for a given flow situation.

The moments technique can now be applied to Equation 7.9, again assuming that $\phi_w = 1.0$, by taking moments with respect to q_o, where $q_o = q_* - q_t$ and q_t is the cumulative discharge about which the moments are taken. The resulting equation after some simplifications is:

$$\frac{d}{dx}\left[\frac{\int_{q_1}^{q_2} \bar{c} q_o^{\,2} dq_o}{\int_{q_1}^{q_2} \bar{c} dq_o}\right] = 2E_{zw} \frac{\int_{q_1}^{q_2} \bar{c} \frac{\partial (\bar{u}D^2 q_o)}{\partial q_o} dq_o}{\int_{q_1}^{q_2} \bar{c} dq_o} \qquad (7.10)$$

in which q_1 and q_2 are the cumulative discharges measured from $q_o=0$. Equation 7.10 can be rewritten as:

$$\frac{dM_{2q}(X)}{dX} = E_{zw} \; B_q(X) \qquad (7.11)$$

where the definitions of $M_{2q}(X)$ and $B_q(X)$ can be obtained by comparing Equations 7.11 and 7.10.

Equation 7.11 was applied to the winter data and the moments were taken about the point of tracer release, that is $q_t = 0.44\ Q$. The numerical values of $M_{2q}(X)$, $B_q(X)$ and E_{zw} are given in Table 7-5. The overall average transverse mixing coefficient was evaluated as 0.1085 and the corresponding E_{zw}/u_*R as 0.34. It is seen that the overall average values of E_{zw} obtained from Equation 7.7 by correcting for the moments and Equation 7.11 are not significantly different.

TABLE 7-5 NUMERICAL VALUES OF $M_{2q}(X)$, $B_q(X)$ AND E_{zw} IN EQUATION 7.11

Section	Distance x, ft	$M_{2q}(X)$ $ft^6 sec^{-2}$	$B_q(X)$ $ft^3 sec^{-1}$	E_{zw} $ft^2 sec^{-1}$	$\frac{E_{zw}}{u_*R}$
0	0	0	0		
				0.294	0.91
1	1150	21882	129.2		
				0.064	0.20
2	3450	39208	103.3		
				0.071	0.22
3	7000	60689	66.4		
				0.052	0.16
4	9400	68886	66		
				0.174	0.54
5	11800	83201	2.6		
Average				0.1085	0.34

Again, because $\overline{\varepsilon}_{zw}$ varies both longitudinally and laterally different values of E_{zw} are obtained depending on the value of q_t about which the moments are taken. Table 7.4 gives a comparison between the values of $E_{zw}/u_{*}R$ evaluated by taking moments about q_t = 0.44 Q and $q_t = 0.55$ Q.

It is evident from the above discussions that if the mixing is considered over a series of bends and provided a high degree of mixing has been achieved then the method of moments (Equation 7.7) combined with the adjustment (Equation 7.8) proposed by Fischer give satisfactory estimates of the overall k irrespective of the point about which the moments are taken.

Flow in a channel of non-uniform cross-section is usually characterised by an average velocity and depth. For this situation the transverse mixing coefficient can be obtained by applying the formula:

$$E_{zw} = \frac{U_o}{2} \frac{d\sigma_z^2}{dX} \tag{7.12}$$

where σ_z^2 is the variance of the concentration distribution. This equation, as outlined by Sayre and Chang (1968), is based on the assumptions of a gradient-type mixing and a uniform downstream velocity at each point on the channel cross-section. Equation 7.12 is valid only until a significant amount of tracer encounters the opposite bank for bank release or both banks for centerline release of tracer.

When Equation 7.12 was used to determine the mixing coefficient for the summer test, it resulted in an average value of E_{zw} = 0.86 ft^2/sec and k = 0.65. This k-value is almost 100% larger than the value predicted by Equation 7.7 which takes account of depth and velocity variations in the lateral direction. That the assumptions of constant depth and uniform velocity give unsatisfactory predictions of k is also confirmed by Holley et al (1972). They demonstrated numerically that if a trapezoidal channel is represented by a rectangular channel having the same area and surface width, the mixing coefficient calculated from the concentration distributions may be larger.

Reports of field measurements of the normalised transverse mixing coefficient are listed in Table 7.6. It is evident from this table that the k-values obtained are within the same range as those observed for idealised meandering laboratory channels.

The results of Holley and Abrahams (1973) particularly demonstrate how increased mixing caused by obstructions can increase the magnitude of k. Their test reaches had relatively mild bends but they were bordered by groins which, according to their laboratory study, can increase k by a factor of 2 to 3.

It was shown by dimensional arguments in Section 6.2.4 that:

$$\frac{E_{zw}}{u_* R} = \pi_6 \left(\frac{W}{R}, \frac{r_c}{R}, f, \frac{L}{r_c} \right) \qquad (6.27)$$

An indication of the importance of r_c/R can be seen in the two results obtained for the Missouri River. It is assumed that d_* is approximately equal to R for open water conditions.

TABLE 7.6 SOME FIELD MEASUREMENTS OF THE NORMALISEDTRANSVERSE MIXING COEFFICIENT.

SOURCE	CHANNEL	ASPECT RATIO, W_s/R	$k(=E_{zw}/u_*R)$	REMARKS
GLOVER (1964)	Columbia River Near Richland	100	0.72	
YOTSUKURA et al (1970)	Missouri River Near Blair, Nebraska.	74	0.60	Test Reach with a Bend of Radius 12000 ft.
FISCHER (1967)	Atrisco Feeder Canal.	27	0.24	Reasonably Straight Reach.
YOTSUKURA and COBB (1972).	South River.	46.2	0.30	Test Reach had a few Mild Bends.
	Bernando Conveyance Canal	28.7	0.30	Straight Reach with Shifting Bed Configuration.
HOLLEY and ABRAHAM (1973)	Ijssel River.	17.3	0.50	River Bordered by Groins.
	Waal River.	56.7	0.60	River Bordered by Groins.
SAYRE and YEH (1973)	Missouri River Near Brownville Nebraska.	59.1	3.3	Test Reach had 2 Bends with Radii 6400 and 3400 ft.
HIGHWAY and RIVER ENGINEERING DIVISION ALBERTA RESEARCH (1974)	Athabasca River Downstream of Fort McMurray (ICE-COVERED)	240	2.5*	Mild Bends with Some Islands.
PRESENT INVESTIGATION	Lesser Slave River.	17	0.33	Test Reach had a Series of fairly Sharp Bends.
	Lesser Slave River (ICE-COVERED)	37	0.35	

*This Result Is A Preliminary Estimate.

The curvature of the Brownville reach was about 2 to 3 more pronounced than that of the Blair reach with the r_c/R ratio 3 to 5 times greater in the Brownville test. According to Sayre and Yeh (1973) the river discharge at the time of the Blair experiment was approximately 40% less than that during the Brownville test. However, they attributed the greater rate of transverse mixing in the Brownville test more to difference in sinuosity of the two reaches than to difference in river discharge. This seems reasonable since the friction factor, f, for both reaches was approximately the same and the aspect ratio was not significantly different.

The effect of width to depth ratio is not clear from Table 7-6. However, if data obtained for rivers with mild bends and no obstructions are compared then the data seem to indicate some dependence of k on the aspect ratio, with k increasing with W/R.

.CHAPTER 8

SUMMARY, CONCLUSIONS AND RECOMMENDATIONS

Transverse diffusion and mixing in straight and meandering ice-covered and open channel flows were investigated by means of a non-buoyant tracer released into the flow at a steady and continuous rate. Tracer concentration and velocity measurements were made in the laboratory for similar conditions of discharge and depth in both open and ice-covered channels. Transverse mixing experiments for both open and ice-covered conditions were also conducted in the Lesser Slave River. The laboratory and field results were analysed and used to evaluate the effect of an ice-cover on the transverse diffusion and mixing coefficients.

8.1 Conclusions

The primary aim of this thesis was to demonstrate the significant reduction in the mixing capacity of a channel (as measured by E_z or E_{zw}) caused by an ice-cover. The laboratory and field tests indicate that this reduction in absolute terms can vary from 50 to 500%. However, when the mixing coefficients are normalised with the product u_*R reductions of up to 300% could be observed. Other findings of this investigation are as follows.

8.2 Results Related to Straight Flume

1. The depth-averaged transverse concentration profiles at various

downstream stations for a given flow condition can be represented by a single curve if $\bar{c}/C_{max}$ is plotted against z/b. This curve was Gaussian for both open and ice-covered tests.

2. From the above suggestion of similarity, a formula was derived for evaluating the transverse diffusion coefficient. This formula, $E_z = U_o b^2/4x\ln 2$, requires only one measured depth-averaged transverse concentration profile and was found to give satisfactory results. It is only applicable to situations with the source located at the channel centerline.

3. For side release of tracer, the transverse diffusion coefficient was found to increase with distance from the source and approached the constant value for centerline injection as the tracer cloud occupied an increasing area of the uniform flow region.

4. For similar conditions of discharge and depth the presence of an ice-cover was observed to reduce the diffusion capacity, as measured by E_z , by as much as one-half the value for open water conditions.

5. The values of the normalised transverse diffusion coefficient, k (= E_z/u_*R), for ice-cover conditions were generally found to be slightly less than those for the corresponding open channel tests. These latter k-values are within the range of previously reported k-values in open channel flows.

6. For fully rough turbulent flow k was found to increase with increase in f when W/R was held constant. No obvious dependence of k on W/R was indicated by the available data.

8.3 Results Related to Meandering Flume

1. The growth of the second mements of the tracer flux distribution with longitudinal distance was non-linear. The growth rate of M_2 was observed to decrease and in some situations became negative, particularly where the spiral motion decayed and reversed.

2. The local depth-averaged mixing coefficient, $\bar{\varepsilon}_{zw}$, was found to vary both laterally and longitudinally and seemed to be associated largely with variations in the intensity of the spiral motions.

3. The magnitude of the averaged normalised mixing coefficient, k , over the test reach for ice-covered flows was observed, on the average, to be about 2 times less than the corresponding value in open channel flows for similar flow conditions. The range of k-values obtained are comparable to those reported in the literature for field conditions.

4. The magnitude of the transverse mixing coefficient, E_{zw} , was observed to be of the order 4 times smaller for ice-cover conditions than for the corresponding open channel. This substantial reduction is presumably due to reduction in the scale of the domi-

nant turbulent eddies and strength of the spiral motions in the presence of an ice-cover.

5. An apparent dependence of the transverse mixing coefficient on source position was observed. It was suggested that it is probably a manifestation of the effects of transverse velocities on the mixing. The mixing coefficient varied longitudinally for all source positions and the averaged lateral mixing coefficient for different source positions was found, in general, to reach a maximum within the middle third of a bend and a minimum at the beginning of a bend. Again this variation would seem to be related to the growth, decay and reversal of the spiral motions.

6. Negative values of the transverse mixing coefficient were sometimes observed, particularly at the beginning of a bend where there is reversal of the spiral motion. A negative E_{zw} value implies convective transport by spiral motions of low depth-averaged concentration fluid to regions of high depth-averaged concentration.

7. The principal parameters controlling the normalised mixing coefficient, k, were identified as ~~the~~ aspect ratio W/d_* (or W/R), r_c/d_* and the friction factor, f. For the present laboratory investigation, k was found to decrease with increasing r_c/d_* ratio, increasing roughness and decreasing aspect ratio.

8. Of the two methods proposed for evaluating the transverse mixing coefficient, the integral method was found to give extremely high

k-values for situations where the tracer was released at the channel centerline. The cause of this could not be clearly identified. Both integral and moments methods yielded similar patterns for the longitudinal variation of E_{zw}. The overall average E_{zw} for a given source location as computed by the integral method was on the average only about 25% higher than the corresponding value estimated by the moments method. However, large differences in the value of E_{zw} for individual sub-reaches were sometimes observed between the two methods.

8.4 Results Related to Field Investigations

Since the present data relate only to field measurements on one stream, general conclusions would be premature but the results do indicate that an ice-cover can reduce the mixing capacity of a river substantially. This is confirmed by the laboratory data. The assumption of quick vertical mixing normally made in the context of field studies was found not to be valid in the case of relatively deep, meandering rivers. This was also found to be true in the laboratory tests.

8.5 Recommendations

No systematic and detailed investigations have so far been carried out to delineate the effects of various parameters controlling

240

the transverse spreading of tracer, even for the idealized conditions in the laboratory. The following recommendations should be considered in planning future research on transverse mixing and diffusion:

1. Detailed measurements of the normalised mixing and diffusion coefficients along lines similar to that adopted by Miller and Richardson (1974) are needed. These measurements should be used to produce a Moody type diagram which should completely describe the dependence of E_z/u_*R or E_{zw}/u_*R on other parameters such as W/R, f and r_c/R.
2. Present knowledge of the hydraulics of flow in ice-covered channels is very limited. Since the mixing phenomena are closely related to the velocity field, detailed velocity measurements, particularly in ice-covered meandering channels are necessary for a better understanding of mixing in channel flows.

LIST OF REFERENCES

Aris, R. "On the Dispersion of a Solute in a Fluid Flowing Through a Tube". Roy.Soc. (London) Proceedings, Ser. A, 235, pp. 67-77, 1956.

Carslaw, H.S., and J.C. Jaeger "Conduction of Heat in Solids". 2nd. Edition, Oxford Press, 1959.

Chang, Y. "Lateral Mixing in Meandering Channels". Ph.D. Thesis, University of Iowa, 1971.

Czernuszenko, W. "Transversal Diffusion in the Open Channel". Proceedings of the 15th. Congress of the I.A.H.R., Istanbul, Vol. 2, pp. 31-38, 1973.

Elder, J.W. "The Dispersion of Marked Fluid in Turbulent Shear Flow". Journal of Fluid Mechanics, Vol. 5, pp. 544-560, 1959.

Fischer, H.B. "Transverse Mixing in a Sand-Bed Canal". U.S. Geological Survey, Professional Paper 575-D, pp. D267-D272, 1967.

Fischer, H.B. "The Effect of Bends on Dispersion in Streams". Water Resources Research, Vol. 5, No. 2, pp. 496-506, 1969.

Fischer, H.B. Discussion of "Dispersivity Tensor for Turbulent Uniform Channel Flow" by G. Dagan, Journal of the Hydraulics Division, ASCE, Vol. 96(HY4), pp. 1096-1100, April 1970.

Fischer, H.B. "Longitudinal Dispersion and Turbulent Mixing in Open Channel Flow". Annual Review of Fluid Mechanics, Vol. 5, No. 1, pp. 59-78, 1973.

Glover, R.E. "Dispersion of Dissolved or Suspended Materials in Flowing Streams". U.S. Geological Survey, Professional Paper 433-B, 1964.

Hanjalic, K., and B.E. Launder "Fully-Developed Flow in Rectangular Ducts of Non-Uniform Surface Texture". Part I - An Experimental Investigation. Imperial College of Science and Technology, Department of Mechanical Engineering Report No. TWF/TN/48, August 1968.

Hinze, J.O. "Turbulence". McGraw-Hill Book Company, New York, p. 25, 1959.

Holley, E.R., J. Siemons and G. Abraham "Some Aspects of Analysing Transverse Diffusion in Rivers". Journal of Hydraulic Research, Vol. 10, No. 1, pp. 27-57, 1972.

Holley, E.R., and G. Abraham "Laboratory Studies on Transverse Mixing in Rivers". Journal of Hydraulic Research, Vol. 11, No. 3, pp. 219-253, 1973a.

Holley, E.R., and G. Abraham "Field Tests in Transverse Mixing in Rivers". Journal of the Hydraulics Division, ASCE, Vol. 99 (HY12), 1973b.

Hollingshead, A.B. "Boundary Shear Stress Distribution in Open Channel Flow". Ph.D. Thesis, University of Alberta, Edmonton, 1972.

Kellerhals, R., C.R. Neill and D.I. Bray "Hydraulic and Geomorphic Characteristics of Rivers in Alberta". River Engineering and Surface Hydrology Report 72-1, Alberta Research, Edmonton, Alberta, 1972.

Laufer, J. "Investigation of Turbulent Flow in a Two-Dimensional Channel". National Advisory Committee for Aeronatics (NACA) Report No. 1053, 1951.

McQuivey, R.S., and T.N. Keefer "Measurement of Velocity-Concentration Covariance". Journal of the Hydraulics Divison, ASCE, Vol. 98 (HY9), pp. 1625-1645, September 1972.

Miller, A.C., and E.V. Richardson "Diffusion and Dispersion in Open Channel Flow". Journal of the Hydraulics Division, ASCE, Vol. 100 (HY1), pp. 159-171, January 1974.

Okoye, J.K. "Characteristics of Transverse Mixing in Open Channel Flows". Ph.D. Thesis, California Institute of Technology, 1970.

Rajaratnam, N., and D. Muralidhar "Hydraulic Instrumentation Series - Yaw and Pitch Probes". Department of Civil Engineering, University of Alberta, Edmonton, September 1967.

Rozovskii, I.L. "Flow of Water in Bends of Open Channels". Academy of Sciences of Ukranian S.S.R., Kiev, 1957, Translated by Prushansky, Y., The Israel Program for Scientific Translations, No.)TS 60-51133, Office of Technical Services, U.S. Dept. Comm., Washington, D.C., 1961.

Sayre, W.W., and F.M. Chang "A Laboratory Investigation of Open Channel Dispersion Processes for Dissolved, Suspended and Floating Dispersants". U.S. Geological Survey, Professional Paper 433-E 71 pages, 1968.

Sayre, W.W., and S. Fukuoka "Longitudinal Dispersion in Sinuous Channels". Journal of the Hydraulics Division, ASCE, Vol. 99 (HY1), pp. 195-218, 1973.

Sayre, W.W., and Tso-Ping Yeh "Transverse Mixing Characteristics of the Missouri River Downstream from the Cooper Nuclear Station". Iowa Institute of Hydraulic Research Report No. 145, 46 pages, April 1973.

Yen, B.C. "Characteristics of Subcritical Flow in a Meandering Channel". Institute of Hydraulic Research, University of Iowa, Iowa City, 155 pages, 1965.

Yen, B.C. "Spiral Motion of Developed Flow in Wide Curved Open Channels". Sedimentation, Symposium to honour Prof. H.A. Einstein. Edited by H.W. Shen, Chapter 22, 1972.

Yotsukura, N., and E.D. Cobb "Transverse Diffusion of Solutes in Natural Streams". U.S. Geological Survey, Professional Paper 582-C 1972.

Yotsukura, N., H.B. Fischer and W.W. Sayre "Measurement of Mixing Characteristics of the Missouri River Between Sioux City, Iowa and Plattsmouth, Nebraska". U.S. Geological Survey, Water Supply Paper 1899-G, pp. 29, 1970.

APPENDIX A

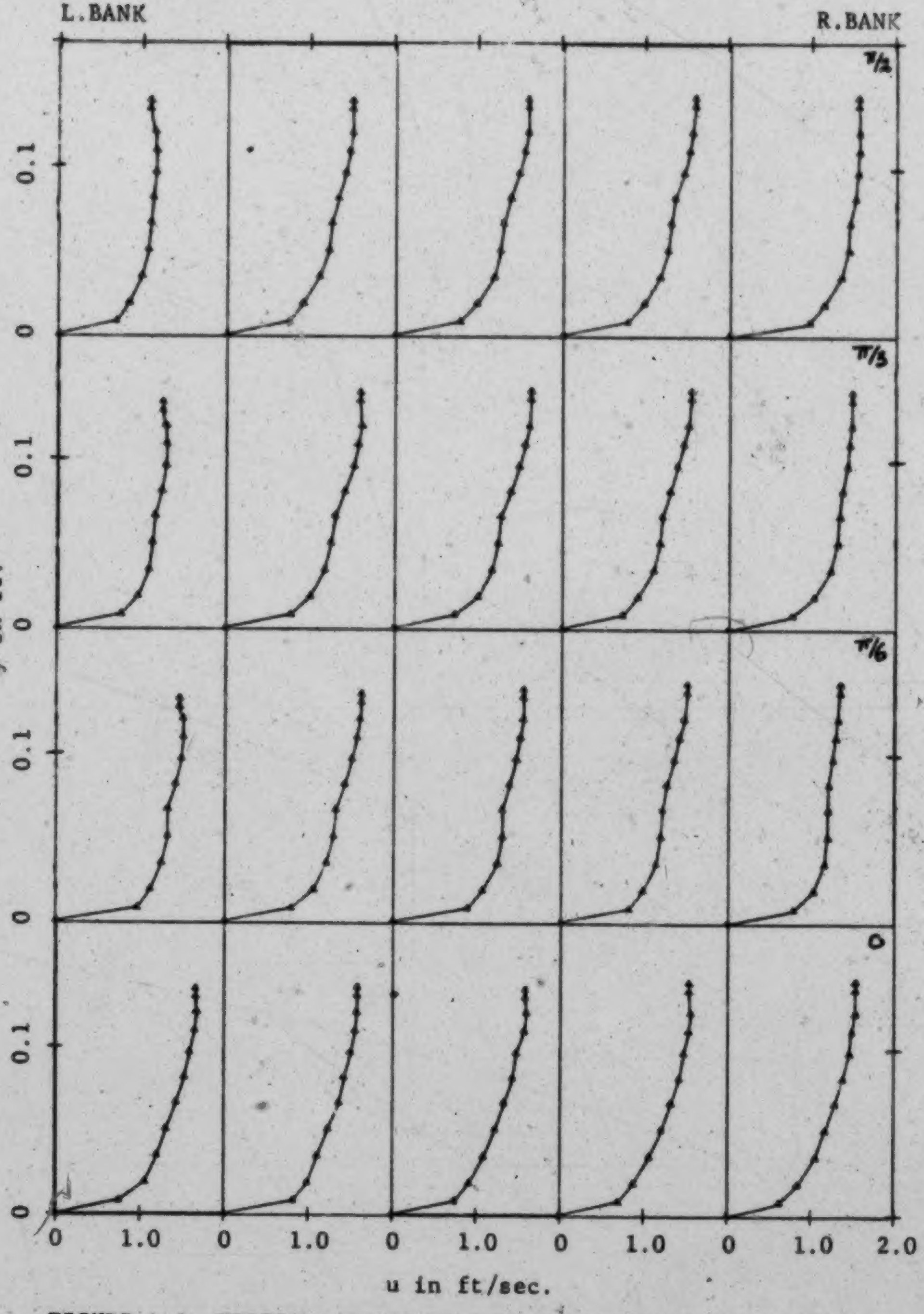

FIGURE A.1a VERTICAL DISTRIBUTIONS OF LONGITUDINAL VELOCITY,
Runs 304/6, SECTIONS θ_1 = 0 TO π/2

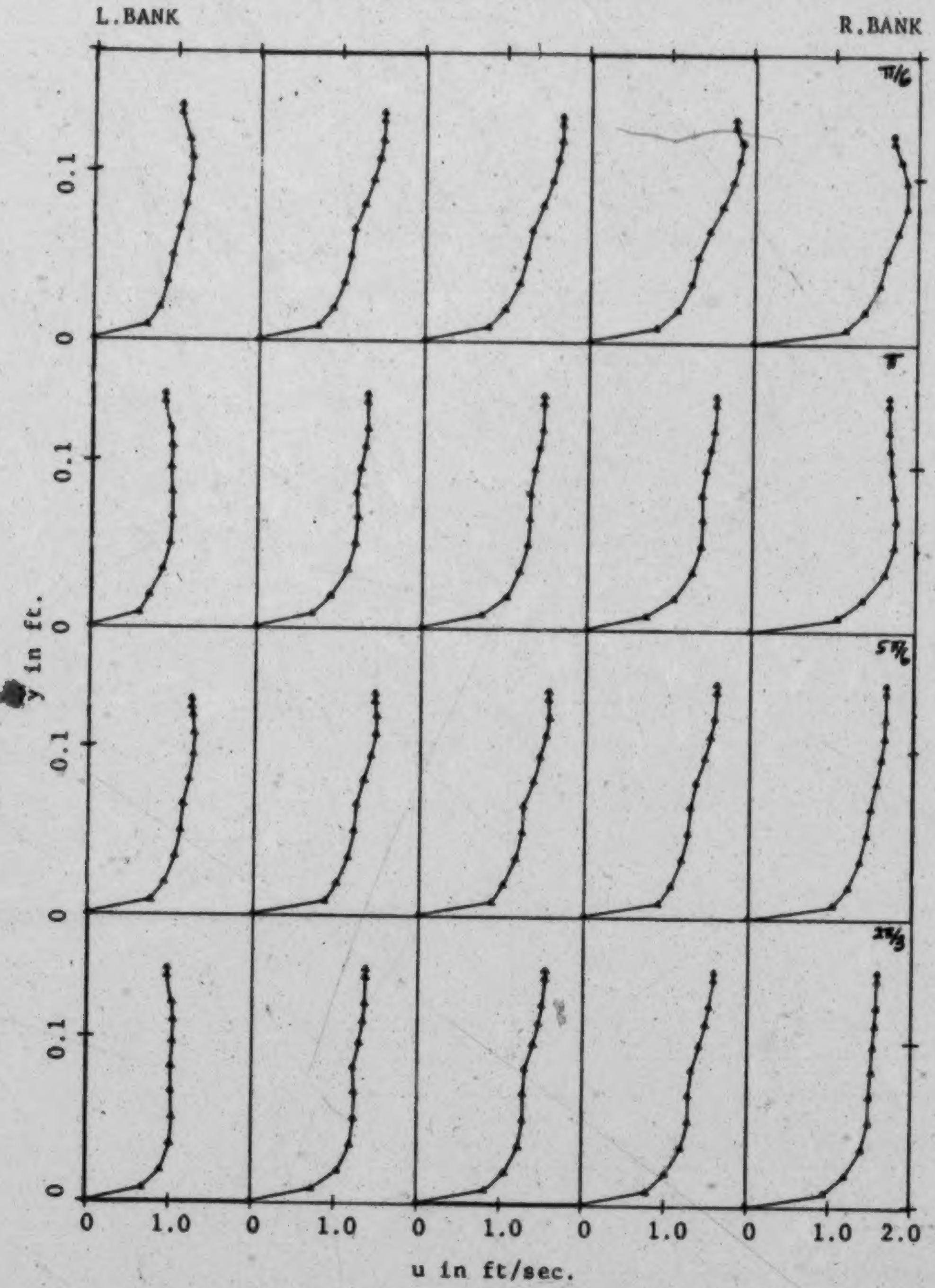

FIGURE A.1b VERTICAL DISTRIBUTIONS OF LONGITUDINAL VELOCITY, Runs, SECTIONS $\theta_1 = 2\pi/3$ TO $\theta_2 = \pi/6$

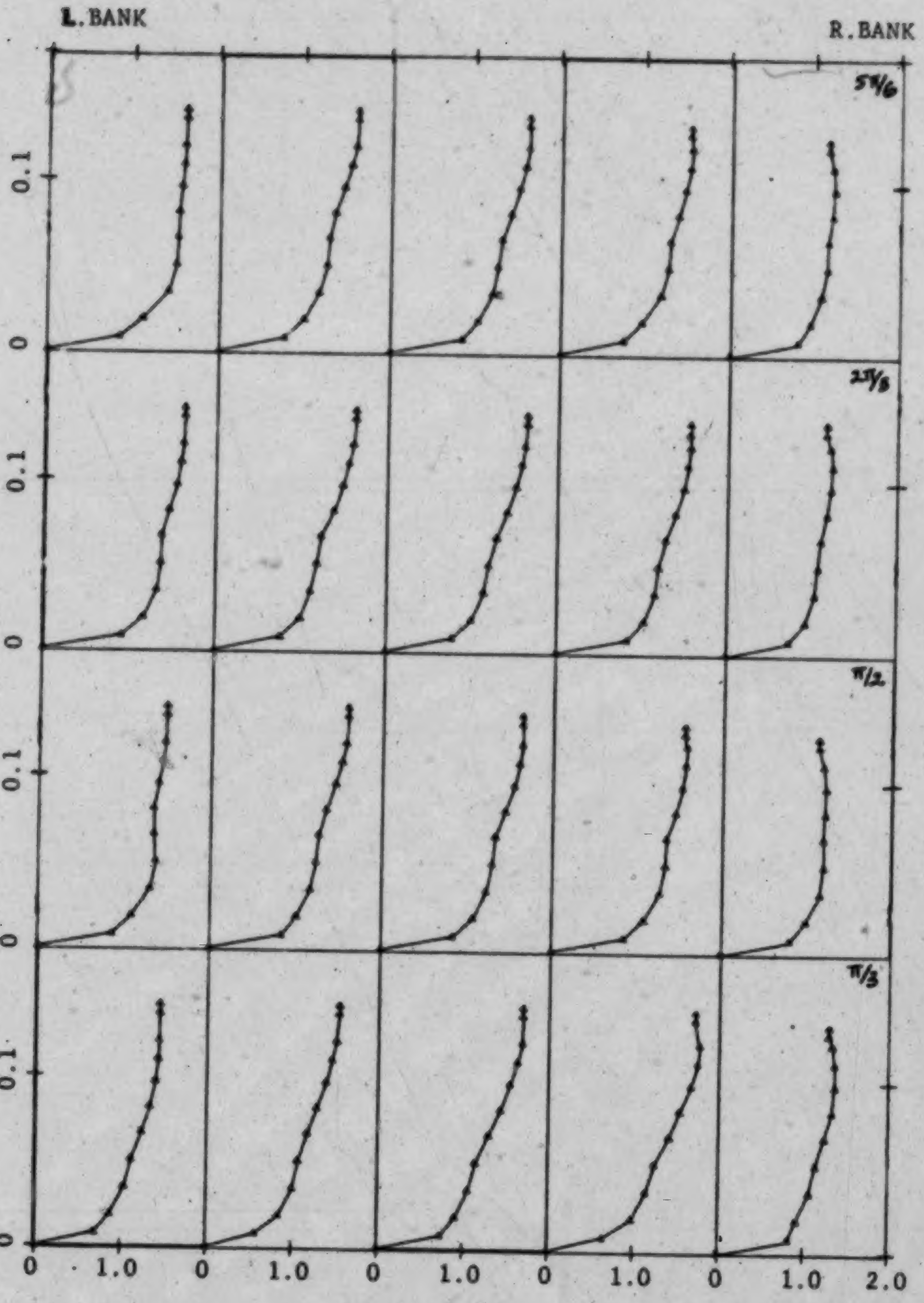

FIGURE A.1c VERTICAL DISTRIBUTIONS OF LONGITUDINAL VELOCITY, Runs, SECTIONS $\theta_2 = \pi/3$ TO $5\pi/6$.

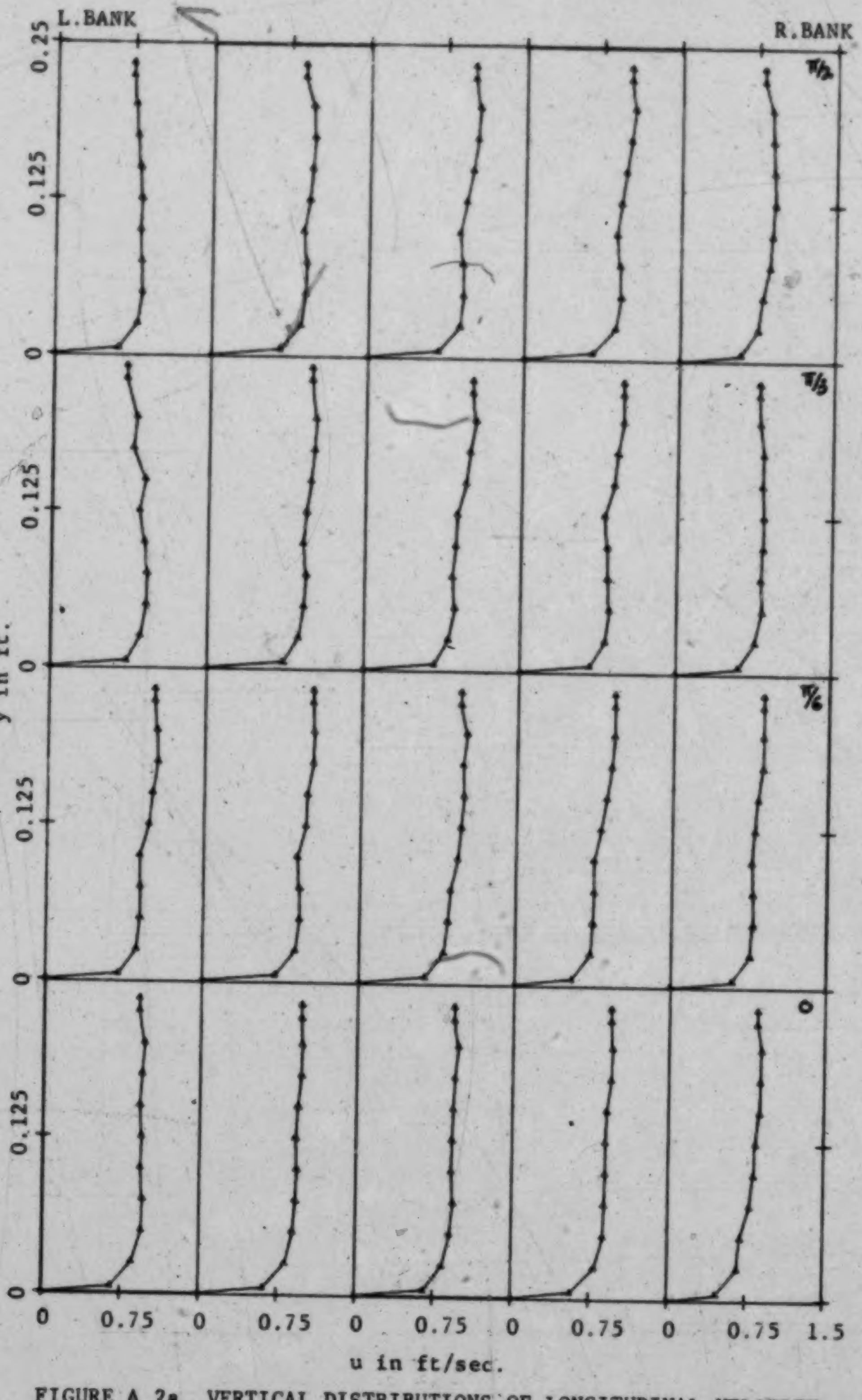

FIGURE A.2a VERTICAL DISTRIBUTIONS OF LONGITUDINAL VELOCITY. Runs 307/8, SECTIONS θ_1 = 0 TO π/2

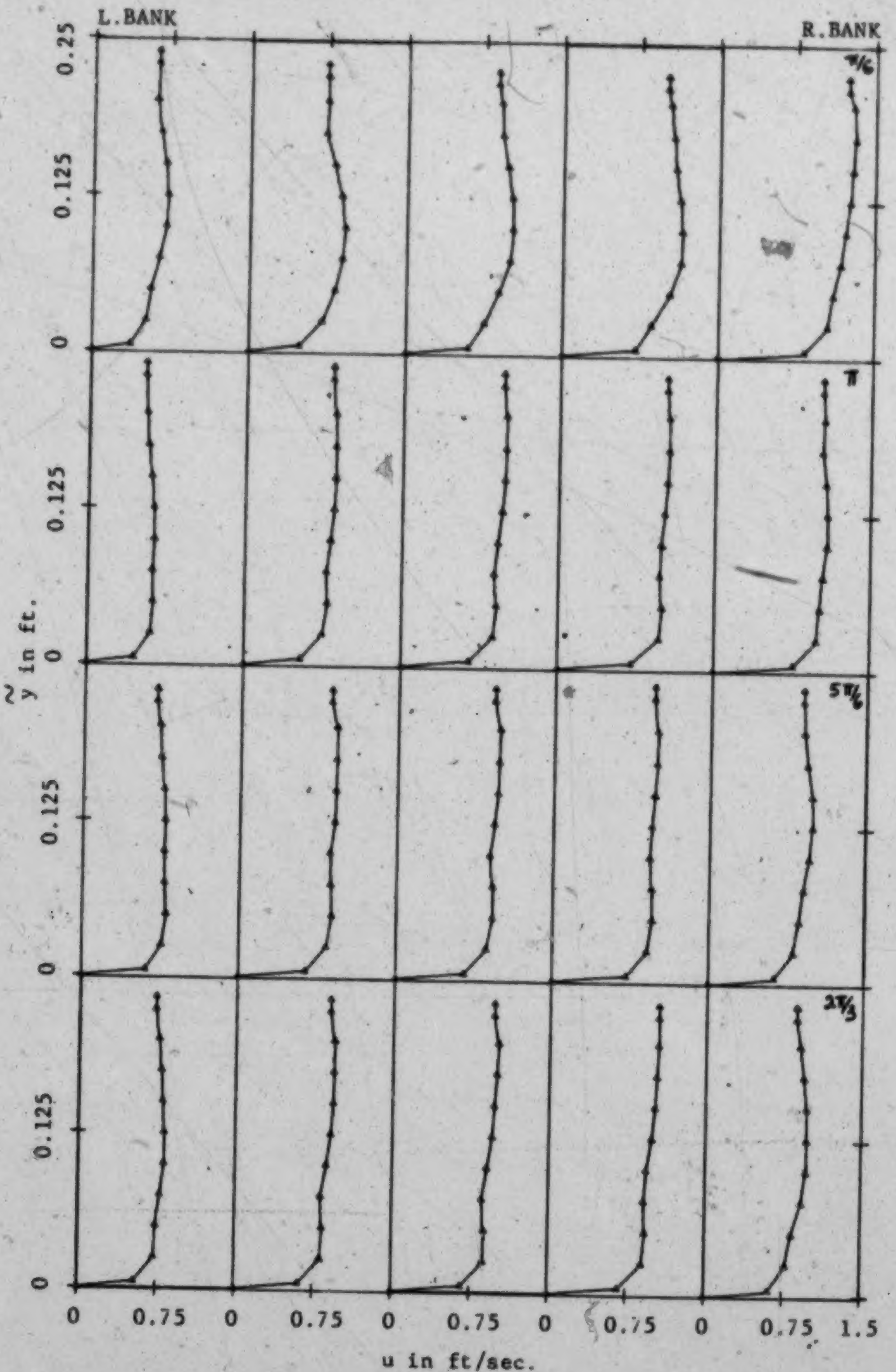

FIGURE A.2b VERTICAL DISTRIBUTIONS OF LONGITUDINAL VELOCITY, Runs 307/8, SECTIONS $\theta_1 = 2\pi/3$ TO $\theta_2 = \pi/6$.

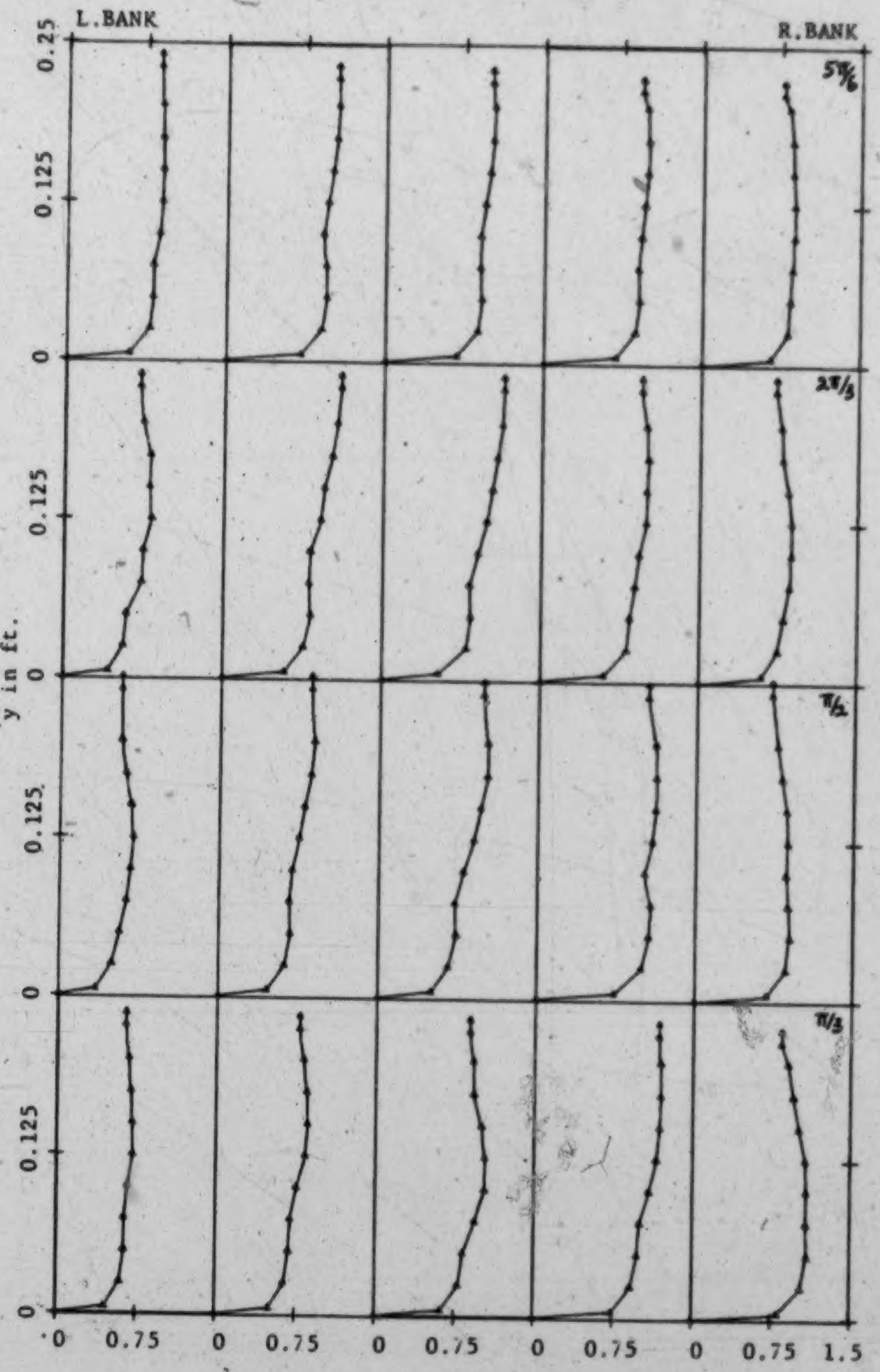

FIGURE A.2c VERTICAL DISTRIBUTIONS OF LONGITUDINAL VELOCITY, Runs 307/8, SECTIONS $\theta_2 = \pi/3$ TO $5\pi/6$.

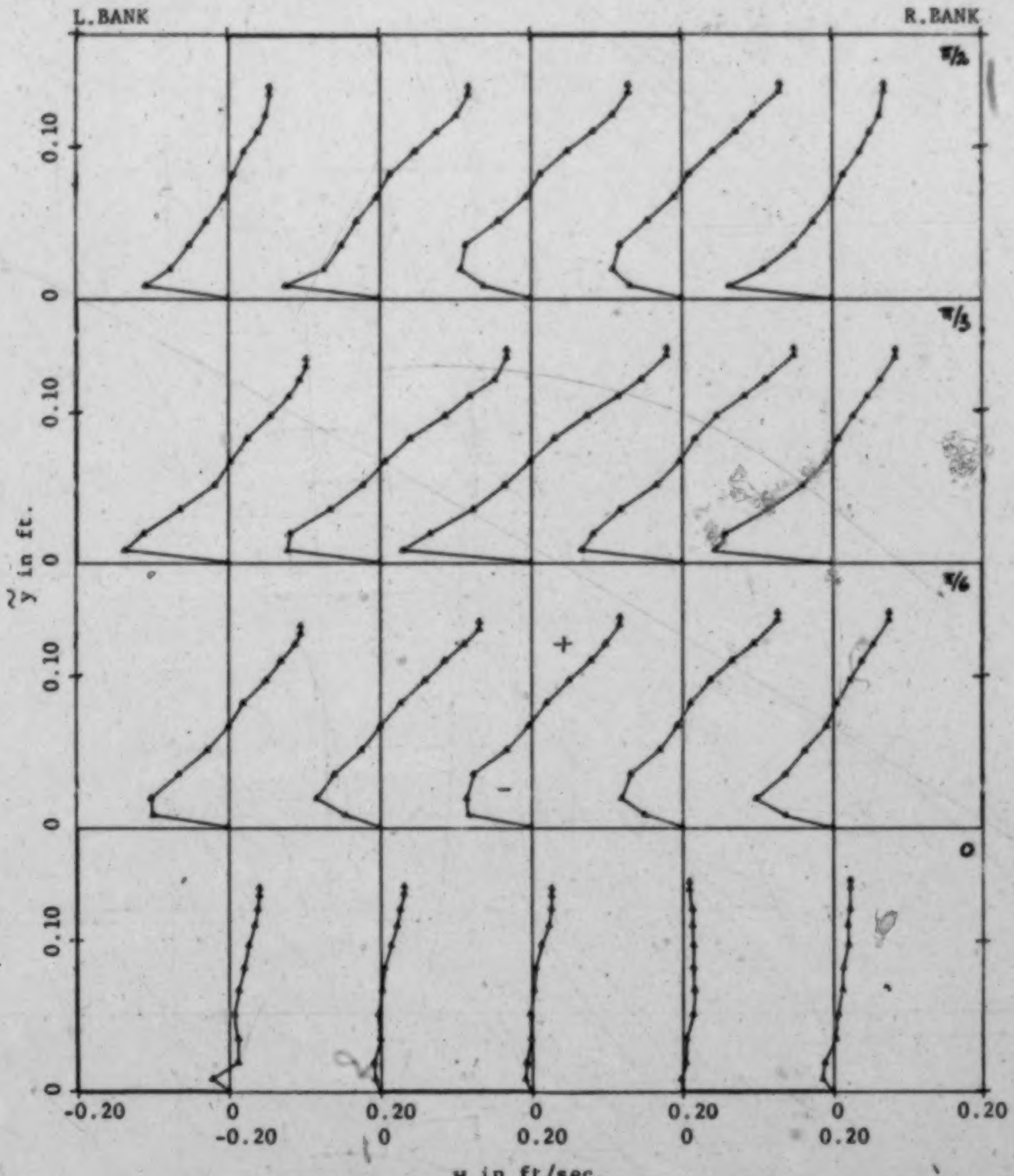

FIGURE A.3a VERTICAL DISTRIBUTIONS OF TRANSVERSE VELOCITY,
Runs 304/6, SECTIONS $\theta_1 = 0$ TO $\pi/2$.

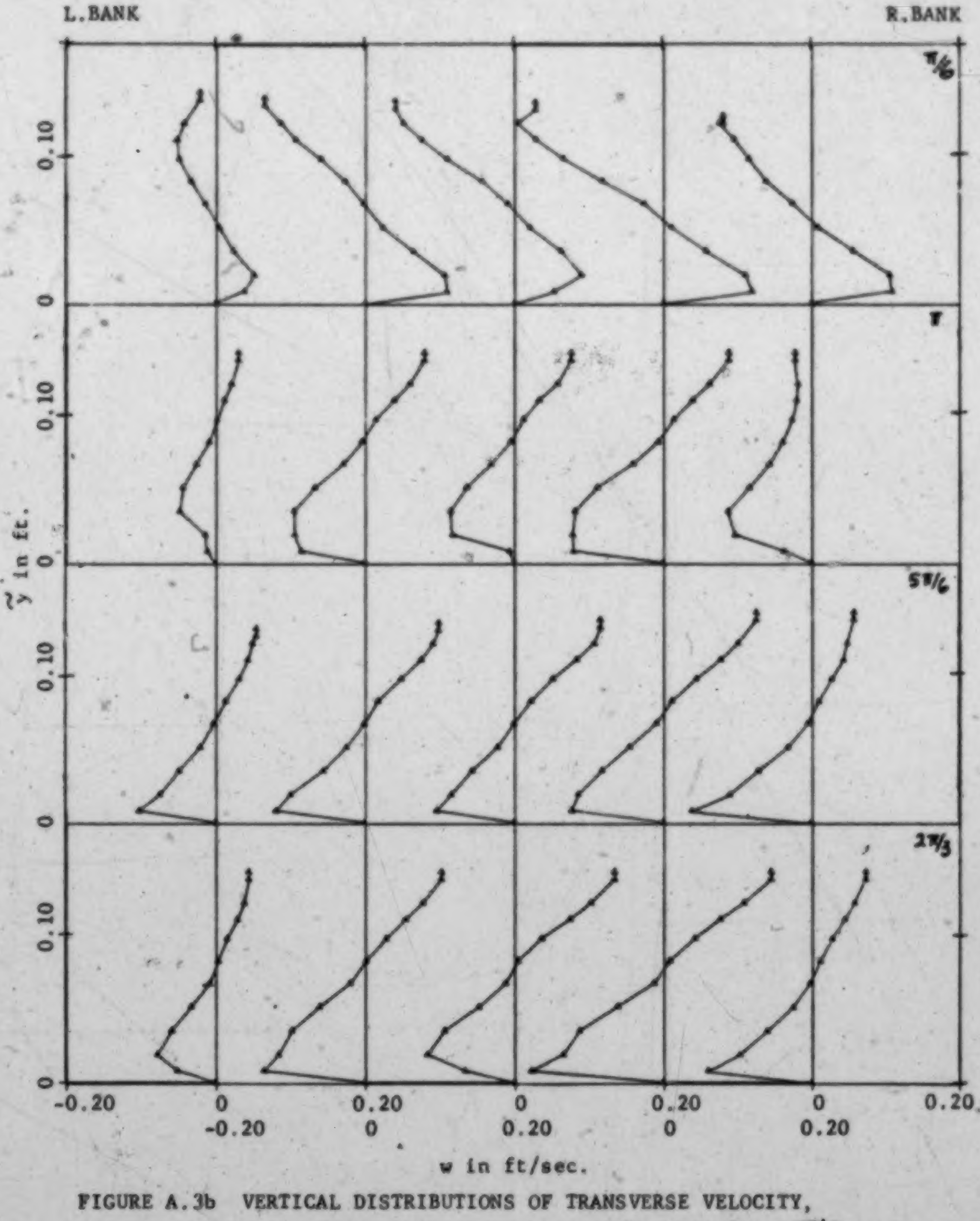

FIGURE A.3b VERTICAL DISTRIBUTIONS OF TRANSVERSE VELOCITY, Runs 304/6, SECTIONS $\theta_1 = 2\pi/3$ TO $\theta_2 = \pi/6$.

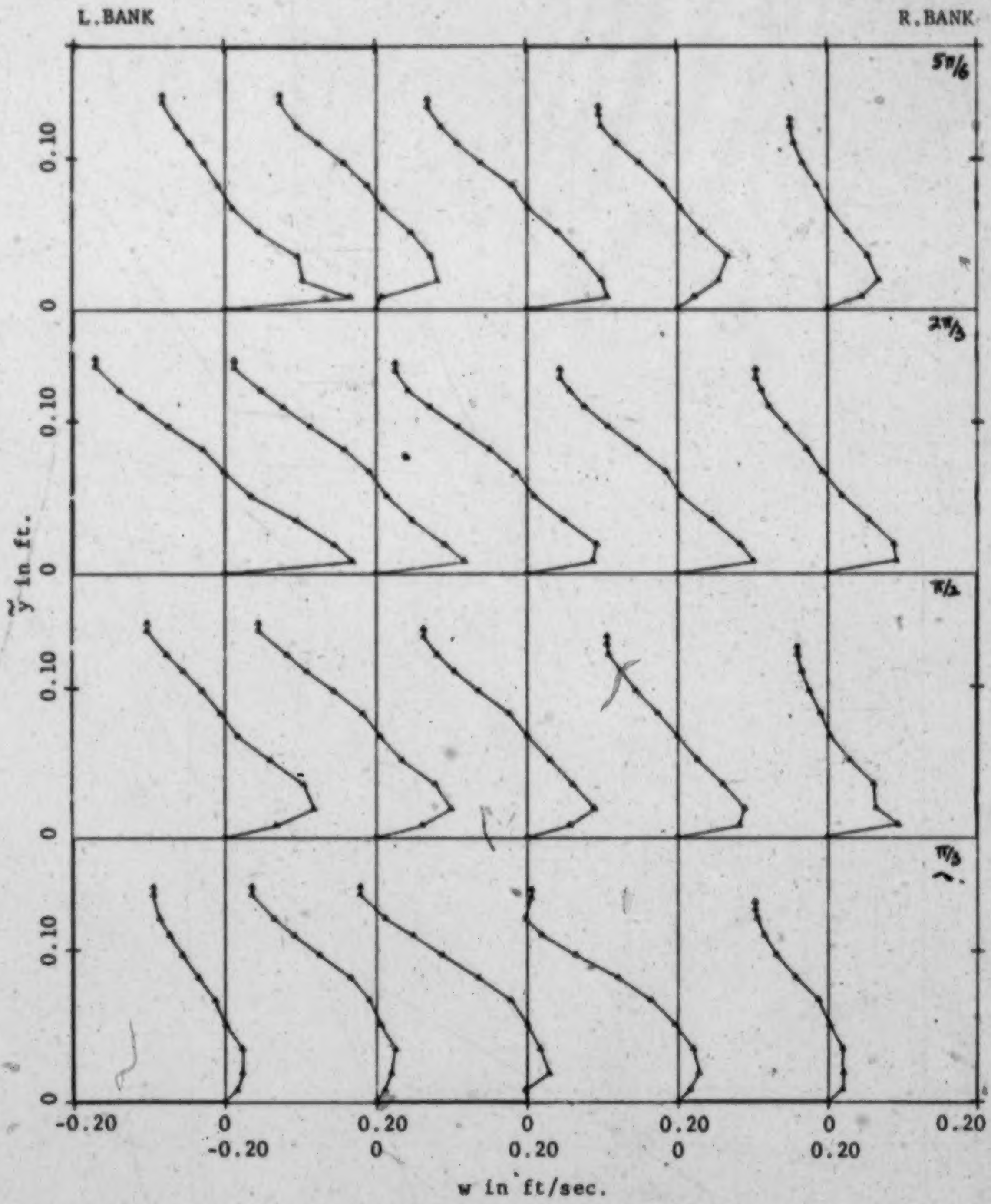

FIGURE A.3c VERTICAL DISTRIBUTIONS OF TRANSVERSE VELOCITY, Runs 304/6, SECTIONS $\theta_2 = \pi/3$ TO $5\pi/6$

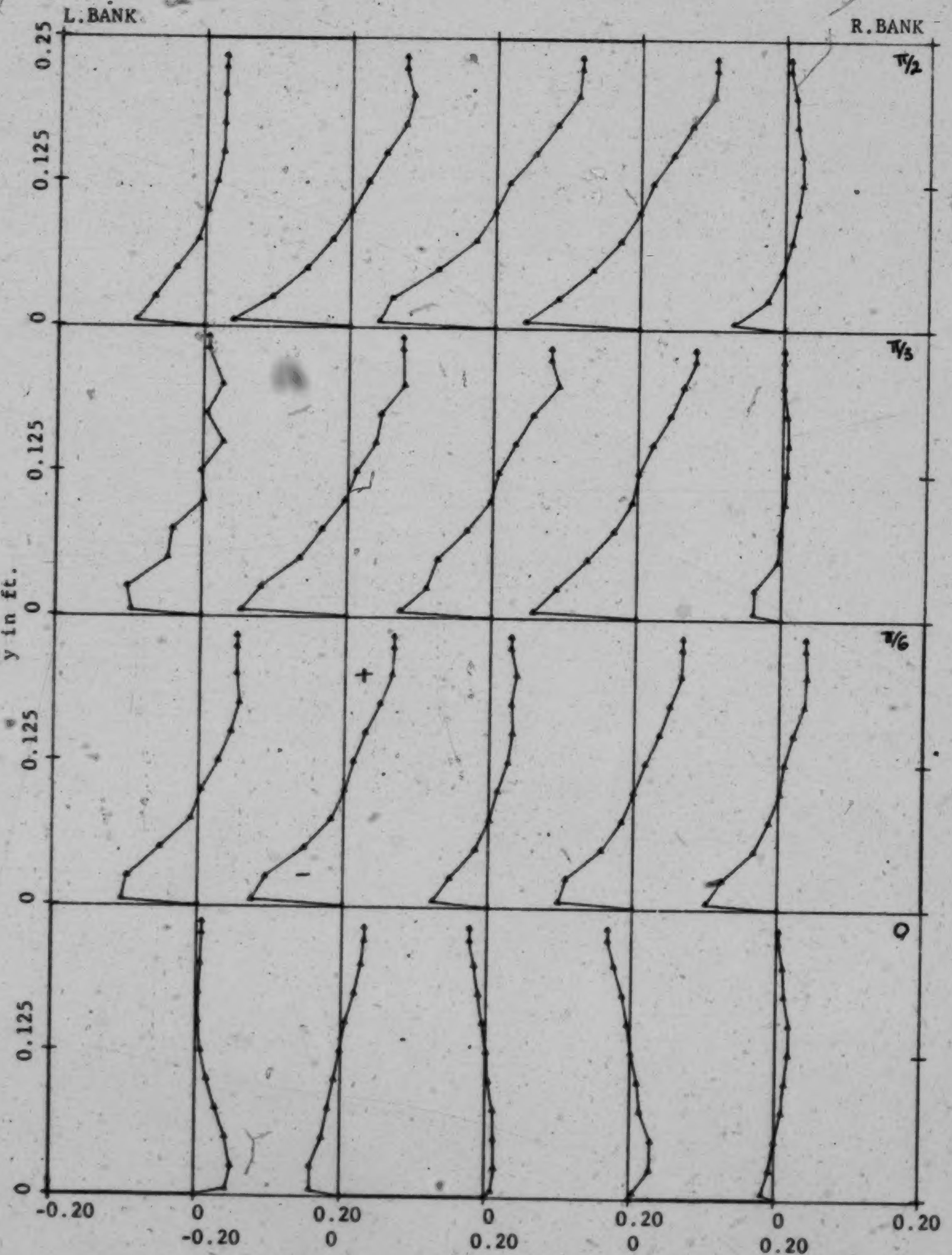

FIGURE A.4a VERTICAL DISTRIBUTIONS OF TRANSVERSE VELOCITY, Runs 307/8, SECTIONS θ_1 = 0 TO π/2.

A11

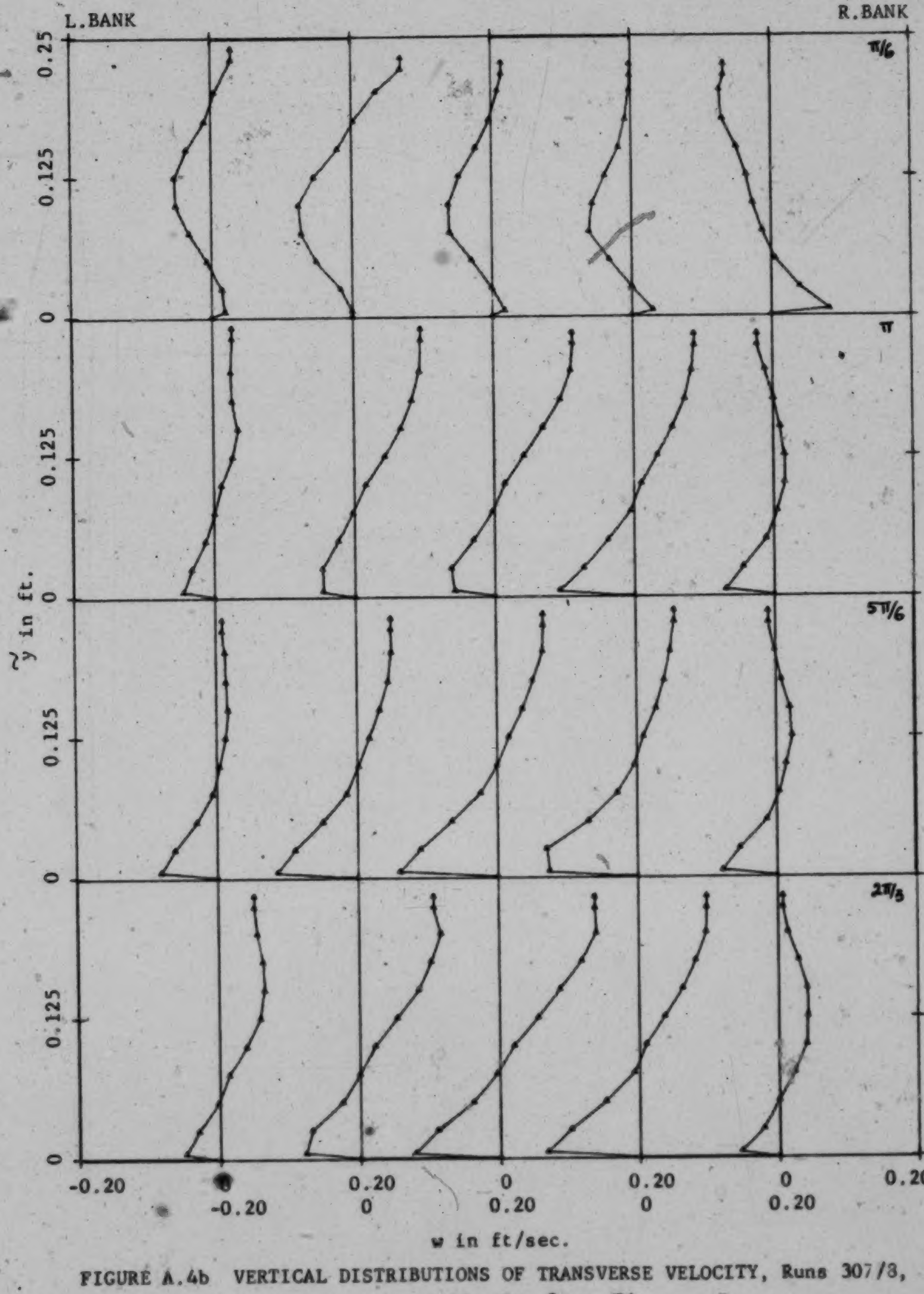

FIGURE A.4b VERTICAL DISTRIBUTIONS OF TRANSVERSE VELOCITY, Runs 307/3, SECTIONS $\theta_1 = 2\pi/3$ TO $\theta_2 = \pi/6$.

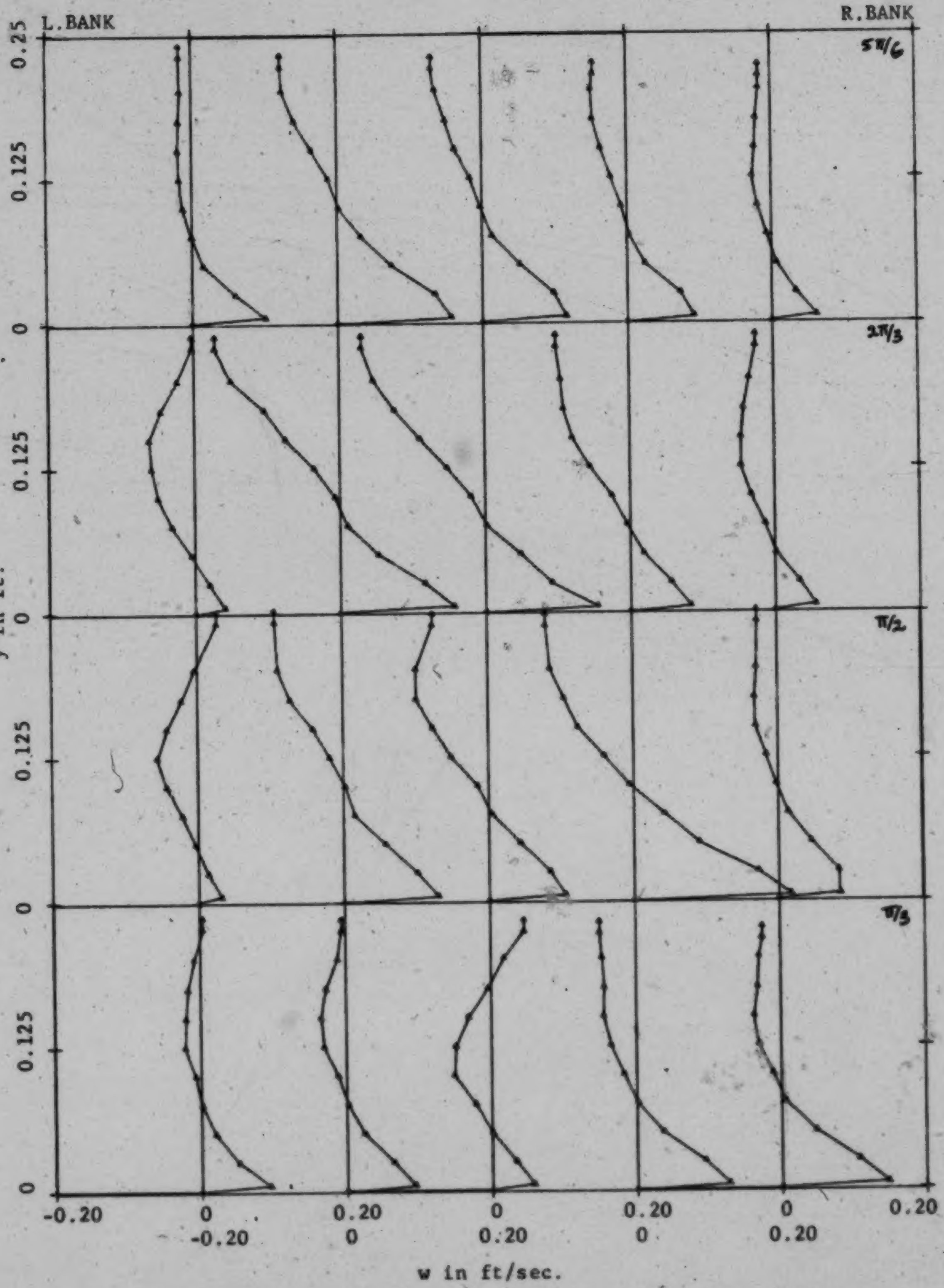

FIGURE A.4c VERTICAL DISTRIBUTIONS OF TRANSVERSE VELOCITY, Runs 307/8, SECTIONS θ_2 = π/3 TO 5π/6.

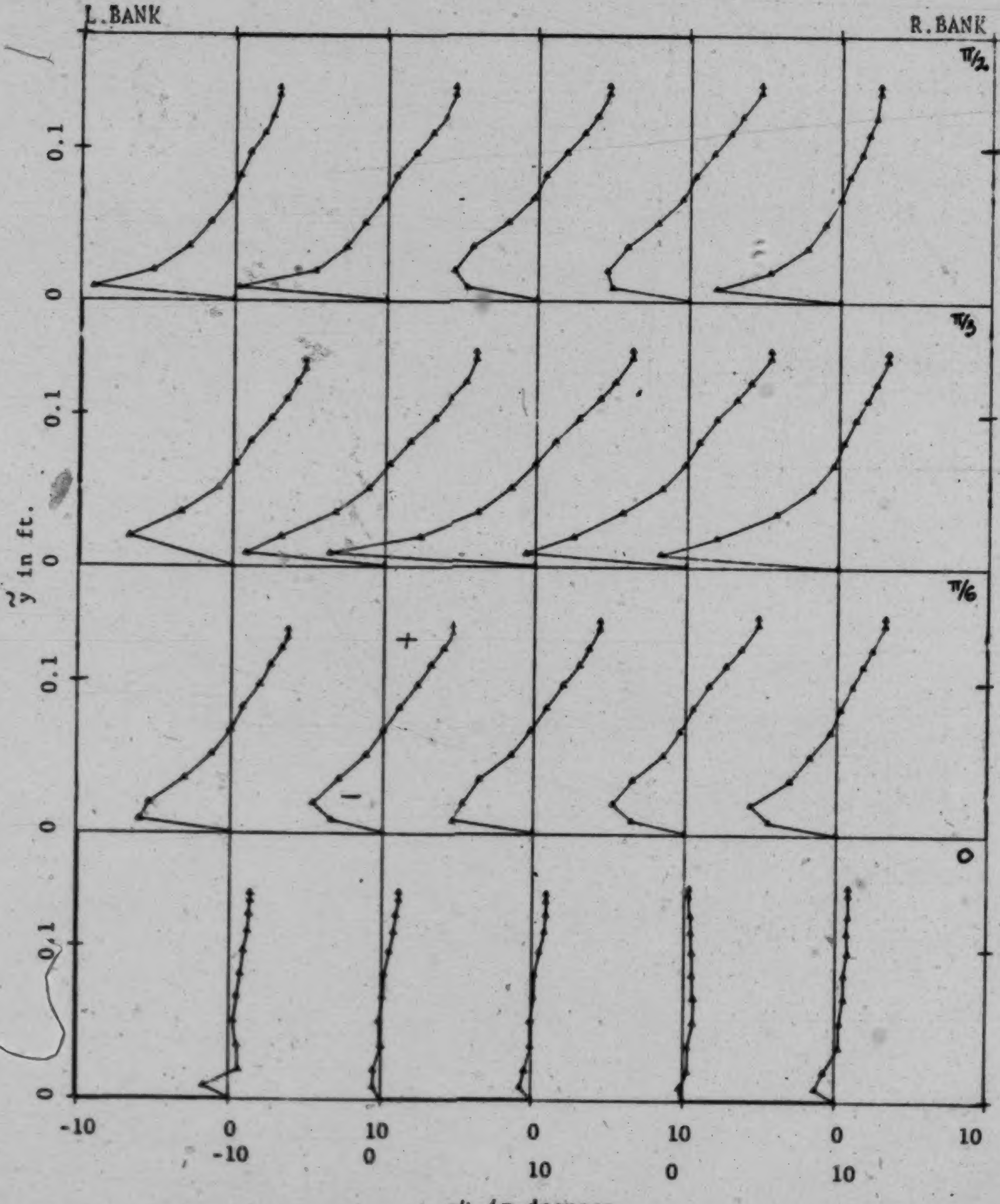

FIGURE A.5a VERTICAL DISTRIBUTIONS OF HORIZONTAL ANGLE OF DEVIATION OF VELOCITY VECTOR, Runs 304/6, SECTIONS ϑ_1 = 0 TO π/2

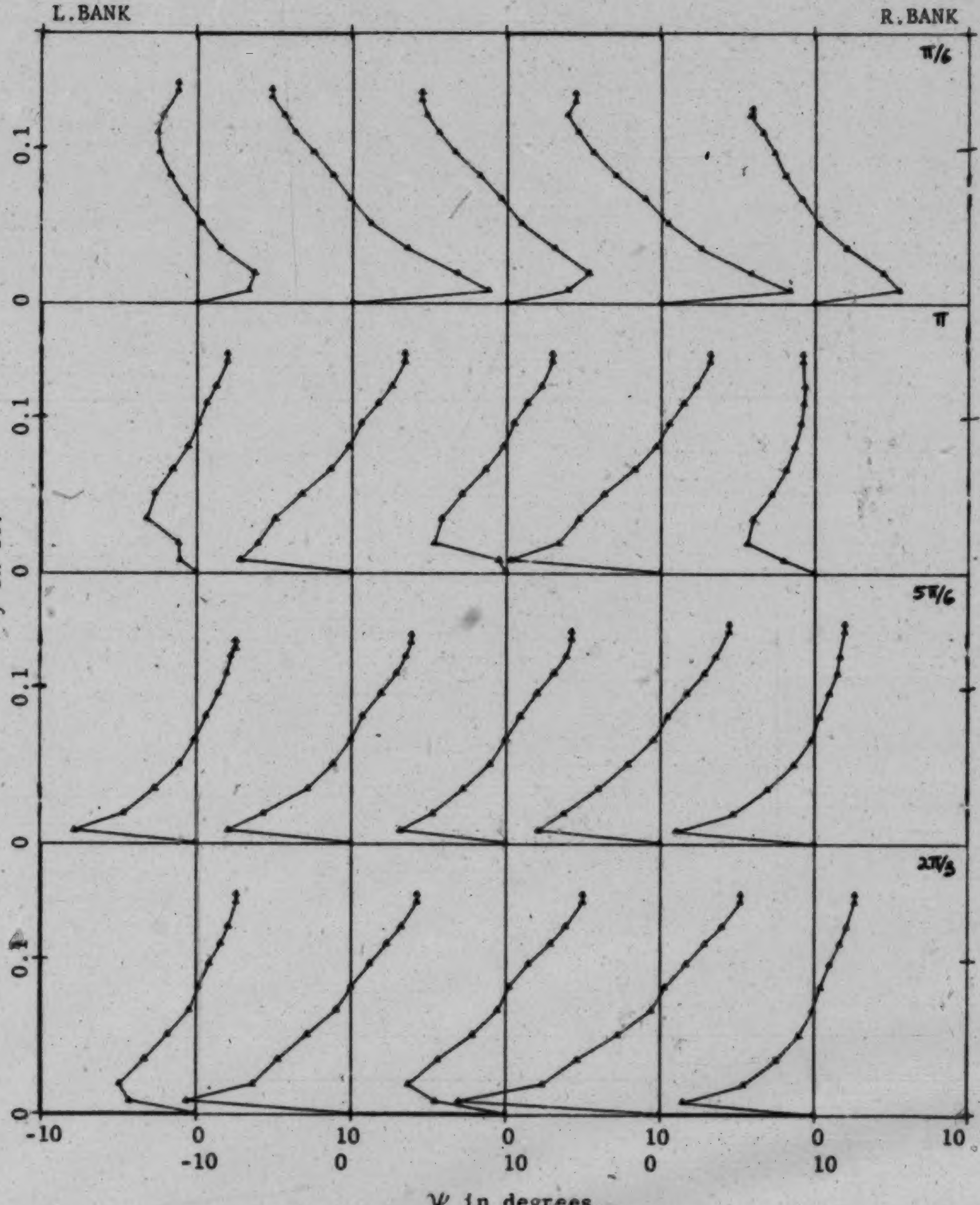

FIGURES A.5b VERTICAL DISTRIBUTIONS OF HORIZONTAL ANGLE OF DEVIATION OF VELOCITY VECTOR, Runs 304/6. SECTIONS $\theta_1 = 2\pi/3$ TO $\theta_2 = \pi/6$

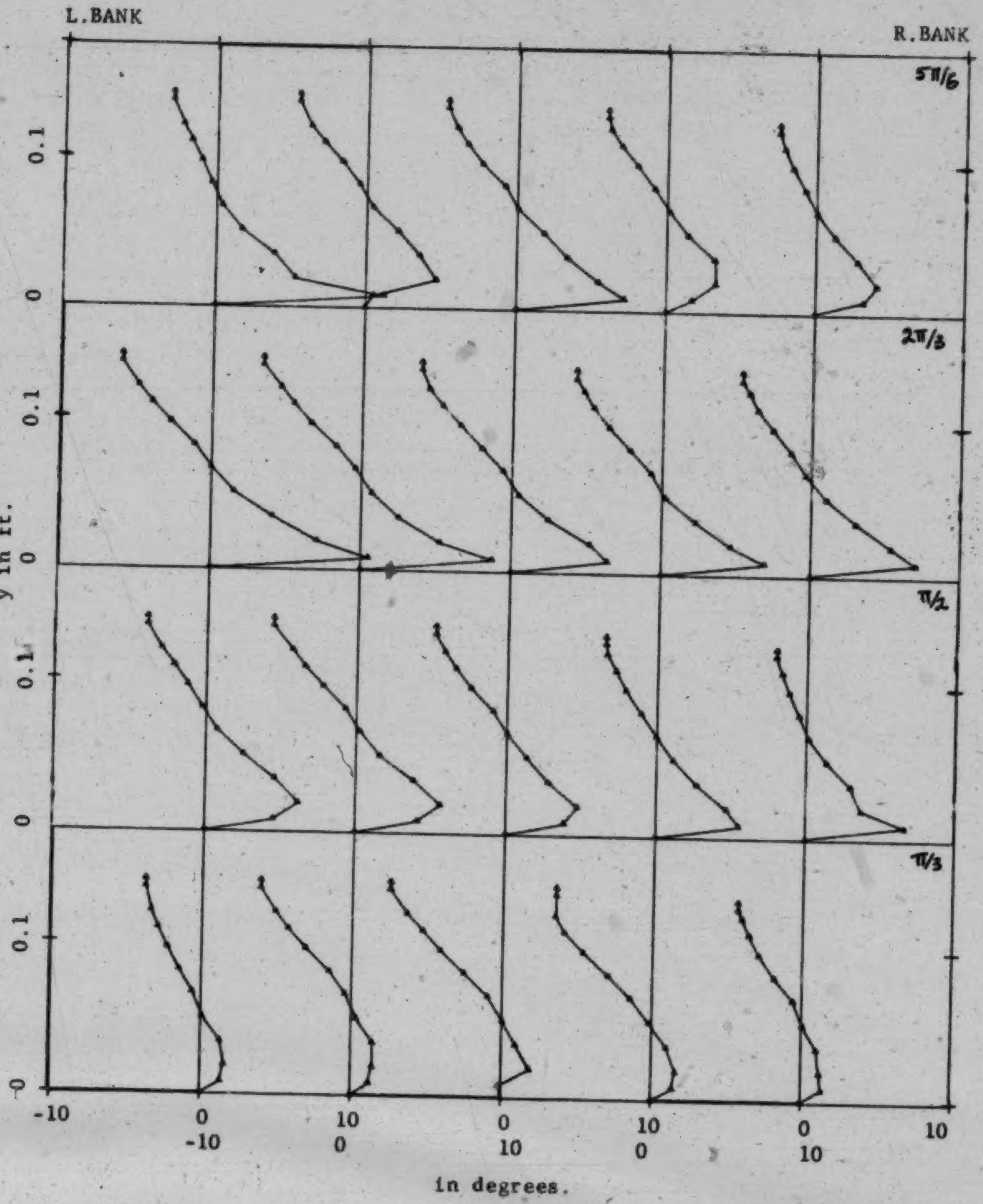

FIGURE A.5c VERTICAL DISTRIBUTIONS OF HORIZONTAL ANGLE OF DEVIATION OF VELOCITY VECTOR, Runs 304/6, SECTIONS $\theta_2 = \pi/3$ TO $5\pi/6$.

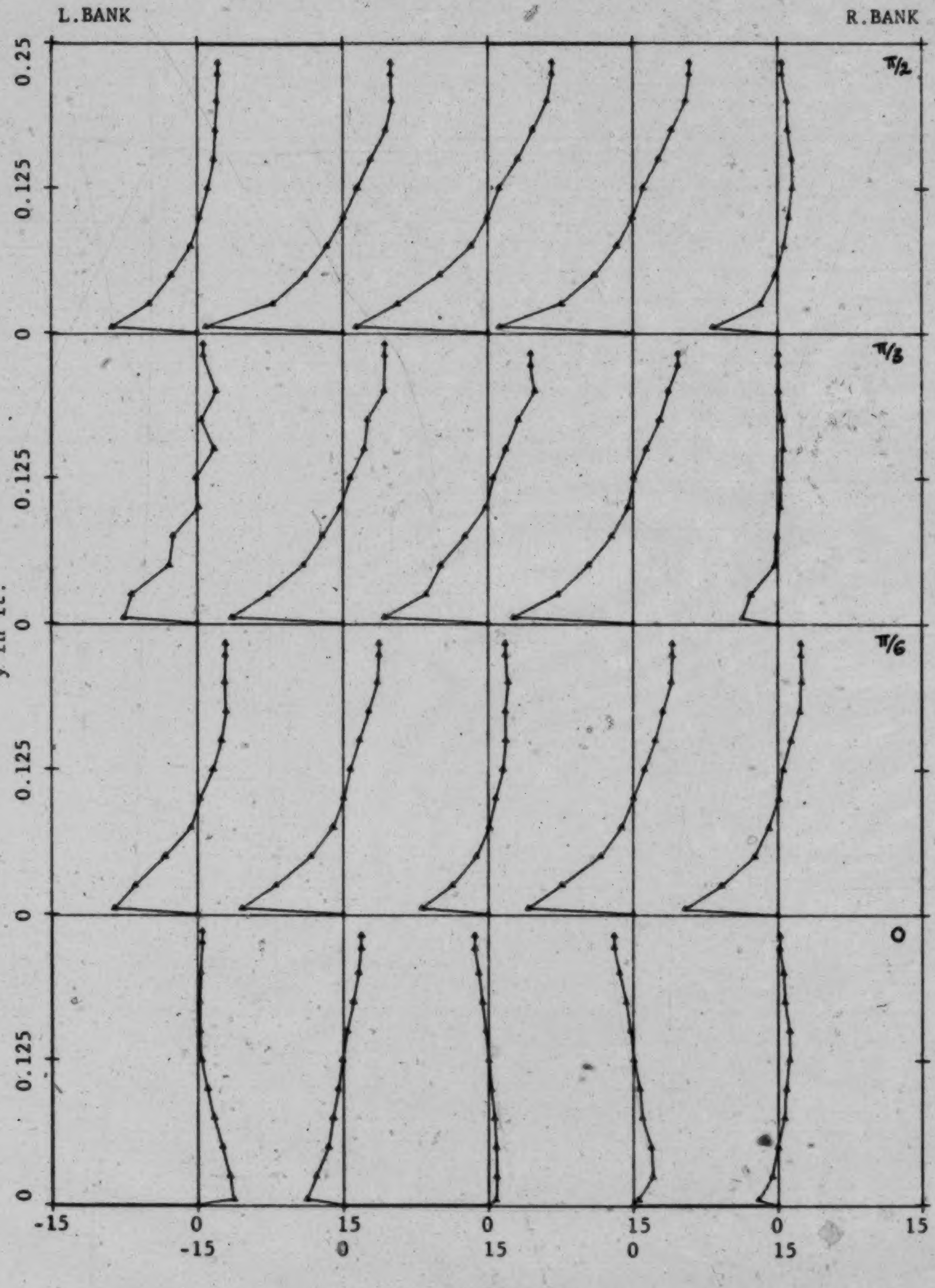

FIGURE A.6a VERTICAL DISTRIBUTIONS OF HORIZONTAL ANGLE OF DEVIATION OF VELOCITY VECTOR, Runs 307/8, SECTIONS $\theta_1 = 0$ TO $\pi/2$.

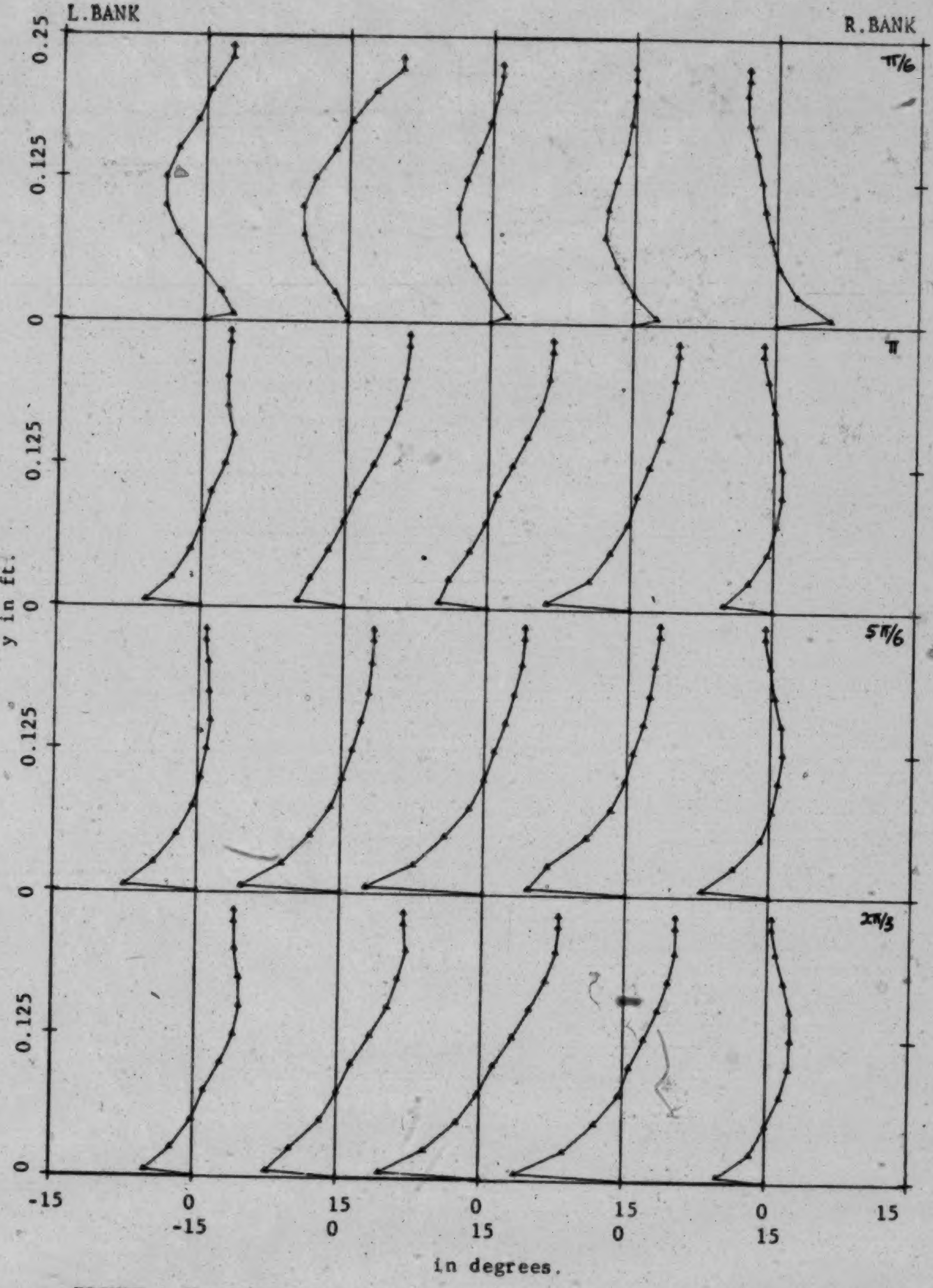

FIGURE A.6b VERTICAL DISTRIBUTIONS OF HORIZONTAL ANGLE OF DEVIATION OF VELOCITY VECTOR, Runs 307/8, SECTIONS $\theta_1 = 2\pi/3$ To $\theta_2 = \pi/6$.

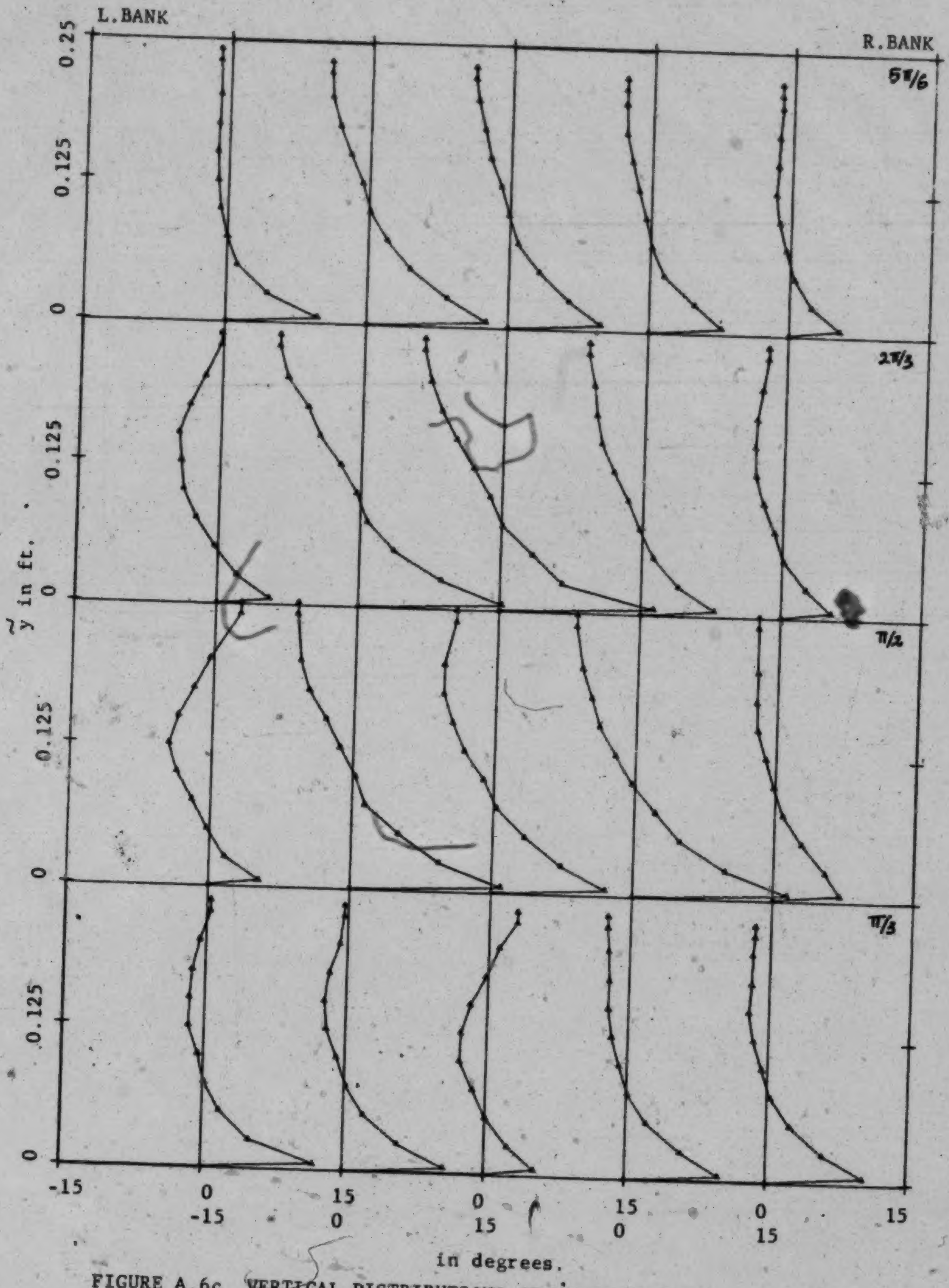

FIGURE A.6c VERTICAL DISTRIBUTIONS OF HORIZONTAL ANGLE OF DEVIATION OF VELOCITY VECTOR, Runs 307/8, SECTIONS $\theta_2 = \pi/3$ TO $5\pi/6$.

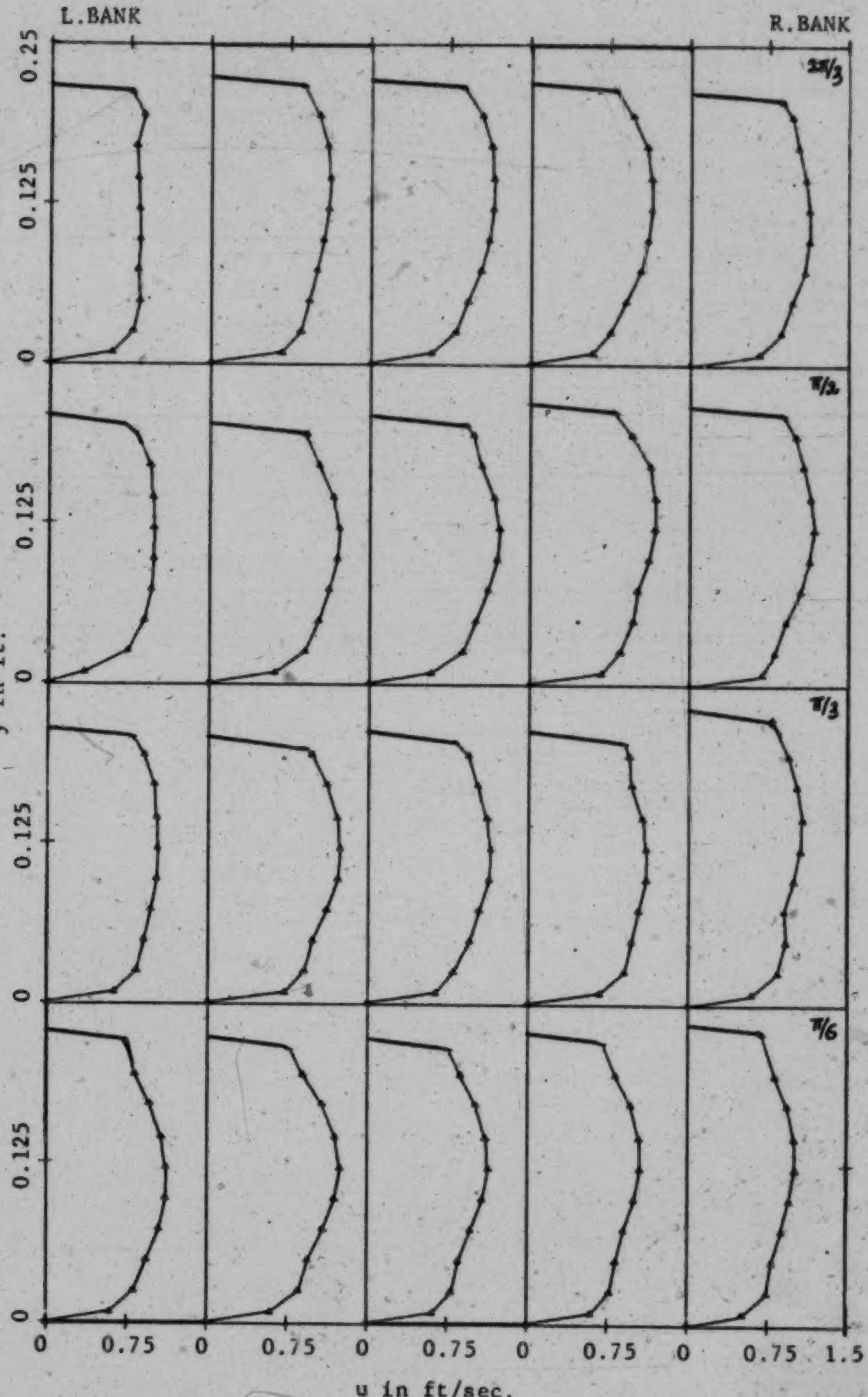

FIGURE A.7a VERTICAL DISTRIBUTIONS OF LONGITUDINAL VELOCITY, Runs 401/2/3, SECTIONS $\theta_1 = \pi/6$ TO $2\pi/3$.

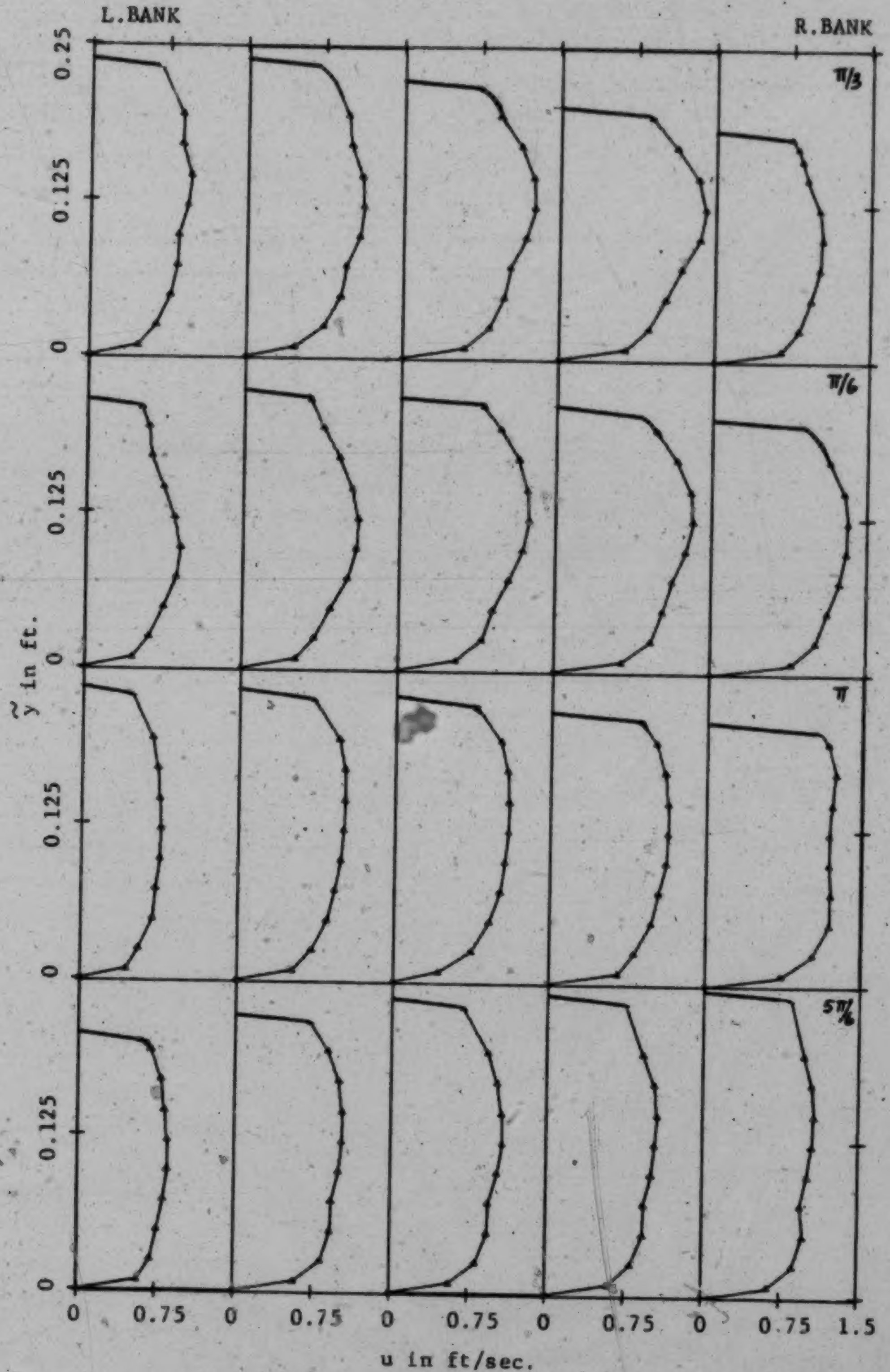

FIGURE [illegible].7b VERTICAL DISTRIBUTIONS OF LONGITUDINAL VELOCITY, Runs 401/2/3, SECTIONS $\theta_1 = 5\pi/6$ TO $\theta_2 = \pi/3$.

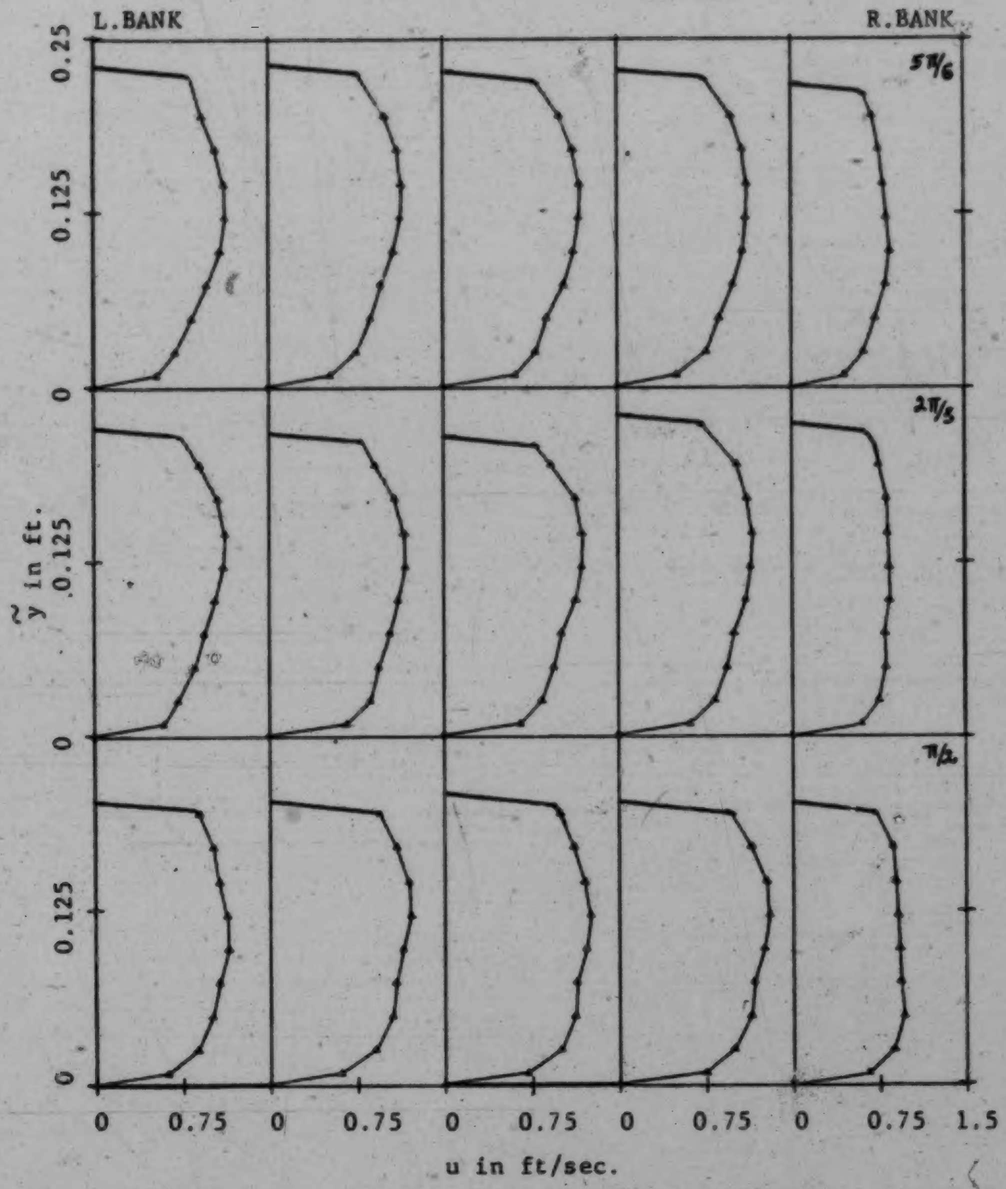

FIGURE A.7c VERTICAL DISTRIBUTIONS OF LONGITUDINAL VELOCITY, Runs 401/2/3, SECTIONS $\theta_2 = \pi/2$ TO $5\pi/6$.

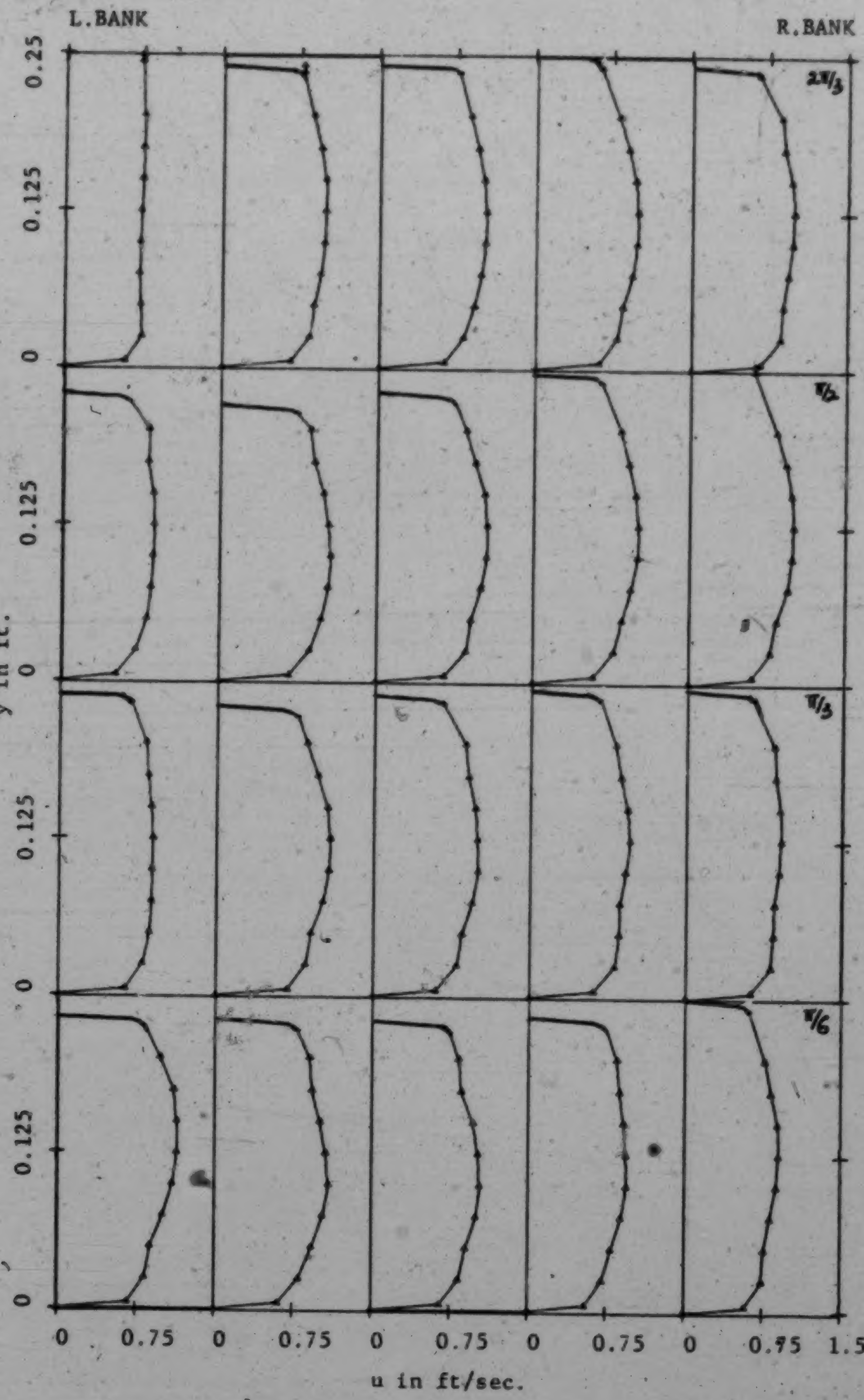

FIGURE A.8a VERTICAL DISTRIBUTIONS OF LONGITUDINAL VELOCITY, Runs 407/8, SECTIONS $\theta_1 = \pi/6$ TO $2\pi/3$.

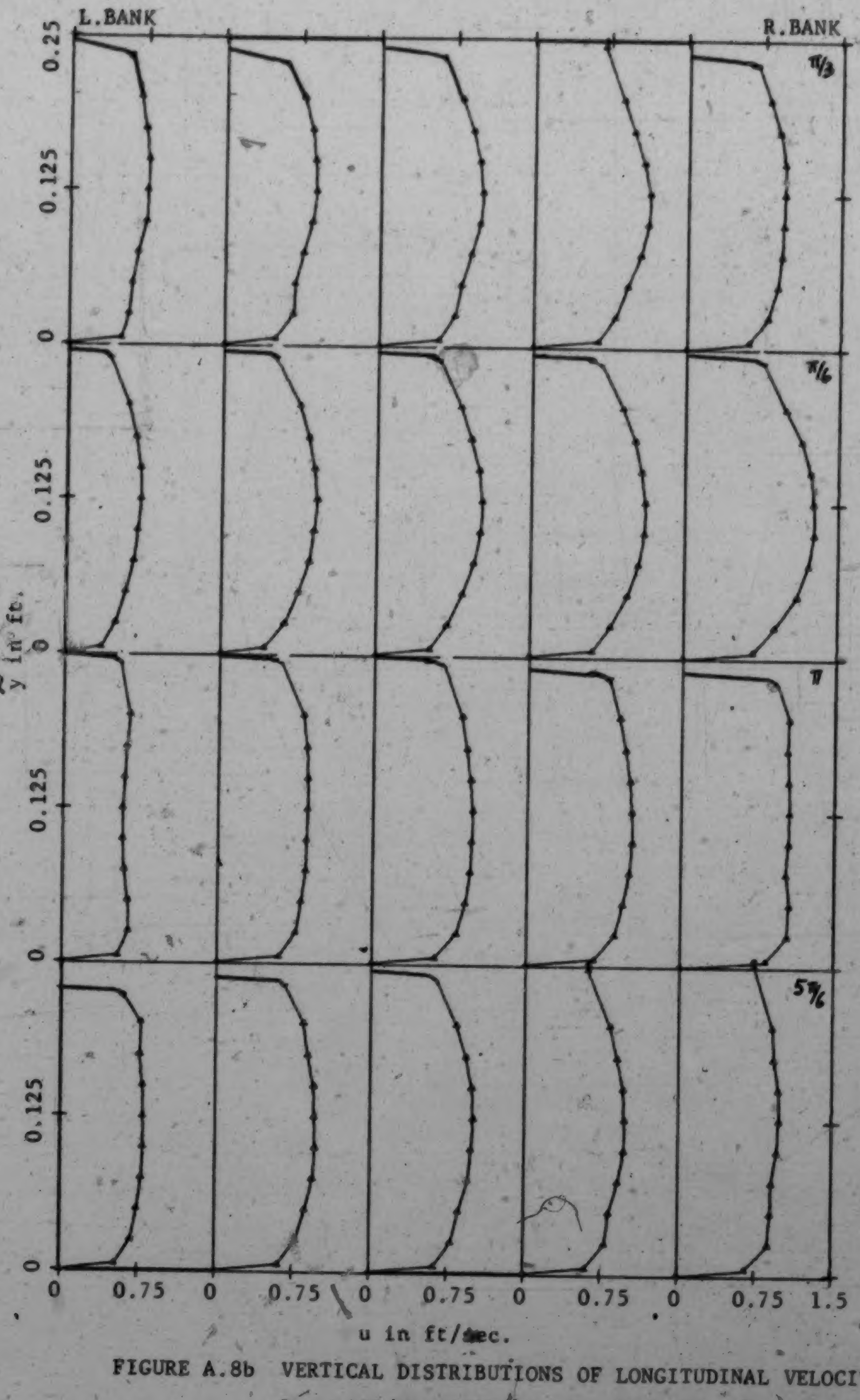

FIGURE A.8b VERTICAL DISTRIBUTIONS OF LONGITUDINAL VELOCITY.
Runs 407/8, SECTIONS $\theta_1 = 5\pi/6$ TO $\theta_2 = \pi/3$.

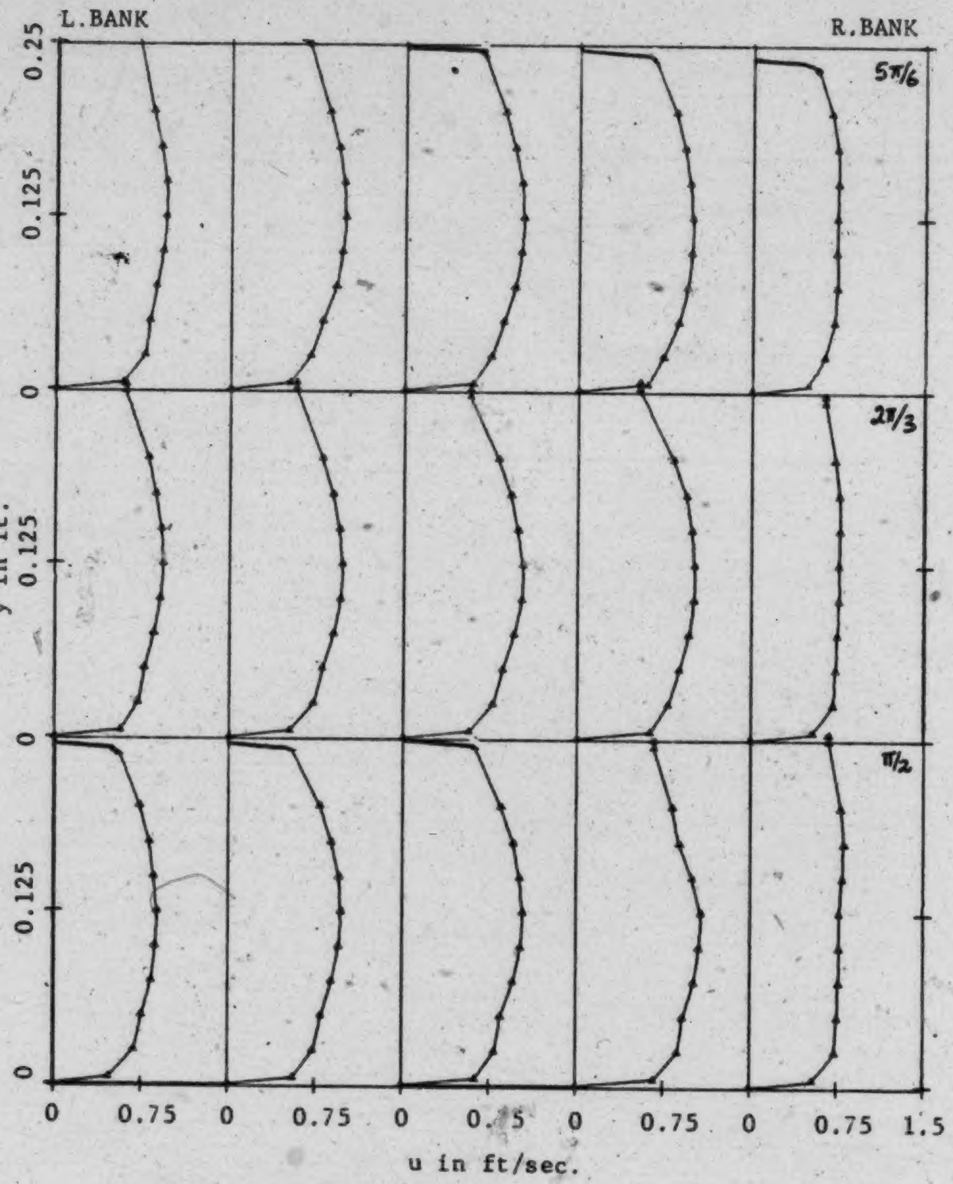

FIGURE A.8c VERTICAL DISTRIBUTIONS OF LONGITUDINAL VELOCITY, Runs 407/8, SECTIONS $\theta_2 = \pi/2$ TO $5\pi/6$.

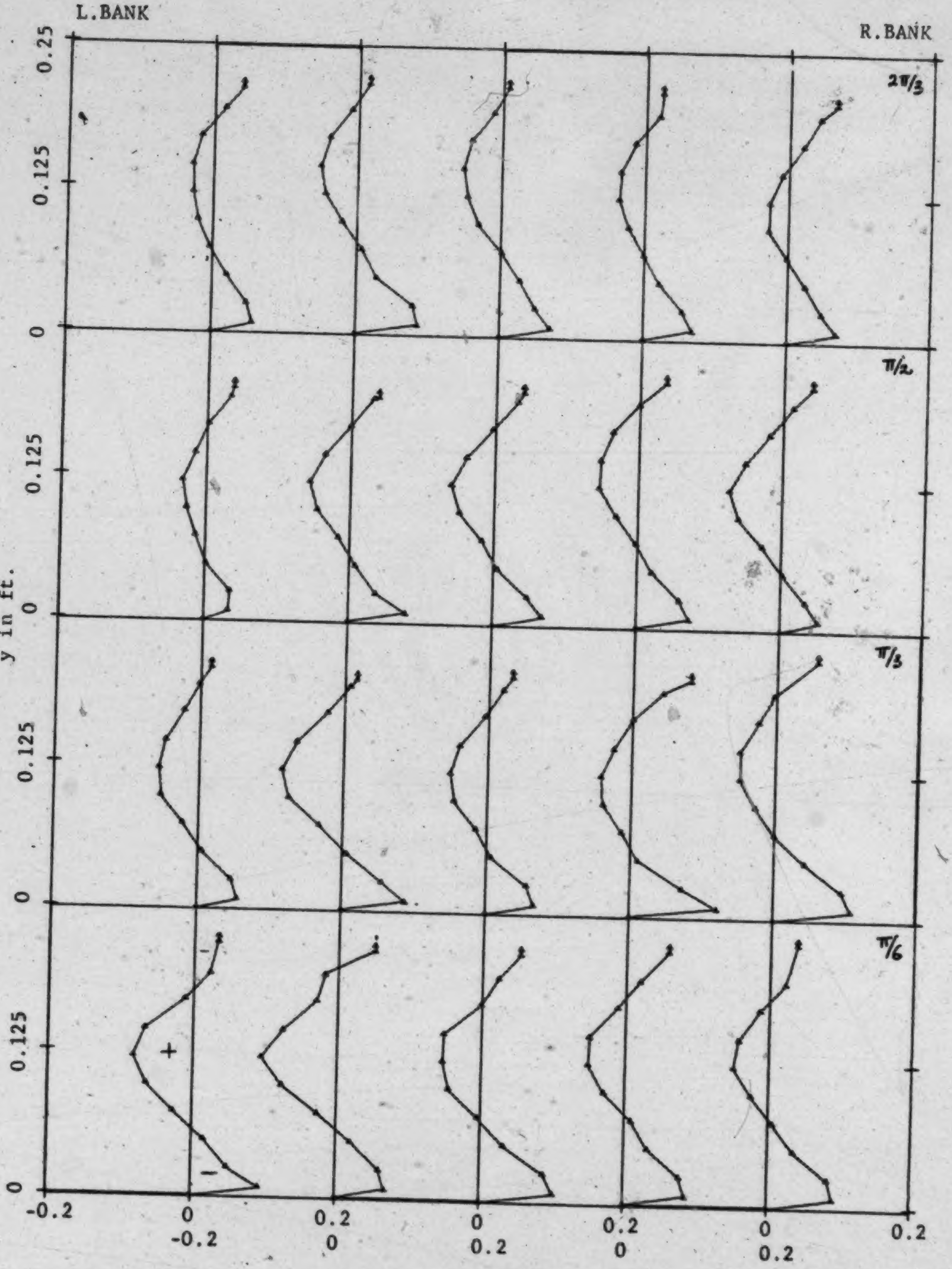

FIGURE A.9a VERTICAL DISTRIBUTIONS OF TRANSVERSE VELOCITY,
Runs 401/2/3, SECTIONS θ_1 = π/6 TO 2π/3

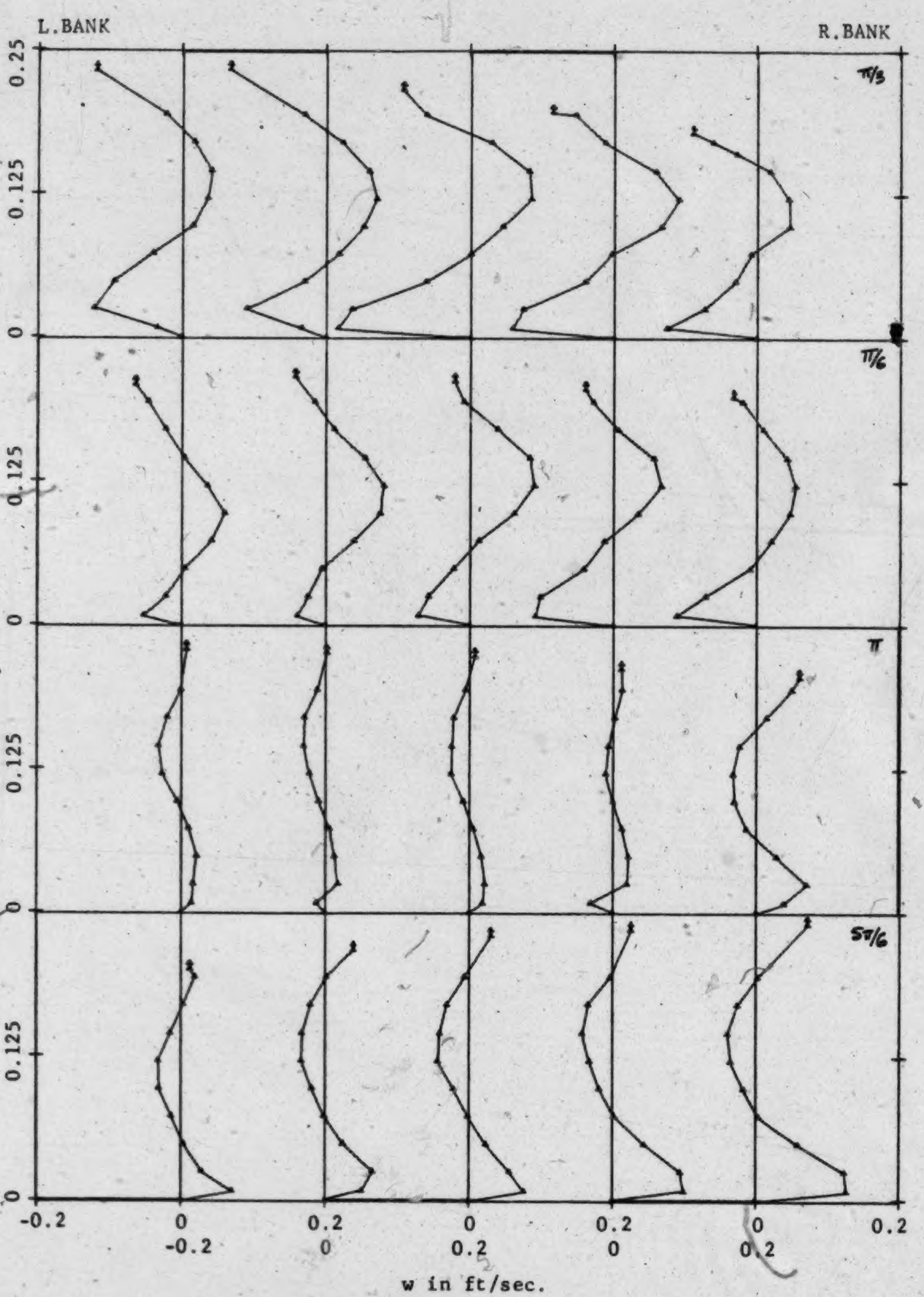

FIGURE A.9b VERTICAL DISTRIBUTIONS OF TRANSVERSE VELOCITY, Runs 401/2/3, SECTIONS $\theta_1 = 5\pi/6$ TO $\theta_2 = \pi/3$

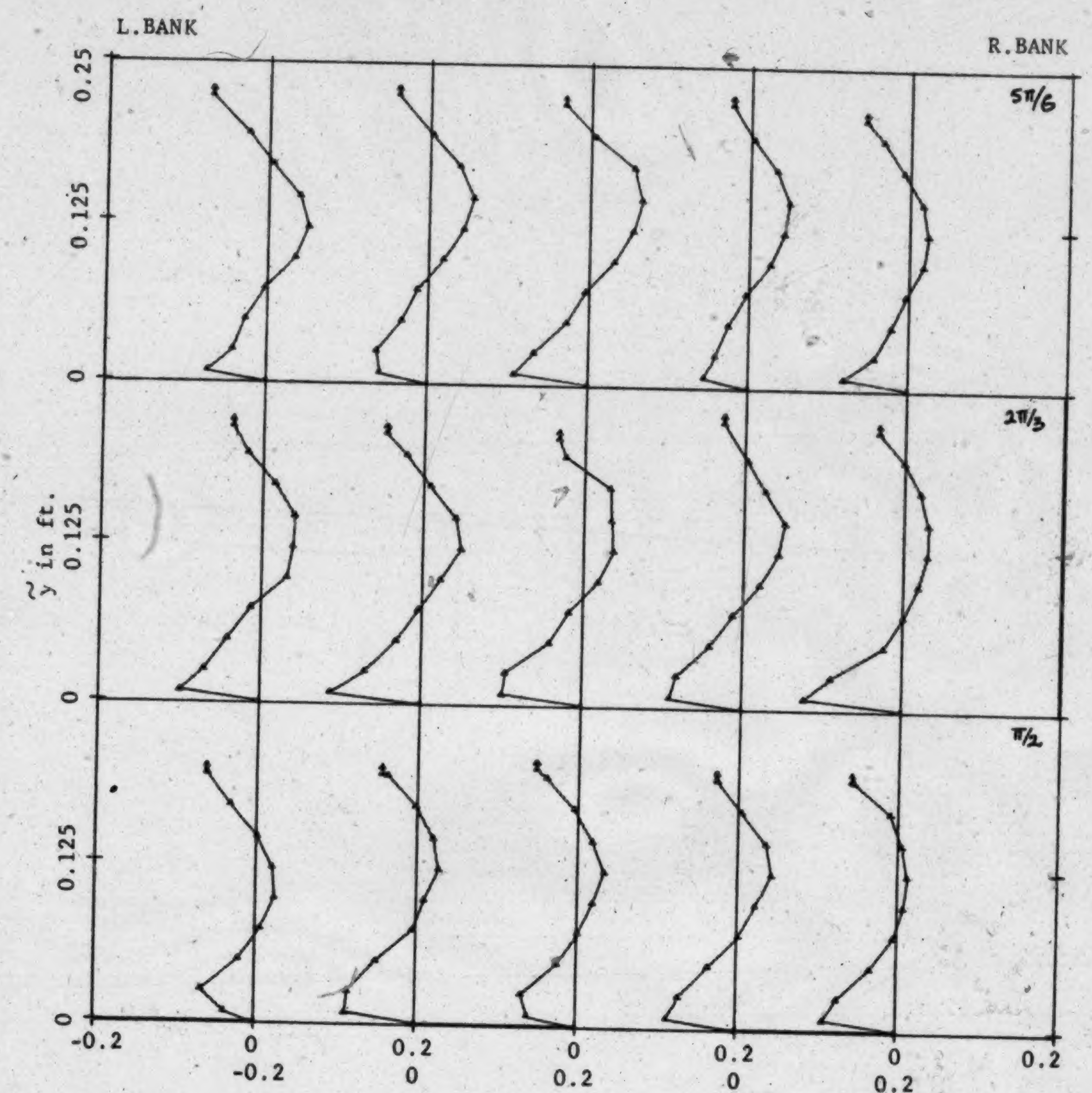

FIGURE A.9c VERTICAL DISTRIBUTIONS OF TRANSVERSE VELOCITY, Runs 401/2/3, SECTIONS $\theta_2 = \pi/2$ TO $5\pi/6$.

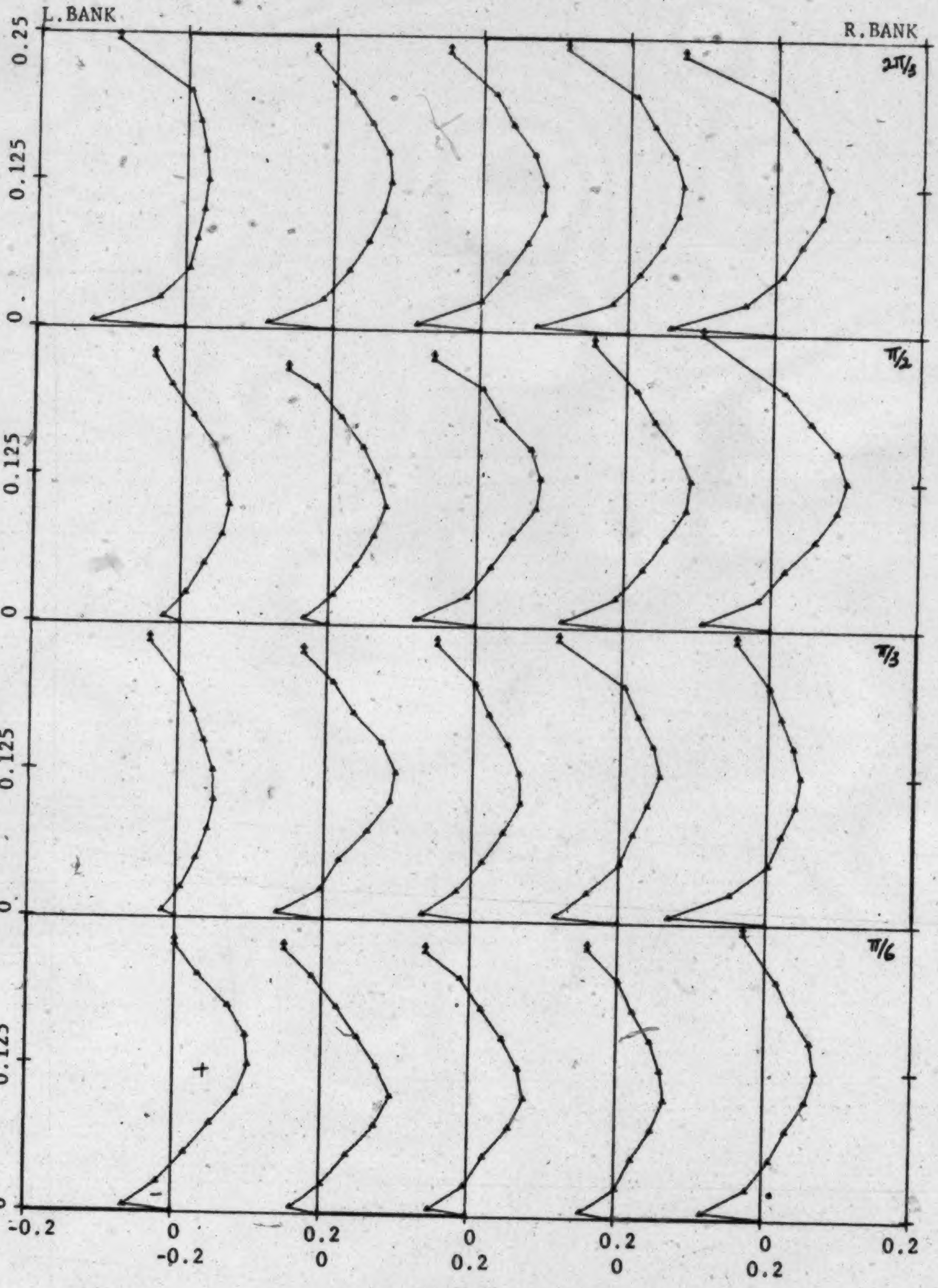

FIGURE A.10a VERTICAL DISTRIBUTIONS OF TRANSVERSE VELOCITY, RUNS 407/8, SECTIONS $\theta_1 = \pi/6$ TO $2\pi/3$.

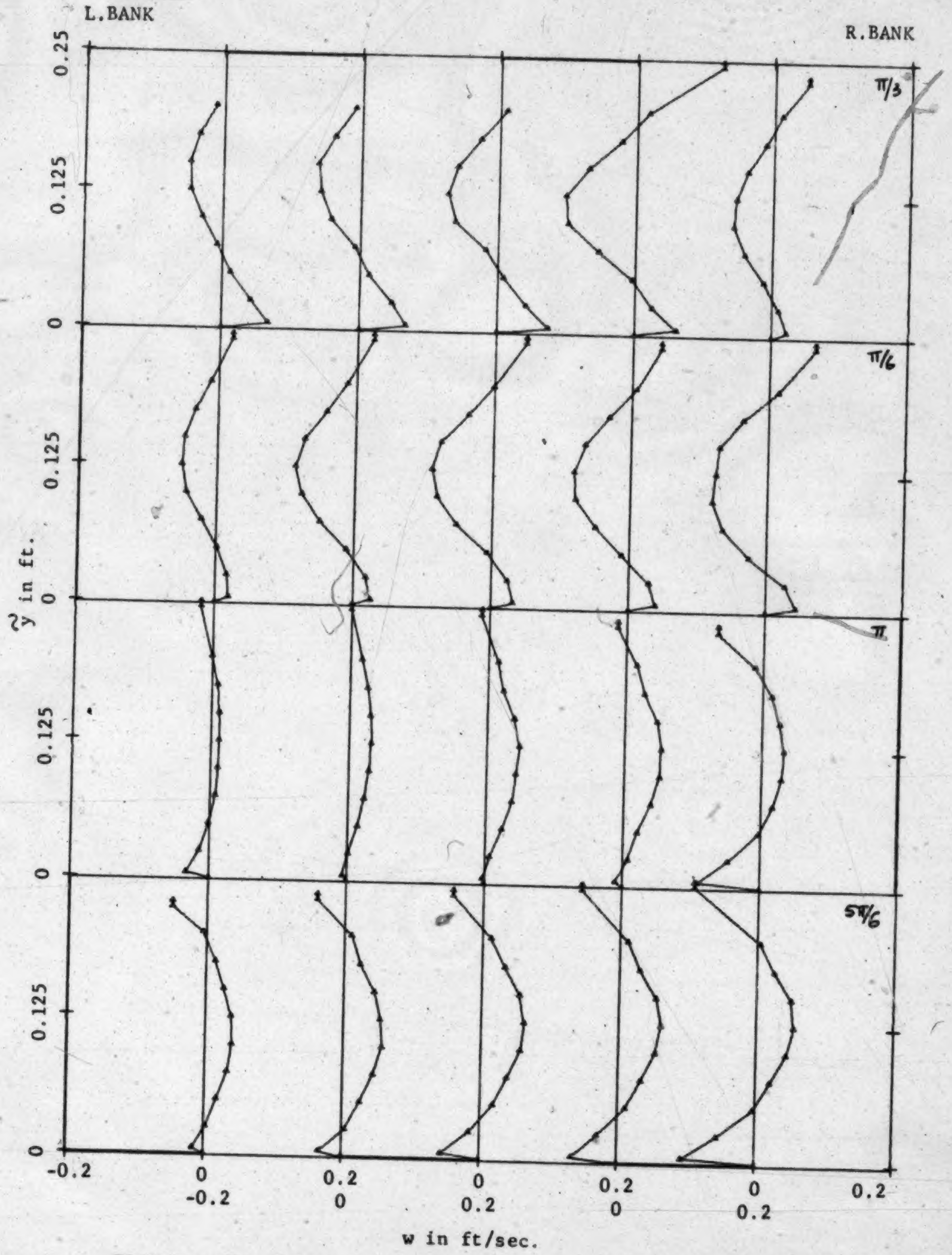

FIGURE A.10b VERTICAL DISTRIBUTIONS OF TRANSVERSE VELOCITY, Runs 407/8, SECTIONS $\theta_1 = 5\pi/6$ TO $\theta_2 = \pi/3$

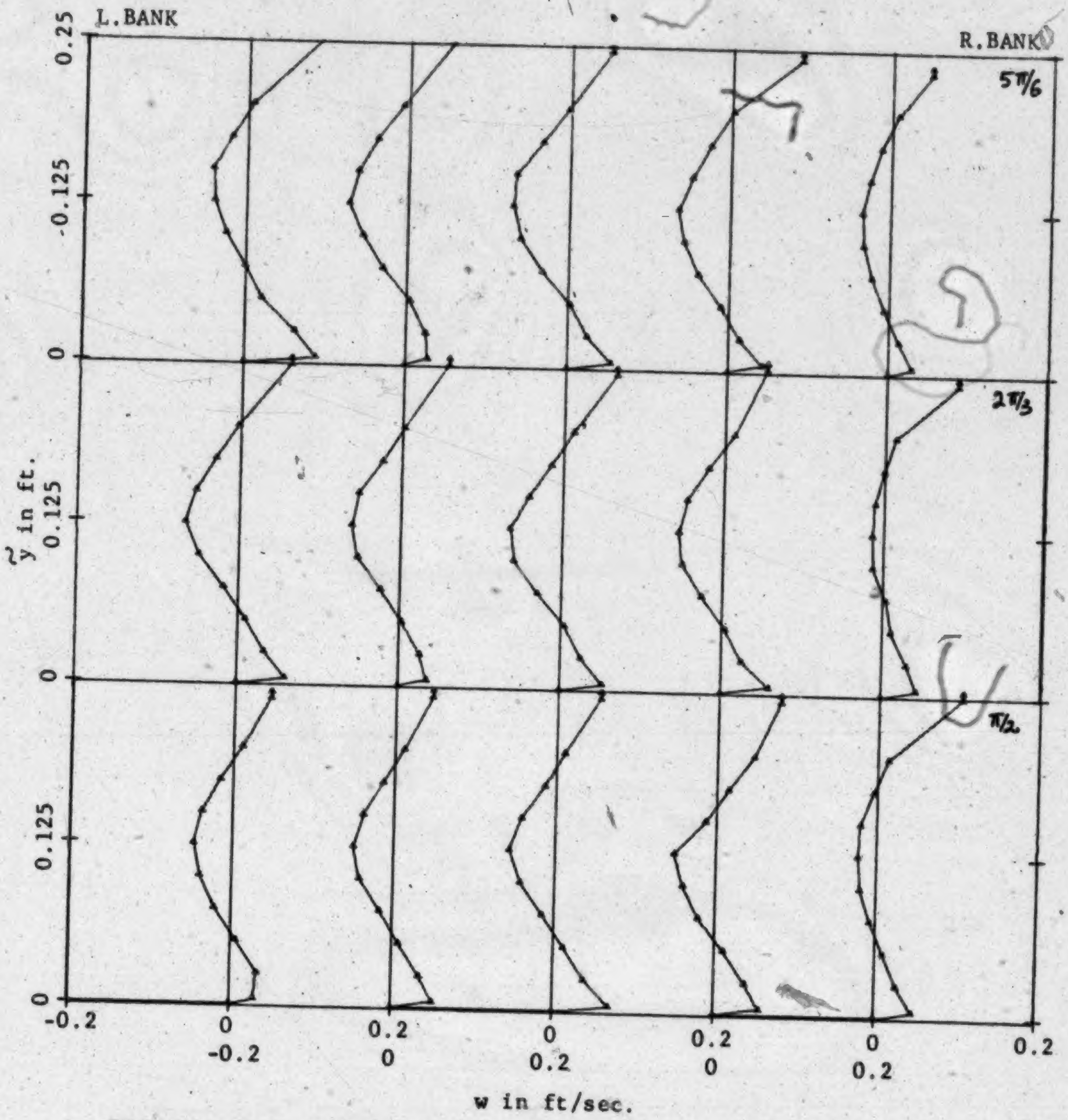

FIGURE A.10c VERTICAL DISTRIBUTIONS OF TRANSVERSE VELOCITY. Runs 407/8, SECTIONS $\theta_2 = \pi/2$ TO $5\pi/6$.

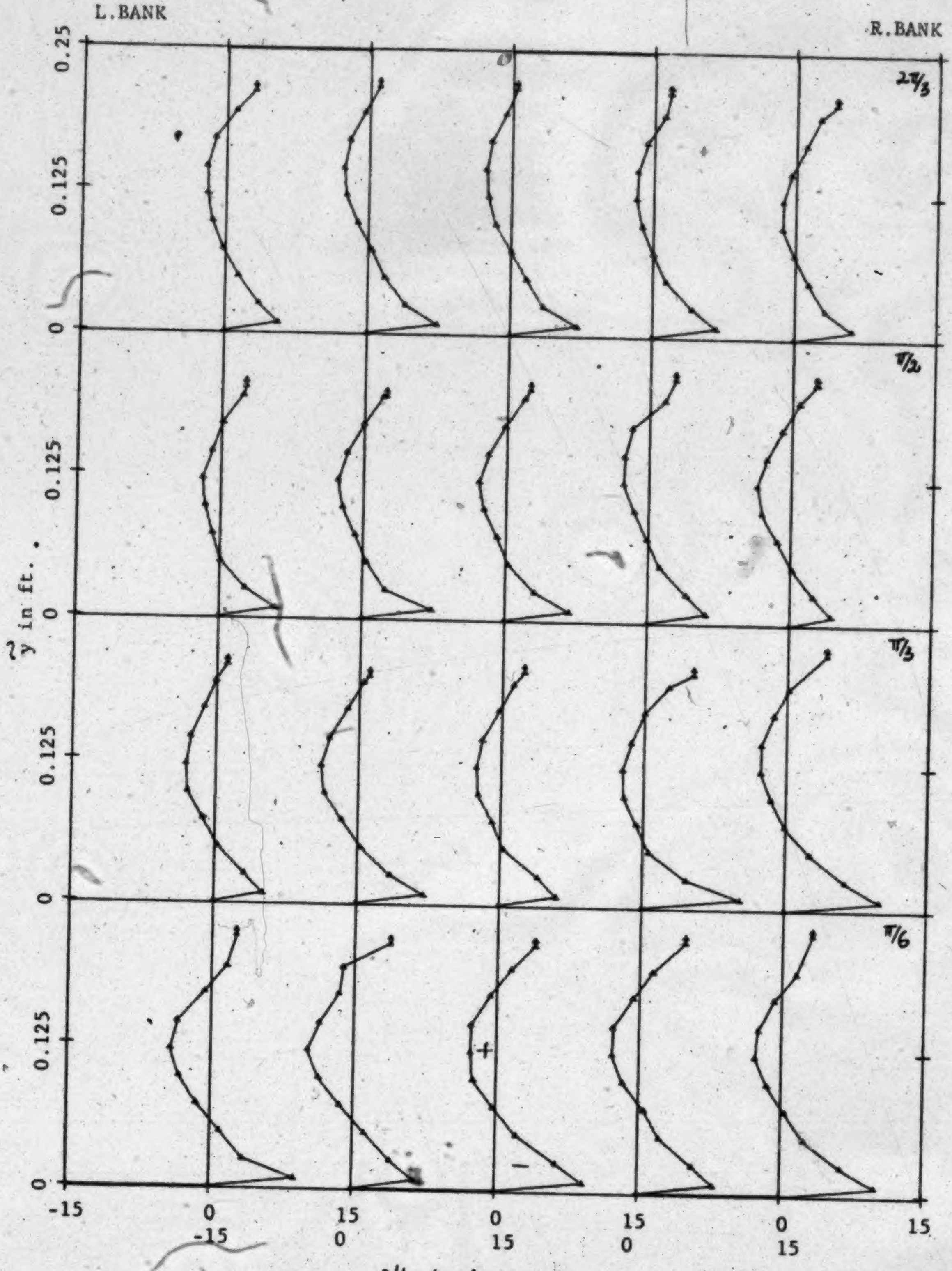

FIGURE A.11a VERTICAL DISTRIBUTIONS OF HORIZONTAL ANGLE OF DEVIATION OF VELOCITY VECTOR, Runs 401/2/3, SECTIONS $\theta_1 = \pi/6$ TO $2\pi/3$

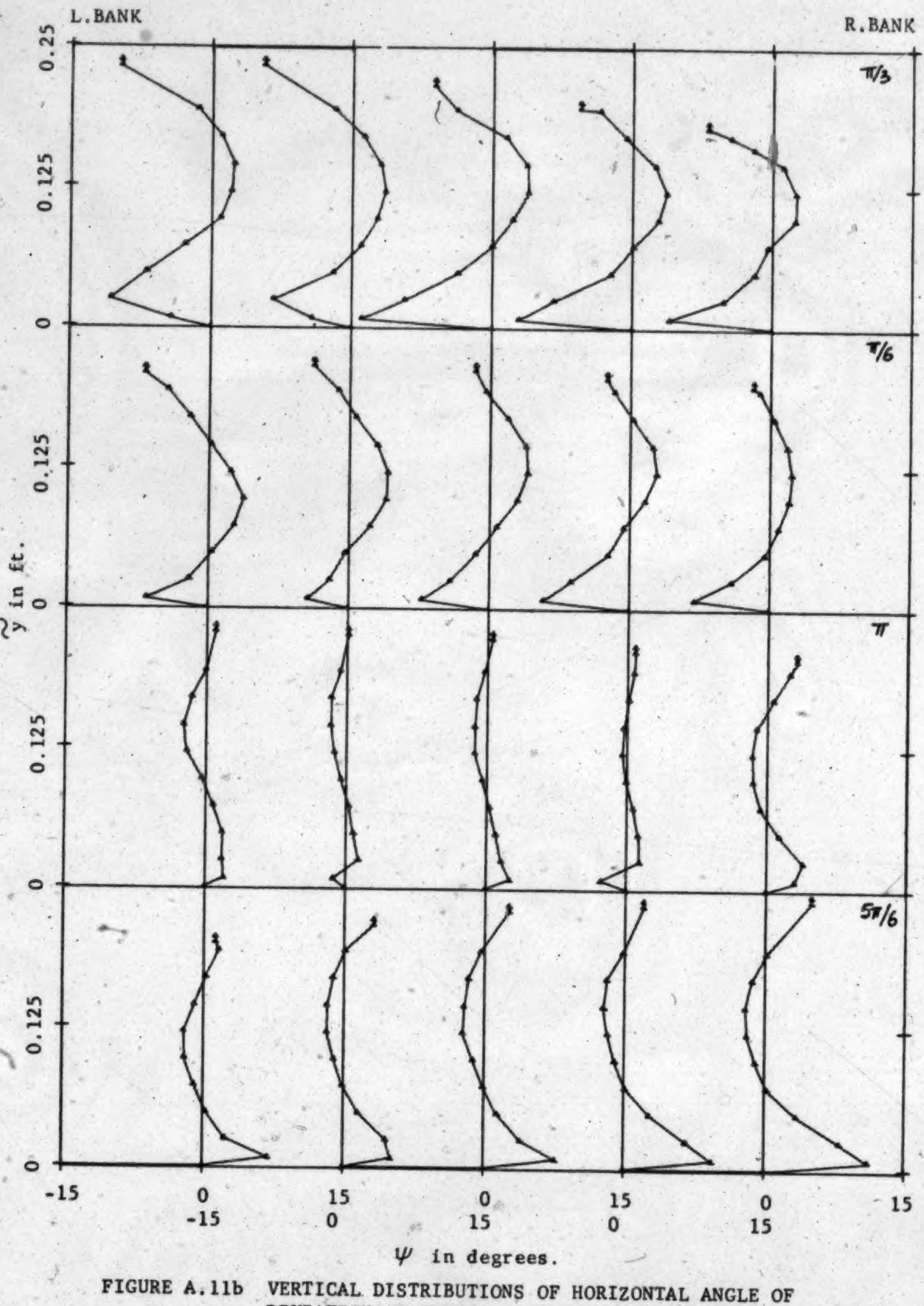

FIGURE A.11b VERTICAL DISTRIBUTIONS OF HORIZONTAL ANGLE OF DEVIATION OF VELOCITY VECTOR, Runs 401/2/3, SECTIONS $\theta_1 = 5\pi/6$ TO $\theta_2 = \pi/3$.

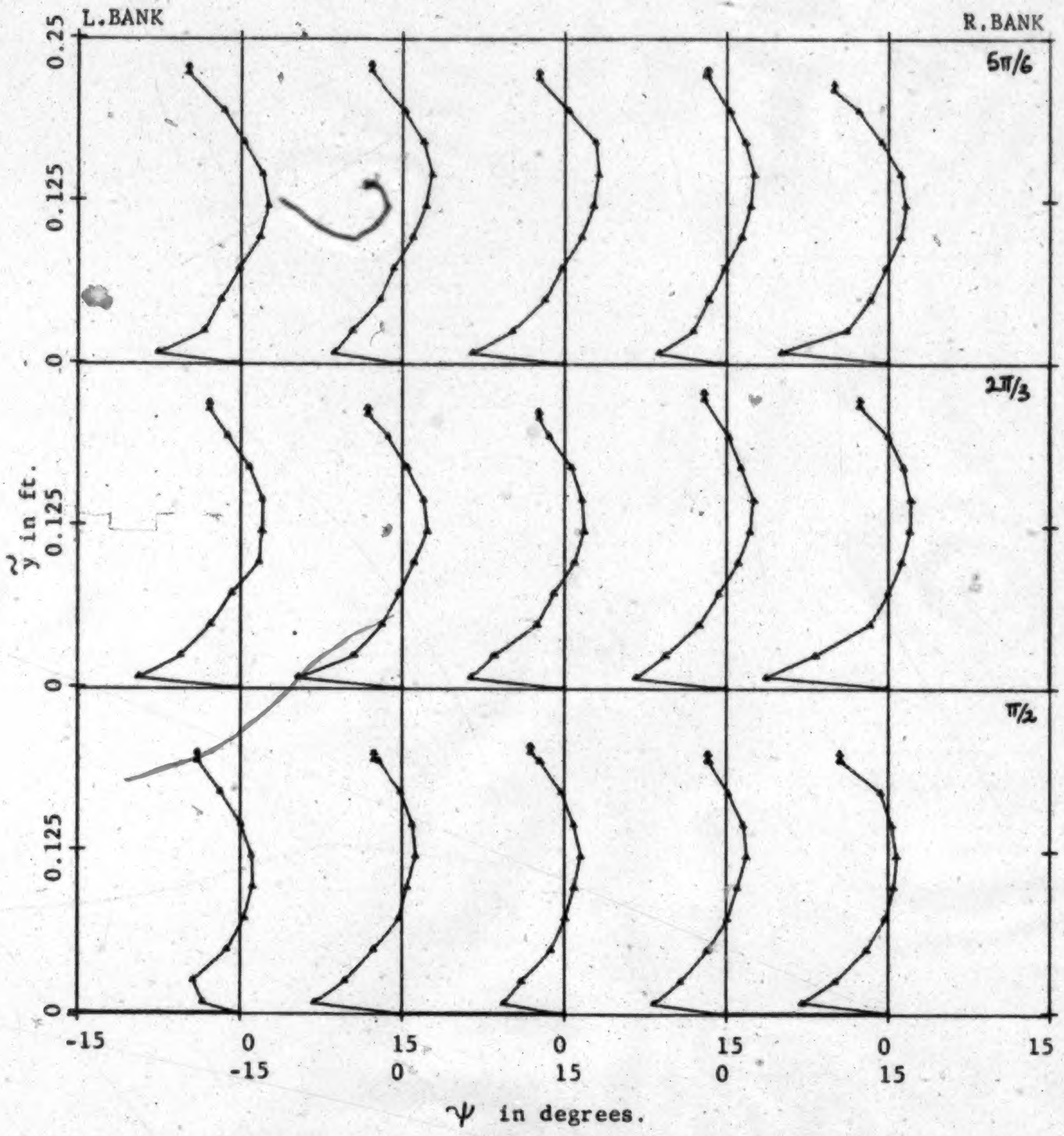

FIGURE A.11c VERTICAL DISTRIBUTIONS OF HORIZONTAL ANGLE OF DEVIATION OF VELOCITY VECTOR, Runs 401/2/3, SECTIONS $\theta_2 = \pi/2$ TO $5\pi/6$.

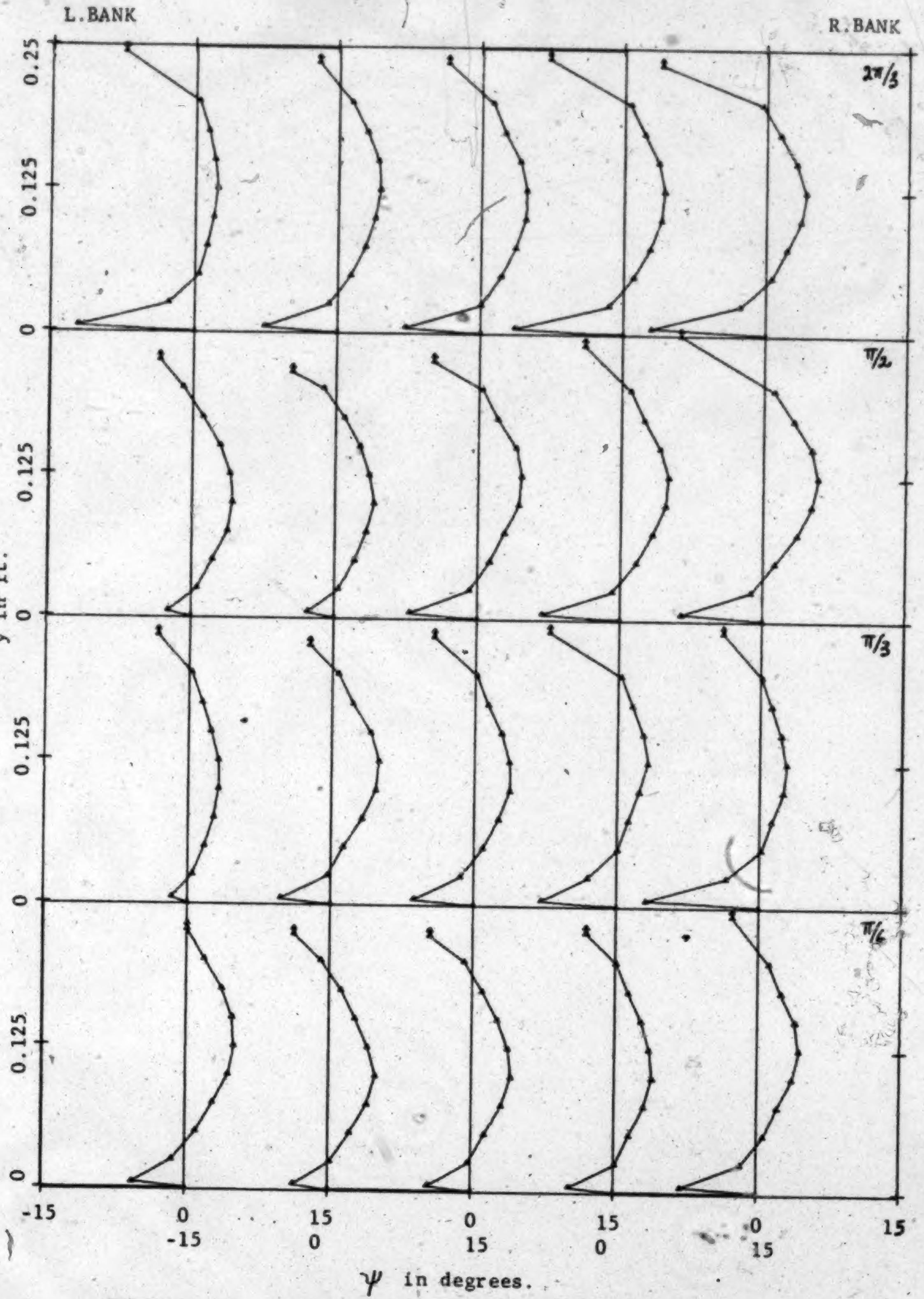

FIGURE A.12a VERTICAL DISTRIBUTIONS OF HORIZONTAL ANGLE OF DEVIATION OF VELOCITY VECTOR, Runs 407/8, SECTIONS $\theta_1 = \pi/6$ TO $\theta_1 = 2\pi/3$.

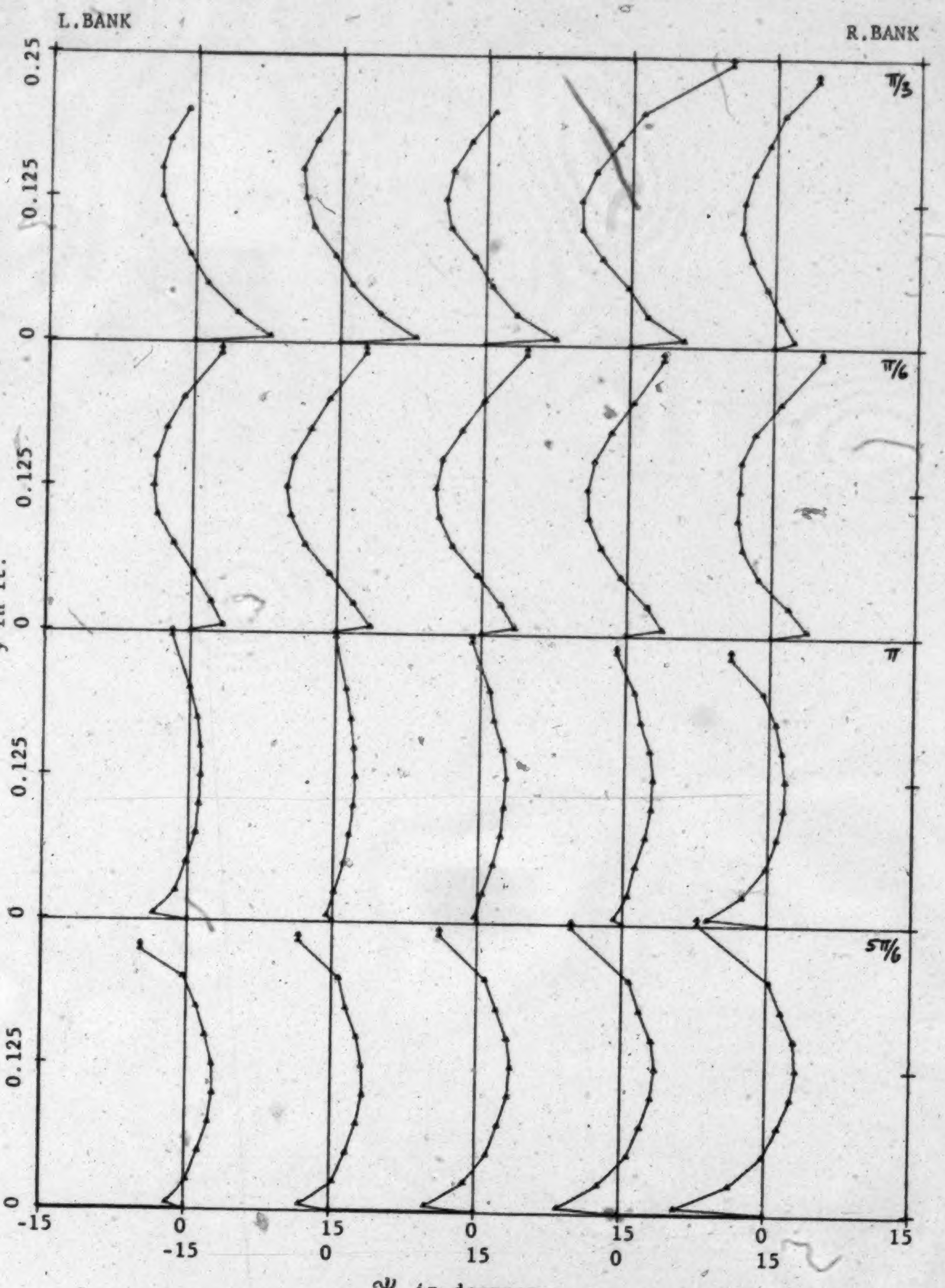

FIGURE A.12b VERTICAL DISTRIBUTIONS OF HORIZONTAL ANGLE OF DEVIATION OF VELOCITY VECTOR, Runs 407/8, SECTIONS $\theta_1 = 5\pi/6$ TO $\theta_2 = \pi/3$.

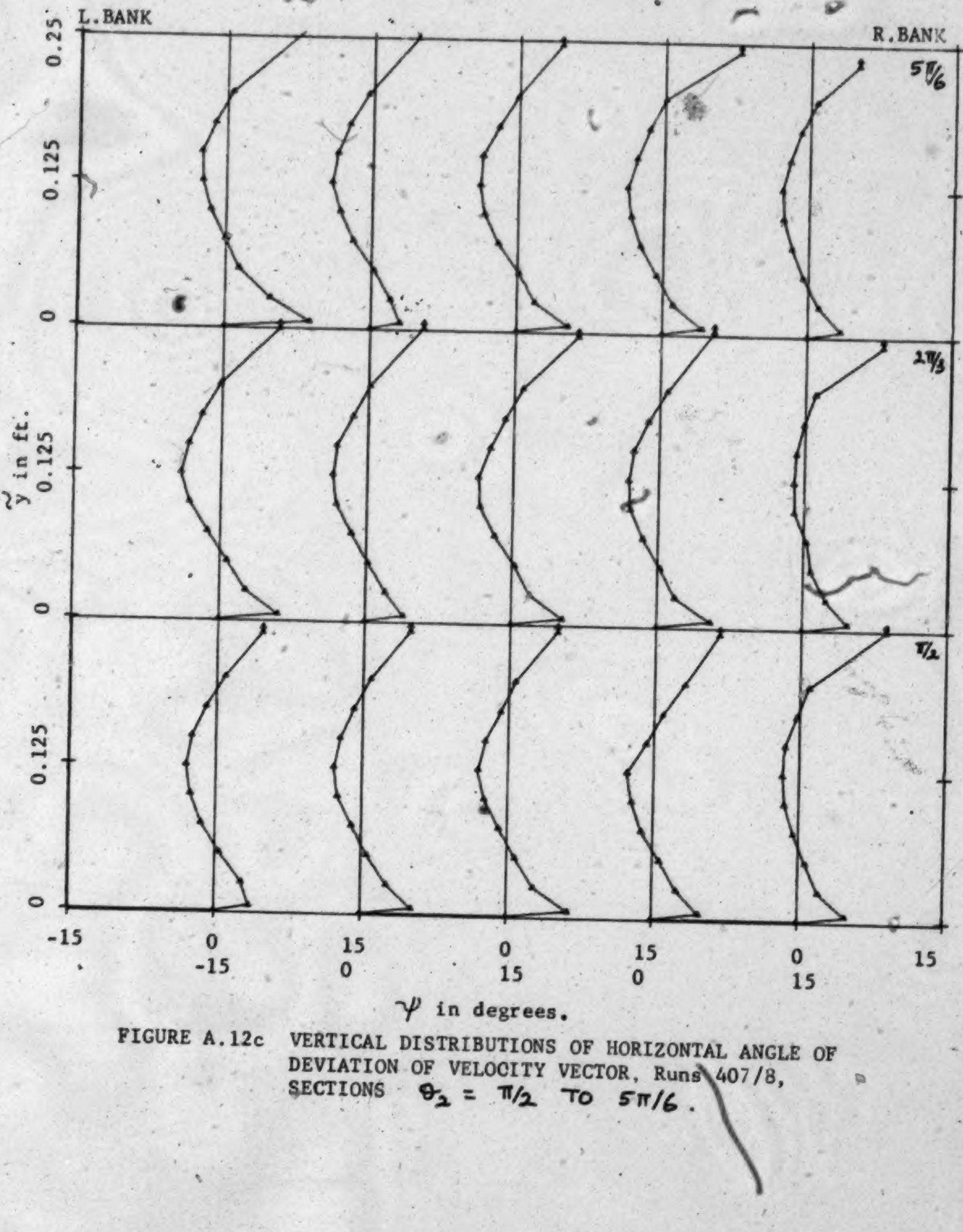

FIGURE A.12c VERTICAL DISTRIBUTIONS OF HORIZONTAL ANGLE OF DEVIATION OF VELOCITY VECTOR, Runs 407/8, SECTIONS $\theta_2 = \pi/2$ TO $5\pi/6$.